A Thesis Entitled

STUDY ON EFFICIENCY OF FIN STRUCTURES IN THE HEAT TRANSFER ANALYSIS

Submitted to the

Faculty of Science and Technology

For the Award of the Degree of

Doctor of Philosophy

in

MATHEMATICS

by

KEERTHI M.L.

Research Supervisor

Dr. B.J. GIREESHA

Professor

Department of P.G. Studies and Research in Mathematics

Jnanasahyadri, Shankaraghatta - 577 451

Shivamogga, Karnataka, India

February 2023

DECLARATION

I hereby declare that the thesis entitled **"Study on Efficiency of Fin Structures in the Heat Transfer Analysis"**, submitted to the Faculty of Science and Technology, Kuvempu University for the award of the degree of Doctor of Philosophy in Mathematics is the result of the research work carried out by me in the Department of Mathematics, Kuvempu University under the guidance of **Dr. B.J. Gireesha**, Professor, Department of P.G. Studies and Research in Mathematics, Kuvempu University, Jnanasahyadri, Shankaraghatta.

The thesis represents original work by the author except where due reference and credit is given. No portion of the work referred to in this thesis has been submitted in any form for another degree or qualification to any other university or institution.

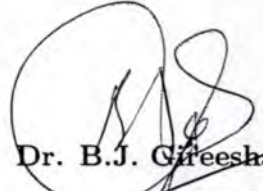Place: Jnanasahyadri

Date: 23|02|2023

Keerthi M.L.

CERTIFICATE

This is to certify that the thesis entitled **"Study on Efficiency of Fin Structures in the Heat Transfer Analysis"** submitted to the Faculty of Science and Technology, Kuvempu University for the award of the degree of Doctor of Philosophy in Mathematics by **Keerthi M.L.** is the result of bonafide research work carried out by her under my guidance in the Department of Mathematics, Kuvempu University, Jnanasahyadri, Shankaraghatta.

The portion of the work embodied in this thesis has not been submitted in part or full to any other University or Institute for the award of any degree.

Place: Jnanasahyadri

Date: 23|02| 2023

Dr. B.J. Gireesha

Research Supervisor

Dr. B.J. GIREESHA
M.Sc., M.Phil.,Ph.D., PDF (USA)
Professor
Department of Mathematics
Kuvempu University, Jnana Sahyadri
SHANKARAGHATTA-577 451

ACKNOWLEDGEMENT

strengths and igniting my love for Mathematics.

I greatly admire my seniors Dr. S. Sindhu, Dr. Nagaraja B., Dr. Felicita Almeida, Dr. D.O. Soumya, Dr. Shruthi C., Dr. Aruna Kumara H. and Dr. Devaraja Mallesha Naik for their valuable suggestions and unconditional support. I warmly thank my fellow researchers Kavya N.S., Pavithra C.G., Sushma, Pavan Kumar P.L., Raghavendra R.S., Surekha Desai, Bhanumathi N., Dr. Manohar R Gombi, Dr. K.S. Venkatesha, Dr. H.M. Manjunatha, Rajeshwari M.R., Dhanalakshmi R., Dr. Roja A., Anitha L., Usha B., Dr. Shankaralingappa B.M., Manjunatha Malligawad, Sanjay T., Aishwarya C., Jeevana Jyothi E., Sudharani L., Pooja M.N., Chaitra Chooda Chalavadi, Yashwanth B.R. and Praveen J. for their love and affection.

I am grateful to non-teaching staff of our department Mrs. M.P. Latha, Mr. Rakesh S.M. and Mr. Shivakumar for their valuable favours and kind co-operation. I extend my thanks to staff members of OBC Cell specially Dr. Shrikanth, Mrs. Suma Rao and Mrs. Rani for their invaluable help and best wishes.

Finally, I would like to acknowledge the people who are my inner strength, my grandparents, **Smt Vanajakshamma** and **Sri M. Basavappa**, my parents **Smt Suneetha** and **Sri M. Lohitkumar**, my supportive brother **Manu M.L.**, my loving sister **Shubha M.L.** and my friends **Madhura R.** and **Pavithra M.** for always encouraging and motivating me while chasing my dreams. I consider myself the luckiest in the world to have such a supportive family, standing behind me with their love and support. Finally, I thank each and everyone who have helped me in completing my Ph.D. journey.

Place: Jnanasahyadri   Keerthi M L

Date:

Contents

Preface

Excess heat generation in thermal components is unavoidable in a wide range of engineering applications. This excessive heat might have a negative impact on the operation and functionality of such components. As a result, the reliable operation of such components necessitates the use of appropriate cooling technology. Although different cooling processes have long been used to remove heat, a fin or an extended surface plays a vital role in increasing the heat transfer rate. A fin is a component attached to a primary surface with the aim of increasing the latter's surface area thereby increasing the heat exchange rate. It has a variety of applications in the field of manufacture and engineering where it is essential for the surface of components to work in a threshold temperature range. Some invaluable applications are in aviation engineering, automobile industries, nuclear power plants, microelectronics, home electronic systems, etc.

A fin is an extension on exterior surfaces of objects that increase the rate of heat transfer to or from the object by increasing convection. This is achieved by increasing the surface area of the body, which in turn increases the heat transfer rate by a sufficient degree. Increasing the heat transfer between the object and the surrounding mainly depends on three parameters namely, surface area available, temperature difference between surface and surrounding fluid and the convective heat transfer coefficient. The base surface area is limited by design of the system. The temperature difference depends

on the process and cannot be altered. The heat transfer coefficient also cannot be increased beyond a certain value. Thus, the possible option is to increase the base area by the so called 'Extended surface' or 'Fin'. The fin structures extended from the base surfaces provide additional convection area for the heat conducted into the fin at base. Fin structures are thus used whenever the available surface area are found insufficient to transfer the required quantity of heat with the available temperature deep and heat transfer coefficient.

On request from the Engineering Division of the U.S. Army and the U.S. Bureau of Standards in connection with the heat dissipating features of air-cooled aircraft engines, a paper by Harper and Brown (1922) appeared as an NACA report. It was an elegant piece of work and appears to be the first really significant attempt to provide a mathematical analysis of the interesting interplay between convection and conduction in and upon a single extended surface called fin. Murray (1938) proposed that the analysis of extended surface is based on a set of assumptions that have been known since 1945 as the Murray-Gardner assumptions. Gardner (1945) derived general equations for the temperature excess profile and fin efficiency for any form of extended surface for which the Murray-Gardner assumptions are applicable.

Research in the field of heat transfer enhancement via fin is going on since decades. Because of their widespread use in industry, researchers have always sought new techniques to improve their performance and make them more flexible to the needs of the field. Kraus et al (2002) have put in an encyclopaedic effort in compiling the advancements in the field of extended surface technology. In recent years fin problems were proposed and studied under different circumstances by Gorla and Bakier (2011), Aziz and Torabi (2012), Khani et al (2016), Sowmya et al (2019), Das and Kundu (2021), Kundu and Yook (2021) and

many others.

The fin geometry can be broadly classified into longitudinal (straight), radial, and pin fin structures. Each fin geometry can assume distinct profiles like rectangular, trapezoidal, exponential, convex, concave etc depending on the variation in the fin thickness along its length. The longitudinal fin structures of distinct profiles were mainly concentrated by Torabi et al (2013), Moradi et al (2014), Hatami and Ganji (2014), Kundu and Lee (2015), Ma et al (2017) and Sowmya and Gireesha (2022). On the other hand the radial or circular fin structures were examined by Arslanturk (2009), Aziz et al (2013), Gireesha et al (2019) and Ndlovu (2020). The pin fin structures or spines have applications in gas turbine blades, computer chips, and heat sinks and were mainly discussed by Hajabdollahi et al (2012), Hatami and Ganji (2013), Vahabzadeh et al (2015), Fallo et al (2018), and Turkyilmazoglu (2020, 2021). On the other hand, the semi-spherical shaped fin structures have gained enormous applications due to the ease of manufacturing as well as the low resistance which they offer to the flow as compared to other shapes. They are mainly employed by embedding them on the surface of heat sinks, plate fin heat exchangers, microchannels etc. Sabbaghi et al (2011), Hatami et al (2014), Atouei et al (2015) and Manohar et al (2021) have carried out research on the semi-spherical fin structures.

With flexibility in the context of weight, size, and shape fin has gained employment in numerous areas. The manufacturing cost is also a necessary aspect to be taken into consideration while designing the fin structures. In airborne and space applications fin structures of tapered profiles are preferred over rectangular fin structures, because of their lighter structures. On the other hand, the inverted fin profiles have applications in the area of double pipe heat exchangers. In this regard, the tapered and inverted profiles of trapezoidal fin structures have been investigated by Lane and Heggs (2005),

Khani and Aziz (2010), Das (2016) and Turkyilmazoglu (2017) whilst that of exponential fin structures has been examined by Turkyilmazoglu (2014), Kundu et al (2015) and Turkyilmazoglu (2018).

Kiwan and Al-Nimr (2001) were the foremost to consider the light-weighted porous fin structures as a substitution for the solid ones. The porous fin structures have higher surface area to volume ratio as compared to solid ones and thus enhance the heat transfer rate. The researchers namely Kiwan (2007a, 2007b), Bhanja et al (2013), Hatami et al (2013), Nabati (2021), etc., mainly focused on porous fin structures. The fully wet environment is an emerging technology in the field of heat transfer enhancement. Sharqawy and Zubair (2008) explored the thermal performance of fin structures operating under wet conditions. Further, Hatami and Ganji (2014), Darvishi et al (2016), Kundu et al (2018), Das and Kundu (2019), etc have discussed distinct fin structures exposed to wet environment. The angle of inclination has a significant impact on the thermal performance of fin structures as analysed by Kiwan (2019), Gireesha and Sowmya (2020) and other researchers.

Coolants utilised in industries and other disciplines, such as water, ethylene glycol, etc., are often weak at temperature conduction. The injection of nanoparticles into coolants can overcome this nature, and Choi and Eastman (1995) were the first to suggest this approach. Inspired by the use of nanofluids in several heat transfer enhancement fields, Baslem et al (2020) investigated heat transfer through fin structures wetted in nanofluids. However, while such a nanofluid may have superior thermal conductivity, it may not have improved rheological characteristics, and its stability is also an issue. To address this, hybrid nanofluids were developed, which are nanofluid composites made up of a perfect blend of two distinct nanoparticles that are acceptable for the field's application needs.

Taking notice of hybrid nanofluids' increased efficacy, the heat transmission through a porous fin structure under motion in the presence of a hybrid nanofluid was explored by Gireesha et al (2020). With the ground-breaking works of Sowmya et al (2019), Hosseinzadeh et al (2022) and Talbi et al (2022) the nanotechnology-assisted extended surface technology is reaching new heights.

The functionally graded materials (FGM) are composite materials that are graded for a smooth transition of properties. But the composite materials show a sharp transition in properties which may result in failure of the components. Hence, FGMs have replaced composite materials in the fields of mining, nuclear, chemical, biomedical, etc. An overview of FGMs has been recorded in the article by Zhang [20]. The works by Hassanzadeh and Pekel (2013), Oguntala et al (2019), Sowmya et al (2020) and Yildrim et al (2020) are some of the important ones on the application of FGMs in the field of extended surfaces.

Extrusion, casting, glass fibre drawing, hot rolling, etc. are some of the most essential production processes and, in the automobile industry, there is also continuous movement of fin surfaces. Since fin is under continuous motion in a variety of applications, there is a necessity to analyse the effect of movement on its thermal profile. Aziz and Khani (2011), Bhanja et al (2014), Singla and Das (2014), Sun and Xu (2015), Roy et al (2018), Najafabadi et al (2021) and many other researchers have incorporated fin motion in distinct fin problems. A moving fin surface can be mounted with a stretching/shrinking mechanism similar to a conveyer belt. Turkyilmazoglu (2015) were the first to study the impact of stretching/shrinking on the thermal performance of fin structures and were followed by Mosavat et al (2018).

The surface roughness artificially created by MEMS (Microelectromechanical systems)

technologies during the production have a significant impact on the thermal performance of structures of smaller dimension. Diez et al (2010) modelled the rough pin fin problem which were further analysed by Oguntala et al (2018a, 2018b), Ayoobi (2021) and others. On the other hand internal heat generation in the fin structures when exposed to various circumstances has been concentrated by Aziz and Bouaziz (2011), Ghasemi et al (2014), Sowmya et al (2020) and other researchers.

Understanding the operation of fin structures in transient temperature circumstances is crucial for many cooling applications, such as energy storage devices, automatic control systems, electronic equipment, and others. In this regard, distinct fin structures were investigated under unsteady conditions by Moitsheki and Harley (2011), Khan and Aziz (2012), Mosayebidorcheh et al (2014), Sowmya et al (2021) and others. All these studies dealt with performance of fin structures are subject to constant base temperature. But in realistic applications the fin base encounters a non-constant or periodic variation in the temperature. Fin structures in applications like electronic equipment, solar collectors, cutting tools, internal combustion engines, etc., experience a periodic variation in the thermal conditions. Thus, results obtained by analysing a fin with constant base temperature cannot be satisfactorily applied to the real-life applications. In this regard, Aziz and Na (1981), Aziz and Luardini (1994), Yang (2008), Singh et al (2018) and others have analysed the fin structures when exposed to periodic variations in the base temperature.

The classic concept of heat conduction, i.e., Fourier's law, has produced a reasonable pact at most time and spatial dimensions. The parabolic nature of Fourier's laws indicates that heat flux arises concurrently with the establishment of the thermal gradient and heat dispersion speed will be infinite. The Fourier's law fails when heat is transferred in exceedingly short durations, especially elevated temperature differences or extremely

minimal temperature levels closer to absolute zero. Thus, the effect of non-Fourier heat conduction which leads to the formulation of the hyperbolic heat conduction equation is considered for discussing the transmission of thermal waves with finite speed. Numerous researchers like Kundu and Lee (2012, 2013), Bhowmik et al (2014), Varun Kumar et al (2022) and others have considered hyperbolic heat conduction for a wide range of initial and boundary value problems.

Analysing the fin thermal performance when it is exposed to various circumstances can be done by calculating the thermal efficiency and entropy generation. Fin efficiency is defined as the ratio of heat transfer from the fin to the maximum heat that can be transferred from the fin. This quantity is more often used to determine the heat flow when variable area fin atructures are used. Joneidi et al (2009), Ganji et al (2011), Torabi and Aziz (2012) are among the ones who have analysed the performance of fin structures by calculating their efficiency. Further, entropy generation denotes the energy degradation during a process and helps estimate the wasted energy. With this, fin optimization has been driven towards a new direction with the assessment of entropy generation in distinct fin structures. Thus the entropy generation in distinct fin structures was concentrated by Poulikakos and Bejan (1982), Aziz and Makinde (2010), Khatami and Rahbar (2019) and Din et al (2022a, 2022b).

With regard to the above noted research contributions the current work focuses on the impact of various circumstances on the heat transfer through a fin structure. Different fin geometries namely rectangular, trapezoidal and exponential profiled longitudinal fin; semi-spherical fin; rectangular profiled radial fin and cylindrical, conical and convex profiled pin fin are subject to circumstances like inclination, stretching/shrinking, periodic boundary, non-Fourier heat flux, hybrid nanofluid flow, surface roughness, etc. The gov-

erning equations have been modelled for fin thermal profile, heat transfer rate, efficiency, entropy generation and average entropy generation. The derived ordinary and partial differential equations have been respectively solved by employing the Runge Kutta Fehlberg fourth fifth order and finite difference methods. Based on these aspects, the thesis is divided into **EIGHT** chapters.

The **FIRST** chapter emphasises on the trapezoidal and dovetail profiled longitudinal fin structures exposed to a convective-radiative environment and mounted on an inclined surface have been considered for the analysis. The fin structures have been assumed to be porous and fully wet in nature. The Darcy model has been implemented to simulate the fluid-solid interactions. Further, the convective and radiative heat transfer coefficients have been taken to be temperature-dependent. The resulting equation which is a nonlinear ordinary differential equation (ODE) has been reduced by introducing the non-dimensional quantities and then solved by employing the Runge-Kutta Fehlberg $4^{th} - 5^{th}$ order (RKF45) method. The effect pertinent parameters on the fin thermal profile and fin heat transfer rate has been presented graphically and discussed. It has been inferred that the dovetail fin profile achieves the highest heat transfer rate followed by rectangular and trapezoidal fin profiles provided the internal heat generation is minimal.

In the **SECOND** chapter trapezoidal and exponential profiled convective-radiative porous longitudinal fin structures wetted in a single-phase fluid have been considered. The periodic variation in the fin base temperature has been taken into account along with the temperature sensitive thermal conductivity, internal heat generation and convective heat transfer coefficients. The modelled problem which is resolved into a nonlinear partial differential equation (PDE) is made dimensionless and solved by employing the centered implicit finite difference method (FDM). The results have been visually displayed through

graphs and discussed with their physical interpretations. The impact relevant quantities on the distribution of temperature along the fin length and also with dimensionless time has been investigated. It has been deciphered that the periodic heat transfer gives rise to wavy nature of fin thermal profile against time.

In the **THIRD** chapter, trapezoidal and exponential profiled convective-radiative wet porous longitudinal fin structures subject to motion have been considered. Here, the fin structures are allowed to stretch or shrink by mounting a conveyer belt like mechanism on the fin surface. An analysis of the transient thermal behaviour of both fin structures exposed to Fourier and non-Fourier heat conduction has been performed. By using the centered implicit FDM, the modelled problem which is a nonlinear PDE has been numerically solved. The results have been graphically displayed using graphs and further reviewed with regard to their physical interpretations. On the variations in the fin temperature with its length and also with dimensionless time, the effects of Vernotte number, wet porous nature, stretching/shrinking parameter, Peclet number and other pertinent factors have been studied.

In the **FOURTH** chapter transient heat transfer characteristics of a convective-radiative longitudinal fin of exponential profile fully wetted in a hybrid nanofluid have been analysed. The fin medium is porous and Darcy law has been implemented to formulate the fluid-solid interactions. The hybrid nanofluid is obtained by immersing Silver and Graphene nanoparticles in the base fluid water and the study is based on a mass-based model. The scrutiny presented in dimensionless form is a nonlinear PDE which is solved by employing the FDM. The effect of relevant parameters on the thermal field and thermal efficiency of the fin structures has been graphically analysed and discussed. The examination has resulted in a novel outcome that the presence of hybrid nanofluid

enhances the fin efficiency.

The **FIFTH** chapter focuses on a fully wet porous fin of radial profile exposed to convective-radiative heat exchange with the hybrid nanofluid flowing past it with a constant velocity of $\bar{U}$. In the analysis, spherical-spherical, spherical-cylindrical, and spherical-platelet shape combinations of two nanoparticles are considered. The mixture model is employed to assess all the thermophysical attributes of the hybrid nanofluid except thermal conductivity and dynamic viscosity, which are estimated by applying the nanoparticle volume fraction-based interpolation method. The fin model with the applied conditions results in an ODE which is made dimensionless and then numerically resolved by applying the RKF45 technique. The effect of significant parameters on the energy field and thermal gradient profiles of the radial fin subjected to shape-dependent hybrid nanofluid flow has been graphically analysed. Furthermore, the thermal fin efficiency has been modelled and its variation with the significant parameters has been examined. One of the major outcomes was that efficiency increases with nanoparticle volume fraction. Further, it is significantly affected by the shape factor of the nanoparticles and achieves the highest value for spherical-platelet combination.

The **SIXTH** chapter intends to examine the unsteady thermal behaviour of fully wet, porous, and rough micro-pin fin structures under convective-radiative conditions. Here, pin fin structures of cylindrical, conical and convex parabolic profiles have been chosen. The problem is modelled by incorporating the roughness parameters in the perimeter and cross-sectional area of the pin fin. The resulting PDEs are nonlinear and of second order which have been solved by employing the FDM. The impact of roughness parameter, wet porous parameter, dimensionless time and other relevant parameters on the thermal performance and efficiency of rough micro-pin fin structures has been established graphically.

According to the findings, rise in roughness causes an increase in efficiency.

The **SEVENTH** chapter numerically investigates the transient thermal behaviour of a fully wet semi-spherical fin composed of functionally graded material (FGM). The study incorporates the Darcy model as the fin is made up of porous material. Further, the fin is exposed to convective-radiative heat exchange and is subject to uniform motion. The heat balance equation has been reduced to get a nonlinear PDE which is computed by employing the FDM. The dimensionless terms are grouped together and their influence on the temperature distribution in a semi-spherical fin is studied. The transient fin efficiency has been modelled and its variation with relevant parameters has been graphically depicted. And these are found to be greatly affected by Peclet number, wet porous nature and dimensionless time.

The **EIGHTH** chapter emphasizes on a wet porous moving longitudinal fin composed of linear FGM has been chosen for the analysis. The fin is allowed to stretch/shrink by mounting a mechanism similar to a conveyer belt. The thermal behaviour of the fin and its entropy generation in the presence of convective-radiative heat transmission are the focus of the study. Further, three distinct cases of FGM namely homogeneous, type I (higher thermal grading towards the fin base) and type II (higher thermal grading towards the fin tip) have been comparatively investigated. The derived energy equation is a 2nd order nonlinear ODE and is solved with the aid of the RKF45 method. The fin thermal profile, entropy generation profile, and average entropy generation have been graphically analysed for the significant parameters. The entropy generation along fin length as well as the average entropy generated in a fin are discovered to be lowest in the case of homogeneous fin structures followed by type I and type II FGM fin structures. The present investigation benefits the manufacture and design of FGM fin structures.

Chapter 1

Heat Transfer Analysis of Longitudinal Fins of Trapezoidal and Dovetail Profile on an Inclined Surface

1.1 Prelims

The trapezoidal and dovetail profiled longitudinal fin structures exposed to a convective-radiative environment and mounted on an inclined surface have been considered for the analysis. The fin structures have been assumed to be porous and fully wet in nature. The Darcy model has been implemented to simulate the fluid-solid interactions. Further, the convective and radiative heat transfer coefficients have been taken to be temperature-dependent. The resulting equation which is a nonlinear ordinary differential equation (ODE) has been reduced by introducing the non-dimensional quantities and then solved by employing the Runge-Kutta Fehlberg $4^{th} - 5^{th}$ order (RKF45) method. The effect of tip tapering, angle of inclination, fully wet nature, porosity, internal heat generation, and other pertinent parameters on the fin thermal profile and fin heat transfer rate has

been presented graphically and discussed. It has been inferred that the dovetail fin profile achieves the highest heat transfer rate followed by rectangular and trapezoidal fin profiles provided the internal heat generation is minimal. The present work is significant for fin design purposes and also acts as a verification tool for future research.

1.2   Modeling and Interpretation

Consider a longitudinal fin of length L, width W and base thickness t_b mounted on a surface inclined at an angle Ω as shown in figure 1.1 a. Varying the fin tip thickness we obtain longitudinal fin of trapezoidal, rectangular and dovetail profiles as shown in figure 1.1 b. The heat enters the fin through the base kept at temperature T_b. The convection and radiation heat sinks are maintained at temperatures T_a and T_s respectively. The internal heat generation in fin is taken as a linear function of temperature.
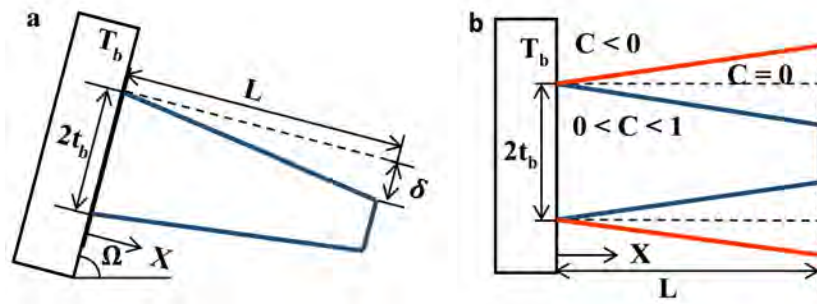

Figure 1.1: a) Inclined trapezoidal fin. b) Comparison of fin profiles for different values of fin taper ratio C.

The problem formulation is abridged by employing certain assumptions as followed.

- The fin medium is porous, homogeneous, isotropic, and completely infused with single-phase fluid.

- Darcy's law governs the porous medium and clear fluid interaction.

2

- The fin is fully wetted in a fluid and the solid matrix and the fluid are in local thermodynamic equilibrium.

- The temperature inside the fin varies only along the axial direction as its variation along the non-axial direction is negligible.

- The surface radiant exchange is neglected.

- The convective and radiative heat transfer coefficients are temperature-dependent.

- The fin tip is adiabatic in nature as the transfer of heat through it is negligible compared to the heat transferred through the lateral surface.

- The fin operates under the steady state condition.

In view of the stated assumptions, the general energy transmission equation of a steady state fin problem may be written as,

$$q_x - q_{x+dx} + q^*(T)Wt(x) - 2\bar{m}C_p(T - T_a) - 2\varepsilon(T)\sigma W dx(T^4 - T_s^4)$$

$$- 2h(T)W dx(1 - \hat{\phi})(T - T_a) - 2h_D W dx l_{fg}(1 - \hat{\phi})(\bar{\omega} - \bar{\omega}_s) = 0. \tag{1.2.1}$$

Here the coefficient "2" is for considering the upper and lower surfaces.

From Fourier's law of conduction,

$$q = -k_{eff}A_c(x)\frac{dT}{dx}, \tag{1.2.2}$$

where $A_c(x)$ is the cross-sectional area of the fin at distance x.

k_{eff} is the effective thermal conductivity and it is calculated from the following equation,

$$k_{eff} = (1 - \hat{\phi})k_S + \hat{\phi}k_f. \tag{1.2.3}$$

3

Here $\hat{\phi}$ is porosity and $1 - \hat{\phi}$ is taken for effective solid surface.

The area of cross-section of the fin is given by,

$$A_c(x) = Wt^*(x), \tag{1.2.4}$$

where $t^*(x)$ is the fin thickness at distance x.

$\bar{m}$ is the fluid's mass flow rate through a porous fin and is defined as,

$$\bar{m} = \rho_f \bar{v}(x) W dx. \tag{1.2.5}$$

The fluid velocity through the porous fin, according to Darcy's model, is defined as,

$$\bar{v}(x) = \frac{gK\beta_f(T - T_a)sin(\Omega)}{\nu_f}. \tag{1.2.6}$$

The fin surface emissivity ε as a function of temperature is given by,

$$\varepsilon(T) = \varepsilon_s(1 + \beta^*(T - T_s)). \tag{1.2.7}$$

Assume that the internal heat generation is non-uniform and varies linearly with fin surface temperature as,

$$q^*(T) = q_a^*(1 + \epsilon_g(T - T_a)). \tag{1.2.8}$$

The temperature sensitive convective heat transfer coefficient $h(T)$ and its relation with the mass transfer coefficient h_D as per Chiltone-Colburn analogy is given by,

$$h(T) = h_a \left(\frac{T - T_a}{T_b - T_a} \right)^m = h_D C_p Le^{\frac{2}{3}}. \tag{1.2.9}$$

The nonlinear ODE regulating the temperature distribution in the fin is obtained by substituting equations (1.2.2) – (1.2.9) into equation (1.2.1),

$$k_{eff} \frac{d}{dx} \left[t^*(x) \frac{dT}{dx} \right] + q_a^*(1 + \epsilon_g(T - T_a))t^*(x) - \frac{2\rho_f g K \beta_f C_p \sin(\Omega)}{\nu_f}(T - T_a)^2$$

$$- \frac{2(1 - \hat{\phi})h_a(T - T_a)^{m+1}}{(T_b - T_a)^m} - \frac{2h_a l_{fg}(1 - \hat{\phi})(\bar{\omega} - \bar{\omega}_s)(T - T_a)^m}{C_p Le^{\frac{2}{3}}(T_b - T_a)^m}$$

$$- 2\sigma \varepsilon_s(1 + \beta^*(T - T_s))(T^4 - T_s^4) = 0. \quad (1.2.10)$$

For longitudinal fin structures of trapezoidal, rectangular, and dovetail shape, the local semi-fin thickness is given by,

$$t^*(x) = t_b - \delta\left(\frac{x}{L}\right). \quad (1.2.11)$$

The above formula for semi-fin thickness is obtained by modifying the one mentioned in [?]. Here value of δ determines the profile. Substituting equation (1.2.11) in equation (1.2.10), the resulting equation is,

$$k_{eff} \frac{d}{dx} \left[\left(t_b - \delta\left(\frac{x}{L}\right) \right) \frac{dT}{dx} \right] - \frac{2\rho_f g K \beta_f C_p \sin(\Omega)}{\nu_f}(T - T_a)^2 - \frac{2(1 - \hat{\phi})h_a(T - T_a)^{m+1}}{(T_b - T_a)^m}$$

$$- \frac{2h_a l_{fg}(1 - \hat{\phi})(\bar{\omega} - \bar{\omega}_s)(T - T_a)^m}{C_p Le^{\frac{2}{3}}(T_b - T_a)^m} - 2\sigma \varepsilon_s(1 + \beta^*(T - T_s))(T^4 - T_s^4)$$

$$+ q_a^*(1 + \epsilon_g(T - T_a)) \left(t_b - \delta\left(\frac{x}{L}\right) \right) = 0$$

$$(1.2.12)$$

The associated boundary conditions are given by,

$$T = T_b \ at \ x = 0,$$

$$\frac{dT}{dx} = 0 \ at \ x = L. \quad (1.2.13)$$

5

The dimensionless quantities listed below are introduced.

$$\theta = \frac{T}{T_b}, \theta_a = \frac{T_a}{T_b}, \theta_s = \frac{T_s}{T_b}, X = \frac{x}{L}, C = \frac{\delta}{t_b}, B^* = \frac{\beta^*}{t_b}, Nc = \frac{2\rho_f g \beta_f K C_p T_b L^2}{\nu_f k_{eff} t_b},$$

$$Nr = \frac{2\varepsilon_s \sigma L^2 T_b^3}{k_{eff} t_b}, m_0 = \frac{2h_a L^2 (1-\hat{\phi})}{k_{eff} t_b}, G = \frac{q_a^* L^2}{k_{eff} T_b}, m_1 = \frac{2h_a l_{fg}(1-\hat{\phi}) b_2 L^2}{k_{eff} t_b C_p L^2},$$

$$\epsilon_G = \epsilon_g T_b, \bar{\omega} - \bar{\omega}_s = b_2(T - T_a), m_2 = m_0 + m_1. \tag{1.2.14}$$

Here Nc is the natural convective parameter, Nr is the radiative parameter, B^* is the emissivity parameter, m_2 is the wet porous parameter, C is the fin taper ratio, θ_a is the ambient temperature, θ_s is the sink temperature, G is the generation parameter, ϵ_G is the non-dimensional internal heat generation parameter.

The equation (1.2.12) on non-dimensionalizing reduces to,

$$\frac{d^2\theta}{dX^2} - C\frac{d\theta}{dX} - CX\frac{d^2\theta}{dX^2} + G(1 + \epsilon_G(\theta - \theta_a))(1 - CX) - m_2\frac{(\theta - \theta_a)^{m+1}}{(1 - \theta_a)^m}$$

$$- Nc(\theta - \theta_a)^2 sin(\Omega) - Nr(1 + B^*(\theta - \theta_s))(\theta^4 - \theta_s^4) = 0. \tag{1.2.15}$$

Here,

$0 < C < 1$ corresponds to longitudinal fin of trapezoidal profile,

$C = 0$ corresponds to longitudinal fin of rectangular profile, and

$C < 0$ corresponds to longitudinal fin of dovetail profile.

The associated reduced boundary conditions are,

$$\theta = 1 \ at \ X = 0,$$

$$\frac{d\theta}{dX} = 0 \ at \ X = 1. \tag{1.2.16}$$

The fin rate of heat transfer is calculated by using the Fourier's equation at its base and

6

is given by,

$$q = -k_{eff} A_b \frac{dT(0)}{dx} \tag{1.2.17}$$

where, A_b is the area of the fin base.

The fin rate of heat transfer in dimensionless form is,

$$Q = \frac{qL}{k_{eff} A_b T_b} = -\theta'(0) \tag{1.2.18}$$

1.3   Numerical Elucidation

The nonlinear second order ODE with insulated boundary conditions is solved by applying the RKF45 method. The first step is to convert the boundary value problem into an initial value problem by employing the shooting technique. Then the obtained initial value problem is solved via RKF method as followed.

$$q_1 = h^* z(u_l, v_l), \tag{1.3.1}$$

$$q_2 = h^* z \left(u_l + \frac{1}{4} h^*, v_l + \frac{1}{4} q_1 \right), \tag{1.3.2}$$

$$q_3 = h^* z \left(u_l + \frac{3}{8} h^*, v_l + \frac{3}{32} q_1 + \frac{9}{32} q_2 \right), \tag{1.3.3}$$

$$q_4 = h^* z \left(u_l + \frac{12}{13} h^*, v_l + \frac{1932}{2197} q_1 - \frac{7200}{2197} q_2 + \frac{7296}{2197} q_3 \right), \tag{1.3.4}$$

$$q_5 = h^* z \left(u_l + h^*, v_l + \frac{439}{216} q_1 - 8q_2 + \frac{3680}{513} q_3 - \frac{845}{4104} q_4 \right), \tag{1.3.5}$$

$$q_6 = h^* z \left(u_l + \frac{h^*}{2}, v_l - \frac{8}{27} q_1 + 2q_2 - \frac{3544}{2565} q_3 + \frac{1859}{4104} q_4 - \frac{11}{40} q_5 \right). \tag{1.3.6}$$

An approximate solution to the resolved initial value problem is determined by using the Runge Kutta 4th order method.

$$v_{l+1} = v_l + \frac{25}{216} q_1 + \frac{1408}{2565} q_3 + \frac{2197}{4101} q_4 - \frac{1}{5} q_5. \tag{1.3.7}$$

7

And, the approximated value of the solution is improved by applying the Runge Kutta 5th order method.

$$w_{l+1}^* = v_l + \frac{16}{135}q_1 + \frac{6656}{12825}q_3 + \frac{28561}{56430}q_4 - \frac{9}{50}q_5 + \frac{2}{55}q_6. \tag{1.3.8}$$

The difference between the two obtained solutions is taken as the error term. If we get a large error value, then the process is repeated by choosing a smaller step size. In the present analysis, solutions are obtained for the step size 0.001 with the convergence criteria set to 10^{-6}.

1.4 Deliberation of Results

The performance of an inclined porous fin under fully wet condition in the presence of natural convection as well as radiation for trapezoidal and dovetail profiles has been studied parametrically. Each parameter is varied keeping others constant and the constant values considered are $Nc = 1, Nr = 1, m = 2, m_2 = 1, \theta_a = 0.5, \theta_s = 0.5, B^* = 0.2, \Omega = 45^0, G = 0.1$ and $\epsilon_G = 0.2$.

In the special cases of the current problem, the results obtained via RKF45 method have been validated with the analytical solutions (Homotopy Perturbation Method) of Hoshyar et al. [?] as depicted in table (1.1).

The influence of power index m on the thermal profile of fully wet porous fin has been depicted in figure 1.2. It can be inferred that an increase in values of m from 0 to 2 negatively affects the thermal drop rate in fin. Here, $m = 0$ corresponds to fin with constant heat transfer coefficient and $m > 0$ corresponds to fin with temperature-dependent heat transfer coefficient. As h becomes temperature-dependent it can be observed from equation (1.2.9) that its value decreases resulting in a decrease in convective heat loss

from the fin surface. Hence the fin temperature increases with the increase in the value of m. On the other hand, it can be inferred that the thermal drop rate is high in the case of trapezoidal profiled fin followed by rectangular and dovetail profiles.

Figure 1.3 corresponds to the variations in the thermal profile of fin with surface emissivity parameter B^*. It is deciphered that; higher values of B^* correspond to lower thermal profiles. This is because, the positive values of B^* correspond to fin materials whose surface emissivity is directly proportional to temperature, and as the surface emissivity largely increases with temperature more heat is lost by radiation, resulting in a rapid decrease in the temperature of the fin. Thus, a higher heat transfer rate is achieved for higher values of B^*. Further, the thermal profile of the trapezoidal profiled fin stays below that of a rectangular profiled fin followed by a dovetail profiled one.

The variation in the thermal characteristic of trapezoidal, rectangular, and dovetail profiled inclined fin structures with dimensionless ambient and sink temperatures is illustrated through figures 1.4 and 1.5 respectively. The higher value of ambient and sink temperatures negatively influence the fin cooling process. This is because a rise in the ambient temperature values decreases the temperature difference between the fin surface and the surrounding thereby depressing the natural convection process. Thus, there is a decrease in the fin thermal drop rate. Similarly, there is a negative impact on radiative heat loss due to higher values of sink temperature. Hence in both cases, lower values of θ_a and θ_s are favoured. Further, the three different profiles are affected in a similar manner.

The figure 1.6 depicts the degrading temperature profile of inclined fin of various profiles with the progressive natural convective parameter Nc. It is noted that, the portion of heat transferred through convection to that by conduction is measured in terms of Nc. Thus, a progressive rise in the Nc values result in a quicker loss of heat by fin and hence

there is a steep decline in temperature towards the fin tip. Besides, the trapezoidal, rectangular and dovetail profiles are in the ascending order of temperature distribution.

The relation between the dimensionless radiative parameter Nr and the distribution of temperature along the length of the fin is as represented in figure 1.7. It is derived that, there is a depression in temperature along the length of the fin with ascending values of Nr. Since, the strength of surface radiation against conduction is indicated by the radiative parameter Nr, the rise in its value intensifies radiative heat loss, thus hiking the heat transfer rate. Thus, higher values of Nr are preferred for quicker heat loss. Further, all the three longitudinal fin profiles are affected in a similar trend.

The temperature distribution along the fin is reliant on its angle of inclination Ω and it varies as captured in figure 1.8. From the plot it is derived that an increase in the tilt angle positively affects the cooling process of fin. The ascending value of tilt angle acts as a propelling force for convective heat loss resulting in a gradual decrease in the temperature from fin base to fin tip. Hence for an optimum fin, angle of inclination must be at the apex. On the other hand, the thermal profile of trapezoidal fin is steeper than the other two profiles.

The influence of the wet porous parameter m_2 on the thermal profile of a fully wet, porous fin is as framed in figure 1.9. Here it is noticed that the enhancing values of m_2 result in an accelerating decrease in the temperature of the fin. This can be explained as follows. The wet nature of the fin aids in excess heat loss by absorbing more heat from the fin surface, and the porous nature of the fin increases the surface area of fin resulting in more heat loss via convection. Thus, the higher values of m_2 are favoured for quicker loss of heat. Further, the three profiles namely trapezoidal, rectangular and dovetail are in the decreasing order of the thermal drop rate.

Figure 1.10 draws attention on the influence of generation parameter G on the temperature profile of the fin. Here temperature is observed to be an escalating function of generation parameter. This is because with the rise in generation parameter, more heat generation occurs inside the fin negatively impacting the process of heat loss. Thus, lower values of generation parameter G help in the fin cooling process. The effect of G on thermal drop rate is more pronounced in the fin of dovetail profile followed by rectangular and trapezoidal profiles.

The importance of angle of inclination Ω and fin taper ratio C on the rate of heat transfer in a fin is illustrated in figure 1.11. It is observed that as the fin structure diminishes from dovetail profiles to trapezoidal profiles through the rectangular profile, the rate of heat transfer through the fin decreases steeply. This is due to decrease in the available surface area for heat loss. Further, it is noticed that as the angle of inclination ascends from 15^0 to 90^0 there is a notable increase in the rate of heat transfer through the fin. Thus, the dovetail profiled fin with angle of inclination equal to 90^0 has the highest heat transfer rate.

Figure 1.12 captures the impact of variation in the wet porous parameter m_2 and the power index m on the rate of heat transfer through the fin. As depicted in the figure, the rate of heat transfer through the fin increases prominently with an increase in wet porous parameter. Whereas the power index m negatively affects the rate of heat transfer. As it can be seen, the effect is more pronounced for the higher values of the wet porous parameter. Thus, higher heat transfer rate is achieved by considering higher values of wet porous parameter m_2 and lower values of power index m. Besides, the dovetail profiled fin has the highest heat transfer rate followed by rectangular and trapezoidal fin profiles.

The impact of convective and radiative parameters on the dimensionless rate of heat

11

transfer through the fin can be understood by figure 1.13. It is noticed that both the convective parameter Nc and the radiative parameter Nr amplify the cooling process of the fin by fastening the rate of heat transfer. Hence, for intensifying the fin cooling process, values of Nc and Nr must be kept high. Further, the rate of heat transfer is high for the dovetail profiled fin compared to the other two fin structures.

As represented in figure 1.14, the generation parameter G and the non-dimensional internal heat generation parameter ϵ_G have a negative influence on the rate of heat transfer through the fin. In addition, at minimal values of G, the rate of heat transfer is more for the fin of the dovetail profile followed by rectangular and trapezoidal profiles. Whereas at peak values of G, the fin of the trapezoidal profile has higher heat transfer rate followed by rectangular and dovetail profiles. Thus, dovetail fin profile is preferable at lower values of G and the trapezoidal profile is favourable at higher values of G.

1.5   Denouement

The thermal performance of an inclined porous longitudinal fin of trapezoidal, rectangular, and dovetail profiles is considered for numerical investigation. From the study, the following can be derived. The dimensionless parameters of convection, radiation, and surface emissivity enhance the thermal drop rate in fin. The dimensionless parameters of ambient temperature, sink temperature, power index and heat generation negatively dominate the fin tip temperature. The wet porous parameter and the inclination angle strengthen the cooling process of the fin. The thermal profile of the trapezoidal fin structure is lower preceded by rectangular and dovetail structures. The fin heat transfer rate is better in the case of dovetail fin structure followed by rectangular and trapezoidal structures provided the internal heat generation is minimal. The present investigation

can be developed by analysing the efficiency and transient response of the trapezoidal and dovetail fin structures on application of magnetic field thereby increasing the scope of the study. Further the inverse solutions can be attempted for the present problem.

Table 1.1: Comparison of $\theta(X)$ values of the present work with the published literature when $Nc = 0.1, Nr = 0, m_2 = 0.09, m = 0, \theta_a = \theta_s = 0, B^* = 0, C = 0, G = 0.036, \epsilon_G = 0.2, \Omega = 90^0$

X	Hoshyar et al (HPM) [?]	Present Results
0.0	1.000000000	1.000000000
0.2	0.975973539	0.975973537
0.4	0.957555090	0.957555088
0.6	0.944540815	0.944540812
0.8	0.936788323	0.936788321
1.0	0.934213444	0.934213441
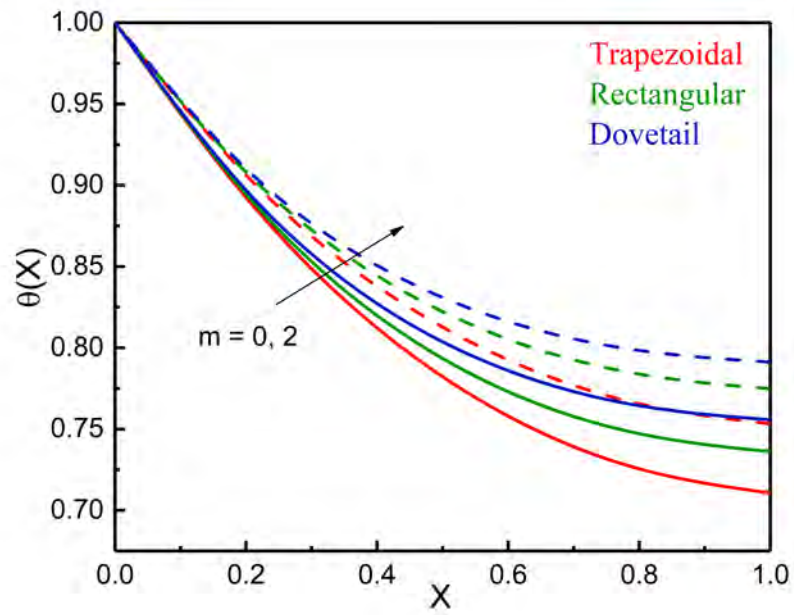
Figure 1.2: Fin thermal profile as a function of power index m.
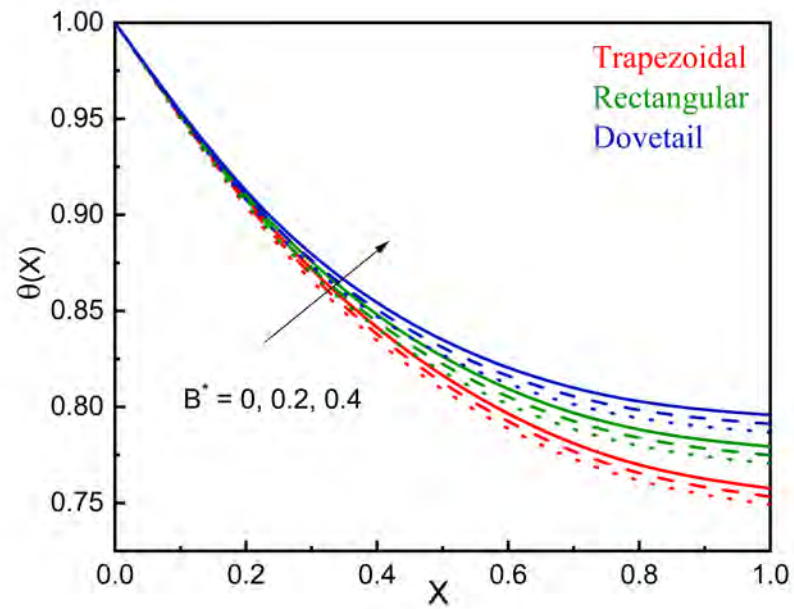
Figure 1.3: Fin thermal profile as a function of emissivity parameter B^*.
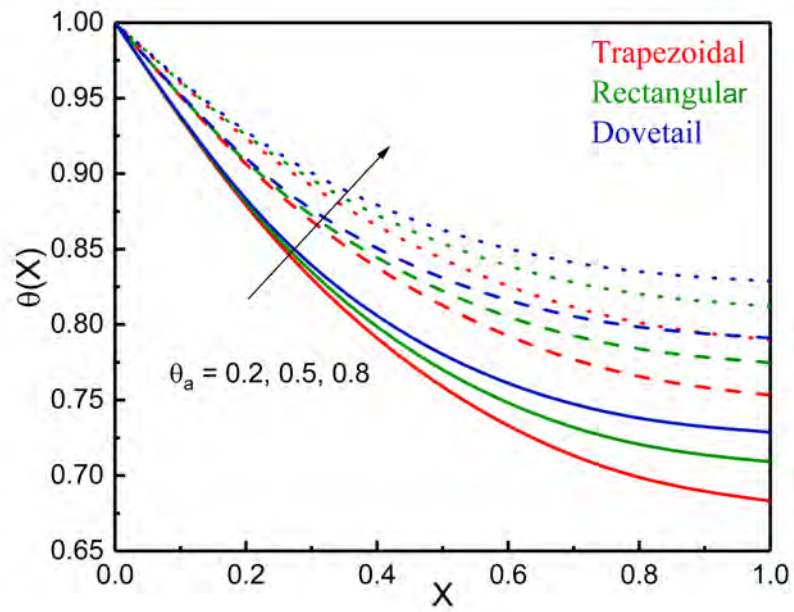
Figure 1.4: Fin thermal profile as a function of ambient temperature θ_a.
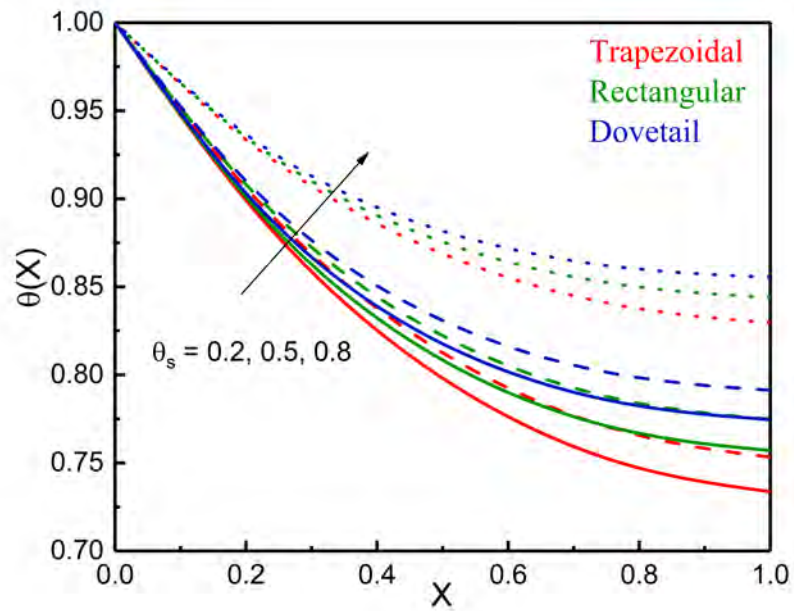
Figure 1.5: Fin thermal profile as a function of sink temperature θ_s.
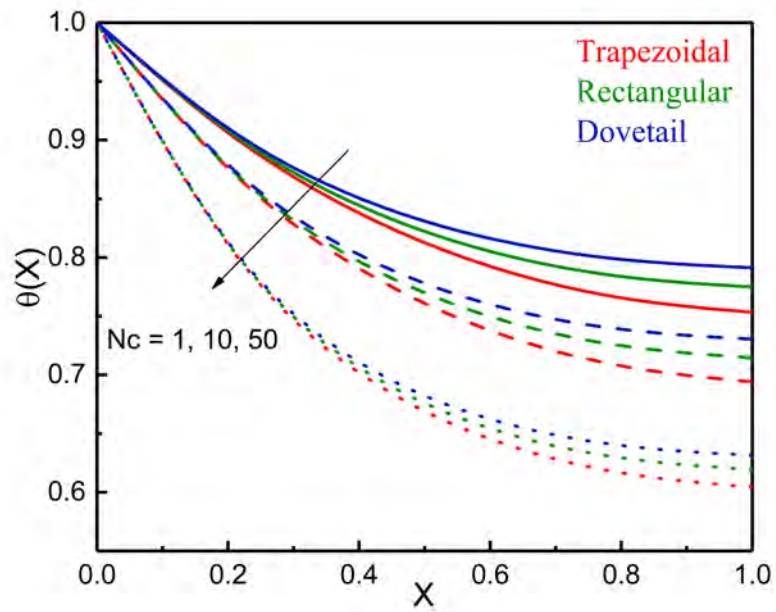
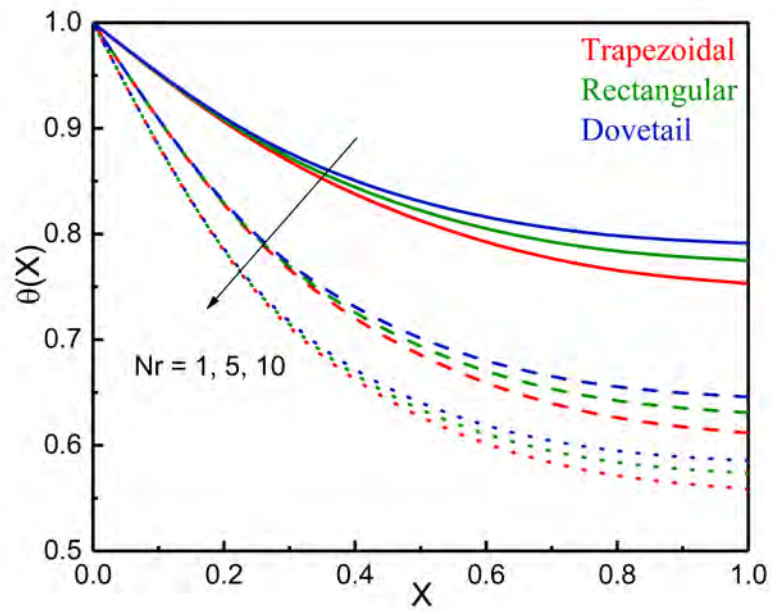Figure 1.6: Fin thermal profile as a function of convective parameter Nc.

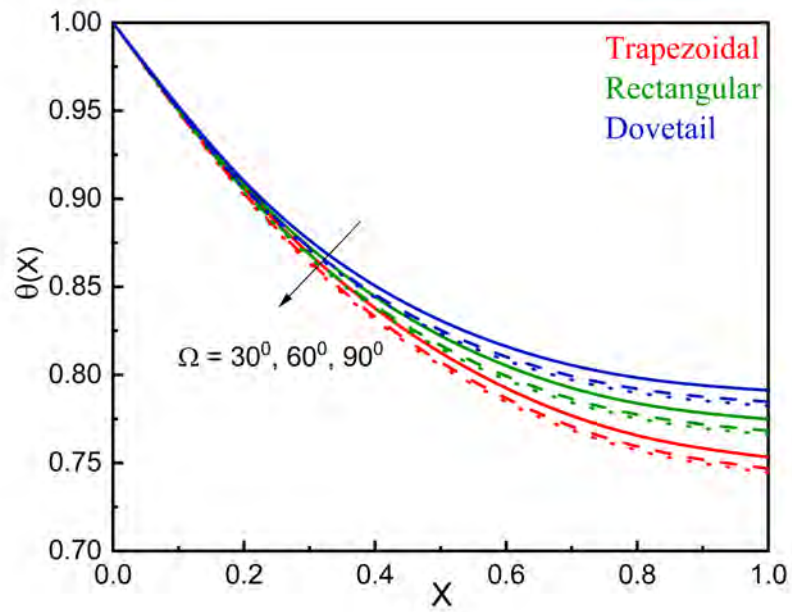Figure 1.7: Fin thermal profile as a function of radiative parameter Nr.

Figure 1.8: Fin thermal profile as a function of angle of inclination Ω
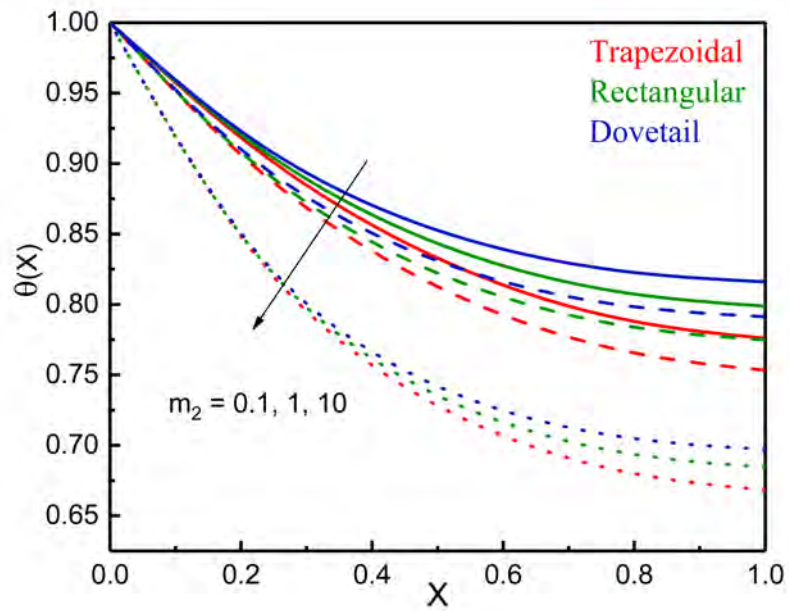
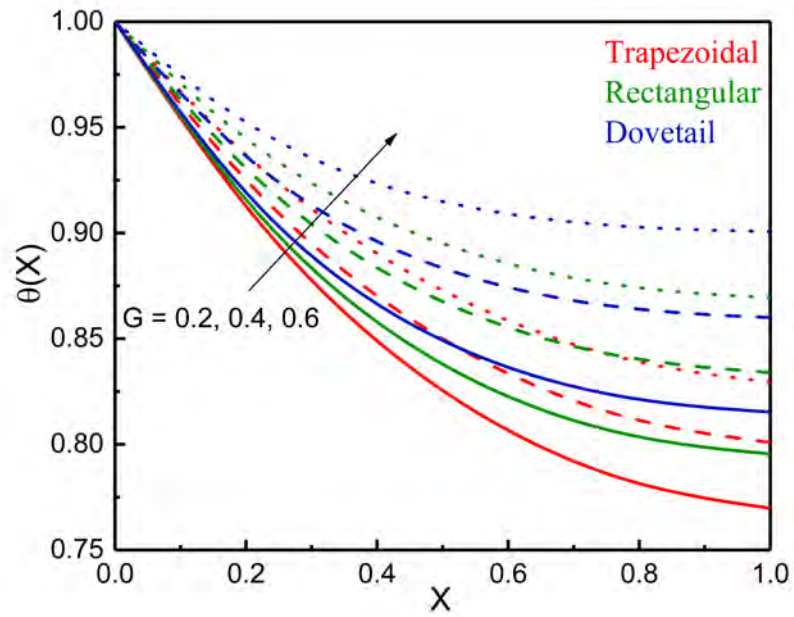Figure 1.9: Fin thermal profile as a function of wet porous parameter m_2.

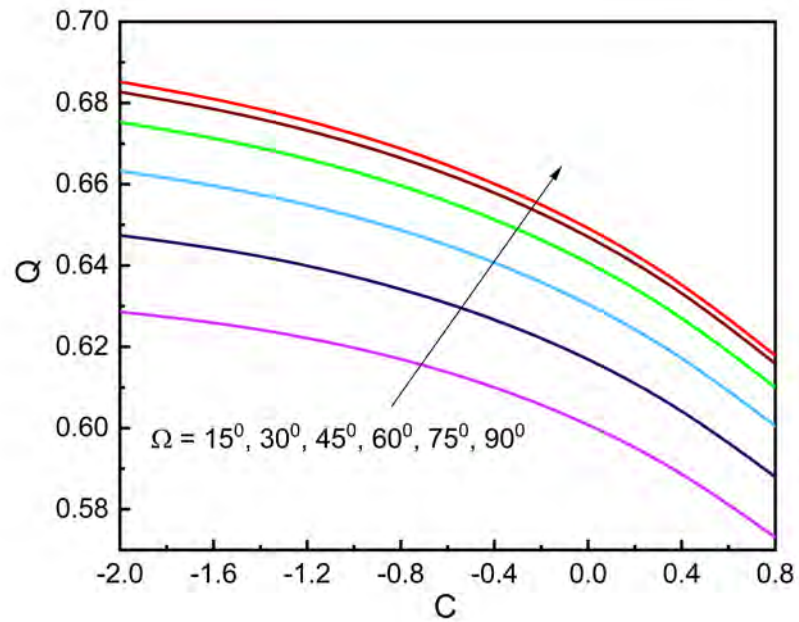Figure 1.10: Fin thermal profile as a function of generation parameter G.

Figure 1.11: Base heat transfer rate of the fin as a function of angle of inclination Ω and fin taper ratio C.
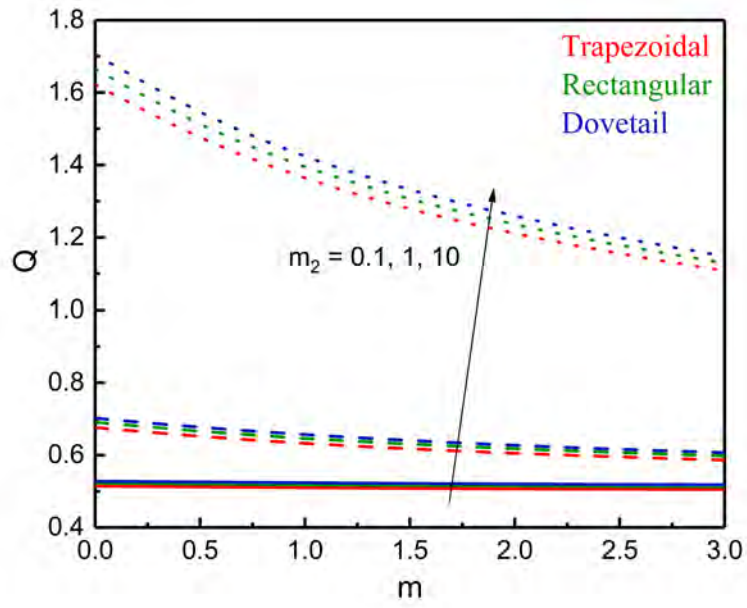
Figure 1.12: Base heat transfer rate of the fin as a function of wet porous parameter m_2 and power index m.
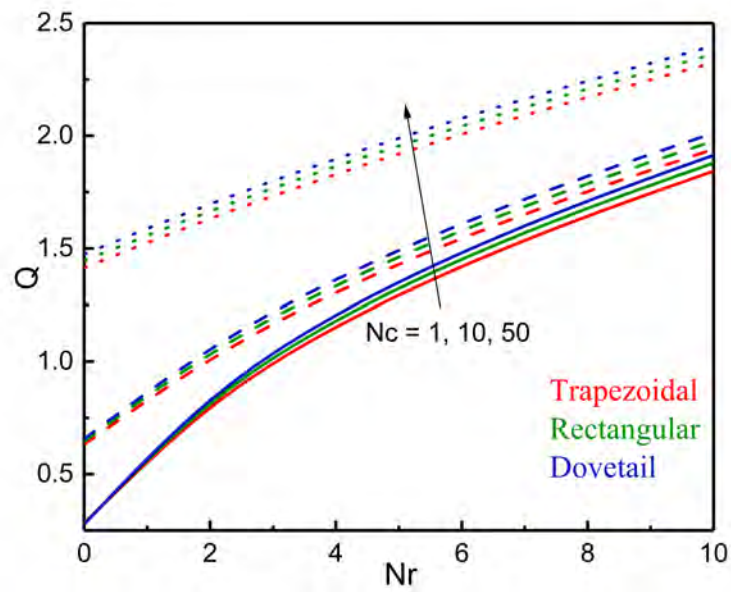

Figure 1.13: Base heat transfer rate of the fin as a function of convective parameter Nc and radiative parameter Nr.
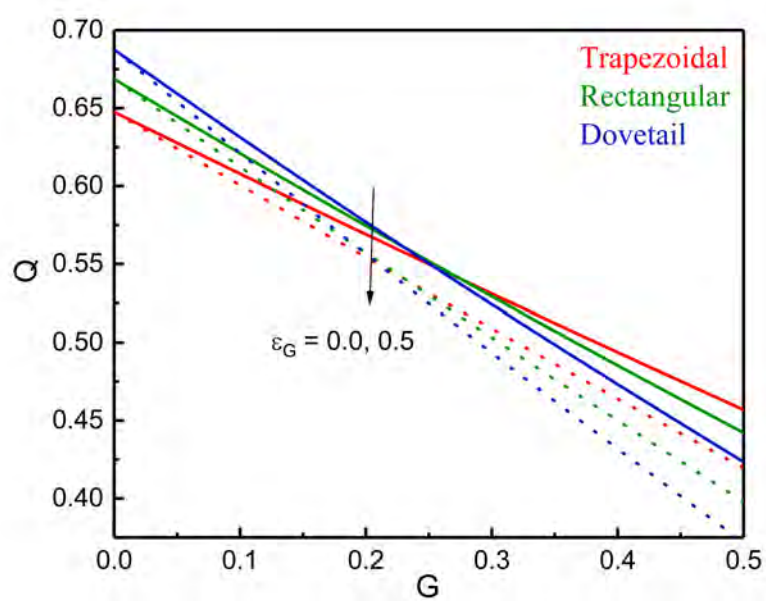
Figure 1.14: Base heat transfer rate of the fin as a function of ϵ_G and generation parameter G.

Chapter 2

Effect of Periodic Heat Transfer on the Transient Thermal Behaviour of Trapezoidal and Exponential Fin Structures

2.1 Prelims

In the current chapter, trapezoidal and exponential profiled convective-radiative porous longitudinal fin structures wetted in a single-phase fluid have been considered. The periodic variation in the fin base temperature has been taken into account along with the temperature sensitive thermal conductivity, internal heat generation and convective heat transfer coefficients. The modelled problem which is resolved into a nonlinear partial differential equation (PDE) is made dimensionless and solved by employing the centered implicit finite difference method (FDM). The results have been visually displayed through graphs and discussed with their physical interpretations. The impact of amplitude, frequency of oscillation, fully wet nature, porosity and other relevant quantities on the distribution of temperature along the fin length and alos with dimensionless time has been investigated. It has been deciphered that the periodic heat transfer gives rise to wavy nature of fin thermal profile against time. The outcomes of the analysis benefit in the

design of fin structures for the applications such as solar collectors, space and airborne applications, refrigeration industries etc.

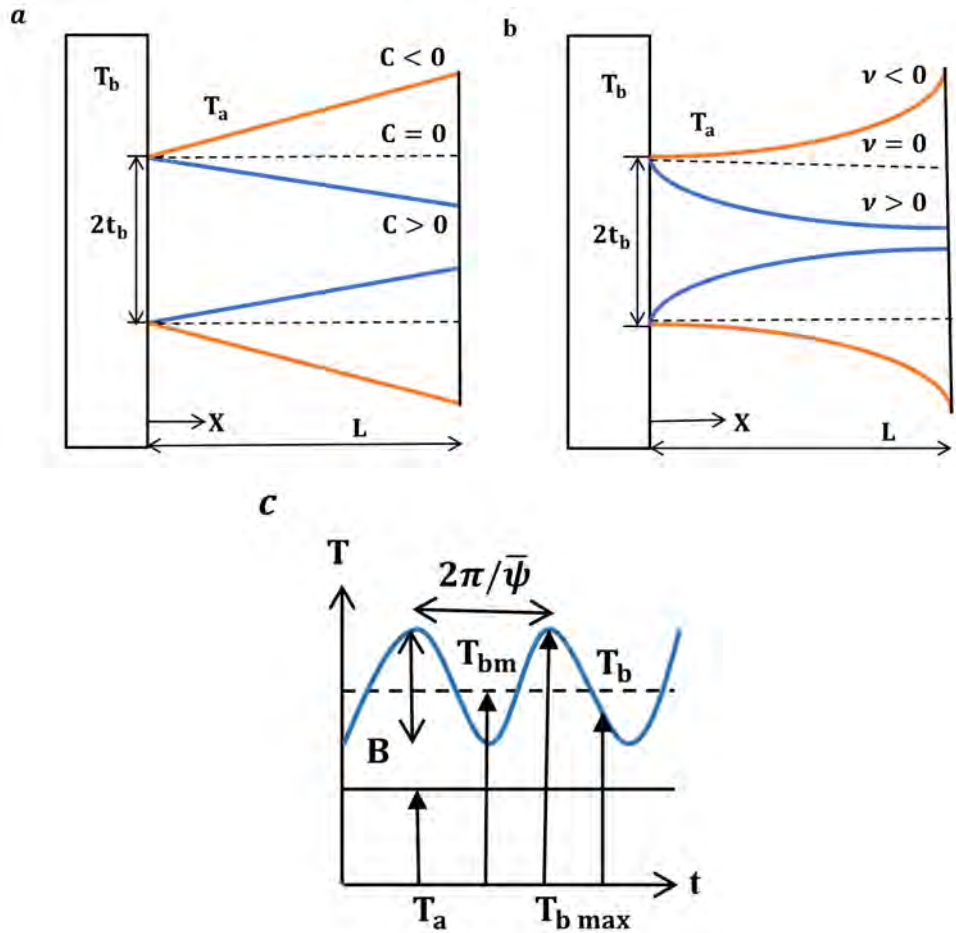## 2.2 Modeling and Interpretation

Figure 2.1: Schematic representation of trapezoidal fin (a), exponential fin (b) and periodic variation in the base temperature (c).

As depicted in figure 2.1, trapezoidal and exponential profiled longitudinal fin structures with length L and thickness t_b have been considered for the analysis. The fin material is porous, homogeneous, isotropic and has thermal conductivity k sensitive to

local temperature. The fin is wetted in a single phase fluid at temperature T_a which penetrates through its pores and their interaction is governed by the Darcy's law. Further, the convective heat transfer coefficient and the heat generation are assumed to be sensitive to temperature variations. The fin structure is mounted on a prime surface having oscillating temperature T_b. Here, the amplitude of input temperature is given by B and the frequency of oscillation is given by $\bar{\psi}$. Because there is a minute temperature variation in the fin's non-axial direction, the fin temperature varies only along the axial axis. Keeping in mind the above circumstances, the energy balance equation of fin per unit width is given by,

$$\rho C_p t_b \frac{\partial T}{\partial t} = \frac{\partial}{\partial x}\left[t^*(x)k(T)\frac{\partial T}{\partial x}\right] - 2\sigma\varepsilon(T^4 - T_a^4) - \frac{2\rho g K \beta_f C_p}{\nu_f}(T - T_a)^2$$

$$+ q^*(T)t^*(x) - 2h(T)(1-\hat{\phi})(T - T_a) - 2h_D l_{fg}(1-\hat{\phi})(\bar{\omega} - \bar{\omega}_s). \qquad (2.2.1)$$

In the above equation the term on the LHS accounts for the unsteady state of the fin, the terms on the RHS respectively account for heat transmission due to conduction, radiation, buoyancy effect, heat generation, convection due to porosity and wet environment. The semi-fin thickness $t^*(x)$ for different profiles of longitudinal fin is given by

Case 1: Trapezoidal profile

$$t^*(x) = t_b - \delta\left(\frac{x}{L}\right). \qquad (2.2.2)$$

Here, δ can be positive, negative or equated to zero depending on the direction in which the fin tip thickness varies and thus determines the resultant profile.

Case 2: Exponential profile

$$t^*(x) = t_b e^{-\nu\frac{x}{L}}. \qquad (2.2.3)$$

Here, ν can be positive, negative or equated to zero depending on the direction in which the fin tip thickness varies and thus determines the resultant profile.

The temperature sensitive thermal conductivity $k(T)$ is given by,

$$k(T) = k_{eff}(1 + \alpha^*(T - T_a)). \qquad (2.2.4)$$

Here, k_{eff} is the effective thermal conductivity of the porous fin medium.

The temperature sensitive heat generation $q^*(T)$ and convective heat transfer coefficient $h(T)$ are respectively given by equations (1.2.8) and (1.2.9).

By utilizing the equations (1.2.8)-(1.2.9) along with the equations (2.2.2)-(2.2.4), the equation (2.2.1) reduces to,

Case 1: Trapezoidal profile

$$\rho C_p t_b \frac{\partial T}{\partial t} = \frac{\partial}{\partial x}\left[t_b\left(1 - \frac{\delta}{t_b}\left(\frac{x}{L}\right)\right)k_{eff}(1 + \alpha^*(T - T_a))\frac{\partial T}{\partial x}\right] - 2\sigma\varepsilon(T^4 - T_a^4)$$

$$- \frac{2h_a(1 - \hat{\phi})(T - T_a)^{m+1}}{(T_b - T_a)^m} - \frac{2h_a l_{fg}(\bar{\omega} - \bar{\omega}_s)(1 - \hat{\phi})(T - T_a)^m}{C_p Le^{\frac{2}{3}}(T_b - T_a)^m}$$

$$- \frac{2\rho g K \beta_f C_p}{\nu_f}(T - T_a)^2 + q_a^*(1 + \epsilon_g(T - T_a))t_b\left(1 - \frac{\delta}{t_b}\left(\frac{x}{L}\right)\right). \qquad (2.2.5)$$

Case 2: Exponential profile

$$\rho C_p t_b \frac{\partial T}{\partial t} = \frac{\partial}{\partial x}\left[t_b e^{-\nu\frac{x}{L}}k_{eff}(1 + \alpha^*(T - T_a))\frac{\partial T}{\partial x}\right] - 2\sigma\varepsilon(T^4 - T_a^4)$$

$$- \frac{2h_a(1 - \hat{\phi})(T - T_a)^{m+1}}{(T_b - T_a)^m} - \frac{2h_a l_{fg}(1 - \hat{\phi})(\bar{\omega} - \bar{\omega}_s)(T - T_a)^m}{C_p Le^{\frac{2}{3}}(T_b - T_a)^m}$$

$$- \frac{2\rho g K \beta_f C_p}{\nu_f}(T - T_a)^2 + q_a^*(1 + \epsilon_g(T - T_a))t_b e^{-\nu\frac{x}{L}}. \qquad (2.2.6)$$

The following are the required physical quantities of interest for the current analysis,

$$\theta = \frac{T - T_a}{T_{bm} - T_a}, C_T = \frac{T_a}{T_{bm} - T_a}, X = \frac{x}{L}, A = \alpha^*(T_{bm} - T_a), C = \frac{\delta}{t_b}, \tau = \frac{k_{eff}}{\rho C_p L^2}t,$$

$$G = \frac{q_a^* L^2}{k_{eff}t_b}, \bar{\omega} - \bar{\omega}_s = b_2(T - T_a), m_0 = \frac{2h_a(1 - \hat{\phi})L^2}{k_{eff}t_b}, m_1 = \frac{2h_a(1 - \hat{\phi})L^2 l_{fg}b_2}{k_{eff}t_b Le^{\frac{2}{3}}C_p},$$

$$m_2 = m_0 + m_1, Nr = \frac{2\sigma\varepsilon(T_{bm} - T_a)^3 L^2}{k_{eff}t_b}, Nc = \frac{2gK\rho C_p\beta_f(T_{bm} - T_a)L^2}{\nu_f k_{eff}t_b},$$

$$\psi = \frac{\bar{\psi}\rho C_p L^2}{k_{eff}}, \epsilon_G = \epsilon_g(T_{bm} - T_a). \tag{2.2.7}$$

The temperature at the fin base is set to oscillate with amplitude B and frequency of oscillation $\bar{\psi}$. Thus, the required initial and boundary conditions are given by [?],

$$T(x, 0) = T_a,$$

$$T(0, t) = T_b = T_{bm} + (T_{bm} - T_a)Bcos(\bar{\psi}t),$$

$$\frac{\partial}{\partial x}T(L, t) = 0. \tag{2.2.8}$$

On non-dimensionalizing equations (2.2.5) and (2.2.6) by employing the parameters in equation (2.2.7), we get,

Case 1: Trapezoidal profile

$$\frac{\partial\theta}{\partial\tau} = (1 - CX)(1 + A\theta)\frac{\partial^2\theta}{\partial X^2} + A(1 - CX)\left(\frac{\partial\theta}{\partial X}\right)^2 - C(1 + A\theta)\frac{\partial\theta}{\partial X} - m_2\theta^{m+1}$$

$$- Nr\left((\theta + C_T)^4 - C_T^4\right) - Nc\theta^2 + G(1 + \epsilon_G\theta)(1 - CX) \tag{2.2.9}$$

Here, $0 < C < 1$ and $C = 0$ correspond to trapezoidal and rectangular profiles.

Case 2: Exponential profile

$$\frac{\partial\theta}{\partial\tau} = e^{-\nu X}(1 + A\theta)\frac{\partial^2\theta}{\partial X^2} + Ae^{-\nu X}\left(\frac{\partial\theta}{\partial X}\right)^2 - \nu e^{-\nu X}(1 + A\theta)\frac{\partial\theta}{\partial X} - m_2\theta^{m+1}$$

$$- Nr\left((\theta + C_T)^4 - C_T^4\right) - Nc\theta^2 + G(1 + \epsilon_G\theta)e^{-\nu X} \tag{2.2.10}$$

Here, $0 < \nu < 1$ and $\nu = 0$ correspond to exponential and rectangular profiles.

The above initial and boundary conditions get reduced to,

$$\theta(X,0) = 0,$$

$$\theta(0,\tau) = 1 + Bcos(\psi\tau),$$

$$\frac{\partial}{\partial X}\theta(1,\tau) = 0. \tag{2.2.11}$$

2.3 Numerical Elucidation

The second order nonlinear PDEs of parabolic nature named equation (2.2.9) and (2.2.10) and their corresponding initial and boundary conditions labelled as equation (2.2.11) are the concerned equations. Using the FDM with centered-implicit scheme the solution of the PDEs has been found via the Maple software. The time interval and the spatial domain are initially split into a finite number of steps with step sizes of $\Delta\tau$ and ΔX, respectively by partitioning the (X,τ) plane into smaller rectangles. By employing the forward difference for time and a 2nd order central difference for the space derivative, the derivatives in the differential equations are substituted by their approximate finite difference solutions. Through this, the nonlinear PDE is restructured into a system of linear equations. Now, the solution at the required discrete point can be computed by implementing the reliable techniques of matrix algebra. The software's algorithm handles the calculations rather easily and presents the result as a component from which quantitative data can be retrieved. The results of the present investigation for both the PDEs have been extracted by setting $\Delta X = 0.008$ and $\Delta\tau = 0.008$.

2.4   Deliberation of Results

The solutions obtained numerically have been displayed through graphs and discussed parametrically. Each physical quantity is varied keeping others constant and the constant values considered for the analysis unless otherwise mentioned are: $Nc = 1, Nr = 1, m_2 = 1, G = 0.1, \epsilon_G = 0.1, A = 0.2, C = 0.4, \nu = 1, C_T = 0.2, m = 2, B = 0.5, \psi = 1, \tau = 0.8$ and $X = 0.5$.

In the special cases of the current problem, the results obtained via FDM have been validated with the analytical solutions (Differential Transformation Method) of Ganji et al. [?] as depicted in table (2.1).

The effect of fin taper ratio C and fin shape parameter ν on the temperature characteristic of trapezoidal and exponential fin structures for variation in the dimensionless length X and dimensionless time τ has been pictured in figure 2.2 (a-c). The fin temperature at a particular axial location is found to decrease with increase in the values of C and ν. Here $C < 0, \nu < 0$ depict inverted fin profiles, $C = 0, \nu = 0$ depict fin of rectangular profile, $C > 0, \nu > 0$ depict tapered fin profiles. Thus, as fin geometry transits from inverted profile to tapered one, the fin temperature distribution decreases. It can be observed that with increase in time parameter, the fin temperature increases steeply in the beginning and then achieves a steady value for the non-periodic case. But in the case of periodic thermal conditions one can observe a steep rise followed by variation in temperature with a constant amplitude. This can be explained as follows. At time $\tau = 0$, the temperature of the entire fin is same as that of ambient temperature and no heat transfer occurs. But at time $\tau > 0$, there will be a step rise in base temperature resulting in heat flow through the fin structure. Further, the heat flow proportion varies with the amount of heat that

enters through the fin base, thus causing a wavy natured thermal profile in the case of periodic heat transfer.

The distribution of temperature in trapezoidal and exponential fin structures for simultaneous variation in the dimensionless length coordinate X and time τ for both periodic and non-periodic thermal conditions has been depicted in figure 2.3 (a-b). It is known that temperature of the fin is highest at the base and gradually decreases towards the fin tip. This statement is validated by this figure as temperature decreases from $X = 0$ (fin base) to $X = 1$ (fin tip). Further, wavy nature can be observed in the thermal characteristics of both the fin structures in the case of periodic thermal conditions.

Figure 2.4 (a-c) represents the trapezoidal and exponential fin thermal profiles for distinct values of the frequency of oscillation ψ for variation in the dimensionless length coordinate X (at $\tau = 0.8$) and time τ (at $X = 0.5$). Here $\psi = 0$ represents the case of non-periodic heat transfer and $\psi \neq 0$ represents periodic heat transfer. It can be observed that the rise in ψ values lower the fin thermal profile and induce more wave characteristics to the temperature curve. This is because the rise in ψ values reduce the amplitude of input temperature and thus lower the average value of base temperature resulting in lower thermal profiles. Further the behaviour of thermal characteristic along the fin length and with time is similar as explained before.

The impact of amplitude of input temperature B on the thermal field of trapezoidal and exponential fin structures along the fin length X (at $\tau = 0.8$) and with dimensionless time τ (at $X = 0.5$) has been illustrated in figure 2.5 (a-c). Here, $B = 0$ represents non-periodic thermal condition and $B \neq 0$ represents periodic boundary condition. When $B = 0$ the thermal profile of fin validates with the ones available in the literature. From the figures it can be observed that for $B \neq 0$ the fin temperature curve is wavy in nature,

and it attains higher values of amplitude for elevating values of parameter B. This is because the fin base temperature oscillates with the time parameter and achieves highest or lowest values for higher values of parameter B.

Figure 2.6 (a-c) respectively depict the variation in temperature of trapezoidal and exponential fin structures for distinct values of radiative parameter Nr with dimensionless length coordinate X and time coordinate τ. It can be inferred from the figures that as Nr value rises, there is a steep decrease in the fin temperature. This is because, the elevation in the value of Nr means rise in heat transmission via radiation leading to dip in the local fin temperature. On the other hand, from figures 2.6 (b-c) we can observe that the fin temperature at a particular point oscillates with the time parameter due to oscillating nature of the base temperature.

The impact of convective parameter Nc on the fluctuations in the local temperature of trapezoidal and exponential fin structures with length coordinate (dimensionless) X has been depicted in figure 2.7 (a) and for dimensionless time τ has been pictured in figure 2.7 (b-c). For higher values of parameter Nc, lower thermal profiles have been produced. This can be explained as follows. The elevation in Nc value represents increased permeability of the porous medium which results in better movement of the ambient fluid through the fin pores. This leads to increased heat transmission via convection thus resulting in lower values of fin temperature. Further the figure 2.7 (b-c) represents the oscillating behaviour of the temperature.

Figure 2.8 (a-c) depicts the fluctuations in the temperature values of the trapezoidal and exponential fin structures for varying values of thermal conductivity parameter A. Here figure 2.8 (a) and figure 2.8 (b-c) correspondingly represent the variations with respect to length (dimensionless) X and time (dimensionless) τ. It can be noted from the

figure that as values of A rise, there is elevation in the temperature values. This is due to increase in average thermal conductivity of the fin material resulting in increased heat transmission via conduction. Further as a result of oscillating base temperature, the fin temperature at a particular location is found to oscillate with time.

The influence of heat generation G on the thermal performance of trapezoidal and exponential fin structures under periodic as well as non-periodic conditions has been illustrated in figure 2.9 (a-c). Here figure 2.9 (a) and figure 2.9 (b-c) respectively correspond to variations in length (dimensionless) X and time (dimensionless) τ. An increase in the temperature values at a particular axial location can be observed from the figures. This is because of the increase in generation of internal heat which adds up to the fin temperature resulting in hike in the local temperature values. Further the influence of periodic thermal conditions on the temperature curve can be observed from the wavy nature of the fin thermal profile with the time parameter.

The repercussion of wet porous parameter m_2 on the thermal behaviour of trapezoidal and exponential fin structures has been recorded in figure 2.10 (a-c). Here, figure 2.10 (a) is for varying non-dimensional length X and figure 2.10 (b-c) is for varying non-dimensional time τ. It can be seen that, m_2 has a negative effect on the distribution of temperature. The effect of porosity and wet nature on the fin thermal performance can be estimated via the parameter m_2. Thus, as m_2 increases, porosity and/or wet nature increase resulting in better heat removal via convection. This results in decrease in the temperature towards the fin tip. On the other hand, in the case of periodic heat transfer wavy nature of fin thermal profile with time can be observed due to oscillating base temperature.

2.5   Denouement

The convective-radiative fully wet porous trapezoidal and exponential fin structures subject to periodic thermal conditions have been numerically investigated by employing the FDM. The following conclusions have been derived from the graphical analysis of both trapezoidal and exponential fin structures.

- As the fin geometry transits from inverted profile to tapered one, fin surface temperature is found to decrease.

- The fin temperature values at a particular axial location are found to steeply increase in the beginning and gradually attain a steady state in the case of non-periodic heat transfer.

- In the case of periodic heat transfer the fin temperature values at a particular axial location are found to oscillate with time.

- The rise in the values of frequency of oscillation induces more wave characteristics to the thermal profile simultaneously lowering the curve.

- The amplitude of input temperature has a significant impact on the height of the thermal wave.

- The convective, radiative and wet porous parameters are found to decrease the fin surface temperature.

- The thermal conductivity parameter and generation number are found to raise the fin tip temperature.

Table 2.1: Comparison of $\theta(X, \tau)$ values of the present work with the published literature when $Nr = 0.2, m_2 = 1, A = 0.2, \tau = 5, Nc = 0, G = 0, \epsilon_G = 0, C = 0, \nu = 0, C_T = 0, m = 0, B = 0, \psi = 0.$

X	Ganji et al (DTM) [?]	Present Results
0.0	0.99999999	1.00000000
0.2	0.87497225	0.87497225
0.4	0.78185489	0.78185489
0.6	0.71739957	0.71739958
0.8	0.67951379	0.67951380
1.0	0.66701337	0.66701339
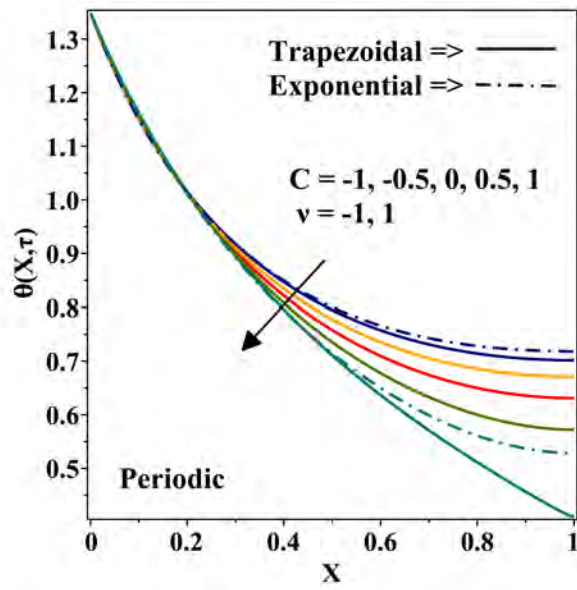
(a)
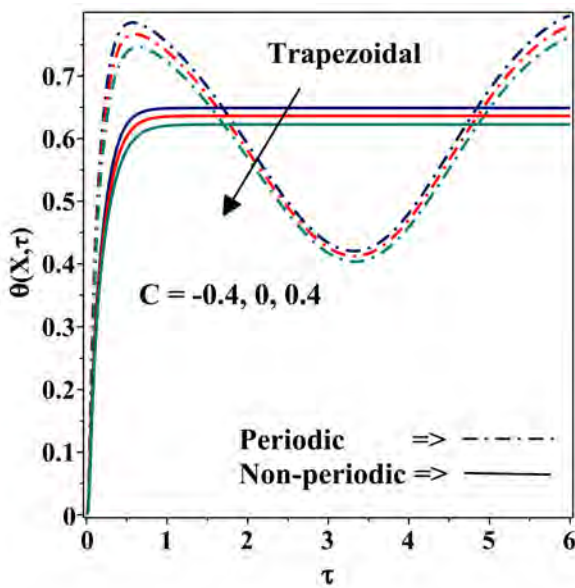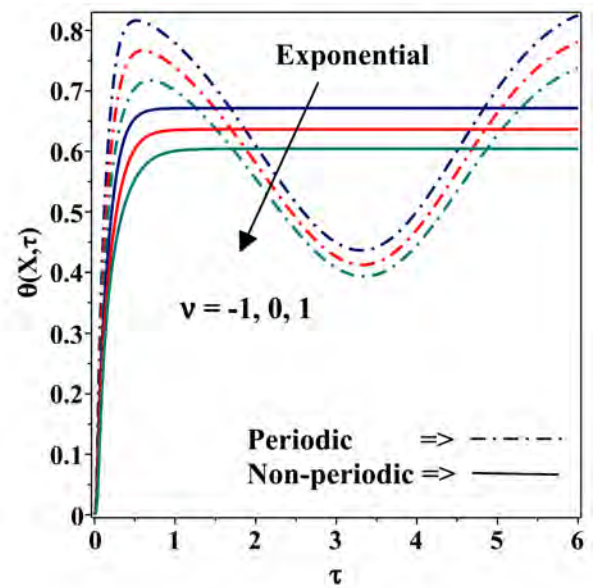
(b)   (c)

Figure 2.2: Plot of fin temperature values for distinct values of fin taper ratio C and shape parameter ν.

.
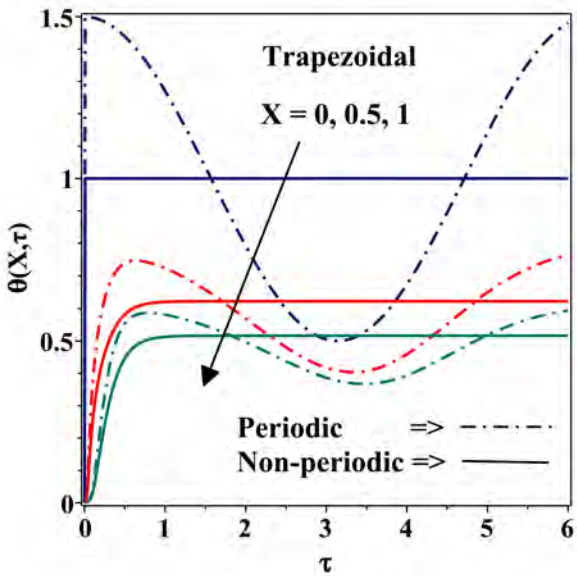
(a)
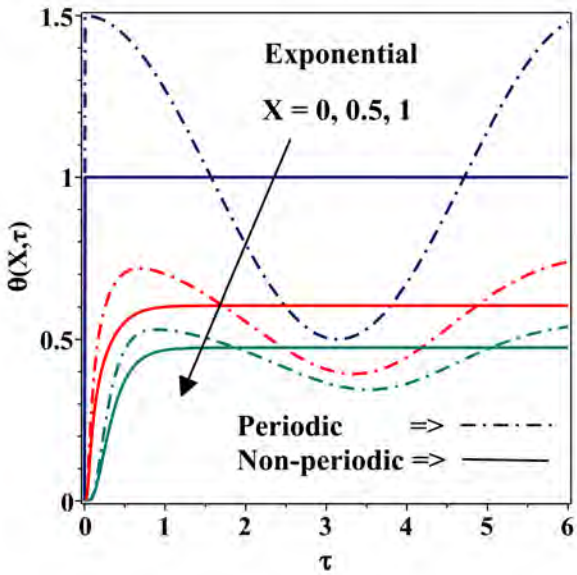
(b)

Figure 2.3: Plot of fin temperature values against dimensionless time τ for distinct values of dimensionless length X.
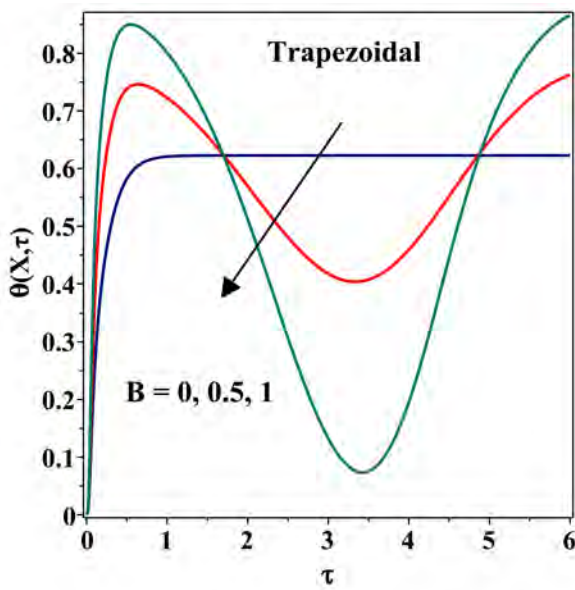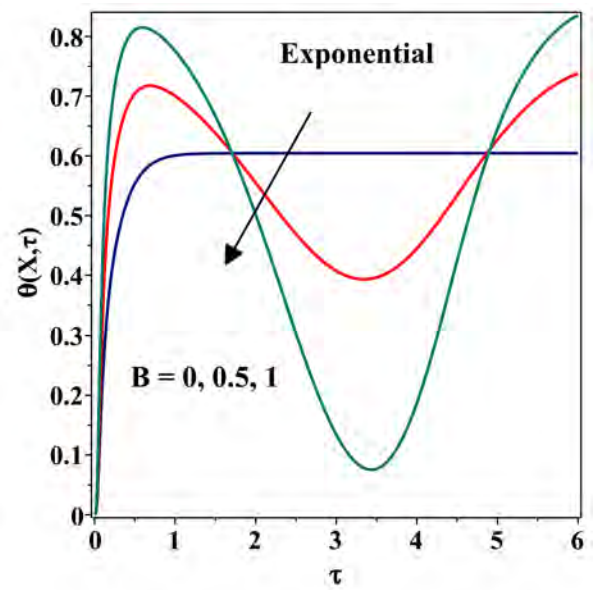
.
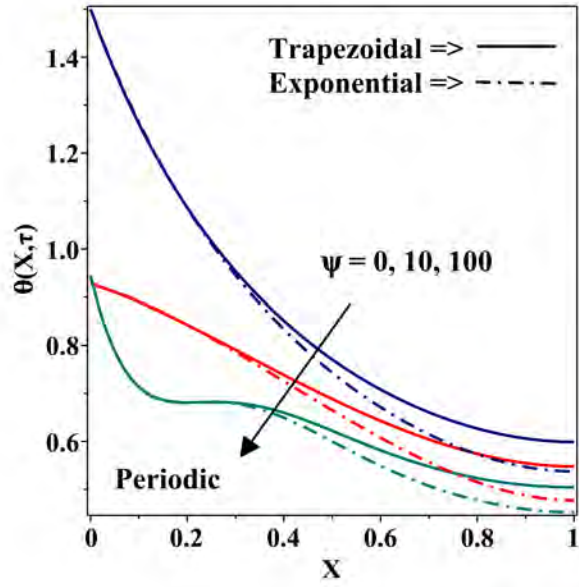
(a)
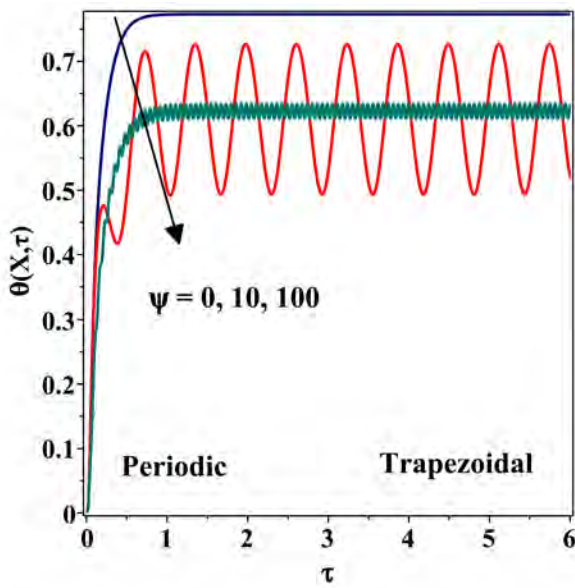
(b)
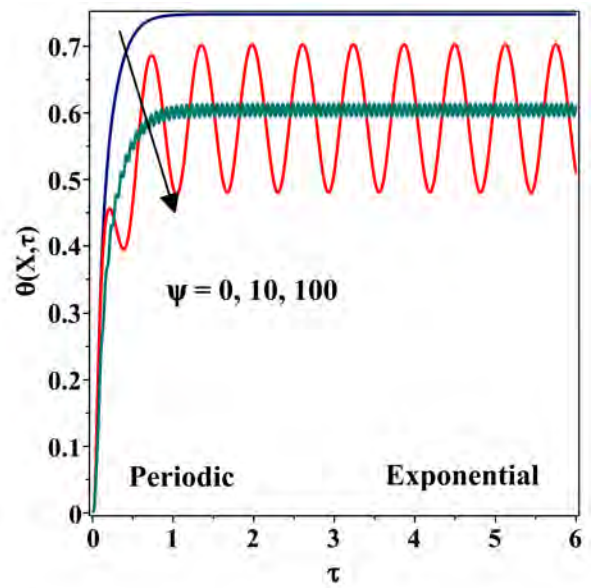
(c)

Figure 2.4: Plot of fin temperature values for distinct values of frequency of oscillation ψ.
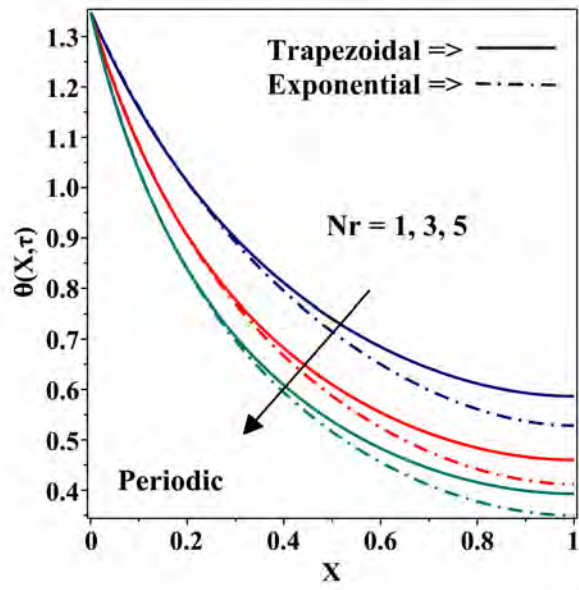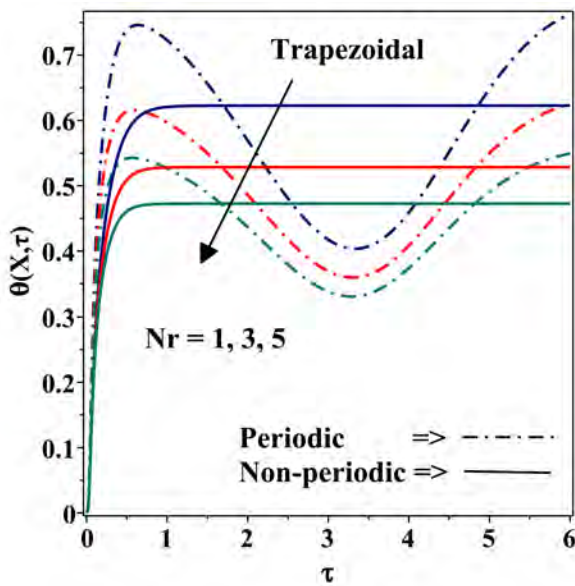
.
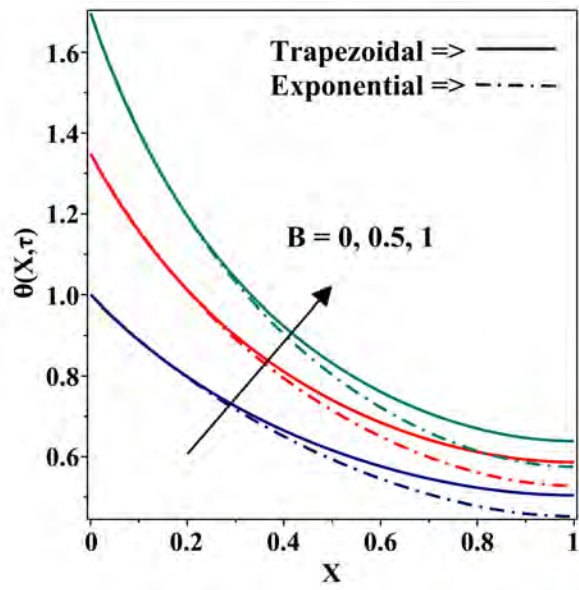
(a)

(b)

(c)

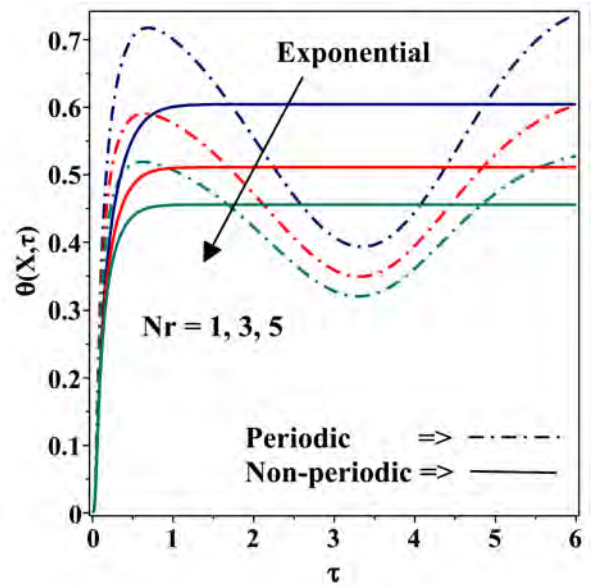Figure 2.5: Plot of fin temperature values for distinct values of amplitude of different temperature B.

.

(a)
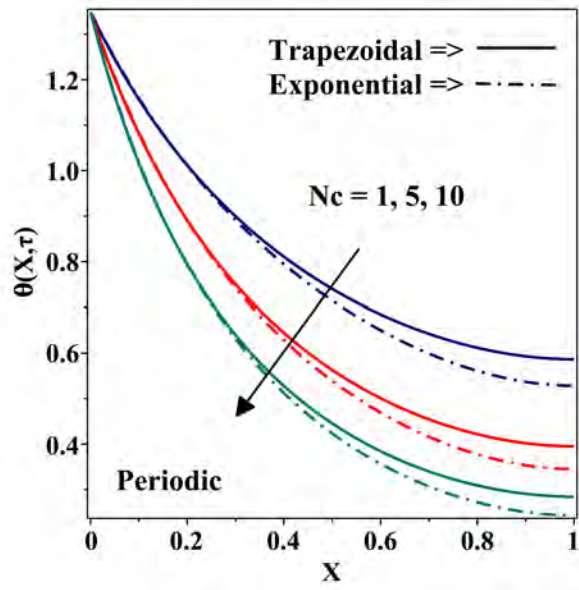

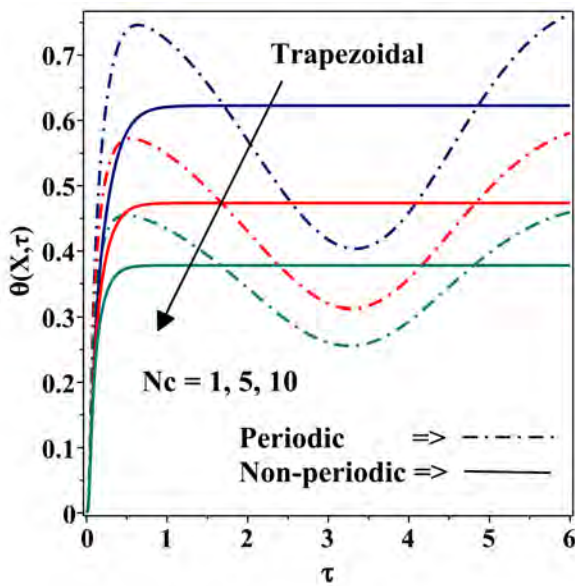(b)   (c)
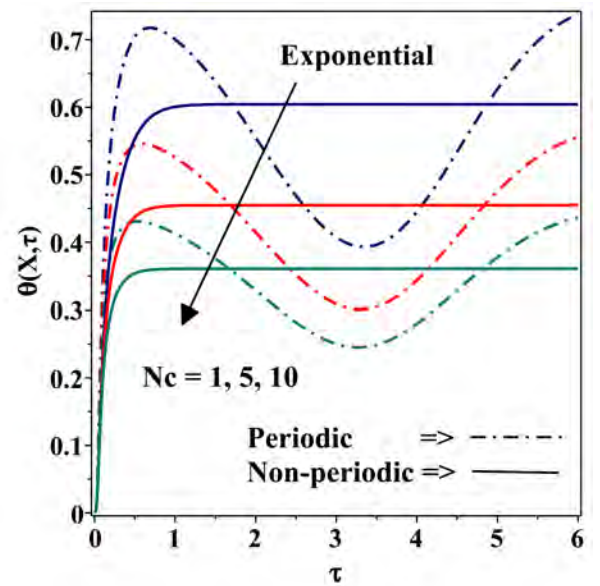
Figure 2.6: Plot of fin temperature values for distinct values of radiative parameter Nr.

.

(a)
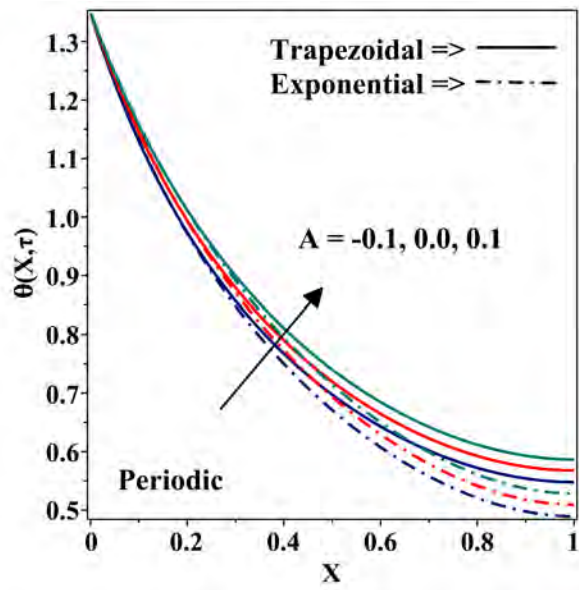

(b)   (c)
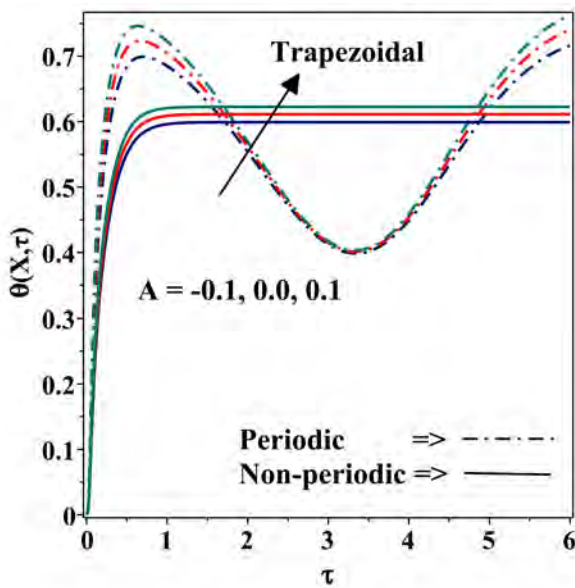
Figure 2.7: Plot of fin temperature values for distinct values of convective parameter Nc.

.

(a)

(b)   (c)

Figure 2.8: Plot of fin temperature values for distinct values of thermal conductivity parameter A.

.

(a)

(b)

(c)
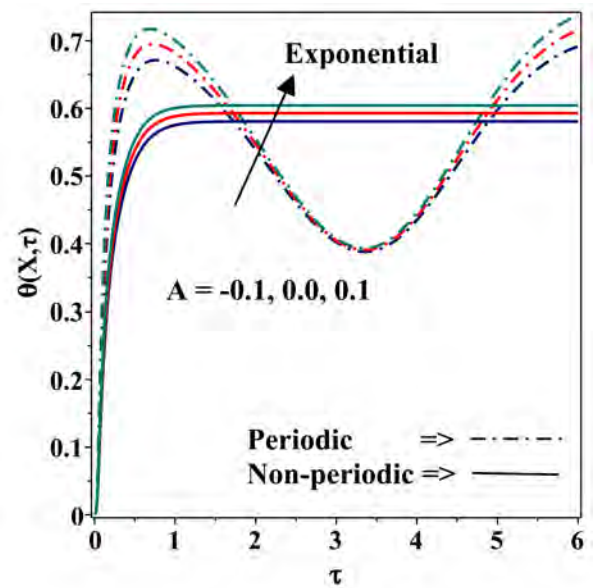
Figure 2.9: Plot of fin temperature values for distinct values of generation parameter G.

.

(a)
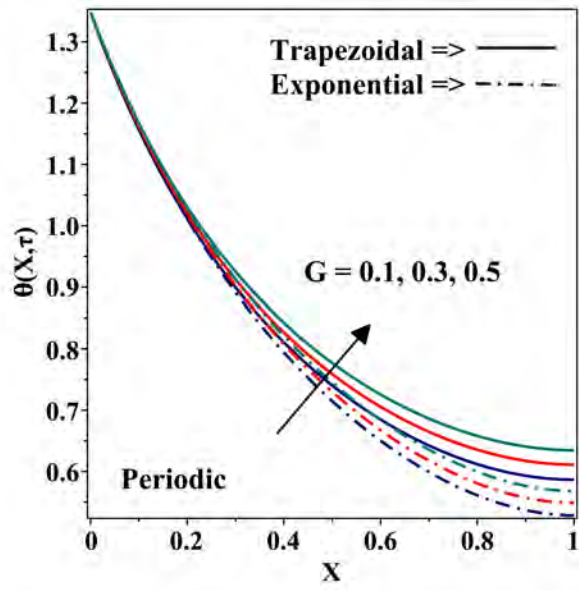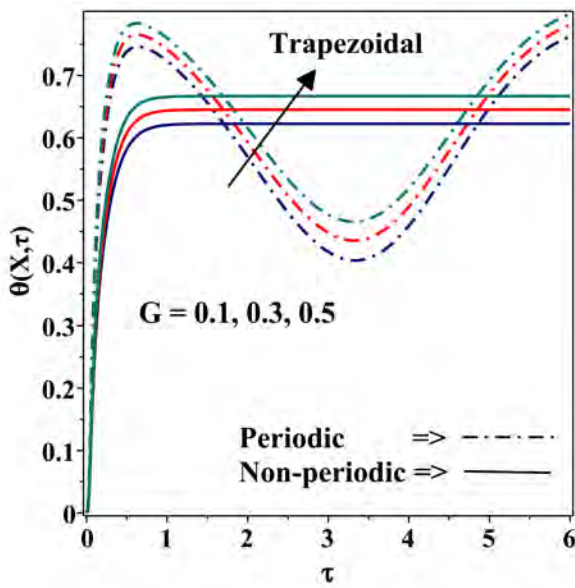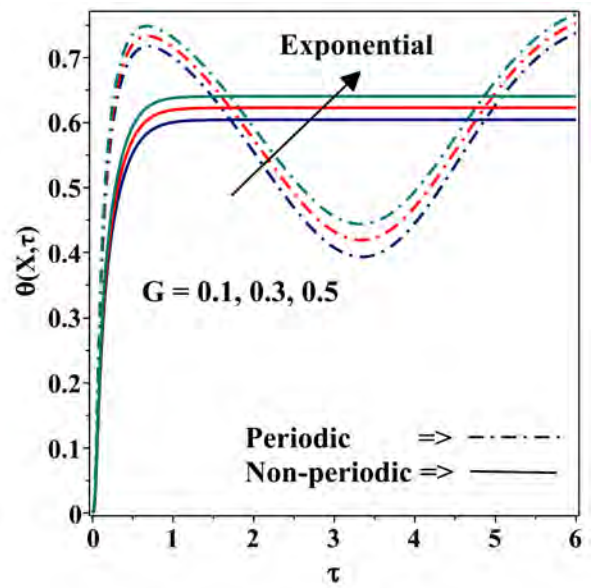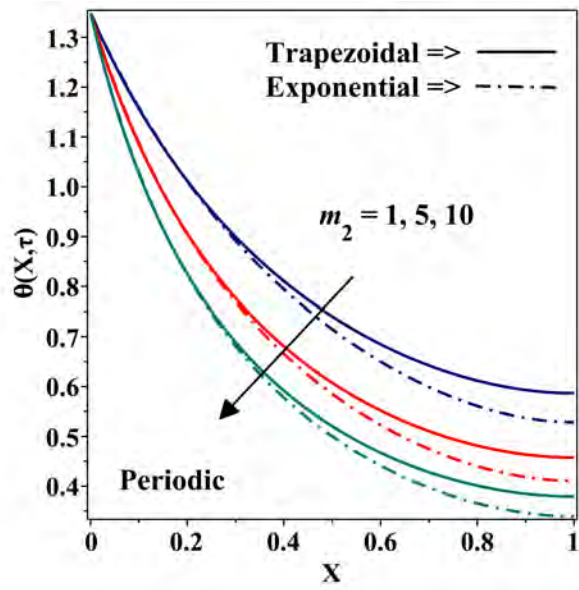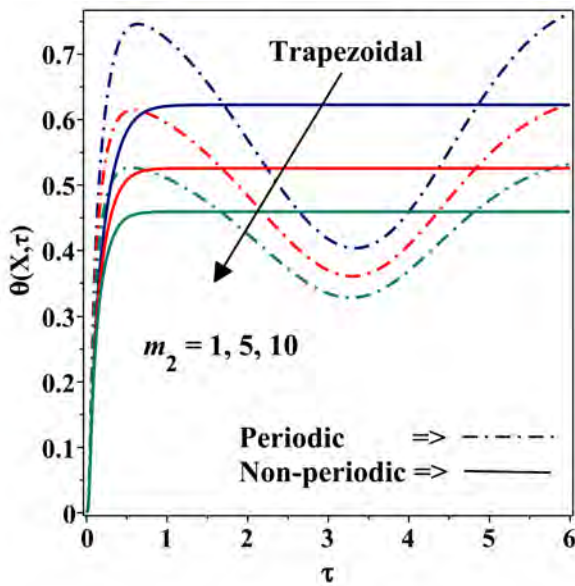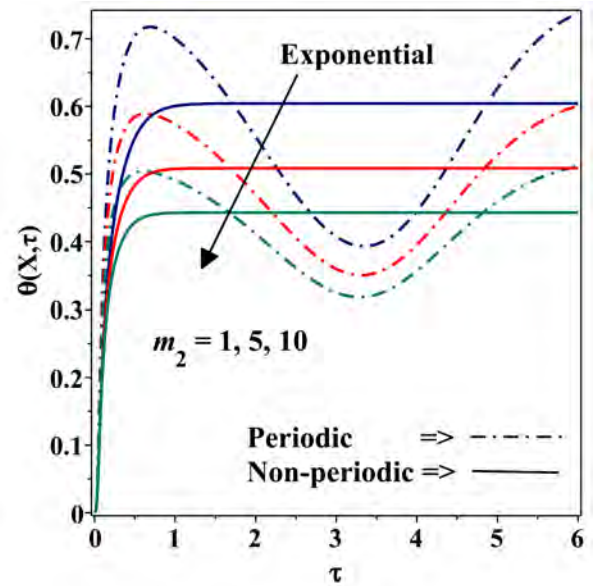

(b)   (c)

Figure 2.10: Plot of fin temperature values for distinct values of wet porous parameter m_2.

.

Chapter 3

Transient Thermal Analysis of Trapezoidal and Exponential Fin Structures subject to Non-Fourier Heat Conduction

3.1   Prelims

In the current chapter, trapezoidal and exponential profiled convective-radiative wet porous longitudinal fin structures subject to motion have been considered. Here, the fin structures are allowed to stretch or shrink by mounting a conveyer belt like mechanism on the fin surface. An analysis of the transient thermal behaviour of both fin structures exposed to Fourier and non-Fourier heat conduction has been performed. By using the centered implicit FDM, the modelled problem which is a nonlinear PDE has been numerically solved. The results have been graphically displayed using graphs and further reviewed with regard to their physical interpretations. On the variations in the fin temperature with its length and also with dimensionless time, the effects of Vernotte number, wet porous nature, stretching/shrinking parameter, Peclet number and other pertinent factors have been studied. The analysis' findings are useful for designing fin structures for solar collectors, airborne and space applications, refrigeration industries, etc.

3.2   Modelling and Interpretation
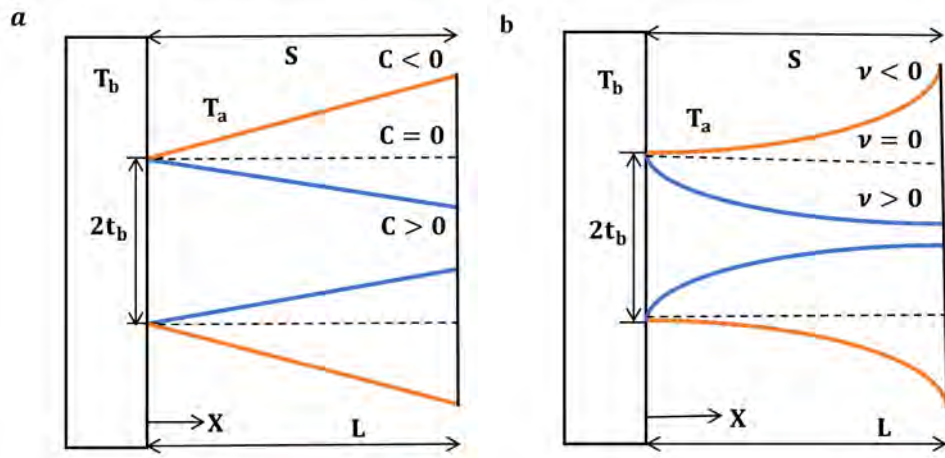
Figure 3.1: Schematic representation of stretching/shrinking (a) trapezoidal and (b) exponential profiled longitudinal fin structures.

The considered fin problem has a geometry as depicted in figure 3.1. Here, trapezoidal and exponential profiled longitudinal fin structures with length L and thickness t_b have been considered for the analysis. The fin material is porous, homogeneous and isotropic. The fin is wetted in a single phase fluid at temperature T_a which penetrates through its pores and their interaction is governed by the Darcy's law. Further, the convective heat transfer coefficient is assumed to be sensitive to local temperature variation. The fin is subject to motion with a uniform velocity $\bar{U}$ and its surface is mounted with a conveyer belt like mechanism which allows it to stretch/ shrink at a rate of $\bar{U}(1 + s^*(L - x))$ in the direction of motion. At time $t = 0$ the fin temperature is equivalent to the ambient temperature. But for $t > 0$ there is a sudden rise in the base temperature to T_b.

The thermal study of the current issue has been carried out by using the Cattaneo-Vernotte non-Fourier heat conduction model. Non-Fourier conduction, which results from the finite propagation speed of the heat front, is more difficult to evaluate than Fourier

conduction. In the Fourier case, the governing equation is parabolic, whereas in the non-Fourier case, it is hyperbolic. Thus, the energy balance equation per unit width for the current fin problem according to hyperbolic heat conduction is given by.

$$\rho C_p t_b \left(\frac{\partial T}{\partial t} + \tau_0 \frac{\partial^2 T}{\partial t^2} \right) = \frac{\partial}{\partial x} \left[k_{eff} t^*(x) \frac{\partial T}{\partial x} \right] - \rho C_p \bar{U} t^*(x) \left(1 + s^*(L - x) \right) \frac{\partial T}{\partial x}$$

$$- 2h(T)(1 - \hat{\phi})(T - T_a) - 2h_D l_{fg}(1 - \hat{\phi})(\bar{\omega} - \bar{\omega}_s) - 2\sigma\varepsilon(T^4 - T_a^4)$$

$$- \frac{2gK\rho C_p \beta_f}{\nu_f}(T - T_a)^2. \tag{3.2.1}$$

The required initial and boundary conditions for fin with adiabatic tip are [**?**],

$$T(x, 0) = T_a, \quad \frac{\partial}{\partial t} T(x, 0) = 0,$$

$$T(0, t) = T_b, \quad \frac{\partial}{\partial x} T(L, t) = 0. \tag{3.2.2}$$

The semi-fin thickness $t^*(x)$ for longitudinal fin of trapezoidal and exponential profiles is respectively given by equations (2.2.2) and (2.2.3). Further, the temperature sensitive convective heat transfer coefficient is given by equation (1.2.9).

Making use of equations (1.2.9), (2.2.2) and (2.2.3) the equation (3.2.1) takes the form,

Case 1: Trapezoidal profile

$$\rho C_p t_b \left(\frac{\partial T}{\partial t} + \tau_0 \frac{\partial^2 T}{\partial t^2} \right) = \frac{\partial}{\partial x} \left[k_{eff} t_b \left(1 - \frac{\delta}{t_b} \left(\frac{x}{L} \right) \right) \frac{\partial T}{\partial x} \right] - \frac{2gK\rho C_p \beta_f}{\nu_f}(T - T_a)^2$$

$$- \frac{2h_a(1 - \hat{\phi})(T - T_a)^{m+1}}{(T_b - T_a)^m} - \frac{2h_a l_{fg}(1 - \hat{\phi})(\bar{\omega} - \bar{\omega}_s)(T - T_a)^m}{C_p Le^{\frac{2}{3}}(T_b - T_a)^m}$$

$$- 2\sigma\varepsilon(T^4 - T_a^4) - \rho C_p \bar{U} t_b \left(1 - \frac{\delta}{t_b} \left(\frac{x}{L} \right) \right) \left(1 + s^*(L - x) \right) \frac{\partial T}{\partial x}. \tag{3.2.3}$$

Case 2: Exponential profile

$$\rho C_p t_b \left(\frac{\partial T}{\partial t} + \tau_0 \frac{\partial^2 T}{\partial t^2} \right) = \frac{\partial}{\partial x} \left[k_{eff} t_b e^{-\nu \frac{x}{L}} \frac{\partial T}{\partial x} \right] - \frac{2gK\rho C_p \beta_f}{\nu_f} (T - T_a)^2$$

$$- \frac{2h_a(1 - \hat{\phi})(T - T_a)^{m+1}}{(T_b - T_a)^m} - \frac{2h_a l_{fg}(1 - \hat{\phi})(\bar{\omega} - \bar{\omega}_s)(T - T_a)^m}{C_p Le^{\frac{2}{3}}(T_b - T_a)^m}$$

$$- 2\sigma\varepsilon(T^4 - T_a^4) - \rho C_p \bar{U} t_b e^{-\nu \frac{x}{L}} \left(1 + s^*(L - x)\right) \frac{\partial T}{\partial x}. \tag{3.2.4}$$

The dimensionless forms of equation (3.2.3) and equation (3.2.4) are nonlinear PDEs of second order given by,

Case 1: Trapezoidal profile

$$Ve^2 \frac{\partial^2 \theta}{\partial \tau^2} + \frac{\partial \theta}{\partial \tau} = (1 - CX)\frac{\partial^2 \theta}{\partial X^2} - C\frac{\partial \theta}{\partial X} - m_2\theta^{m+1} - Nr\left((\theta + C_T)^4 - C_T^4\right)$$

$$- Nc\theta^2 - Pe(1 - CX)\left(1 + S(1 - X)\right)\frac{\partial \theta}{\partial X}. \tag{3.2.5}$$

Case 2: Exponential profile

$$Ve^2 \frac{\partial^2 \theta}{\partial \tau^2} + \frac{\partial \theta}{\partial \tau} = e^{-\nu X}\frac{\partial^2 \theta}{\partial X^2} - \nu e^{-\nu X}\frac{\partial \theta}{\partial X} - m_2\theta^{m+1} - Nr\left((\theta + C_T)^4 - C_T^4\right)$$

$$- Nc\theta^2 - Pee^{-\nu X}\left(1 + S(1 - X)\right)\frac{\partial \theta}{\partial X}. \tag{3.2.6}$$

The respective dimensionless initial and boundary conditions are,

$$\theta(X, 0) = 0, \quad \frac{\partial}{\partial \tau}\theta(X, 0) = 0,$$

$$\theta(0, \tau) = 1, \quad \frac{\partial}{\partial X}\theta(1, \tau) = 0. \tag{3.2.7}$$

This is achieved by utilizing the following parameters,

$$\theta = \frac{T - T_a}{T_b - T_a}, C_T = \frac{T_a}{T_b - T_a}, X = \frac{x}{L}, \tau = \frac{k_{eff}}{\rho C_p L^2}t, Ve = \sqrt{\frac{\tau_0 k_{eff}}{\rho C_p L^2}}, Pe = \frac{\rho C_p \bar{U} L}{k_{eff}},$$

$$Nc = \frac{2g\rho\beta_f KC_p(T_b - T_a)L^2}{\nu_f k_{eff} t_b}, Nr = \frac{2\varepsilon\sigma L^2(T_b - T_a)^3}{k_{eff} t_b}, m_0 = \frac{2h_a(1 - \hat{\phi})L^2}{k_{eff} t_b}, C = \frac{\delta}{t_b},$$

$$m_1 = \frac{2h_a(1 - \hat{\phi})L^2 l_{fg} b_2}{k_{eff} t_b C_p Le^{\frac{2}{3}}}, m_2 = m_0 + m_1, S = s^*L, \bar{\omega} - \bar{\omega}_s = b_2(T - T_a). \qquad (3.2.8)$$

3.3 Numerical Elucidation

The second order nonlinear PDEs of hyperbolic nature named equation (3.2.5) and (3.2.6) and their corresponding initial and boundary conditions labelled as equation (3.2.7) are the concerned equations. Using the FDM with centered-implicit scheme the PDE's solutions have been found via the Maple software. The detailed procedure is explained in section (2.3). The results of the present investigation for both the PDEs have been extracted by setting $\Delta X = 0.008$ and $\Delta \tau = 0.008$.

3.4 Deliberation of Results

The solutions obtained numerically have been displayed through graphs and discussed parametrically. Each physical quantity is varied keeping others constant and the constant values considered for the analysis unless otherwise mentioned are: $Nc = 1, Nr = 1, m_2 = 1, C = 0.4, \nu = 1, C_T = 0.2, m = 2, Ve = 1, Pe = 1, S = 0, \tau = 0.8$ and $X = 0.5$.

The variation in the thermal characteristics of trapezoidal and exponential profiled longitudinal fin structures subject to Fourier and non-Fourier heat conduction for distinct values of dimensionless time τ (X=0.5) has been pictured in figure 3.2 (a-c). It can be observed from the figures that from the fin base to the fin tip, the temperature distribu-

tion steadily decreases in the case of Fourier heat conduction. However, non-Fourier heat conduction has a noticeable impact on the transient temperature response at the fin base i.e., the temperature distribution in the fin as a function of time exhibits an unusual variance even though constant base temperature is maintained. This is due to the hyperbolic governing equation which induces a thermal shock in the temperature. Each time, the temperature drops for a short period of time before rising quickly and at last a spot on the fin experiences an instantaneous temperature drop (thermal shock) in comparison to the surrounding value, and this low temperature is maintained throughout the remainder of the fin. Due to its finite velocity, the thermal wave is near the base of the fin and moves farther with time. Gradually the fluctuations in the temperature variation stabilise and the resultant thermal profile exactly fits with the one from the Fourier case.

The distribution of temperature in trapezoidal and exponential fin structures for simultaneous variation in the dimensionless length coordinate X and time τ for non-Fourier heat conduction has been depicted in figure 3.3 (a-b). It can be observed that at each axial position there is a peak achieved followed by fluctuations which finally lead to a steady value. The time taken by the thermal wave to reach the respective axial position can also be noted from the figures. On the other hand, as expected there is a decrease in the temperature value from fin base to its tip.

Figure 3.4 (a-b) represents the trapezoidal and exponential fin thermal profiles for distinct values of the Vernotte number Ve. For $Ve = 0.001$ we receive a thermal curve similar to that from a Fourier case. It can be observed from the figures that with a rise in the value of Ve the thermal wave is more close to the base of the fin. This can be explained as follows. With elevation in the values of Ve there is an increase in the relaxation time τ_0 resulting in slow propagation of wave towards the fin tip. Thus, higher values of Ve

signify enhanced non-Fourier influence.

The effect of fin taper ratio C and fin shape parameter ν on the temperature characteristic of trapezoidal and exponential fin structures for both the cases of Fourier and non-Fourier heat conduction has been pictured in figure 3.5 (a-c). In the Fourier case, the fin temperature at a particular axial location is found to decrease with increase in the values of C and ν. Thus, as fin geometry transits from inverted profile to tapered one, the fin temperature distribution decreases. Further, in the case of non-Fourier heat conduction the thermal wave is observed to travel slowly as the fin profile changes from inverted to tapered one.

The impact of convective parameter Nc on the fluctuations in the local temperature of trapezoidal and exponential fin structures for both Fourier and non-Fourier cases has been depicted in figure 3.6 (a-c). For higher values of parameter Nc, lower thermal profiles have been produced in both the cases of heat conduction. This can be explained as follows. The elevation in Nc value represents increased permeability of the porous medium which results in better movement of the ambient fluid through the fin pores. This leads to increased heat transmission via convection thus resulting in lower values of fin temperature. Further it can be observed that Nc values don't have any influence on the speed of the thermal wave.

Figure 3.7 (a-c) respectively depict the variation in temperature of trapezoidal and exponential fin structures for distinct values of radiative parameter Nr for both cases of Fourier and non-Fourier heat conduction. It can be inferred from the figures that as Nr value rises, there is a steep decrease in the fin temperature. This is because, the elevation in the value of Nr means rise in heat transmission via radiation leading to decrease in the local fin temperature. On the other hand, from figures we can observe that Nr values

don't influence the relaxation time of the thermal wave.

The repercussion of wet porous parameter m_2 on the thermal behaviour of trapezoidal and exponential fin structures for both cases of Fourier and non-Fourier heat conduction has been recorded in figure 3.8 (a-c). It can be seen that, m_2 has a negative effect on the distribution of temperature. The effect of porosity and wet nature on the fin thermal performance can be estimated via the parameter m_2. Thus, as m_2 increases, porosity and/or wet nature increase resulting in better heat removal via convection. This results in decrease in the temperature towards the fin tip. On the other hand, similar to the convective and radiative parameters, wet porous parameter does not have any impact on the speed of the thermal wave.

Figure 3.9 (a-c) depicts the fluctuations in the temperature values of the trapezoidal and exponential fin structures for varying values of Peclet number Pe. Here figure 3.9 (a) and figure 3.9 (b-c) correspondingly represent the thermal variations for Fourier and non-Fourier cases. It can be noted from the figure that as values of Pe rise, there is elevation in the temperature values. This is because of decrease in the time available for interaction between ambient fluid and the fin surface leading to negative influence on heat transmission via convection. Further, it can be observed that rise in Pe hikes the amplitude of the thermal wave.

The influence of stretching/shrinking parameter S on the thermal performance of trapezoidal and exponential fin structures under Fourier as well as non-Fourier cases of heat conduction has been illustrated in figure 3.10 (a-c). It can be observed that stretching ($S = 1$) increases the local fin temperature whereas shrinking ($S = -1$) decreases the same. This can be explained as follows. The elevation in stretching parameter adds to fin motion thus increasing the fin temperature whereas the hike in shrinking parameter

49

negates the fin motion resulting in lesser fin temperature. On the otherhand, similar to Peclet number, the stretching/shrinking parameter is observed to vary the amplitude of the thermal wave.

3.5 Denouement

The convective-radiative fully wet porous trapezoidal and exponential fin structures subject to motion have been numerically investigated by employing the FDM. The fin structures have been examined under two cases namely: Fourier and non-Fourier heat conduction. The following are the conclusions derived from their graphical analysis.

- In the case of non-Fourier heat conduction a thermal shock is induced to the temperature resulting in a thermal wave travelling towards the fin tip with a finite velocity. Gradually the induced fluctuations in the temperature variation stabilise and the resultant thermal profile fits with the one from the Fourier case.

- The Vernotte number is found to increase the relaxation time resulting in slower movement of thermal wave. Further, the case of non-Fourier heat conduction reduces to Fourier one at lower values of Vernotte number.

- As the fin geometry transits from inverted profile to tapered one, fin surface temperature is found to decrease.

- The convective, radiative, shrinking and wet porous parameters are found to decrease the fin surface temperature.

- The stretching parameter and the Peclet number are found to enhance the distribution of temperature towards the fin tip.
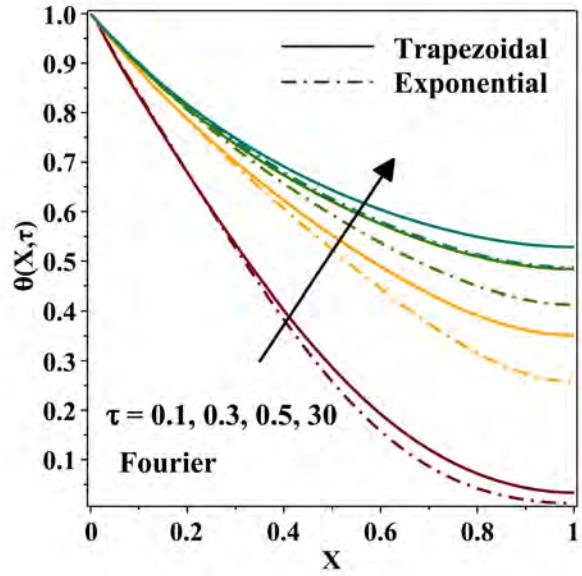
(a)
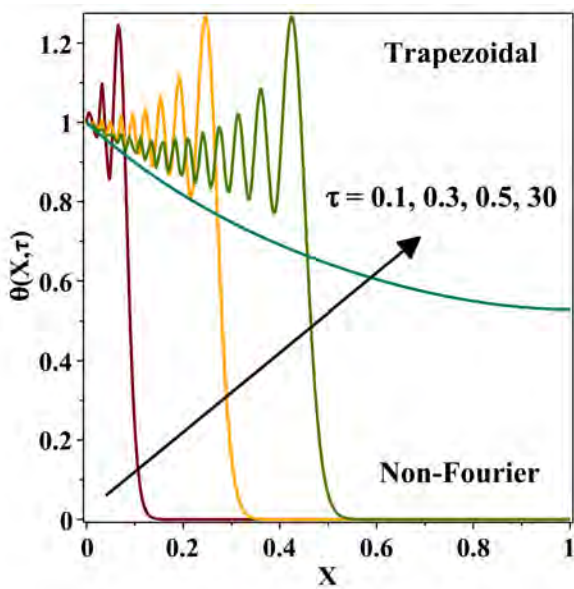
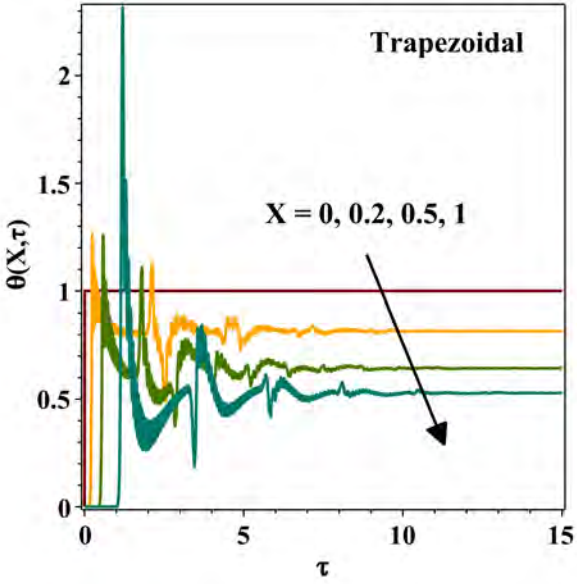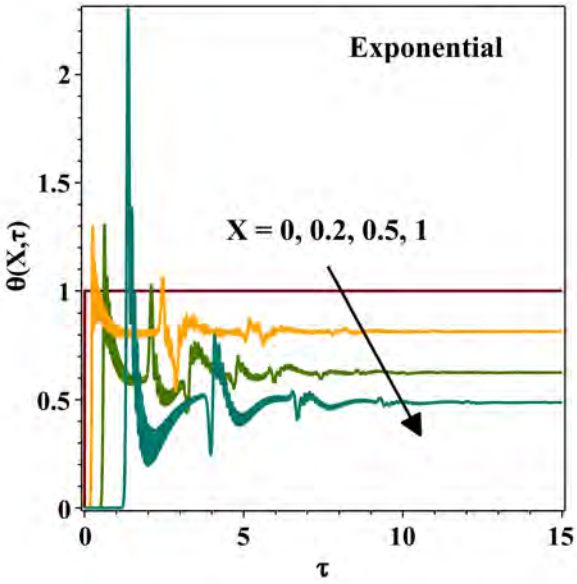**(b)**
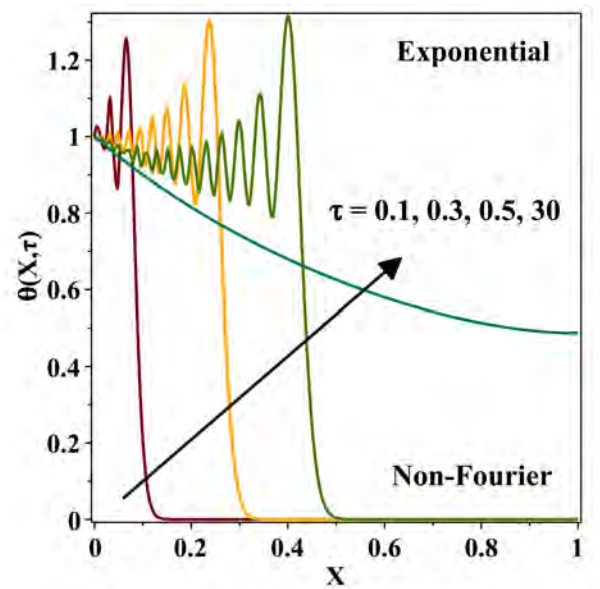
(c)

Figure 3.2: Plot of fin temperature values for distinct values of dimensionless time τ.

.

51

(a)

(b)

Figure 3.3: Plot of fin temperature values against dimensionless time τ for distinct values of dimensionless length X.

.
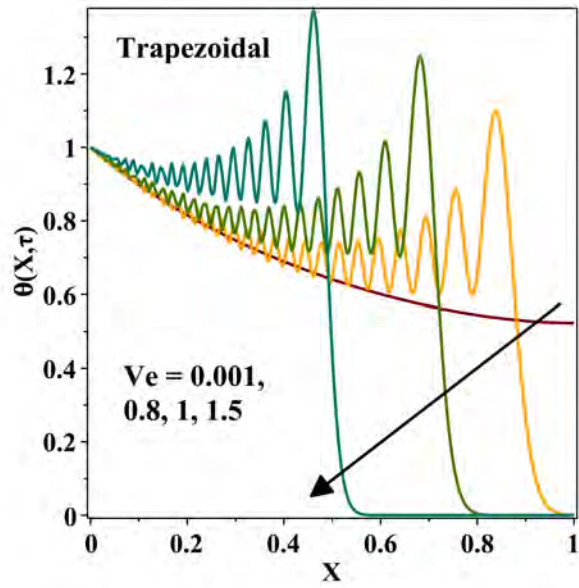
(a)
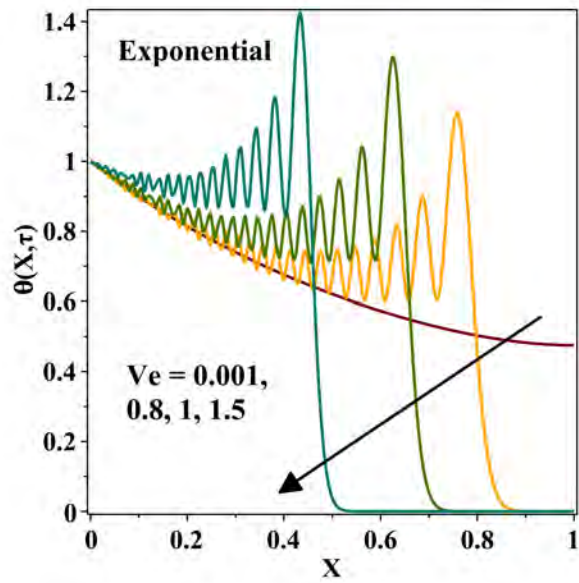
(b)

Figure 3.4: Plot of fin temperature values for distinct values of Vernotte number Ve.

.

(a)

(b)   **(c)**

Figure 3.5: Plot of fin temperature values for distinct values of fin taper ratio C and shape parameter ν.

.

(a)

(b)

(c)

Figure 3.6: Plot of fin temperature values for distinct values of convective parameter Nc.

.
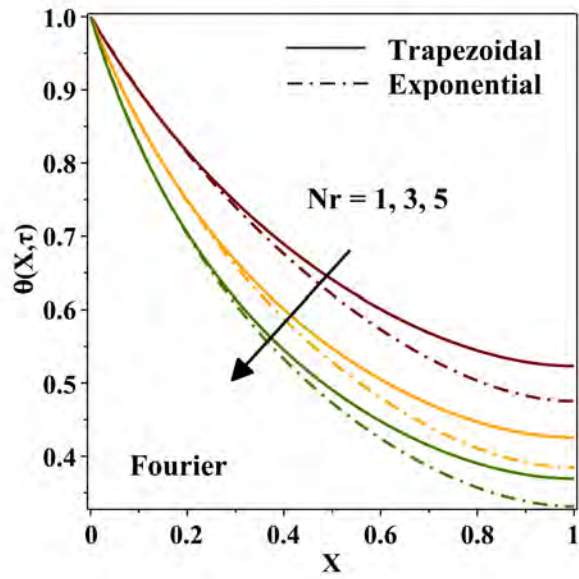
(a)
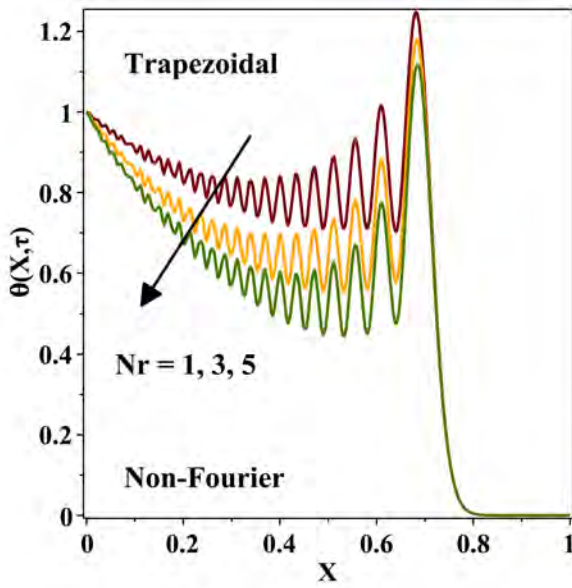
(b)
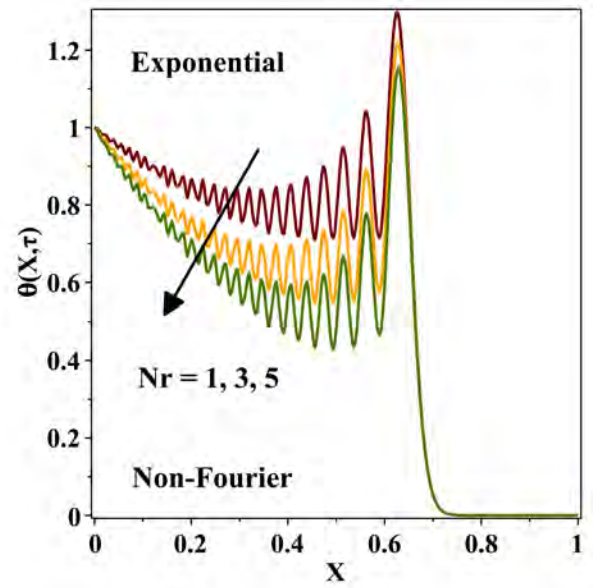
(c)

Figure 3.7: Plot of fin temperature values for distinct values of radiative parameter Nr.

.
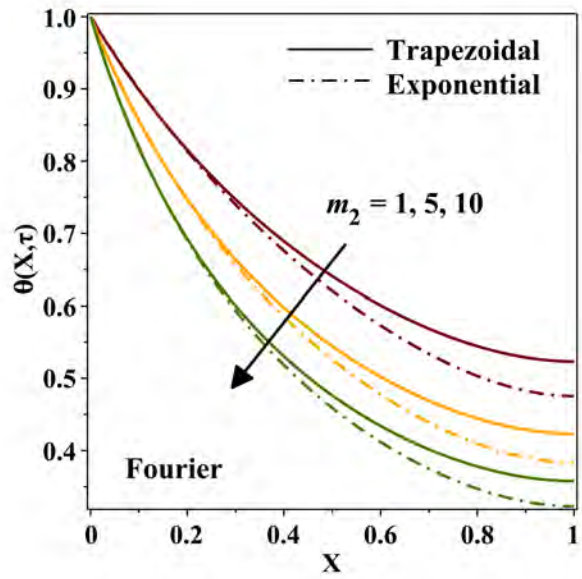
(a)
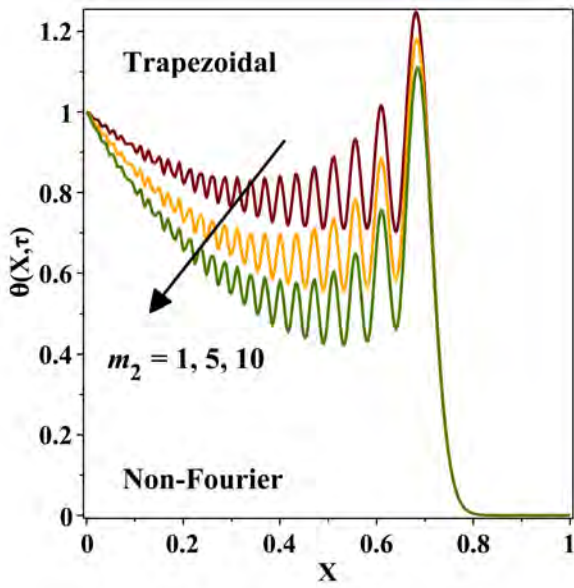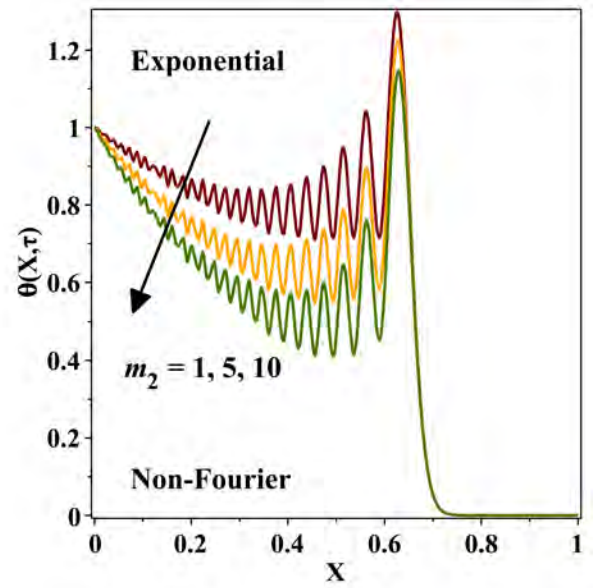
(b)   (c)

Figure 3.8: Plot of fin temperature values for distinct values of wet porous parameter m_2.
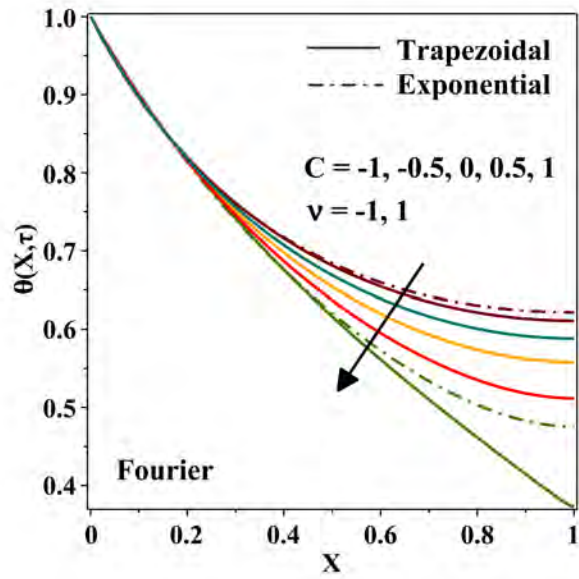
.
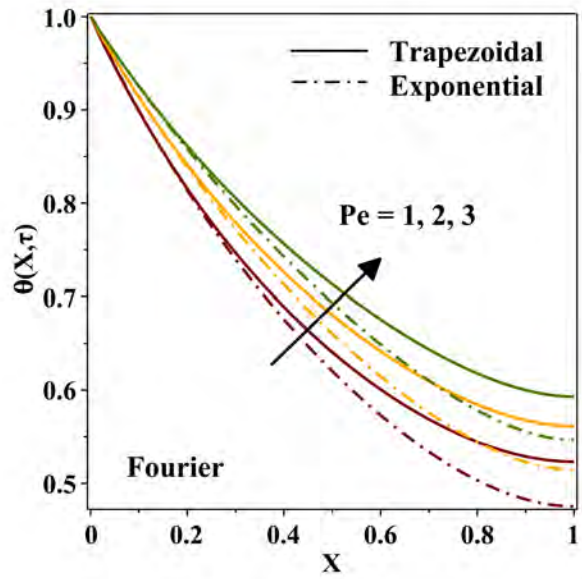
(a)
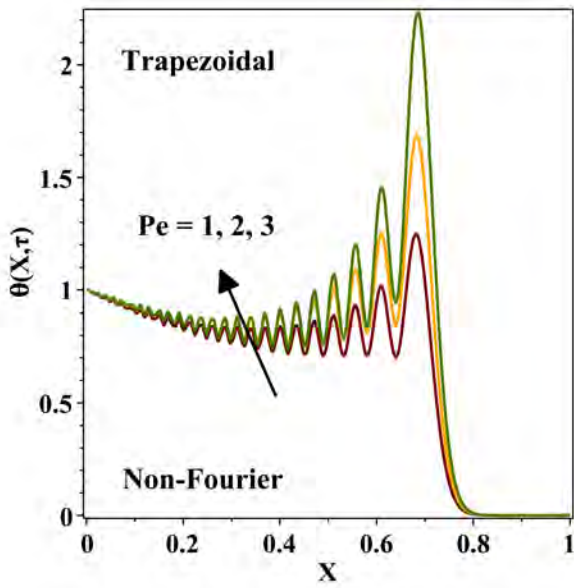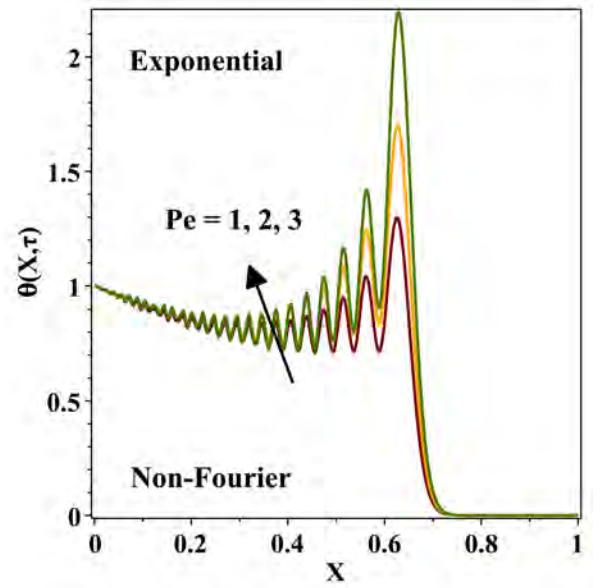
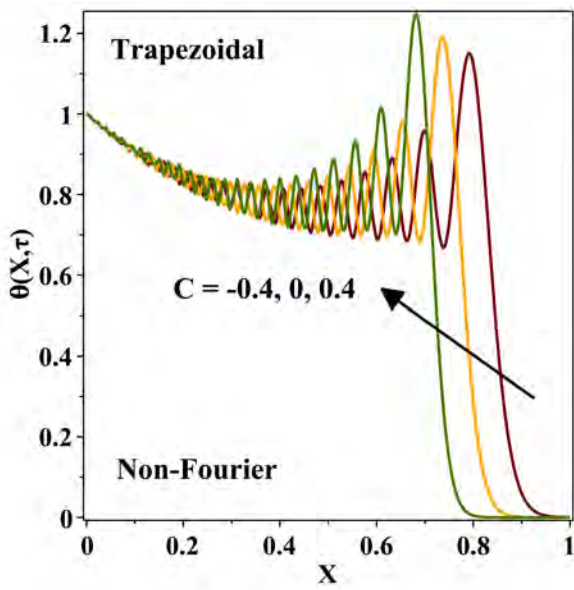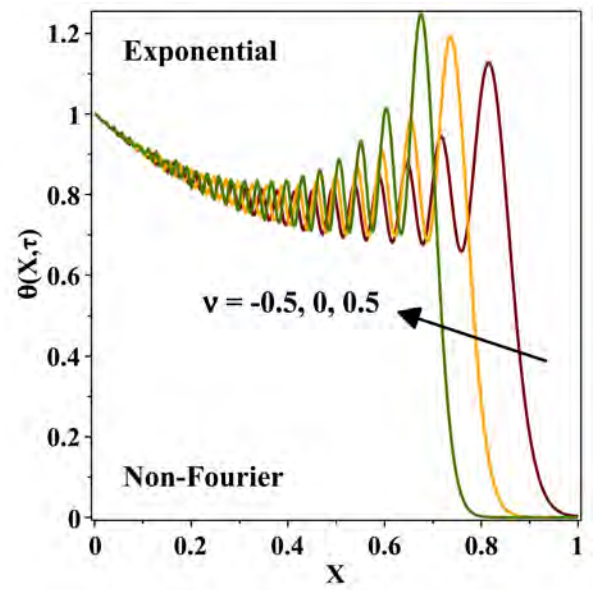(b)   (c)

Figure 3.9: Plot of fin temperature values for distinct values of Peclet number Pe.
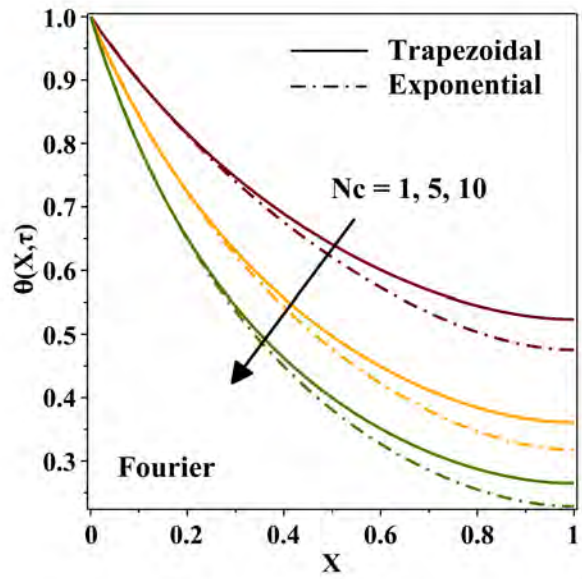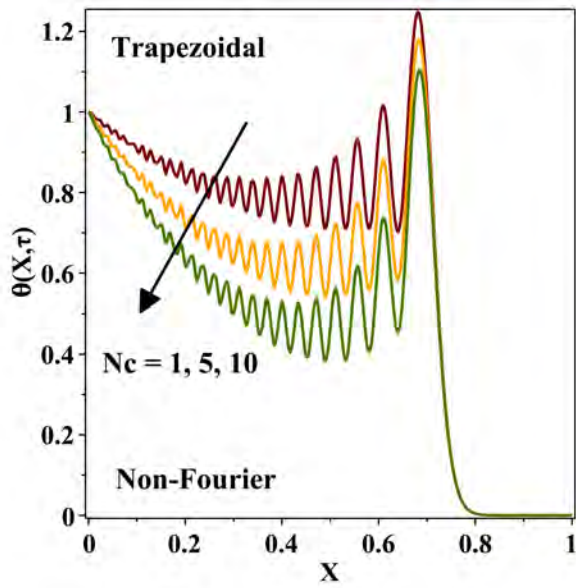
.
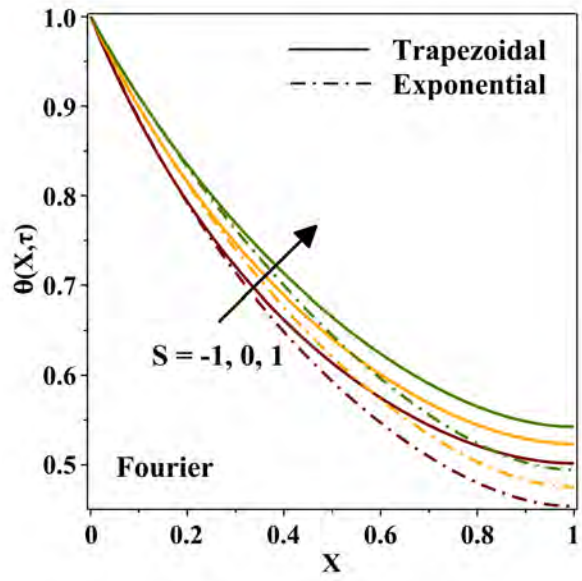
(a)
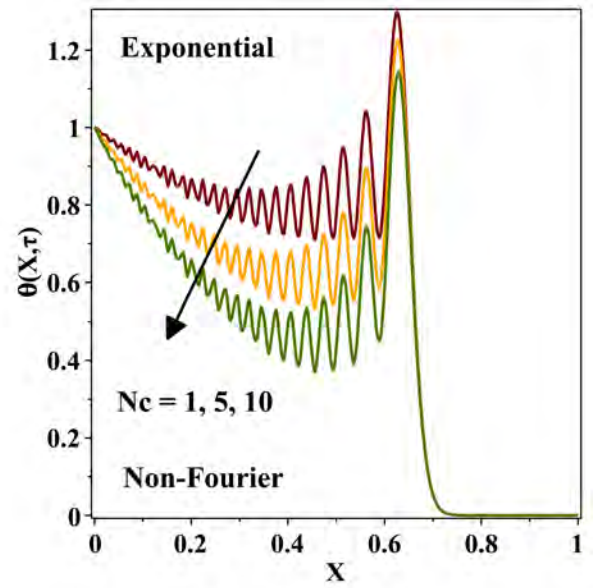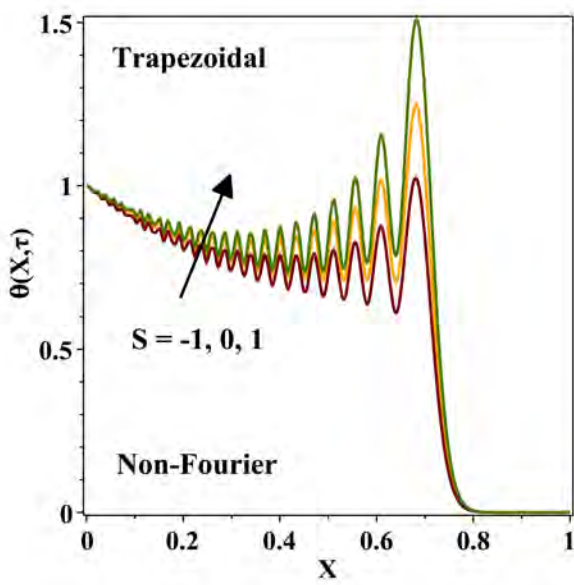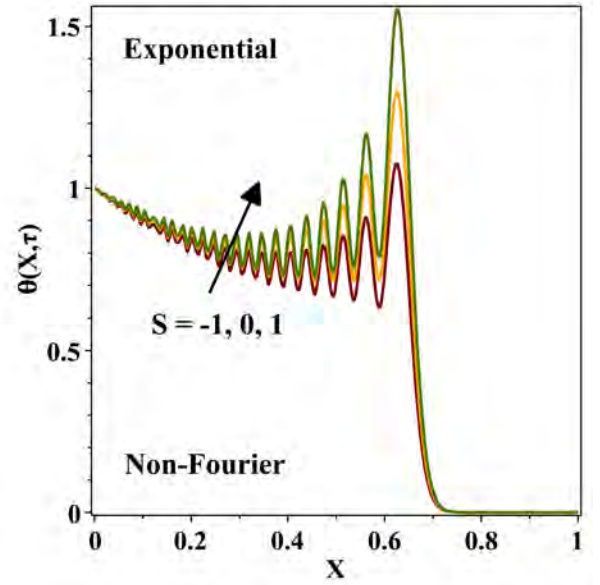

(b)   (c)

Figure 3.10: Plot of fin temperature values for distinct values of stretching/shrinking parameter S.

.

Chapter 4

Impact of Mass-Based Hybrid Nanofluid Flow on Transient Efficiency of Exponential Fin

4.1   Prelims

In the chapter, transient heat transfer characteristics of a convective-radiative longitudinal fin of exponential profile fully wetted in a hybrid nanofluid have been analysed. The fin medium is porous and Darcy law has been implemented to formulate the fluid-solid interactions. The hybrid nanofluid is obtained by immersing Silver and Graphene nanoparticles in the base fluid water and the study is based on a mass-based model. The scrutiny presented in dimensionless form is a nonlinear PDE which is solved by employing the FDM. The effect of nanoparticle shape factor, dimensionless time, wet porous parameter, and other relevant parameters on the thermal field and thermal efficiency of the fin structures has been graphically analysed and discussed. The examination has resulted in a novel outcome that the presence of hybrid nanofluid enhances the fin efficiency. The findings of the investigation play a prominent role in the heat transfer enhancement of industrial processes.

4.2 Modeling and Interpretation

4.2.1 Heat Transfer
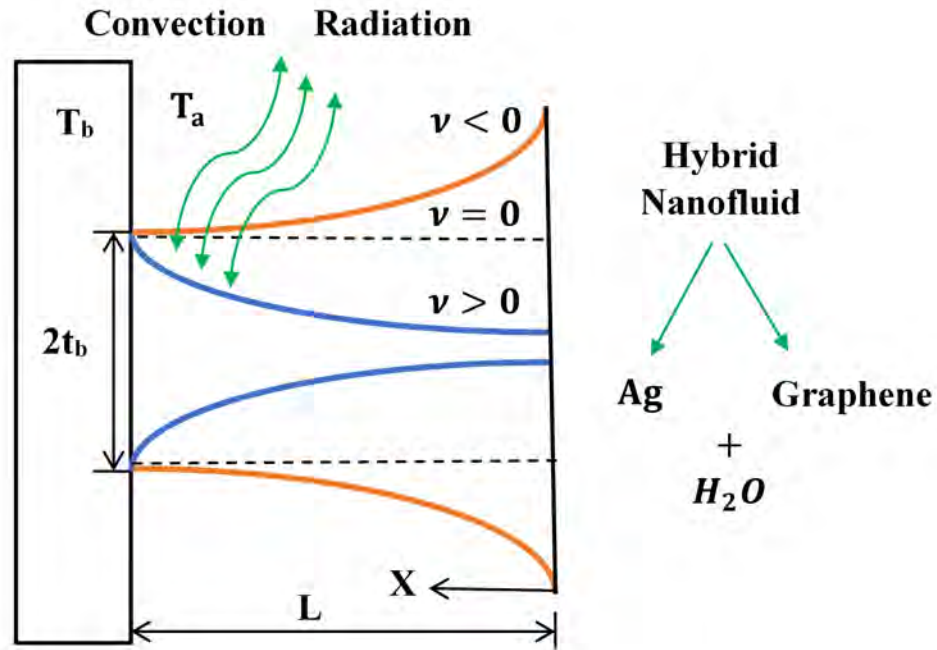
Figure 4.1: Physical depiction of exponential profiled longitudinal fin structure wetted in hybrid nanofluid.

Consider an exponential profiled longitudinal fin with dimensions as depicted in figure 4.1. The fin material is considered to be porous, isotropic and homogeneous in nature. The fin is fully wetted in a hybrid nanofluid and further allows the penetration of the ambient fluid through its pores. The Darcy model has been employed to govern the fluid-solid interactions in the fin model. The ambient hybrid nanofluid with temperature T_a is in contact with the entire fin surface. At time $t = 0$, the fin surface is maintained at the same temperature as the ambient fluid. But at $t > 0$, there is a step rise in temperature of the surface to which the fin base is attached. As heat enters the fin through its base, it flows through the entire fin length. As the difference in temperature between the ambient fluid

and the fin surface rises, the heat in the fin structure is exchanged with the ambient fluid through convective-radiative transmissions. Since the fin thickness is negligible compared to its length the temperature is assumed to vary only along the axial direction of the fin. The energy balance equation for a one-dimensional fin structure under unsteady conditions subject to the above assumptions is given by [**?**],

$$\frac{(\rho C_p)_{hnf} t_b}{k_{hnf}} \frac{\partial T}{\partial t} = \frac{\partial}{\partial x}\left[t^*(x)\frac{\partial T}{\partial x}\right] - \frac{2gK(\rho\beta)_{hnf}(\rho C_p)_{hnf}}{k_{hnf}\mu_{hnf}}(T - T_a)^2 - \frac{2\sigma\varepsilon(T^4 - T_a^4)}{k_{hnf}}$$

$$- \frac{2(1 - \hat{\phi})h(T)(T - T_a)}{k_{hnf}} - \frac{2h_D l_{fg}(\bar{\omega} - \bar{\omega}_s)(1 - \hat{\phi})}{k_{hnf}}. \tag{4.2.1}$$

The respective adiabatic initial and boundary conditions are given by [**?**],

$$T(x, 0) = 0, \quad T(L, t) = T_b, \quad \frac{\partial}{\partial x}T(0, t) = 0. \tag{4.2.2}$$

For an exponential fin structure the fin thickness is a function of x and is given by,

$$t^*(x) = t_b e^{\nu\left(\frac{x}{L} - 1\right)}. \tag{4.2.3}$$

Here, ν is the shape factor and determines the exponential fin shape as,

$\nu = 1$ corresponds to a tapered exponential fin,

$\nu = 0$ corresponds to a rectangular fin and

$\nu = -1$ corresponds to an inverted exponential fin.

Consider,

$$\theta = \frac{T}{T_b}, \theta_a = \frac{T_a}{T_b}, X = \frac{x}{L}, \tau = \frac{k_f}{(\rho C_p)_f L^2}t, Nc = \frac{2gK(\rho\beta)_f(\rho C_p)_f T_b L^2}{k_f \mu_f t_b},$$

$$Nr = \frac{2\sigma\varepsilon T_b^3 L^2}{k_f t_b}, \bar{\omega} - \bar{\omega}_s = b_2(T - T_a), M^2 = \frac{2h_a L^2(1 - \hat{\phi})}{k_f t_b}, n_1 = \frac{l_{fg} b_2}{Le^{\frac{2}{3}}(C_p)_f}. \tag{4.2.4}$$

Equation (4.2.1) after the substitution of equations (1.2.9) and (4.2.3) is non-dimensionalized

by utilizing the above dimensionless quantities to generate the following equation (4.2.5).

$$
\frac{\partial \theta}{\partial \tau} = \left(\frac{(\rho C_p)_f}{(\rho C_p)_{hnf}} \right) \left(\frac{k_{hnf}}{k_f} \right) \frac{\partial}{\partial X} \left[e^{\nu(X-1)} \frac{\partial \theta}{\partial X} \right] - Nc \left(\frac{(\rho \beta)_{hnf}}{(\rho \beta)_f} \right) \left(\frac{\mu_f}{\mu_{hnf}} \right) (\theta - \theta_a)^2
$$

$$
- M^2 \left(\frac{(\rho C_p)_f}{(\rho C_p)_{hnf}} \right) \left(1 + n_1 \left(\frac{(\rho C_p)_f}{(\rho C_p)_{hnf}} \right) \left(\frac{\rho_{hnf}}{\rho_f} \right) \right) \frac{(\theta - \theta_a)^{m+1}}{(1 - \theta_a)^m}
$$

$$
- Nr \left(\frac{(\rho C_p)_f}{(\rho C_p)_{hnf}} \right) (\theta^4 - \theta_a^4). \tag{4.2.5}
$$

The respective dimensionless initial and boundary conditions are given by,

$$
\theta(X,0) = 0, \quad \theta(1,\tau) = 1, \quad \frac{\partial}{\partial X} \theta(0,\tau) = 0. \tag{4.2.6}
$$

4.2.2 Mass-Based Hybrid Nanofluid Model

The hybrid nanofluid formulation according to the mass-based model is as given below [?] [?]. It is worth mentioning that w_1, w_2 and w_f are masses of the 1st nanoparticle ($AgNPs$), the 2nd nanoparticle ($GrNPs$) and the base fluid ($H2O$), respectively. The sphericity χ and the empirical shape factor s for applied nanoparticles have been depicted in Table (4.1). Further, the thermophysical properties of the nanoparticles and the base fluid have been recorded in Table (4.2).

Heat Capacity:

$$
\frac{(\rho C_p)_{hnf}}{(\rho C_p)_f} = (1 - \varphi) + \varphi \frac{(\rho C_p)_s}{(\rho C_p)_f}. \tag{4.2.7}
$$

Viscosity:

$$
\frac{\mu_{hnf}}{\mu_f} = \frac{1}{(1 - \varphi)^{2.5}}. \tag{4.2.8}
$$

Thermal Expansion Capacity:

$$
\frac{(\rho \beta)_{hnf}}{(\rho \beta)_f} = (1 - \varphi) + \varphi_1 \frac{(\rho \beta)_1}{(\rho \beta)_f} + \varphi_2 \frac{(\rho \beta)_2}{(\rho \beta)_f}. \tag{4.2.9}
$$

Density:

$$\frac{\rho_{hnf}}{\rho_f} = (1 - \varphi) + \varphi \frac{\rho_s}{\rho_f}. \tag{4.2.10}$$

Thermal Conductivity:

$$\frac{k_{hnf}}{k_{nf}} = \frac{k_2 + (s-1)k_{nf} - (s-1)\varphi_2(k_{nf} - k_2)}{k_2 + (s-1)k_{nf} + \varphi_2(k_{nf} - k_2)},$$

$$\frac{k_{nf}}{k_f} = \frac{k_1 + (s-1)k_f - (s-1)\varphi_1(k_f - k_1)}{k_1 + (s-1)k_f + \varphi_1(k_f - k_1)}. \tag{4.2.11}$$

where,

$$\rho_s = \frac{(\rho_1 \times w_1) + (\rho_2 \times w_2)}{w_1 + w_2}, \tag{4.2.12}$$

$$(C_p)_s = \frac{(C_p)_1 \times w_1 + (C_p)_2 \times w_2}{w_1 + w_2}, \tag{4.2.13}$$

$$\varphi_1 = \frac{\frac{w_1}{\rho_1}}{\frac{w_1}{\rho_1} + \frac{w_2}{\rho_2} + \frac{w_f}{\rho_f}}, \tag{4.2.14}$$

$$\varphi_2 = \frac{\frac{w_2}{\rho_2}}{\frac{w_1}{\rho_1} + \frac{w_2}{\rho_2} + \frac{w_f}{\rho_f}}, \tag{4.2.15}$$

$$\varphi = \varphi_1 + \varphi_2. \tag{4.2.16}$$

4.2.3 Fin Efficiency

The instantaneous heat transfer rate of the fin wetted in a hybrid nanofluid is given by,

$$Q_f = \int_0^L \left[\begin{array}{c} \frac{2gKW(\rho\beta)_{hnf}(\rho C_p)_{hnf}}{\mu_{hnf}}(T - T_a)^2 + 2\sigma W\varepsilon(T^4 - T_a^4) \\ + \left(2(1 - \hat{\phi})h_a W + \frac{2h_D l_{fg} W b_2 (1-\hat{\phi})}{(C_p)_{hnf} Le^{\frac{2}{3}}} \right) \frac{(T-T_a)^{m+1}}{(T_b - T_a)^m} \end{array} \right] dx. \tag{4.2.17}$$

The ideal heat transfer through the fin when the surface temperature of the entire fin is

equal to base temperature is given by,

$$Q_{ideal} = \left[\begin{array}{c} \frac{2gKW(\rho\beta)_{hnf}(\rho C_p)_{hnf}L}{\mu_{hnf}}(T_b - T_a)^2 + 2\sigma W\varepsilon L(T_b^4 - T_a^4) \\ + \left(2(1 - \hat{\phi})h_a WL + \frac{2h_D l_{fg} W L b_2 (1-\hat{\phi})}{(C_p)_{hnf} Le^{\frac{2}{3}}} \right) (T_b - T_a) \end{array} \right]. \tag{4.2.18}$$

The thermal fin efficiency is calculated as,

$$\eta = \frac{Q_f}{Q_{ideal}}.$$

In dimensionless form the efficiency of fin immersed in a hybrid nanofluid is given by,

$$\eta = \frac{\int_0^1 \left[\begin{array}{c} Nc \left(\frac{(\rho\beta)_{hnf}}{(\rho\beta)_f} \right) \left(\frac{\mu_f}{\mu_{hnf}} \right) \left(\frac{(\rho C_p)_{hnf}}{(\rho C_p)_f} \right) \left(\frac{k_f}{k_{hnf}} \right) (\theta - \theta_a)^2 + Nr \left(\frac{k_f}{k_{hnf}} \right) (\theta^4 - \theta_a^4) \\ \\ + M^2 \left(\frac{k_f}{k_{hnf}} \right) \left(1 + n_1 \left(\frac{(\rho C_p)_f}{(\rho C_p)_{hnf}} \right) \left(\frac{\rho_{hnf}}{\rho_f} \right) \right) \frac{(\theta - \theta_a)^{m+1}}{(1 - \theta_a)^m} \end{array} \right] dX}{\left[\begin{array}{c} Nc \left(\frac{(\rho\beta)_{hnf}}{(\rho\beta)_f} \right) \left(\frac{\mu_f}{\mu_{hnf}} \right) \left(\frac{(\rho C_p)_{hnf}}{(\rho C_p)_f} \right) \left(\frac{k_f}{k_{hnf}} \right) (1 - \theta_a)^2 + Nr \left(\frac{k_f}{k_{hnf}} \right) (1 - \theta_a^4) \\ \\ + M^2 \left(\frac{k_f}{k_{hnf}} \right) \left(1 + n_1 \left(\frac{(\rho C_p)_f}{(\rho C_p)_{hnf}} \right) \left(\frac{\rho_{hnf}}{\rho_f} \right) \right) (1 - \theta_a) \end{array} \right]}.$$

$$(4.2.19)$$

4.3 Numerical Elucidation

The second order nonlinear PDE of parabolic nature named equation (4.2.5) and its corresponding initial and boundary conditions labelled as equation (4.2.6) are the concerned equations. Using the FDM with centered-implicit scheme the PDE's solutions have been found via the Maple software. The detailed procedure is explained in section (2.3). The results of the present investigation have been extracted by setting $\Delta X = 0.001$ and $\Delta\tau = 0.001$.

4.4 Deliberation of Results

The thermal characteristics of tapered and inverted exponential fin structures have been comparatively analysed along with the rectangular fin profile by employing the mass-based hybrid nanofluid model. The numerical solutions extracted from the governing equations have been represented graphically in figures 4.2−4.13 for better analysis and their physical descriptions have been discussed.

The response of thermal characteristics of exponential fin profiles and rectangular fin profile in the presence of silver-graphene-water hybrid nanofluid with the convective parameter Nc and radiative parameter Nr has been depicted in figures 4.2 and 4.3. Both Nc and Nr have provided an affirmative response in accelerating the fin cooling process. The positive influence of Nc is due to the buoyancy effect which can be explained as follows. With increase in Nc values the permeability of the porous medium increases resulting in improved movement of fluid through the pores of the fin. Thus, leading to increased convective heat loss and decrease in the fin temperature. On the other hand, parameter Nr is associated with heat loss through radiation. Hence its rise results in more heat loss and better cooling of the fin. Further, inverted exponential fin has higher difference in temperature along the length of the fin and hence provides higher rate of heat loss. It is followed by rectangular and tapered exponential fin.

The wet parameter n_1 and ambient temperature (dimensionless) θ_a have a remarkable influence on the temperature distribution of exponential (both tapered and inverted) and rectangular fin profiles when immersed in a hybrid nanofluid as pictured in figures 4.4 and 4.5. It can be observed that rise in m_2 lowers the fin thermal profile whereas rise in θ_a does the opposite. This is because m_2 is associated with the wet nature of the fin and thus enhances the convective heat loss leading to decrease in fin temperature. On the other hand, increase in parameter θ_a results in decrease in temperature difference between fin surface and the ambient fluid resulting in slower transmission of heat between the two entities. This phenomenon is backed up by Newton's law of cooling and hence lower values of θ_a are preferrable for better fin cooling. Further, similar trend is followed by all the three longitudinal fin profiles.

Figures 4.6 and 4.7 have captured the impact of exponential index m and thermoge-

ometric parameter M on the thermal response of three different longitudinal fin profiles when hybrid nanofluid silver-graphene-water is allowed to pass through the porous fin structures. It can be observed that exponential index m gives rise to higher thermal profiles but the thermogeometric parameter M does the opposite. This can be explained as follows. The variation in the value of heat transfer coefficient h with temperature is governed by parameter m and an increase in its value decreases the value of h. This results in lesser heat loss through convection and hence fin temperature rises. On the other hand, the parameter M is employed to gauge the influence of the ratio of convective to conductive heat transfer coefficients and also the porosity of the fin material. Hence rise in M signifies increased convective heat transfer due to an increase in the ratio because of increased surface area due to hike in porosity. Thus, lower values of m and higher values of M are preferable in the fin cooling process.

Figures 4.8 and 4.9 depict the variation in the thermal profile of inverted exponential, rectangular and tapered exponential fin structures with mass of the second nanoparticle w_2 and shape of the nanoparticle s. It can be noted that w_2 improves the distribution of temperature along the fin length. In addition, disc shaped nanoparticle gives rise to higher thermal profiles followed by cylindrical and sphere shaped ones. This is because rise in value of w_2 as well as s increases the thermal conductivity of the hybrid nanofluid leading to increase in the effective thermal conductivity of the fin structure. This results in increase in the fin temperature towards the tip of the fin. Thus, both these parameters provide better distribution of temperature. Further the behaviour of all three fin profiles is similar in both the cases.

The transient nature of the energy profiles of the three different longitudinal fin structures in the presence of hybrid nanofluid has been depicted in figure 4.10. It can be noted

that temperature profiles move upward with the passing of time and the fin base reaches steady state quite faster than the tip of the fin. This can be explained as follows. Initially the temperature at the base of the fin will be zero and then there will be a step rise in the base temperature. This results in the entry of heat to fin structure represented by lower thermal profiles and gradually with time there will be a better distribution of temperature represented by higher thermal profiles. Further it can be observed that nature of thermal profiles of all three geometries is similar.

The thermal efficiency of exponential fin structures in the presence of shape-dependent hybrid nanofluid for simultaneous variation in the thermogeometric parameter M and wet fin parameter n_1 has been illustrated in figure 4.11. It can be observed that fin efficiency decreases with increase in the parameters M and n_1. This is because as explained earlier the rise in these parameters results in a decrease in the distribution of temperature along the length of the fin increasing the deviation of the actual fin case from the ideal one.

Figure 4.12 depicts the influence of weight of the second nanoparticle w_2 on the transient thermal efficiency of three distinct profiles of longitudinal fin structure wetted in a shape-dependent hybrid nanofluid. It can be noticed that efficiency increases with an increase in the values of w_2. This is because the elevation in the concentration of the hybrid nanofluid helps in improving the effective thermal conductivity of the porous fin and thus enhancing the spatial distribution of temperature. Thus, the application of hybrid nanofluid instead of simple base fluid enhances the fin efficiency.

The influence of nanoparticle shape factor s and convective parameter Nc on the efficiency of tapered exponential, rectangular and inverted exponential fin structures has been illustrated in figure 4.13. It can be noted that efficiency increases with rise in the value of s whereas decrases with the hike in the values of Nc. Thus, the hybrid nanofluid

with disc shaped nanoparticles attains highest efficiency than those from spherical and cylindrical ones.

4.5 Denouement

The transient thermal performance of three distinct profiles of longitudinal fin fully wetted in a hybrid nanofluid has been analysed by employing the FDM. A novel mass-based hybrid nanofluid model has been implemented in the place of a fraction based model. The major outcomes of the study are:

- The fin temperature field gradually rises with time and finally attains a steady state.

- The convective-radiative heat transmission environment accelerates the fin cooling process. The wet and porous nature of the fin produces lower tip temperatures whereas the exponential index and ambient temperature negatively affect the fin heat loss.

- The speed of the fin has a significant impact on the its surface temperature. Slower the movement of fin, higher is the heat loss rate.

- The fin surface temperature is greatly influenced by mass and shape of the nanoparticles. Both these parameters enhance the temperature distribution through the fin.

- The tip temperature of an exponential fin with thick tip is lower than that of a rectangular fin followed by an exponential fin with thin tip. Thus, an exponential fin with thick tip performs better than the other two profiles in the process of fin cooling.

Table 4.1: Sphericity χ and empirical shape factor s for applied nanoparticles [?] [?].

Structure	Sphere	Cylinder	Disc
χ	1	0.81	0.52
s	3	3.7	5.7

Table 4.2: Thermophysical properties of base fluid and nanoparticles [?] [?].

Thermophysical properties	Pure water	Silver	Graphene
$\rho(kgm^{-3})$	997.1	10500	2250
$C_p(Jkg^{-1}K^{-1})$	4179	235	2100
$k(Wm^{-1}K^{-1})$	0.613	429	2500
$\beta * 10^{-5}(K^{-1})$	21	1.3	21
Particle size (nm)	-	2-5	10-30
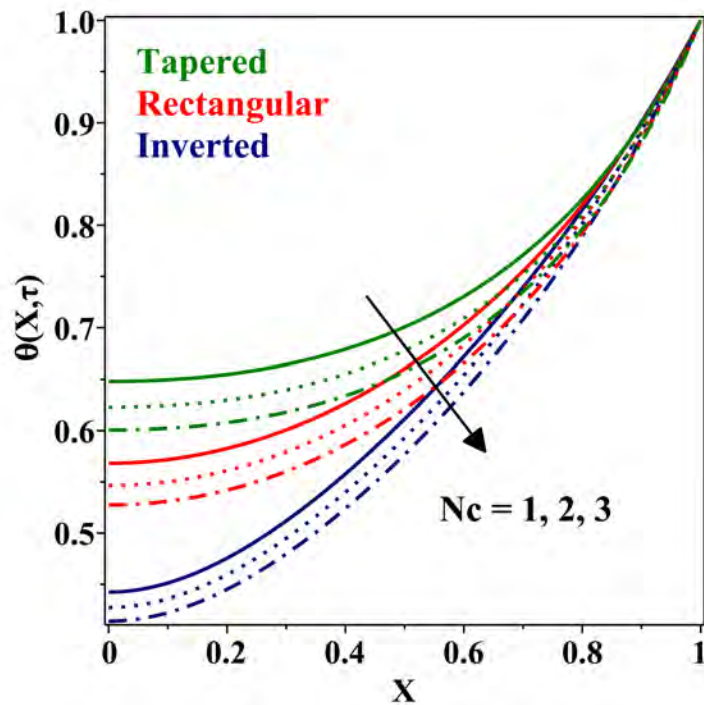
Figure 4.2: Outcome of convective parameter Nc on fin energy field.
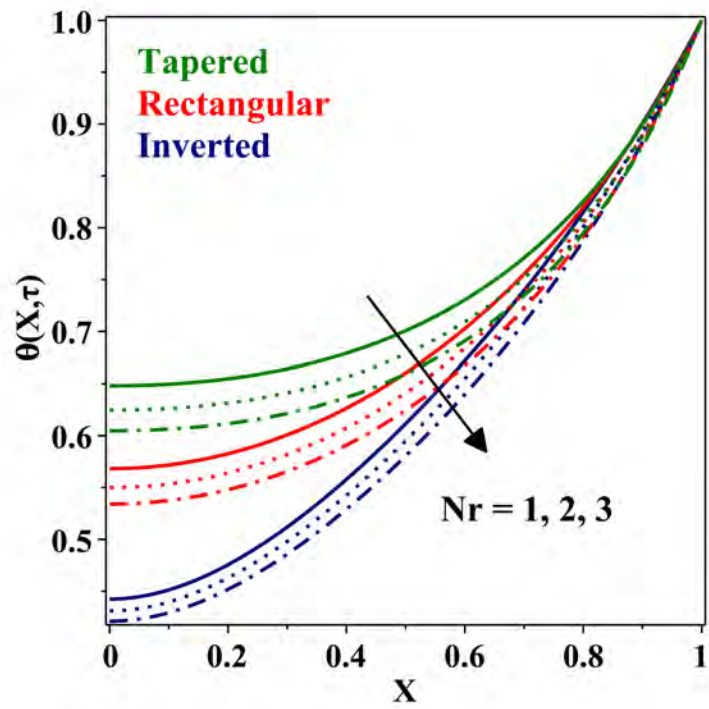
Figure 4.3: Outcome of radiative parameter Nr on fin energy field.
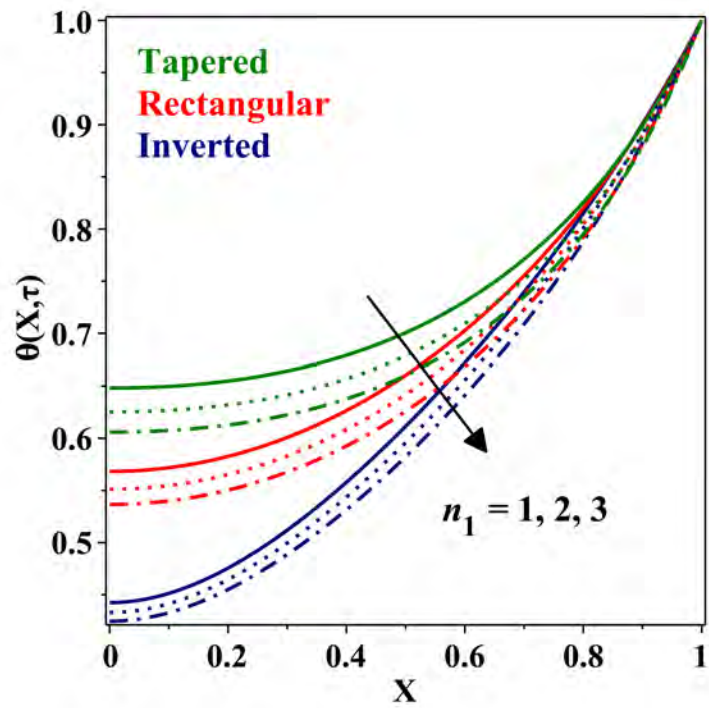
Figure 4.4: Outcome of wet parameter n_1 on fin energy field.
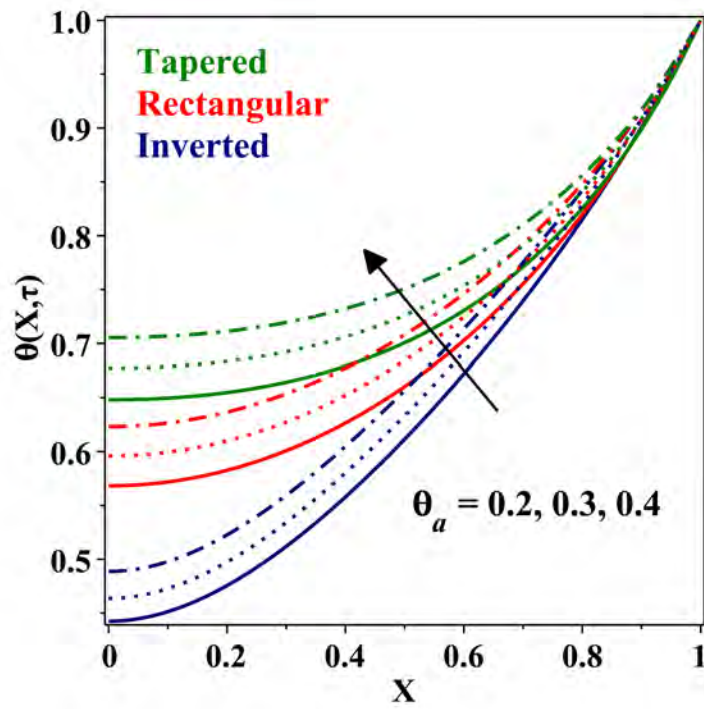
Figure 4.5: Outcome of dimensionless ambient temperature θ_a on fin energy field.
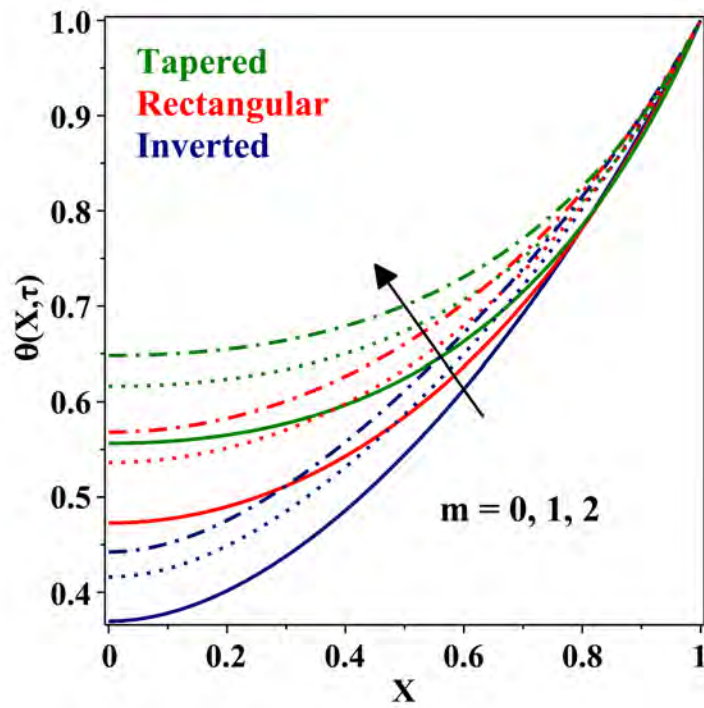
Figure 4.6: Outcome of exponential index m on fin energy field.
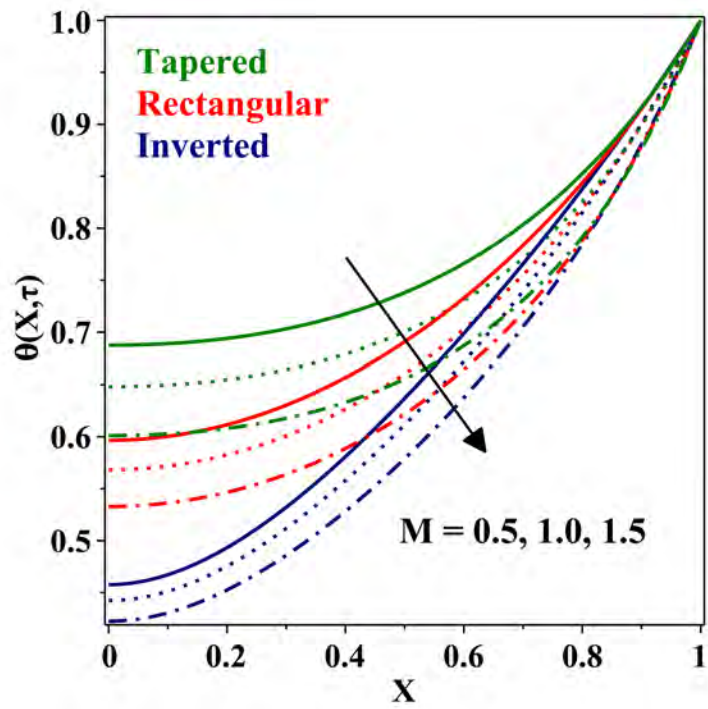
Figure 4.7: Outcome of thermogeometric parameter M on fin energy field.
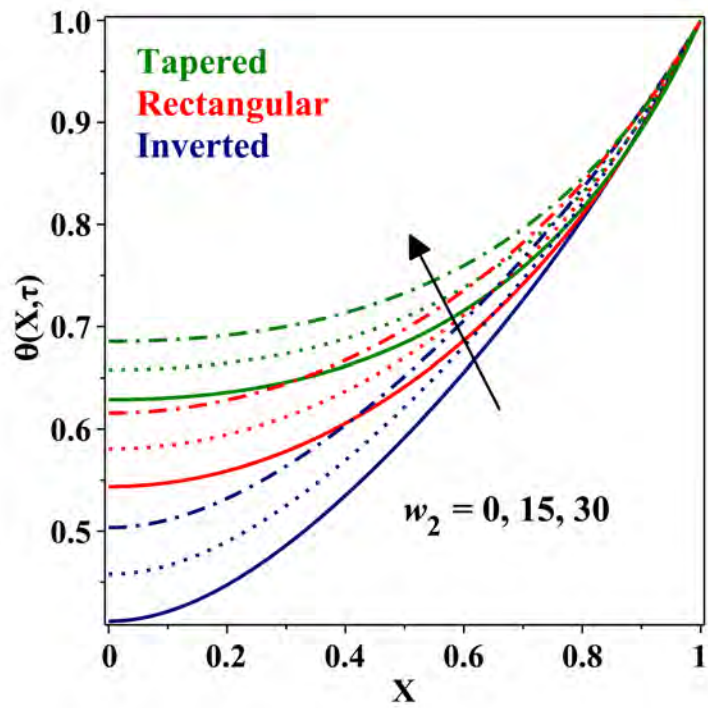
Figure 4.8: Outcome of weight of second nanoparticle w_2 on fin energy field.
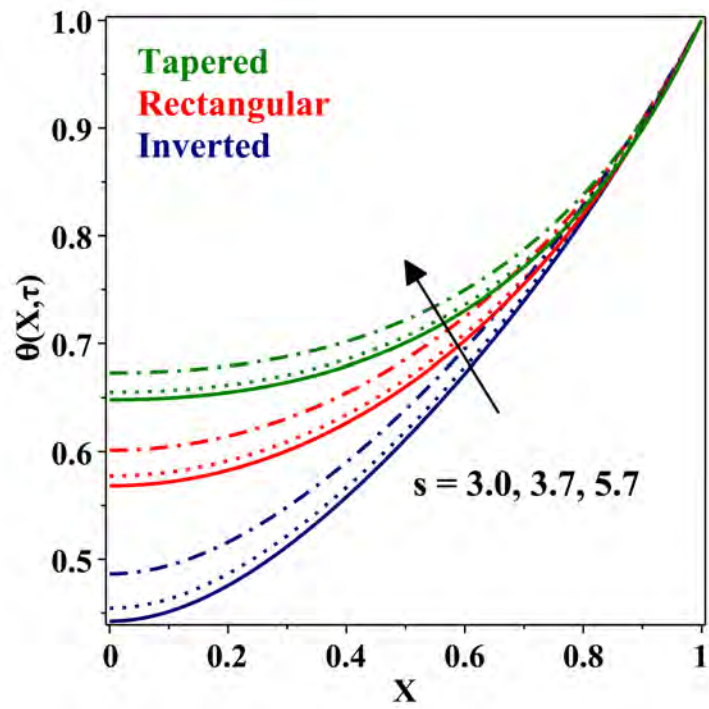
Figure 4.9: Outcome of nanoparticle shape parameter s on fin energy field.
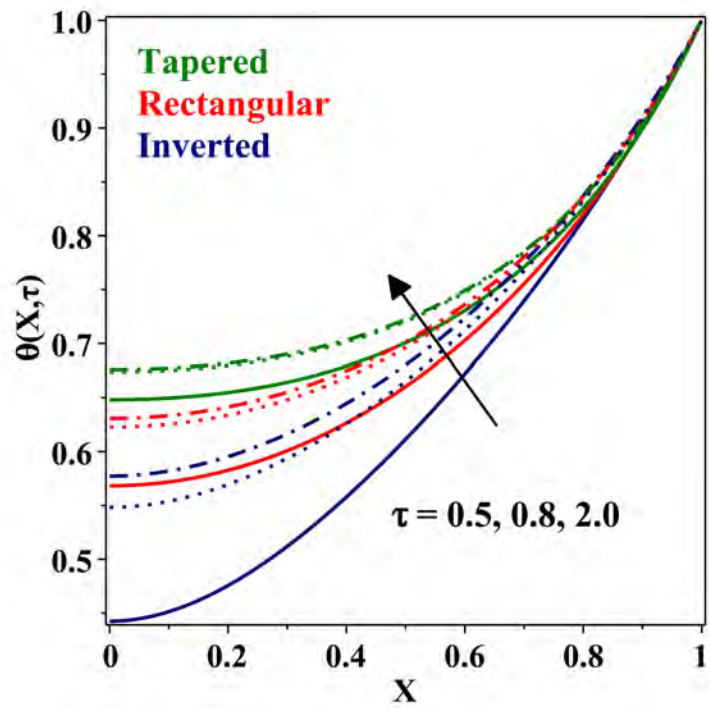
Figure 4.10: Outcome of dimensionless time τ on fin energy field.
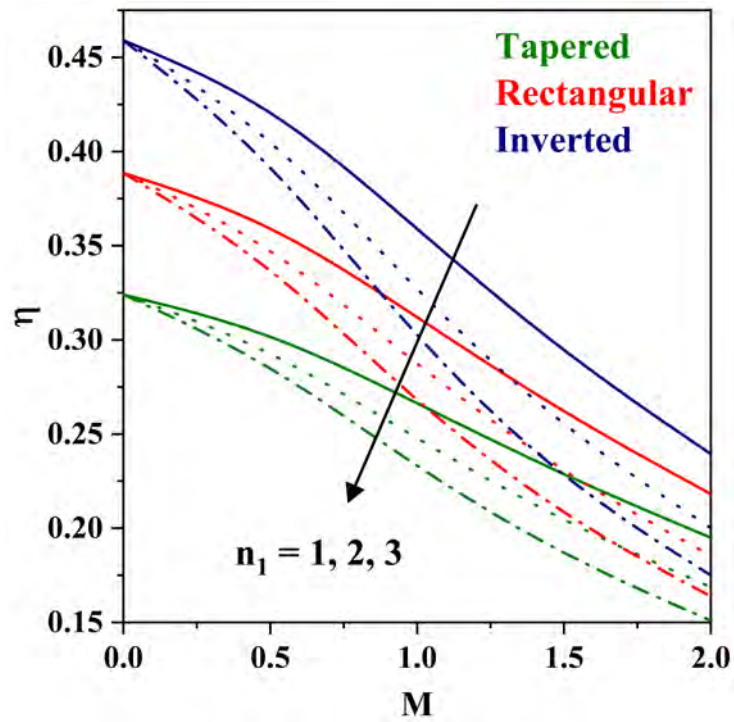
Figure 4.11: Outcome of M and n_1 on fin thermal efficiency.
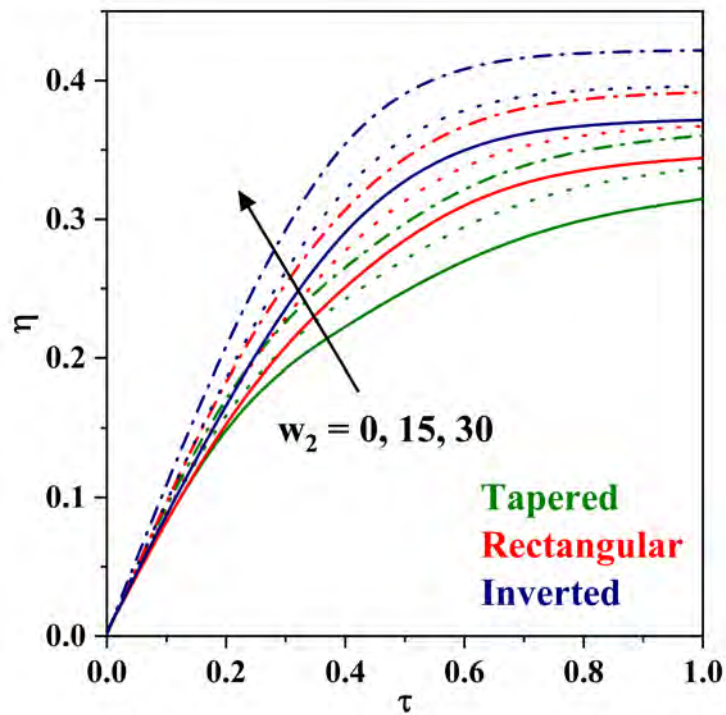
Figure 4.12: Outcome of w_2 and τ on fin thermal efficiency .
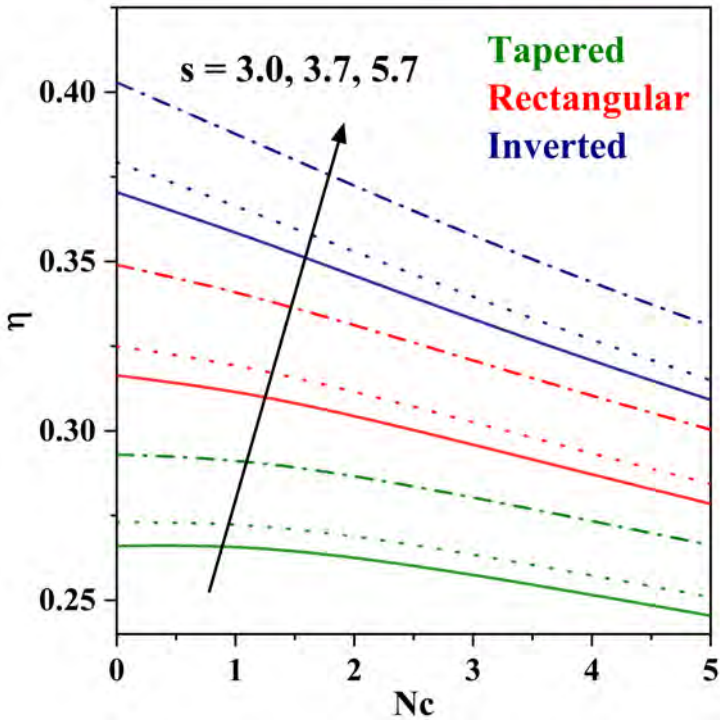
Figure 4.13: Outcome of s and Nc on fin thermal efficiency.

Chapter 5

Numerical Investigation of Efficiency of Fully Wet Porous Convective-Radiative Moving Radial Fin in the Presence of Shape-Dependent Hybrid Nanofluid

5.1   Prelims

The main focus of the study is a fully wet porous fin of radial profile exposed to convective-radiative heat exchange with the hybrid nanofluid flowing past it with a constant velocity of $\bar{U}$. In the analysis, spherical-spherical, spherical-cylindrical, and spherical-platelet shape combinations of two nanoparticles are considered. The mixture model is employed to assess all the thermophysical attributes of the hybrid nanofluid except thermal conductivity and dynamic viscosity, which are estimated by applying the nanoparticle volume fraction-based interpolation method. The fin model with the applied conditions results in an ODE which is made dimensionless and then numerically resolved by applying the RKF45 technique. The effect of Peclet number, wet fin parameter, thermogeometric parameter, nanoparticle volume fraction, convective parameter, radiative parameter, exponential index, empirical shape factor and ambient temperature (dimensionless) on the

77

energy field and thermal gradient profiles of the radial fin subjected to shape-dependent hybrid nanofluid flow has been graphically analysed. Furthermore, the thermal fin efficiency has been modelled and its variation with the significant parameters has been examined. One of the major outcomes was that efficiency increases with nanoparticle volume fraction. Further, it is significantly affected by the shape factor of the nanoparticles and achieves the highest value for spherical-platelet combination. The results obtained motivate further study of nanotechnology assisted extended surface technology.

5.2 Modeling and Interpretation

5.2.1 Heat Transfer
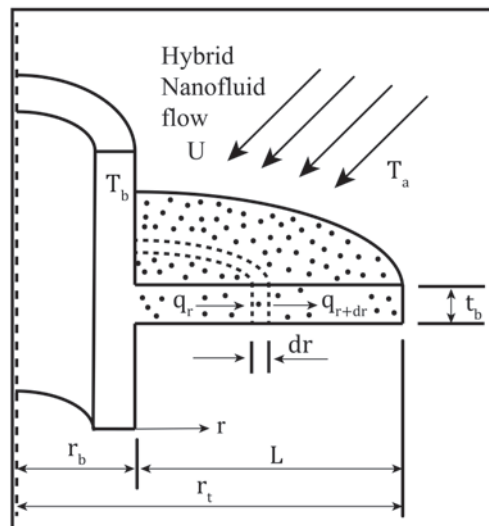
Figure 5.1: Pictorial representation of hybrid nanofluid flow past a porous radial fin.

In this work, a rectangular profiled radial fin is assumed to be fully wetted in the

hybrid nanofluid. As depicted in figure 5.1, a fin with base radius r_b, tip radius r_t, and thickness t_b is considered. The fin is assumed to be moving with a constant velocity $\bar{U}$. This can also be assumed as a hybrid nanofluid moving with a constant velocity $\bar{U}$ past a stationary fin. The fin structure is made up of porous material, enabling the hybrid nanofluid to infiltrate through it, and the Darcy model has been utilised to study the solid-fluid interaction. The fin gathers heat from the prime surface, which is at temperature T_b, and exchanges it with the ambient hybrid nanofluid kept at temperature T_a through convective and radiative modes of heat transmission. Since the fin thickness is small, the heat transmission through the fin tip is negligible and thus the fin tip is assumed to be adiabatic in nature. Also, one dimensional temperature distribution, i.e., only along the radial direction, is assumed in the fin.

The flow of heat energy through a small area of cross-section dr has been modelled under steady state conditions and is given by,

$$(q(r) - q(r + dr))dr - 2\bar{v}(r)2\pi r dr(\rho C_p)_{hnf}(T - T_a) - (\rho C_p)_{hnf}2\pi r t_b \bar{U} \frac{dT}{dr}$$

$$- 2\pi r h dr(1 - \hat{\phi})(T - T_a) - 2\pi r dr h_D l_{fg}(1 - \hat{\phi})(\bar{\omega} - \bar{\omega}_s)dr$$

$$- 2\sigma \varepsilon F_{f-a}2\pi r dr(T^4 - T_a^4) = 0. \tag{5.2.1}$$

Here the first term represents the energy difference for a small distance dr, the second term is introduced via Darcy model to address the fluid's interaction with the porous media, the third term accounts for fin motion, the fourth term is for radiation phenomenon, the fifth and sixth terms are for convective and fully wet nature of the porous fin structure. As per the Fourier's law of heat conduction $q(r)$, the heat energy at radial position r is

given by,

$$q(r) = -k_{hnf} 2\pi r t_b \frac{dT}{dr}.$$

(5.2.2)

As per Darcy's model the velocity of the fluid particles flow through the porous media is

given by,

$$\bar{v}(r) = \frac{gK(\rho\beta)_{hnf}(T - T_a)}{\mu_{hnf}}.$$

(5.2.3)

Upon utilizing equations (5.2.2) and (5.2.3), equation (5.2.1) resolves into,

$$\frac{1}{r}\frac{d}{dr}\left(r\frac{dT}{dr}\right) - \frac{2gK(\rho C_p)_{hnf}(\rho\beta)_{hnf}}{\mu_{hnf}k_{hnf}t_b}(T - T_a)^2 - \frac{2h_D l_{fg}(1 - \hat{\phi})(\bar{\omega} - \bar{\omega}_s)}{k_{hnf}t_b}$$

$$- \frac{2h(1 - \hat{\phi})(T - T_a)}{k_{hnf}t_b} - \frac{2\sigma\varepsilon F_{f-a}}{k_{hnf}t_b}(T^4 - T_a^4) - \frac{(\rho C_p)_{hnf}\bar{U}}{k_{hnf}}\frac{dT}{dr} = 0.$$

(5.2.4)

The respective adiabatic boundary conditions are given by,

$$T(r_b) = T_b,$$

$$\frac{dT(r_t)}{dr} = 0.$$

(5.2.5)

The following are the dimensionless quantities:

$$\theta = \frac{T}{T_b}, \theta_a = \frac{T_a}{T_b}, R = \frac{r}{r_b}, \bar{R} = \frac{r_t}{r_b}, Nc = \frac{2gK(\rho C_p)_f(\rho\beta)_f T_b r_b^2}{\mu_f k_f t_b}, Nr = \frac{2\sigma\varepsilon F_{f-a}T_b^3 r_b^2}{k_f t_b},$$

$$\bar{\omega} - \bar{\omega}_s = b_2(T - T_a), M^2 = \frac{2h_a r_b^2(1 - \hat{\phi})}{k_f t_b}, n_1 = \frac{l_{fg}b_2}{Le^{\frac{2}{3}}(C_p)_f}, Pe = \frac{(\rho C_p)_f \bar{U} r_b}{k_f}.$$

(5.2.6)

Using the equations (1.2.9) and (5.2.6), the equation (5.2.4) reduces to,

$$\frac{1}{R}\frac{d}{dR}\left(R\frac{d\theta}{dR}\right) - Nc\left(\frac{(\rho C_p)_{hnf}}{(\rho C_p)_f}\right)\left(\frac{(\rho\beta)_{hnf}}{(\rho\beta)_f}\right)\left(\frac{k_f}{k_{hnf}}\right)\left(\frac{\mu_f}{\mu_{hnf}}\right)(\theta - \theta_a)^2$$

$$- Nr\left(\frac{k_f}{k_{hnf}}\right)(\theta^4 - \theta_a^4) - Pe\left(\frac{(\rho C_p)_{hnf}}{(\rho C_p)_f}\right)\left(\frac{k_f}{k_{hnf}}\right)\frac{d\theta}{dR}$$

$$- M^2\left(1 + n_1\left(\frac{(\rho C_p)_f}{(\rho C_p)_{hnf}}\right)\left(\frac{\rho_{hnf}}{\rho_f}\right)\right)\left(\frac{k_f}{k_{hnf}}\right)\frac{(\theta - \theta_a)^{m+1}}{(1 - \theta_a)^m} = 0.$$

(5.2.7)

With the reduced boundary conditions,

$$\theta(1) = 1,$$

$$\frac{d}{dR}\theta(\bar{R}) = 0, \bar{R} = 3. \tag{5.2.8}$$

5.2.2 Thermal Efficiency Analysis

Comparison of fin structures based on their thermal efficiency is an effective way in analysing different fin structures under various circumstances. For the calculation of fin efficiency, it is necessary to model the heat transfer through the entire fin structure given by Q_f and heat transfer through an ideal fin structure given by Q_{ideal}.

$$Q_f = \int_{r_b}^{r_t} \left[\begin{array}{c} \frac{2gK(\rho\beta)_{hnf}(\rho C_p)_{hnf}2\pi r(T-T_a)^2}{\mu_{hnf}} + 2\sigma\varepsilon F_{f-a}2\pi r(T^4 - T_a^4) \\ \\ + \frac{2\pi rh_a(1-\hat{\phi})(T-T_a)^{m+1}}{(T_b-T_a)^m} + \frac{2\pi rh_a(1-\hat{\phi})l_{fg}b_2(T-T_a)^{m+1}}{(C_p)_{hnf}Le^{\frac{2}{3}}(T_b-T_a)^m} \end{array} \right] dr.$$

$$Q_{ideal} = \int_{r_b}^{r_t} \left[\begin{array}{c} \frac{2gK(\rho\beta)_{hnf}(\rho C_p)_{hnf}2\pi r(T_b-T_a)^2}{\mu_{hnf}} + 2\sigma\varepsilon F_{f-a}2\pi r(T_b^4 - T_a^4) \\ \\ + 2\pi rh_a(1-\hat{\phi})(T_b - T_a) + \frac{2\pi rh_a(1-\hat{\phi})l_{fg}b_2}{(C_p)_{hnf}Le^{\frac{2}{3}}}(T_b - T_a) \end{array} \right] dr.$$

The thermal fin efficiency is calculated as,

$$\eta = \frac{Q_f}{Q_{ideal}}.$$

$$\eta = \frac{\int_1^{\bar{R}} \left[\begin{array}{c} Nc\left(\frac{(\rho C_p)_{hnf}}{(\rho C_p)_f}\right)\left(\frac{(\rho\beta)_{hnf}}{(\rho\beta)_f}\right)\left(\frac{k_f}{k_{hnf}}\right)\left(\frac{\mu_f}{\mu_{hnf}}\right)(\theta - \theta_a)^2 + Nr\left(\frac{k_f}{k_{hnf}}\right)(\theta^4 - \theta_a^4) \\ \\ +M^2\left(1 + n_1\left(\frac{(\rho C_p)_f}{(\rho C_p)_{hnf}}\right)\left(\frac{\rho_{hnf}}{\rho_f}\right)\right)\left(\frac{k_f}{k_{hnf}}\right)\frac{(\theta-\theta_a)^{m+1}}{(1-\theta_a)^m} \end{array} \right] RdR}{\left[\begin{array}{c} Nc\left(\frac{(\rho C_p)_{hnf}}{(\rho C_p)_f}\right)\left(\frac{(\rho\beta)_{hnf}}{(\rho\beta)_f}\right)\left(\frac{k_f}{k_{hnf}}\right)\left(\frac{\mu_f}{\mu_{hnf}}\right)(1 - \theta_a)^2 + Nr\left(\frac{k_f}{k_{hnf}}\right)(1 - \theta_a^4) \\ \\ +M^2\left(1 + n_1\left(\frac{(\rho C_p)_f}{(\rho C_p)_{hnf}}\right)\left(\frac{\rho_{hnf}}{\rho_f}\right)\right)\left(\frac{k_f}{k_{hnf}}\right)(1 - \theta_a) \end{array} \right]}. \tag{5.2.9}$$

81

5.2.3 Thermophysical Properties of Hybrid Nanofluid

In the above equations (5.2.7) and (5.2.9), $\rho_{hnf}, (C_p)_{hnf}, \beta_{hnf}$ respectively are the density, specific heat capacity and thermal expansion coefficient of the hybrid nanofluid and are assessed based on the mixture model as [?] [?],

$$\rho_{hnf} = \rho_1\varphi_1 + \rho_2\varphi_2 + (1 - \varphi_1 - \varphi_2)\rho_f, \qquad (5.2.10)$$

$$(\rho C_p)_{hnf} = \varphi_1(\rho C_p)_1 + \varphi_2(\rho C_p)_2 + (1 - \varphi_1 - \varphi_2)(\rho C_p)_f, \qquad (5.2.11)$$

$$(\rho\beta)_{hnf} = \varphi_1(\rho\beta)_1 + \varphi_2(\rho\beta)_2 + (1 - \varphi_1 - \varphi_2)(\rho\beta)_f. \qquad (5.2.12)$$

In the current examination the hybrid nanofluid composed of two different nanoparticles of distinct shapes is considered. Here, the interpolation method is implemented to calculate the dynamic viscosity μ_{hnf} and thermal conductivity k_{hnf} of the hybrid nanofluid. Initially for calculating the thermal conductivity of the nanofluid of particular shaped nanoparticle the Maxwell Garnett model given below is utilized.

$$\frac{k_{nf}}{k_f} = \frac{k_p + (s-1)k_f + (s-1)\varphi(k_p - k_f)}{k_p + (s-1)k_f - \varphi(k_p - k_f)}.$$

For spherical shaped 1st nanoparticle:

$$\frac{k_{nf1}}{k_f} = \frac{k_1 + 2k_f + 2\varphi(k_1 - k_f)}{k_1 + 2k_f - \varphi(k_1 - k_f)}.$$

For spherical shaped 2nd nanoparticle:

$$\frac{k_{nf2}}{k_f} = \frac{k_2 + 2k_f + 2\varphi(k_2 - k_f)}{k_2 + 2k_f - \varphi(k_2 - k_f)}.$$

For cylindrical shaped 2nd nanoparticle

$$\frac{k_{nf2}}{k_f} = \frac{k_2 + 3.9k_f + 3.9\varphi(k_2 - k_f)}{k_2 + 3.9k_f - \varphi(k_2 - k_f)}.$$

For platelet shaped 2nd nanoparticle

$$\frac{k_{nf2}}{k_f} = \frac{k_2 + 4.7k_f + 4.7\varphi(k_2 - k_f)}{k_2 + 4.7k_f - \varphi(k_2 - k_f)}.$$

When the 1st and 2nd nanoparticles of concentration φ_1 and φ_2 are considered with the total nanoparticle volume fraction $\varphi = \varphi_1 + \varphi_2$, the resulting thermal conductivity of the hybrid nanofluid is estimated as below,

$$k_{hnf} = \frac{\varphi_1 k_{nf1} \varphi_2 k_{nf2}}{\varphi}. \tag{5.2.13}$$

Similar to the assessment of k_{hnf} the effective dynamic viscosity of the shape-dependent hybrid nanofluid is calculated as follows:

For spherical shaped 1st nanoparticle: $\mu_{nf1} = \mu_f(1 + 2.5\varphi + 6.2\varphi^2)$

For spherical shaped 2nd nanoparticle: $\mu_{nf2} = \mu_f(1 + 2.5\varphi + 6.2\varphi^2)$

For cylindrical shaped 2nd nanoparticle: $\mu_{nf2} = \mu_f(1 + 13.5\varphi + 904.4\varphi^2)$

For platelet shaped 2nd nanoparticle: $\mu_{nf2} = \mu_f(1 + 37.1\varphi + 612.6\varphi^2)$

Thus μ_{hnf} is given by,

$$\mu_{hnf} = \frac{\mu_{nf1}\varphi_1 + \mu_{nf2}\varphi_2}{\varphi}. \tag{5.2.14}$$

For the current investigation, spherical shaped Al_2O_3 is considered to be 1st nanoparticle and spherical shaped Ag, cylindrical shaped CNT or platelet shaped graphene is chosen as the 2nd nanoparticle and water is considered to be the base fluid. The essential details of the nanoparticles and base fluid required for the calculative purpose have been recorded in table 5.1.

5.3 Numerical Elucidation

The nonlinear second-order ODE (5.2.7) with insulated boundary condition in equation (5.2.8) has been solved by applying the RKF45 method. In the present analysis, solutions are obtained for the step size 0.001 with the convergence criteria set to 10^{-6}.

5.4 Deliberation of Results

The discrete numerical output has been reconstructed in the form of graphical structures and in order to better analyse the results thermal profiles as well as thermal gradient profiles along with fin efficiency have been plotted. In figures $5.2 - 5.19$, three different cases of the second nanoparticle's shape namely spherical, cylindrical, and platelet have been depicted for a comparative analysis and are abbreviated as SS (spherical-spherical), SC (spherical-cylindrical), and SP (spherical-platelet) respectively. Throughout the analysis $\varphi_1 = 0.05\%, \varphi_2 = 0.05\%$ thus making $\varphi = 0.1\%$ unless otherwise mentioned.

The variation in the thermal conductivity of the hybrid nanofluid with the nanoparticle volume fraction φ for different combination of nanoparticle shapes has been depicted in figure 5.2. It can be observed that the ratio k_{hnf}/k_f raises with an increase in φ value and is highest in the case of spherical-platelet combination of nanoparticle shapes followed by spherical-cylindrical and spherical-spherical combinations.

5.4.1 Thermal Field Analysis:

Figures 5.3 and 5.4 respectively indicate the temperature outline and thermal gradient of a radial fin immersed in a shape-dependent hybrid nanofluid for distinct values of convective parameter Nc. It can be witnessed from the depiction that the temperature outline is

lower for higher values of Nc and the thermal gradient towards the fin base increases with elevating values of Nc. The parameter Nc accounts for the permeability of the porous medium and the buoyancy effect is the key factor behind this behaviour of temperature and thermal gradient outlines. That is, with a rise in the values of Nc permeability of the porous medium increases leading to quicker movement of heat carrying fluid particles in and out of the fin matrix. This leads to a higher rate of heat loss and better cooling phenomenon. Further, the hybrid nanofluid with spherical-platelet combination of nanoparticles results in better temperature distribution followed by spherical-cylindrical and spherical-spherical combinations. This can be explained as follows. The hybrid nanofluid present in the pores of the fin structure raises the effective thermal conductivity of the fin material and helps in better transmission of heat through conduction from the fin base towards the fin tip. Further, the effective thermal conductivity of the fin structure is highest in the case of spherical-platelet combination as can be observed from figure 5.2.

The temperature profile and thermal gradient plot of a radial fin structure subject to flow of hybrid nanofluid with spherical-spherical, spherical-cylindrical and spherical-platelet combination of nanoparticles for variation in the radiation parameter Nr have been pictured in figures 5.5 and 5.6 likewise. It can be noted that with uplifting values of radiative parameter, the fin surface temperature decreases towards the fin tip and the temperature difference increases towards the fin base. The term Nr accounts for increase in radiative heat exchange as compared to conductive heat transmission. Thus, rise in Nr values increase the heat loss through radiation leading to lower thermal profiles. On the other hand, it can be noted from figure 5.6 that temperature difference at the fin base increases with increase in the values of Nr. As the heat transfer through conduction is influenced by the temperature difference, a hike in the values of Nr results in faster

extraction of heat from the prime surface via the fin base. Also, the variation in the fin thermal profile for distinct combination of nanoparticle shapes follows the same trend as explained before.

The impact of thermogeometric parameter M on the energy profile and temperature gradient profile of a radial fin exposed to hybrid nanofluid flow has been captured in figures 5.7 and 5.8 respectively. As depicted M has a negative influence on the temperature distribution and has a positive effect in rising the temperature difference towards the fin base. Here the parameter M is employed to gauge the influence of convective to conductive heat transfer coefficients ratio and also of porosity of the fin material on the fin thermal behaviour. Hence rise in M signifies increased convective heat transfer due to increase in the ratio or due to increase in surface area with hike in porosity. This results in sharp dip in the fin temperature leading to quick rise in temperature difference as can be seen in the two plots. Thus, higher values of M encourage higher heat transfer rate. Additionally, as can be observed from figure 5.8, the temperature difference at the fin base attains highest value for spherical-spherical combination of nanoparticle shapes. Thus, the considered combination extracts heat quickly from the prime surface via the fin base and results in higher rate of heat loss from the base.

The motive of plotting figures 5.9 and 5.10 is to recognize the behaviour of temperature field and temperature gradient of rectangular profiled radial fin respectively in the presence of hybrid nanofluid upon variation in wet fin parameter n_1. It can be seen from figure 5.9 that lower thermal profiles are th result of higher values of n_1. Also, from figure 5.10 it can be deciphered that n_1 increases the temperature difference at the base of the fin structure. Here, the parameter n_1 encloses the variations in the fin surface temperature due to wet nature of the fin and the wet environment improves the heat transmission via

convection. Further, the spherical-platelet nanoparticle shape combination improves the distribution of temperature towards the fin tip for the similar reasons as explained before.

Figures 5.11 and 5.12 illustrate the dependence of temperature profile and thermal gradient of a radial fin wetted in a hybrid nanofluid on the exponential index m. It can be noticed that with rise in m values there is increased distribution of temperature as shown in figure 5.11. On the other hand, the difference in temperature towards the fin base has decreased with uplifting values of m as depicted in figure 5.12. Here $m = 0$ connects to linear case and $m \neq 0$ connects to nonlinear case. As m moves from 0 to 2 the dependence of heat transfer coefficient on temperature rises whereas its value decreases resulting in lesser heat transmission through convection. Additionally, spherical-spherical nanoparticle combination has lower thermal profiles than spherical-cylindrical ones followed by spherical-platelet combination.

The dimensionless ambient temperature's impact on the thermal profile and temperature gradient of porous radial fin exposed to convective-radiative heat loss has been sketched in figures 5.13 and 5.14 respectively. It is noted that higher values of θ_a result in higher thermal profiles as in figure 5.13. And higher thermal gradient profiles are outcome of lower values of θ_a as in figure 5.14. This is because of direct impact of this parameter on the convective heat removal mechanism. Further the three different combinations of nanoparticle shapes affect the heat transfer in the fin system in a similar trend as explained before.

The influence of Peclet number Pe on the energy graph and thermal gradient graph of a moving radial fin exposed to shape-dependent hybrid nanofluid flow has been depicted in figures 5.15 and 5.16 respectively. As can be seen in figure 5.15 higher thermal profiles correspond to higher values of Peclet number and from figure 5.16 it can be inferred

that Peclet number has a negative influence on the temperature difference parameter. This is because with rise in Peclet number the speed of hybrid nanofluid flow past the fin structure increases resulting in decrease in interaction time between solid and fluid structures leading to rise in the local fin temperature. Further, as explained earlier the spherical-platelet combination of nanoparticles enhance the distribution of temperature throughout the fin length followed by spherical-cylindrical and spherical-spherical ones.

5.4.2 Thermal Efficiency Analysis:

The thermal efficiency of a radial fin exposed to shape-dependent hybrid nanofluid for simultaneous variation in the convective parameter Nc and radiative parameter Nr has been illustrated in figure 5.17. It is observed that thermal efficiency of fin degrades with increase in the parameters Nc and Nr. This is because the rise in these parameters results in decrease in temperature distribution with fin length resulting in increase in the deviation of the actual fin case from the ideal one. On the other hand, the consequence of thermogeometric parameter M and wet parameter n_1 on the thermal efficiency of a radial fin is as depicted in figure 5.18. It can be concluded that fin efficiency has a negative influence from parameters M and n_1. The reason behind this behaviour can be explained with the similar reasons as above.

The figure 5.19 depicts the influence of nanoparticle volume fraction φ and Peclet number Pe on the efficiency of a moving radial fin fully wetted in shape-dependent hybrid nanofluid. It is noticed that efficiency rises with uplifting values of φ and Pe. This is because the elevation in the concentration of the hybrid nanofluid helps in improving the porous fin's overall thermal conductivity and thus enhances the spatial distribution of temperature. On the other hand, Peclet number as explained before helps in better

temperature distribution leading to enhanced fin efficiency. Thus, the application of hybrid nanofluid instead of simple base fluid and the moving fin in the place of a stationary fin enhance the fin efficiency. Additionally, from the figures 5.17, 5.18 and 5.19 one can notice that spherical-platelet shaped nanoparticle combination results in higher fin efficiency as compared to spherical-cylindrical and spherical-spherical combinations. This is because as explained earlier the spherical-platelet combination enhances the temperature distribution leading to increased fin efficiency.

5.5 Denouement

The current study examined the thermal behaviour and efficiency of a radial fin exposed to the flow of a shape-dependent hybrid nanofluid. The results have been graphically described utilizing the solutions obtained via the RKF45 technique. The prominent explorations of the study are as followed:

- The convective and thermogeometric parameters along with the wet and radiative environment hike the temperature drop towards the fin base and thus enhance the heat extraction from the prime surface.

- The temperature distribution along the fin length and the thermal fin efficiency have a hike of 1.2% and 2% respectively as Peclet number varies from 1 to 3.

- The exposure of fin to hybrid nanofluid has a prominent effect on its thermal efficiency. There is a hike of 2% in thermal fin efficiency as the total nanoparticle volume fraction raises from 0.01% to 0.1%.

- Nanoparticle shape also has a significant impact on the temperature distribution

along the fin length as well as the thermal fin efficiency. Both have been recorded highest for spherical-platelet combination of the nanoparticles with spherical-cylindrical and spherical-spherical combinations followed by it.

- The heat transmission rate at the fin base is also affected by the distinct combination of nanoparticle shapes. It is highest in the case of spherical-spherical combination followed by spherical-cylindrical and spherical-platelet ones.

Table 5.1: Thermophysical properties of water and nanoparticles [**?**].

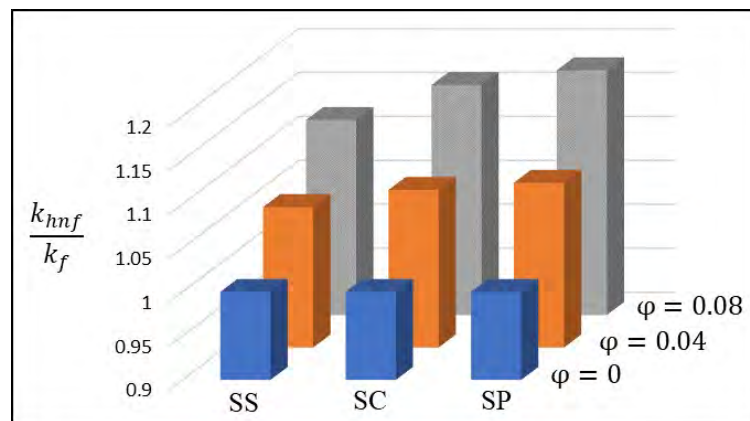| Property	Water	Al_2O_3	Ag	CNT	Graphene
$\rho(kgm^{-3})$	997.1	3970	10500	2100	2200
$C_p(J/kgK)$	4179	765	235	410	790
$k(W/mK)$	0.613	40	429	3007.4	5000
$\beta(K^{-1}) * 10^{-5}$	21	2.4	5.4	2	-0.8
Shape	$-$	Spherical	Spherical	Cylindrical	Platelet

Figure 5.2: Repercussion of nanoparticle volume fraction φ and distinct combination of nanoparticle shapes on thermal conductivity of hybrid nanofluid.
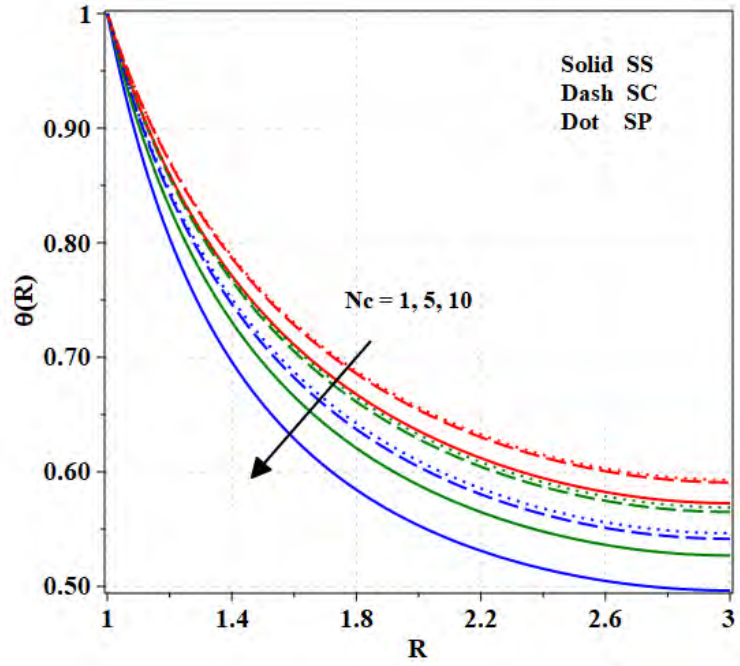
Figure 5.3: Repercussion of convective parameter Nc and distinct combination of nanoparticle shapes on fin thermal field.
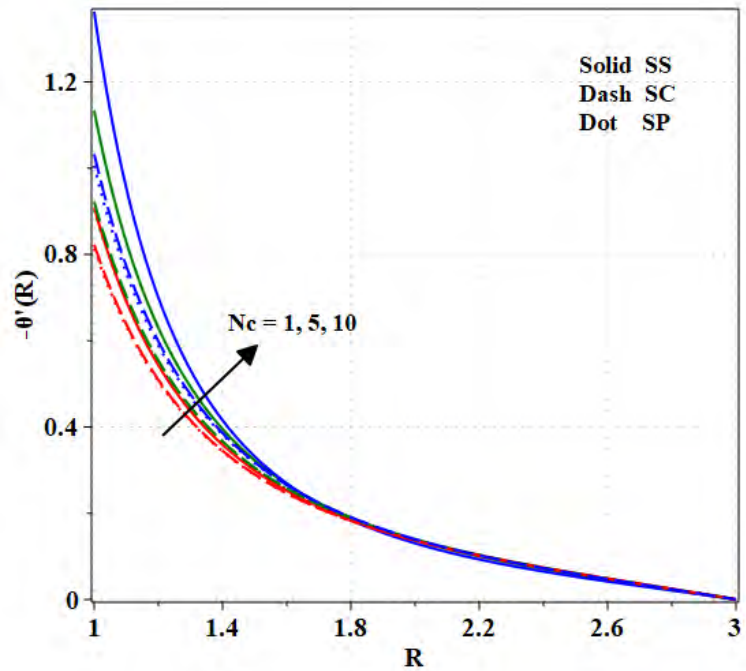

Figure 5.4: Repercussion of convective parameter Nc and distinct combination of nanoparticle shapes on fin thermal gradient.
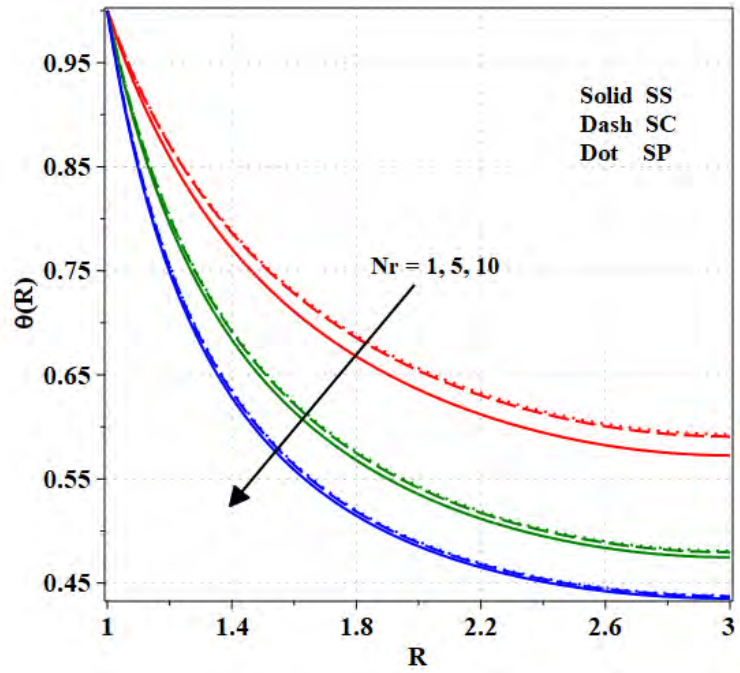
Figure 5.5: Repercussion of radiative parameter Nr and distinct combination of nanoparticle shapes on fin thermal field.
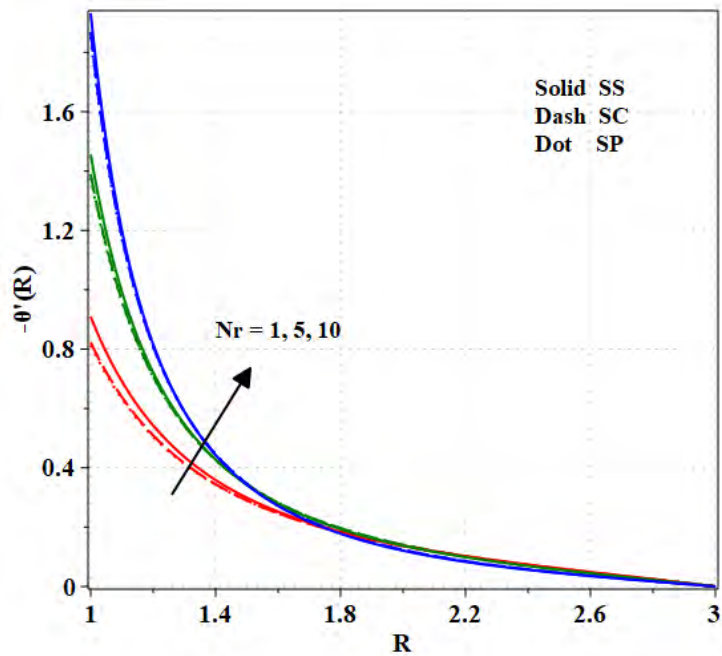

Figure 5.6: Repercussion of radiative parameter Nr and distinct combination of nanoparticle shapes on fin thermal gradient.
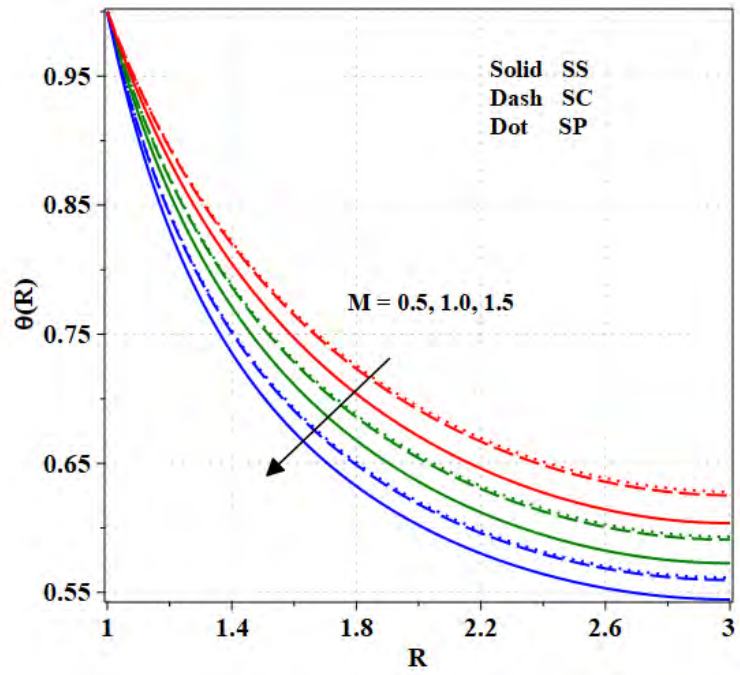
Figure 5.7: Repercussion of thermogeometric parameter M and distinct combination of nanoparticle shapes on fin thermal field.

Figure 5.8: Repercussion of thermogeometric parameter M and distinct combination of nanoparticle shapes on fin thermal gradient.

Figure 5.9: Repercussion of wet fin parameter n_1 and distinct combination of

nanoparticle shapes on fin thermal field.

Figure 5.10: Repercussion of wet fin parameter n_1 and distinct combination of nanopar-

ticle shapes on fin thermal gradient.
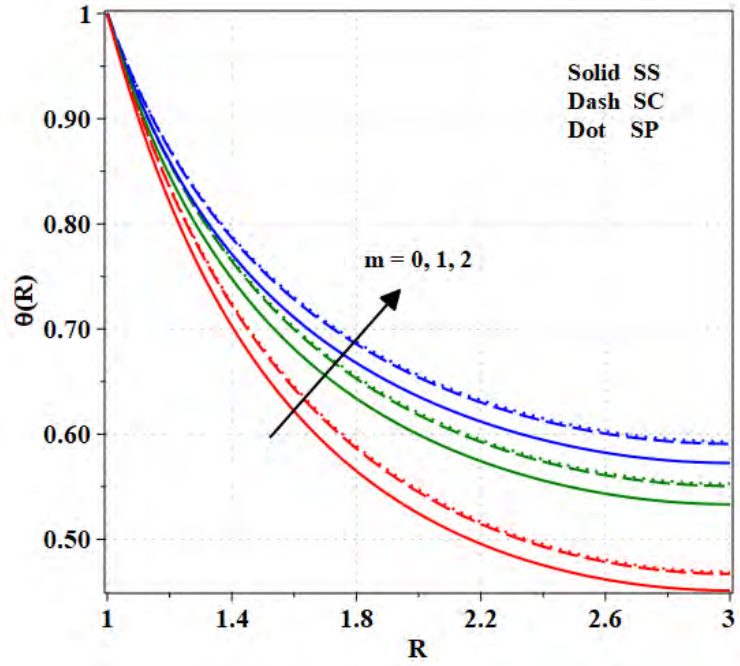
Figure 5.11: Repercussion of exponential index m and distinct combination of nanoparticle shapes on fin thermal field.
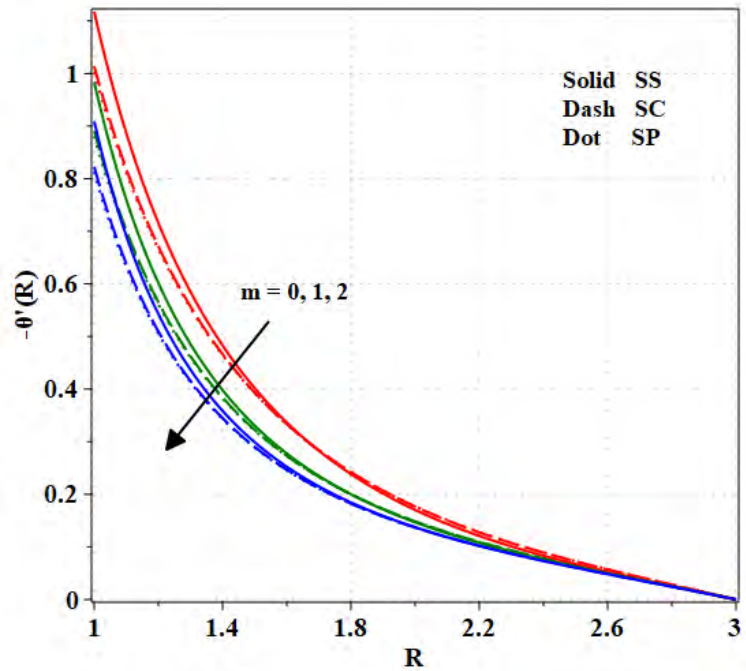
Figure 5.12: Repercussion of exponential index m and distinct combination of nanoparticle shapes on fin thermal gradient.
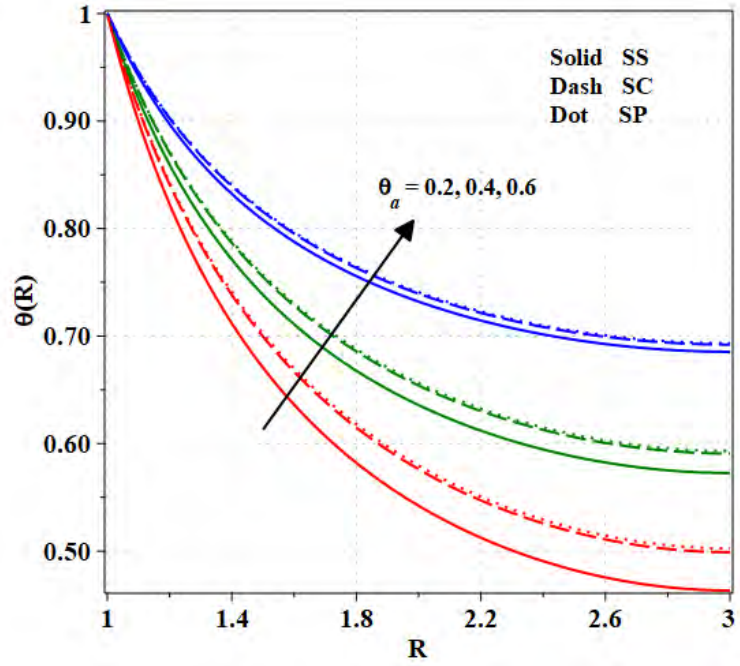
Figure 5.13: Repercussion of dimensionless ambient temperature θ_a and distinct combination of nanoparticle shapes on fin thermal field.
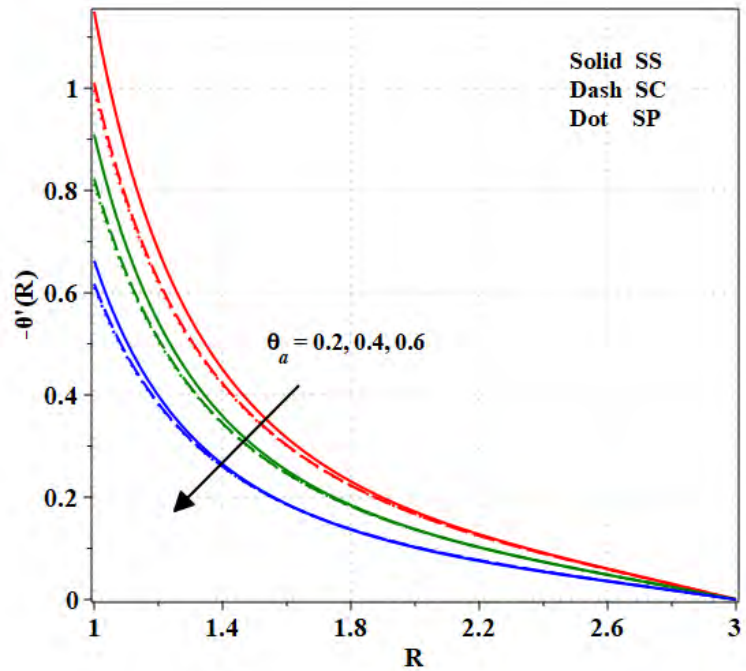
Figure 5.14: Repercussion of dimensionless ambient temperature θ_a and distinct combination of nanoparticle shapes on fin thermal gradient.
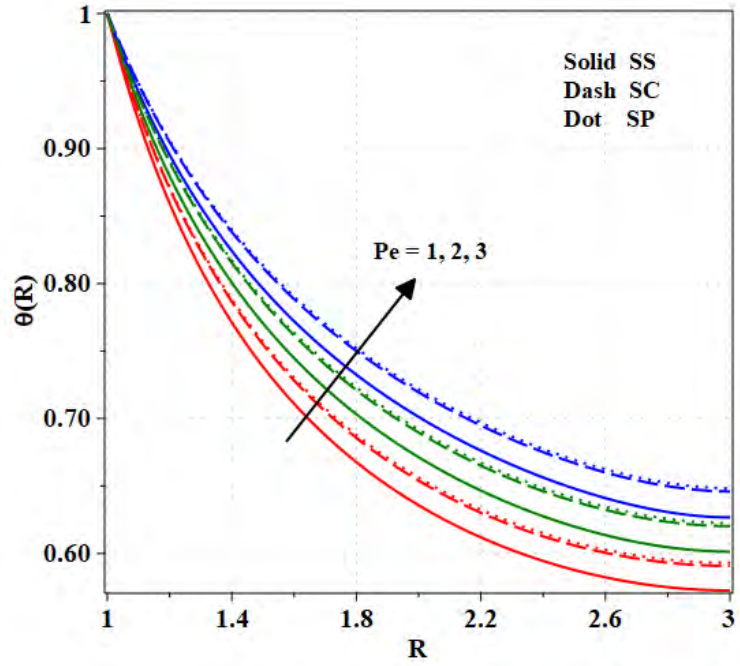
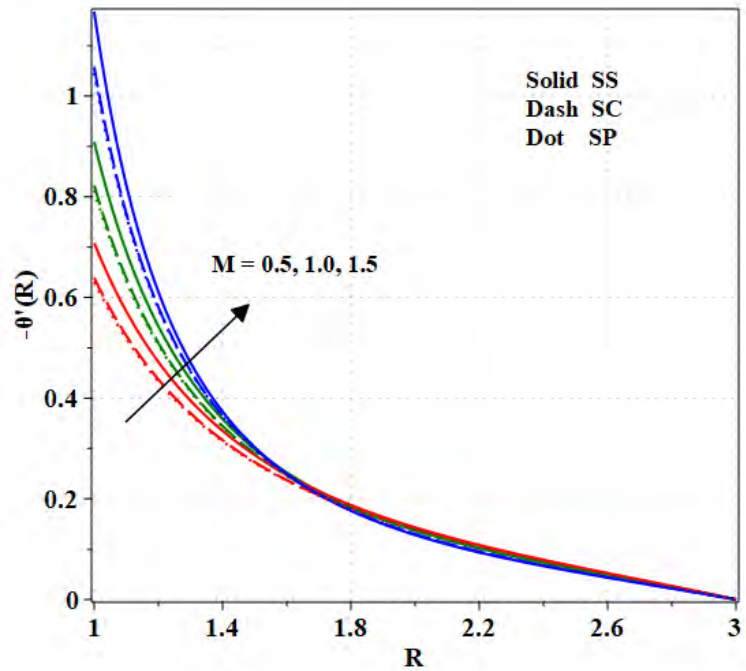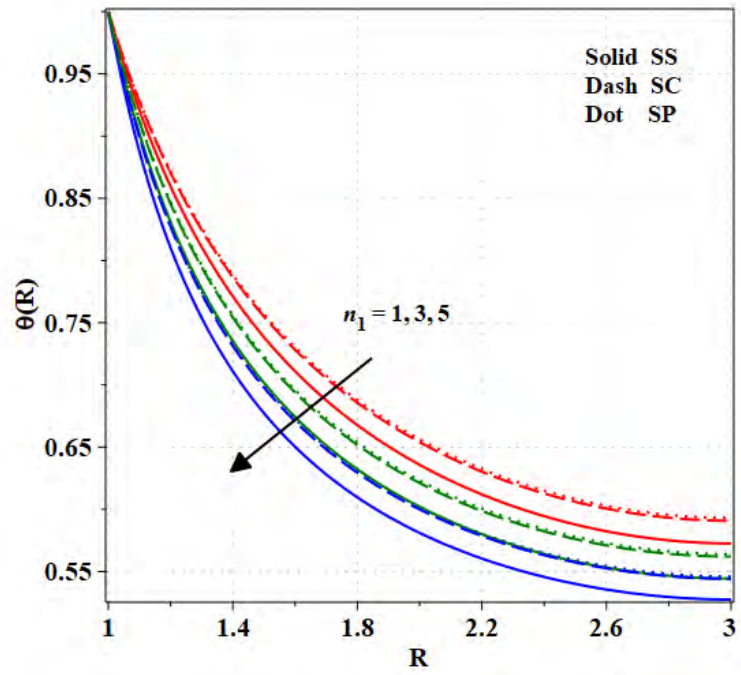Figure 5.15: Repercussion of Peclet number Pe and distinct combination of nanoparticle shapes on fin thermal field.
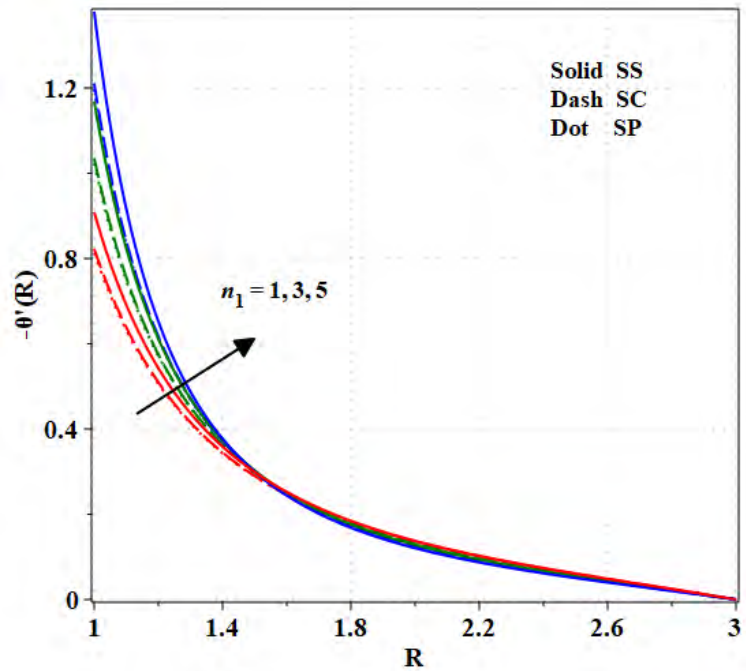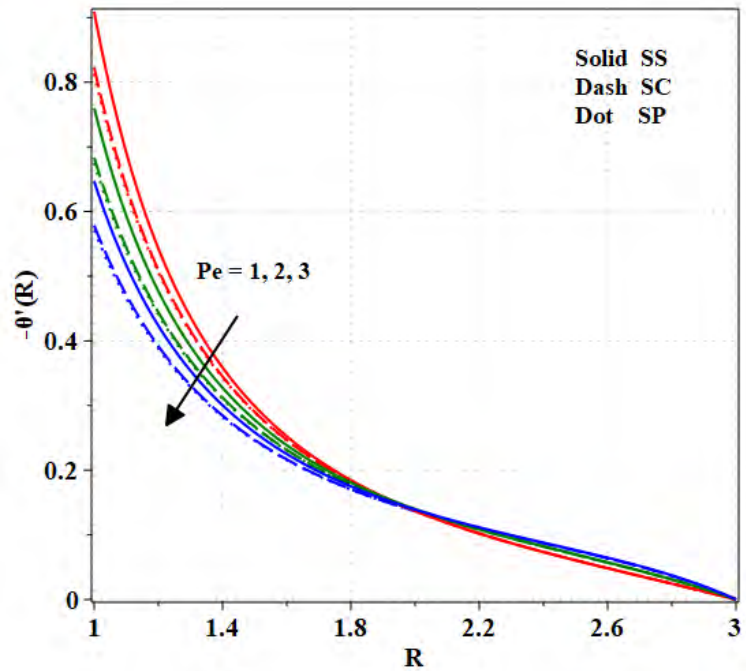

Figure 5.16: Repercussion of Peclet number Pe and distinct combination of nanoparticle shapes on fin thermal gradient.

97
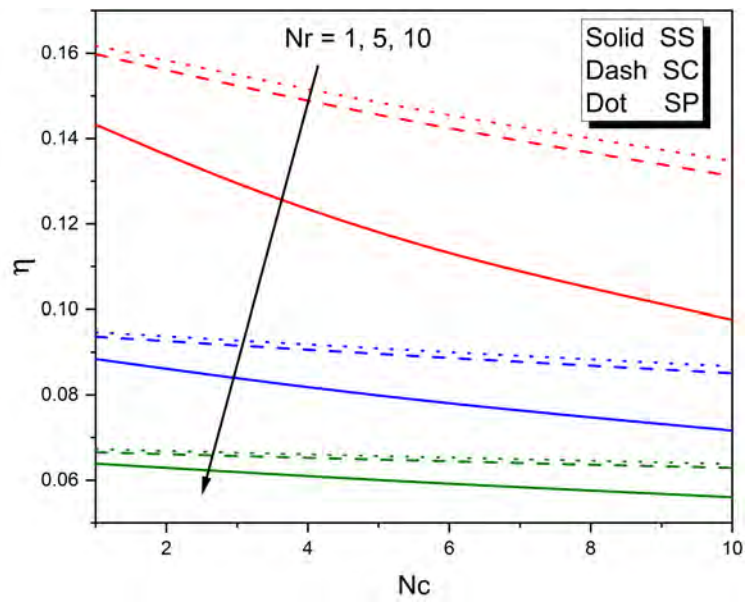
Figure 5.17: Repercussion of Nc and Nr along with distinct combination of nanoparticle shapes on fin thermal efficiency.
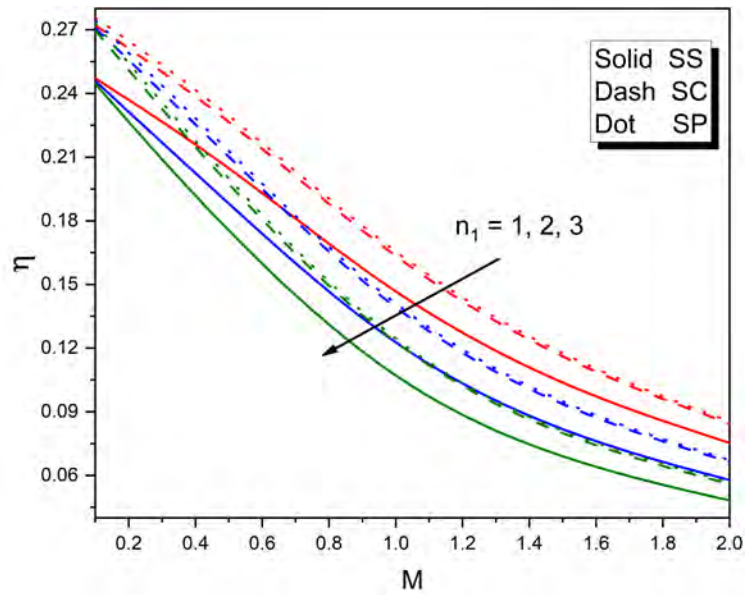
Figure 5.18: Repercussion of n_1 and M along with distinct combination of nanoparticle shapes on fin thermal efficiency.
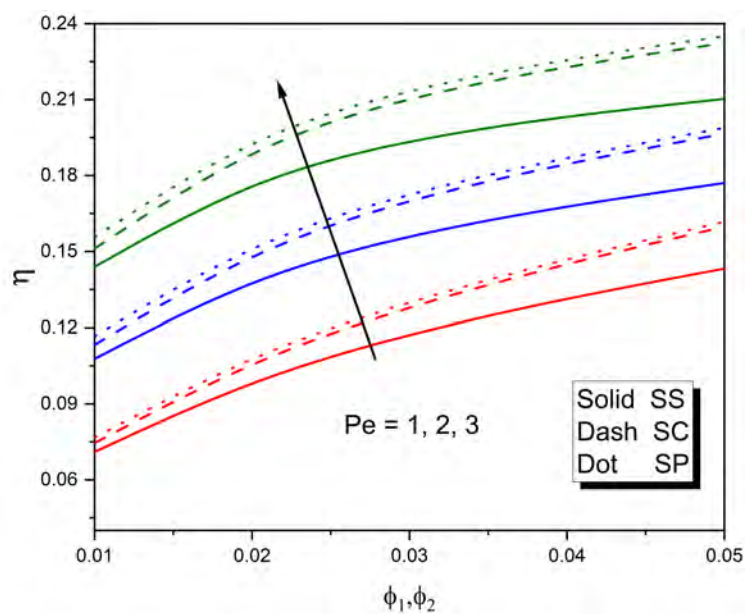
Figure 5.19: Repercussion of φ and Pe along with distinct combination of nanoparticle shapes on fin thermal efficiency.

Chapter 6

Role of Surface Roughness on the Transient Thermal Behaviour of Convective-Radiative Distinct Pin Fin Structures

6.1 Prelims

The MEMS (Microelectromechanical systems) technologies frequently produce rough surfaces and the repercussion of roughness on the thermal performance is more prominent in structures of smaller dimensions. In this regard, the present chapter intends to examine the unsteady thermal behaviour of fully wet, porous, and rough micro-pin fin structures under convective-radiative conditions. Here, pin fin structures of cylindrical, conical and convex parabolic profiles have been chosen. The problem is modelled by incorporating the roughness parameters in the perimeter and cross-sectional area of the pin fin. The resulting PDEs are nonlinear and of second order which have been solved by employing the FDM. The impact of roughness parameter, wet porous parameter, dimensionless time and other relevant parameters on the thermal performance and efficiency of rough micro-pin fin structures has been established graphically. According to the findings, rise in roughness causes an increase in efficiency. Further, the work is beneficial in the field of

microelectronics, especially in the design of micro-pin fin structures.

6.2   Modeling and Interpretation

6.2.1   Heat Transfer
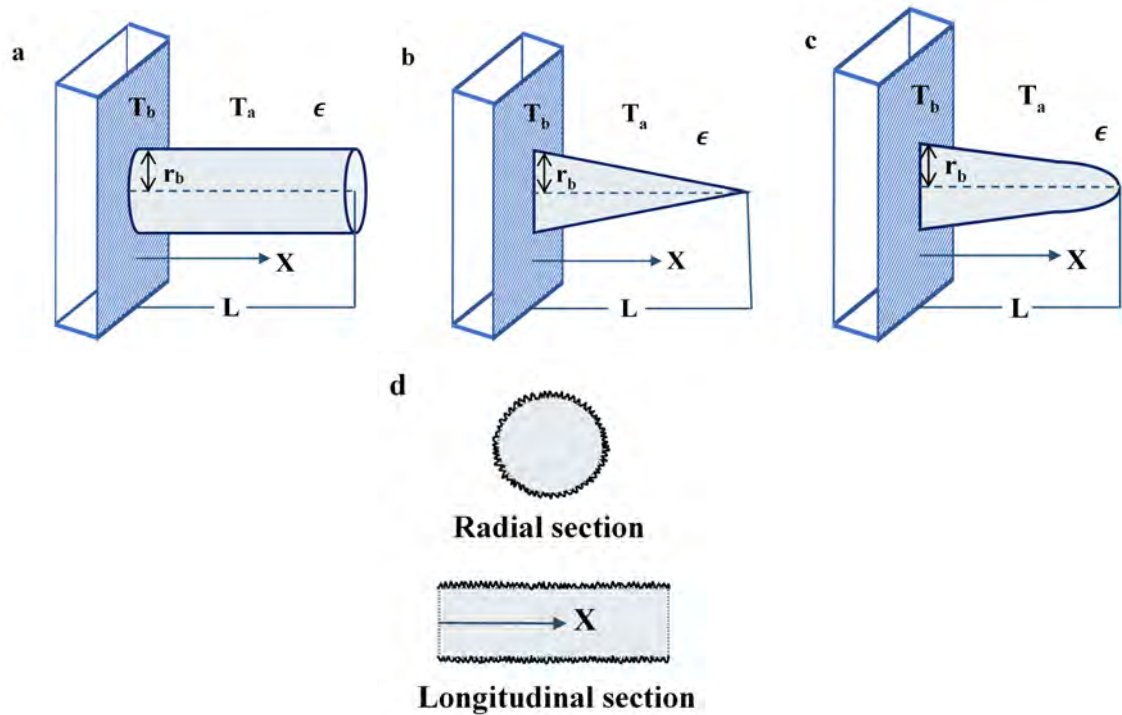
Figure 6.1: Schematic representation of cylindrical pin fin (a), conical pin fin (b), convex parabolic pin fin (c) and variation in roughness along radial and longitudinal cross-sections.

Consider pin fin structures of cylindrical, conical and convex parabolic profiles of length L and base radius r_b as in figure 6.1. The fin material is porous, homogeneous, and isotropic. The solid matrix is fully wetted in a single-phase fluid and the fluid-solid interactions are governed by Darcy's law. At time $t = 0$, the fin surface is maintained at the same temperature as the ambient fluid. But at $t > 0$, there is a step rise in temperature of the surface to which the fin base is attached. Then the fin base starts receiving heat

from the surface maintained at temperature T_b and loses heat through convection and radiation to the ambient fluid at temperature T_a. The fin surface is assumed rough with relative roughness of ϵ. Further, the cross-sectional area and the perimeter of rough pin fin are assumed to be functions of surface roughness. The fin is subject to motion with a uniform velocity $\bar{U}$. Besides, the thermal conductivity and the heat transfer coefficient of convection are assumed to be functions of fin surface temperature. Since for the fin to be effective, the transverse Biot number has to be kept at a minimum, the heat conduction is assumed to be one-dimensional i.e., along the axial direction of the pin fin. Also, the tip of the fin is assumed to be adiabatic in nature.

The energy balance equation for the rough micro-pin fin under unsteady condition is given by,

$$\rho C_p \bar{A}_c(x)\frac{\partial T}{\partial t} = \frac{\partial}{\partial x}\left(k(T)\bar{A}_c(x)\frac{\partial T}{\partial x}\right) - \rho \bar{v}(x)\bar{P}(x)C_p(T - T_a) - \varepsilon\sigma \bar{P}(x)(T^4 - T_a^4)$$

$$- h(T)\bar{P}(x)(1 - \hat{\phi})(T - T_a) - h_D\bar{P}(x)l_{fg}(1 - \hat{\phi})(\bar{\omega} - \bar{\omega}_s)$$

$$+ \rho C_p \bar{U} \bar{A}_c(x)\frac{\partial T}{\partial x}. \tag{6.2.1}$$

The fluid velocity through porous fin $\bar{v}(x)$, the convective heat transfer coefficient $h(T)$ and the thermal conductivity $k(T)$ are respectively given by equations (1.2.6), (1.2.9) and (2.2.4).

The cross-sectional area and perimeter of the rough micro-pin fin are given by [?] [?],

$$\bar{A}_c(x) = \pi \bar{r}(x)^2 + 2\pi r_b^2 \epsilon^2, \tag{6.2.2}$$

$$\bar{P}(x) = 2\pi \bar{r}(x)\sqrt{1 + m_{\bar{\sigma}}^2}. \tag{6.2.3}$$

where, ϵ is the relative roughness and $m_{\bar{\sigma}}$ is the mean absolute surface slope. Consider

[?],

$$\bar{r}(x) = r_b \left(\frac{x}{L}\right)^n,$$ (6.2.4)

where,

$n = 0$ is the cylindrical pin fin,

$n = 1$ is the conical pin fin,

$n = \frac{1}{2}$ is the convex parabolic pin fin.

Further [?] [?],

$$\frac{\partial \bar{A}_c}{\partial x} = \frac{\partial A_c}{\partial x} + 2\pi \bar{r}(x) m_{\bar{\sigma}}.$$ (6.2.5)

The artificial surface roughness parameter ϵ in terms of base radius of the pin fin r_b is

given as [?] [?],

$$\epsilon = \frac{\bar{\sigma}}{r_b}.$$ (6.2.6)

The mean absolute slope of surface roughness is given by [?] [?] [?],

$$m_{\bar{\sigma}} = 0.076 \bar{\sigma}^{0.52}.$$ (6.2.7)

Now, utilizing the parameters in equations (1.2.6), (1.2.9) and (2.2.4) along with equations

(6.2.2) to (6.2.7), the equation (6.2.1) reduces to,

Case 1: Cylindrical pin fin

$$(1 + 2\epsilon^2)\frac{\rho C_p}{k_a}\frac{\partial T}{\partial t} = (1 + \alpha^*(T - T_a))(1 + 2\epsilon^2)\frac{\partial^2 T}{\partial x^2} + (1 + \alpha^*(T - T_a))\frac{2m_{\bar{\sigma}}}{r_b}\frac{\partial T}{\partial x}$$

$$+ \alpha^*(1 + 2\epsilon^2)\left(\frac{\partial T}{\partial x}\right)^2 + \frac{\rho C_p \bar{U}}{k_a}(1 + 2\epsilon^2)\frac{\partial T}{\partial x} - \frac{2\rho g K \beta_f C_p \sqrt{1 + m_{\bar{\sigma}}^2}}{\nu_f k_a r_b}(T - T_a)^2$$

$$- \frac{2h_a l_{fg}(\bar{\omega} - \bar{\omega}_s)\sqrt{1 + m_{\bar{\sigma}}^2}(1 - \hat{\phi})(T - T_a)^m}{k_a r_b C_p Le^{\frac{2}{3}}(T_b - T_a)^m} - \frac{2h_a(1 - \hat{\phi})\sqrt{1 + m_{\bar{\sigma}}^2}(T - T_a)^{m+1}}{(T_b - T_a)^m k_a r_b}$$

$$- \frac{2\sigma\varepsilon\sqrt{1 + m_{\bar{\sigma}}^2}}{k_a r_b}(T^4 - T_a^4).$$ (6.2.8)

Case 2: Conical pin fin

$$\left(\frac{x^2}{L^2} + 2\epsilon^2\right) \frac{\rho C_p}{k_a} \frac{\partial T}{\partial t} = (1 + \alpha^*(T - T_a)) \left(\frac{x^2}{L^2} + 2\epsilon^2\right) \frac{\partial^2 T}{\partial x^2} + \alpha^* \left(\frac{x^2}{L^2} + 2\epsilon^2\right) \left(\frac{\partial T}{\partial x}\right)^2$$

$$+ 2(1 + \alpha^*(T - T_a)) \frac{x}{L^2} \left(1 + \frac{m_{\bar{\sigma}} L}{r_b}\right) \frac{\partial T}{\partial x} + \frac{\rho C_p \bar{U}}{k_a} \left(\frac{x^2}{L^2} + 2\epsilon^2\right) \frac{\partial T}{\partial x}$$

$$- \frac{2\rho g K \beta_f C_p \sqrt{1 + m_{\bar{\sigma}}^2}}{\nu_f k_a r_b} \frac{x}{L} (T - T_a)^2 - \frac{2h_a(1 - \hat{\phi})\sqrt{1 + m_{\bar{\sigma}}^2}}{k_a r_b} \frac{x}{L} \frac{(T - T_a)^{m+1}}{(T_b - T_a)^m}$$

$$- \frac{2h_a l_{fg}(\bar{\omega} - \bar{\omega}_s)\sqrt{1 + m_{\bar{\sigma}}^2}(1 - \hat{\phi})}{k_a r_b C_p Le^{\frac{2}{3}}} \frac{x}{L} \frac{(T - T_a)^m}{(T_b - T_a)^m} - \frac{2\sigma\varepsilon\sqrt{1 + m_{\bar{\sigma}}^2}}{k_a r_b} \frac{x}{L} (T^4 - T_a^4). \tag{6.2.9}$$

Case 3: Convex parabolic pin fin

$$\left(\frac{x}{L} + 2\epsilon^2\right) \frac{\rho C_p}{k_a} \frac{\partial T}{\partial t} = (1 + \alpha^*(T - T_a)) \left(\frac{x}{L} + 2\epsilon^2\right) \frac{\partial^2 T}{\partial x^2} + \alpha^* \left(\frac{x}{L} + 2\epsilon^2\right) \left(\frac{\partial T}{\partial x}\right)^2$$

$$+ \frac{(1 + \alpha^*(T - T_a))}{L} \left(1 + 2\left(\frac{x}{L}\right)^{\frac{1}{2}} \frac{m_{\bar{\sigma}} L}{r_b}\right) \frac{\partial T}{\partial x} + \frac{\rho C_p \bar{U}}{k_a} \left(\frac{x}{L} + 2\epsilon^2\right) \frac{\partial T}{\partial x}$$

$$- \frac{2\rho g K \beta_f C_p \sqrt{1 + m_{\bar{\sigma}}^2}}{\nu_f k_a r_b} \left(\frac{x}{L}\right)^{\frac{1}{2}} (T - T_a)^2 - \frac{2\sigma\varepsilon\sqrt{1 + m_{\bar{\sigma}}^2}}{k_a r_b} \left(\frac{x}{L}\right)^{\frac{1}{2}} (T^4 - T_a^4)$$

$$- \frac{2h_a l_{fg}(\bar{\omega} - \bar{\omega}_s)\sqrt{1 + m_{\bar{\sigma}}^2}(1 - \hat{\phi})}{k_a r_b C_p Le^{\frac{2}{3}}} \left(\frac{x}{L}\right)^{\frac{1}{2}} \frac{(T - T_a)^m}{(T_b - T_a)^m}$$

$$- \frac{2h_a(1 - \hat{\phi})\sqrt{1 + m_{\bar{\sigma}}^2}}{k_a r_b} \left(\frac{x}{L}\right)^{\frac{1}{2}} \frac{(T - T_a)^{m+1}}{(T_b - T_a)^m}. \tag{6.2.10}$$

The initial and boundary conditions for the modelled problem are given by,

$$T(x, 0) = 0, \quad T(L, t) = T_b, \quad \frac{\partial}{\partial x} T(0, t) = 0. \tag{6.2.11}$$

Consider the following dimensionless parameters,

$$\theta = \frac{T}{T_b}, \theta_a = \frac{T_a}{T_b}, X = \frac{x}{L}. \tag{6.2.12}$$

Employing the equation (6.2.12), the equations (6.2.8) to (6.2.10) reduce to second order nonlinear non-dimensionalized PDEs given by,

Case 1: Cylindrical pin fin

$$(1 + 2\epsilon^2)\frac{\partial \theta}{\partial \tau} = (1 + A(\theta - \theta_a))(1 + 2\epsilon^2)\frac{\partial^2 \theta}{\partial X^2} + (1 + A(\theta - \theta_a))\frac{2m_{\bar{\sigma}}}{\psi^*}\frac{\partial \theta}{\partial X}$$

$$+ A(1 + 2\epsilon^2)\left(\frac{\partial \theta}{\partial X}\right)^2 - \frac{Nc}{\psi^{*2}}\sqrt{1 + m_{\bar{\sigma}}^2}(\theta - \theta_a)^2 - \frac{Nr}{\psi^{*2}}\sqrt{1 + m_{\bar{\sigma}}^2}(\theta^4 - \theta_a^4)$$

$$- \frac{m_2}{\psi^{*2}}\sqrt{1 + m_{\bar{\sigma}}^2}\frac{(\theta - \theta_a)^{m+1}}{(1 - \theta_a)^m} + \frac{Pe}{\psi^*}(1 + 2\epsilon^2)\frac{\partial \theta}{\partial X} \qquad (6.2.13)$$

Case 2: Conical pin fin

$$(X^2 + 2\epsilon^2)\frac{\partial \theta}{\partial \tau} = (1 + A(\theta - \theta_a))(X^2 + 2\epsilon^2)\frac{\partial^2 \theta}{\partial X^2} + A(X^2 + 2\epsilon^2)\left(\frac{\partial \theta}{\partial X}\right)^2$$

$$+ (1 + A(\theta - \theta_a))\,2X\left(1 + \frac{m_{\bar{\sigma}}}{\psi^*}\right)\frac{\partial \theta}{\partial X} - \frac{Nc}{\psi^{*2}}X\sqrt{1 + m_{\bar{\sigma}}^2}(\theta - \theta_a)^2$$

$$- \frac{Nr}{\psi^{*2}}X\sqrt{1 + m_{\bar{\sigma}}^2}(\theta^4 - \theta_a^4) - \frac{m_2}{\psi^{*2}}X\sqrt{1 + m_{\bar{\sigma}}^2}\frac{(\theta - \theta_a)^{m+1}}{(1 - \theta_a)^m}$$

$$+ \frac{Pe}{\psi^*}(X^2 + 2\epsilon^2)\frac{\partial \theta}{\partial X} \qquad (6.2.14)$$

Case 3: Convex parabolic pin fin

$$(X + 2\epsilon^2)\frac{\partial \theta}{\partial \tau} = (1 + A(\theta - \theta_a))(X + 2\epsilon^2)\frac{\partial^2 \theta}{\partial X^2} + A(X + 2\epsilon^2)\left(\frac{\partial \theta}{\partial X}\right)^2$$

$$+ (1 + A(\theta - \theta_a))\left(1 + 2X^{\frac{1}{2}}\frac{m_{\bar{\sigma}}}{\psi^*}\right)\frac{\partial \theta}{\partial X} - \frac{Nc}{\psi^{*2}}X^{\frac{1}{2}}\sqrt{1 + m_{\bar{\sigma}}^2}(\theta - \theta_a)^2$$

$$- \frac{Nr}{\psi^{*2}}X^{\frac{1}{2}}\sqrt{1 + m_{\bar{\sigma}}^2}(\theta^4 - \theta_a^4) - \frac{m_2}{\psi^{*2}}X^{\frac{1}{2}}\sqrt{1 + m_{\bar{\sigma}}^2}\frac{(\theta - \theta_a)^{m+1}}{(1 - \theta_a)^m}$$

$$+ \frac{Pe}{\psi^*}(X + 2\epsilon^2)\frac{\partial \theta}{\partial X} \qquad (6.2.15)$$

Here, $\tau = \frac{k_a}{\rho C_p L^2}t$ is the dimensionless time, $A = \alpha^* T_b$ is the dimensionless measure of variation of thermal conductivity with temperature, $\psi^* = \frac{r_b}{L}$ is the base radius to length ratio, $Nc = \frac{2\rho g K \beta_f C_p T_b r_b}{\nu_f k_a}$ is the convective parameter, $Nr = \frac{2\sigma \varepsilon r_b T_b^3}{k_a}$ is the radiative parameter, $m_0 = \frac{2h_a r_b(1-\hat{\phi})}{k_a}$, $m_1 = \frac{2h_a l_{fg}(1-\hat{\phi})b_2 r_b}{k_a C_p Le^{\frac{2}{3}}}$, $m_2 = m_0 + m_1$ is the wet porous parameter,

105

$Pe = \frac{\rho C_p \bar{U} r_b}{k_a}$ is the Peclet number.

The associated initial and boundary conditions are given by,

$$\theta(X, 0) = 0, \quad \theta(1, \tau) = 1, \quad \frac{\partial}{\partial X}\theta(0, \tau) = 0. \tag{6.2.16}$$

6.2.2 Scrutinization of Fin Efficiency

Fin efficiency is one of the important parameters in studying the performance of fin structures. The fin efficiency is calculated as,

$$\eta = \frac{Q_f}{Q_{ideal}}. \tag{6.2.17}$$

Here, Q_f is the heat transfer through the fin,

$$Q_f = \int_0^L \left[\begin{array}{c} \left(\frac{h_a l_{fg} b_2 (1-\hat{\phi})\bar{P}}{C_p Le^{\frac{2}{3}}} + (1-\hat{\phi})h_a \bar{P} \right) \frac{(T-T_a)^{m+1}}{(T_b - T_a)^m} \\ + \sigma \varepsilon \bar{P}(T^4 - T_a^4) + \frac{\rho C_p g K \beta_f \bar{P}}{\nu_f}(T - T_a^2) \end{array} \right] dx. \tag{6.2.18}$$

and Q_{ideal} is the heat transfer through the fin when the entire fin surface is maintained at the base temperature,

$$Q_{ideal} = \int_0^L \left[\begin{array}{c} \left(\frac{h_a l_{fg} b_2 (1-\hat{\phi})\bar{P}}{C_p Le^{\frac{2}{3}}} + (1-\hat{\phi})h_a \bar{P} \right) (T_b - T_a) \\ + \sigma \varepsilon \bar{P}(T_b^4 - T_a^4) + \frac{\rho C_p g K \beta_f \bar{P}}{\nu_f}(T_b - T_a^2) \end{array} \right] dx. \tag{6.2.19}$$

Thus, the dimensionless form of the fin efficiency is given by,

Case 1: Cylindrical pin fin

$$\eta = \frac{\int_0^1 \left[m_2 \frac{(\theta - \theta_a)^{m+1}}{(1-\theta_a)^m} + Nr(\theta^4 - \theta_a^4) + Nc(\theta - \theta_a)^2 \right] dX}{m_2(1 - \theta_a) + Nr(1 - \theta_a^4) + Nc(1 - \theta_a^2)}. \tag{6.2.20}$$

Case 2: Conical pin fin

$$\eta = \frac{\int_0^1 \left[m_2 \frac{(\theta - \theta_a)^{m+1}}{(1-\theta_a)^m} + Nr(\theta^4 - \theta_a^4) + Nc(\theta - \theta_a)^2 \right] X dX}{[m_2(1 - \theta_a) + Nr(1 - \theta_a^4) + Nc(1 - \theta_a^2)] \int_0^1 X dX}. \tag{6.2.21}$$

Case 3: Convex parabolic pin fin

$$\eta = \frac{\int_0^1 \left[m_2 \frac{(\theta - \theta_a)^{m+1}}{(1-\theta_a)^m} + Nr(\theta^4 - \theta_a^4) + Nc(\theta - \theta_a)^2 \right] X^{\frac{1}{2}} dX}{[m_2(1 - \theta_a) + Nr(1 - \theta_a^4) + Nc(1 - \theta_a^2)] \int_0^1 X^{\frac{1}{2}} dX}. \tag{6.2.22}$$

6.3   Numerical Elucidation

The second order nonlinear parabolic PDEs (6.2.13) $-$ (6.2.15) and their corresponding initial and boundary conditions as in equation (6.2.16) are the concerned equations. Using the FDM with centered-implicit scheme the solution of the PDEs have been found via the Maple software. The detailed procedure is explained in section (2.3). The results of the present investigation for both the PDEs have been extracted by setting $\Delta X = 0.005$ and $\Delta \tau = 0.005$.

6.4   Deliberation of Results

In this section, the significance of relevant parameters on the energy profile $\theta(X, \tau)$ and fin efficiency η are discussed with the help of graphs. The constant values taken throughout the study are: $Nc = 0.05, Nr = 0.05, m_2 = 0.01, Pe = 0.1, \tau = 1, \psi^* = 0.10, A = 0.1, \epsilon = 0.15, m = 2$ and $\theta_a = 0.1$.

Figure 6.2 (a-c) depicts the temperature field of moving cylindrical, conical and convex parabolic rough micro-pin fin structures upon variation of relative surface roughness parameter ϵ. A negative impact on the thermal drop rate can be observed from the depiction. The higher the roughness lower is the thermal drop rate and hence the fin cools down slower.

To have a better grasp of the role of thermal conductivity parameter A in the cooling process of the fin, its impact on temperature profiles of rough micro-pin fin structures is represented in figure 6.3 (a-c). It is noted that the fin surface temperature elevates with escalating values of parameter A. This can be explained in the following way. The higher the thermal conductivity parameter stronger is the relation between thermal conductivity

k and local fin temperature T. Thus, with an increase in A value, the average thermal conductivity of the fin increases inducing a higher rate of heat conduction in the fin. This causes better temperature distribution along the axial direction of the pin fin resulting in increased fin surface temperature. Hence, for a higher thermal drop rate, lower values of A are preferable. Besides, the three considered pin fin structures are affected in the same trend.

Figure 6.4 (a-c) captures the transient thermal performance of rough cylindrical, conical and convex parabolic micro-pin fin structures for different values of dimensionless time τ. It can be noted that the thermal profile flattens with time and the variations are significant only at the initial stage. This is because, when $\tau = 0$ the fin base temperature is the same as the surrounding temperature and with an increase in time, the base temperature rises resulting in a rise in fin surface temperature. Initially, the fin temperature rises as per elevation in base temperature and after a certain stage, the local fin temperature remains constant with time i.e., the steady-state is achieved. On the other hand, all three pin fins are affected in an analogous manner.

The energy fields of rough cylindrical, conical and convex parabolic micro-pin fin structures for distinct values of the wet porous parameter m_2 have been plotted in figure 6.5 (a-c). It can be observed that the wet porous parameter has a positive impact on the fin heat transfer rate. The parameter m_2 accounts for both the porosity of the fin material and the wet condition around the fin. Further, an upsurge in porosity increases the surface area of the fin and wet nature causes more absorption of heat from the fin surface leading to increased heat loss through convective-radiative ejections. Thus, higher values of m_2 enhance the fin cooling process. Besides, rough micro-fin structures have a higher thermal drop rate than smooth ones.

Figure 6.6 (a-c) portrays the temperature field of three different rough micro-pin fin profiles for distinct values of the base radius to length ratio ψ^*. According to the figure, the thermal profiles are steeper for the slender fin structures. Thus, with an increase in the length of the pin fin or with the decrease in its radius, the fin surface temperature drops faster leading to steeper profiles. Hence, the slender fin structures enhance the heat transfer rate.

Figure 6.7 (a-c) and figure 6.8 (a-c) respectively highlight the effect of convective parameter Nc and radiative parameter Nr on the energy profiles of three distinct rough micro-pin fin structures. It can be noted that the ascending values of Nc enhance the fin thermal drop rate. This is because the upsurge in Nc values increase the permeability thereby increasing the fluid velocity through the solid fin matrix leading to heat loss due to the buoyancy effect. On the other hand, it can be made out that the boosting values of Nr cause a recession in the fin surface temperature along the axial fin direction. The reason is an increased heat loss through the mechanism of radiation. Thus, the escalating values of Nc and Nr aid to the fin cooling process. Besides, the effect of radiative parameter and convective parameter on all three micro-pin fin profiles is analogous.

The results in figure 6.9 (a-c) provided for the exponential index m associated with the heat transfer coefficient h decipher that, ascending values of m enhance the temperature distribution towards the fin tip. Here, $m = 0$ and $m = 1$ represent the linear case whereas $m = 2$ represents the nonlinear case. From the equation of $h(T)$ it can be deciphered that as the m values transit from 0 to 2, the value of h descends from the value of h_a causing a negative impact on the transfer of heat through convection. Thus, it gives rise to higher fin surface temperature and lesser heat transfer rate. Hence, for quicker fin cooling m values must be at a minimum. Further, the effect of m is similar on all three

rough micro-pin fin profiles.

The effect of ambient temperature θ_a on $\theta(X, \tau)$ is depicted in figure 6.10 (a-c). In all the three cases like cylindrical, conical and convex parabolic rough micro fin structures, an increase in the θ_a value increases the fin surface temperature leading to flatter thermal profiles. This can be explained as follows. According to the Newton's law of cooling and the Stefan Boltzmann's law, the heat transfer rate is a strong function of the temperature gap between the bodies. Thus, the lower the ambient temperature, the more is the gap between the fin surface temperature and the surrounding. This induces increased heat loss through convective and radiative mechanisms leading to a decrease in local fin temperature. Thus, lower values of ambient temperature are preferred in the fin cooling process.

Figure 6.11 (a-c) depicts the impact of Peclet number Pe on the thermal profiles of cylindrical, conical and convex parabolic micro pin-fin profiles. It can be observed that the local fin temperature elevates with the hike in the values of Pe. This is due to the decrease in exposure time of ambient fluid with the fin surface area resulting in lesser heat transmission through convection and radiation. Thus, lower values of Peclet number are preferred for the heat transmission enhancement via fin structures.

The consequences of surface roughness parameter ϵ and dimensionless time τ on the thermal efficiency of cylindrical, conical and convex parabolic micro-pin fin structures have been investigated in figure 6.12. It is shown that elevated values of roughness parameter have a positive impact on the efficiency of fin structures. This can be reasoned as follows. As per fin efficiency definition, it can be interpreted that the structures with surface temperature equal to the base temperature are efficient than those with a lesser surface temperature. As the increase in surface roughness causes a rise in fin surface temperature

110

directing towards more efficient fin structures. Thus, smooth micro-pin fin structures are less efficient than rough ones. On the other hand, the behaviour of fin efficiency with dimensionless time has also been demonstrated in the figure. Initially, at $\tau = 0$ the fin efficiency is zero as there is no heat flow within the fin. Then with the ascending time parameter, the base temperature rises sharply, and the heat starts flowing through the fin resulting in a sharp upliftment in the fin efficiency. Eventually, the fin efficiency achieves a steady state.

Figure 6.13 presents the efficiency of all three distinct rough micro-pin fin structures upon variation of thermal conductivity parameter A and base radius to length ratio ψ^*. It is indicated that the upsurge in the values of thermal conductivity parameter A and the ratio ψ^*, leads to increased fin efficiency. This is expected as the rise in parameters A and ψ^* induce improved distribution of temperature along the fin length. Thus the surface temperature of the pin fin increases leading to increased fin efficiency. Thus, slender micro-pin fin structures with higher thermal conductivity are efficient than their counterparts.

Figure 6.14 brings out the efficiency of three distinct profiled rough micro-pin fin structures for diverse values of convective parameter Nc and radiative parameter Nr. It can be noted that with increment in the parameters Nc and Nr the fin efficiency has declined for all three rough fin structures. This is due to subsiding fin surface temperature towards the tip of the fin for escalating values of the considered parameters. Thus, for achieving higher fin efficiency the values of Nc and Nr must be curtailed.

Figure 6.15 presents the efficiency of all three distinct rough micro-pin fin structures upon variation of wet porous parameter m_2 and Peclet number Pe. It is indicated that the upsurge in the values of wet porous parameter m_2 leads to decrease in efficiency and

elevation in the values of Peclet number Pe, leads to increase in fin efficiency. This is expected as the rise in parameter m_2 decreases the fin temperature whereas the hike in the parameter Pe induce improved distribution of temperature along the fin length. Thus the parameter m_2 causes a decrease in the fin temperature resulting in reduced efficiency of fin structures whereas the parameter Pe results in an increase in the surface temperature of the pin fin leading to increased fin efficiency.

Futher in all the figures from (6.12) to (6.15), it can be observed that efficiency of conical profile is the highest followed by convex parabolic and cylindrical micro pin-fin profiles.

6.5   Denouement

The convective-radiative cylindrical, conical and convex parabolic micro-pin fin structures of smooth and rough surfaces subject to motion have been numerically investigated under unsteady conditions. The following conclusions have been derived. The moving pin fin structures with a smooth surface have more thermal drop rate than those with a rough surface. The heat exchange process is driven by the radiative and convective surroundings at the expense of fin efficiency. The porous fin material and the humidity around fin surface accelerate the temperature decline. The surrounding temperature and the exponent related to the coefficient of heat transfer negatively affect the fin heat transfer rate. The thin and long pin fin structures have higher thermal drop rate whereas the thick and short ones are more efficient. The elevation in thermal conductivity with local fin temperature enhances the temperature distribution in the micro-pin fin. Further, it promotes the fin efficiency. The rough micro-pin fin structures are found more efficient than the smooth ones. Fin efficiency increases with time to a certain extent after which it attains a steady
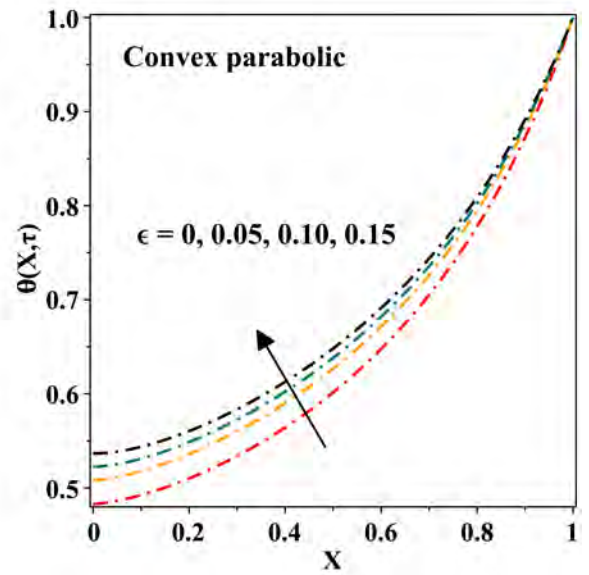
state. Fin efficiency as well as its temperature field achieve higher values with ascending values of Peclet number. The efficiency of conical pin fin is the highest followed by that of convex parabolic and cylindrical ones.
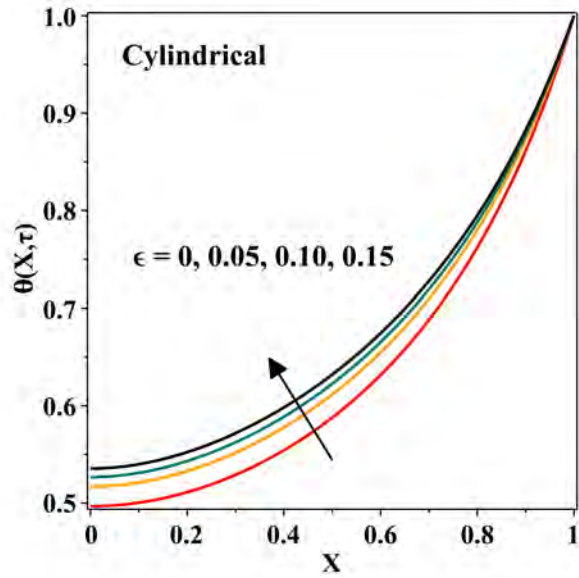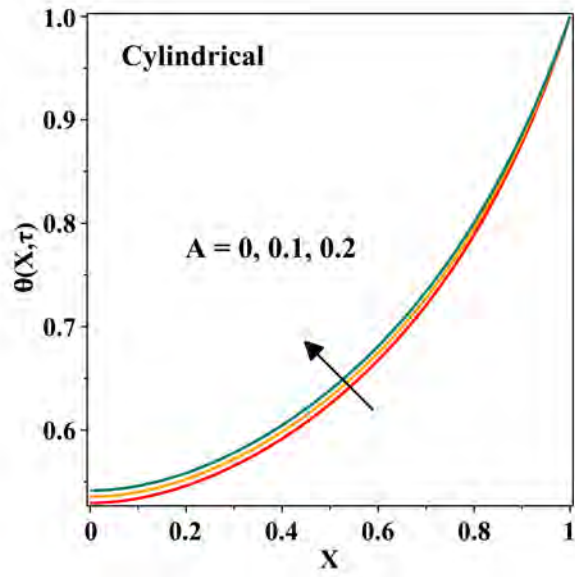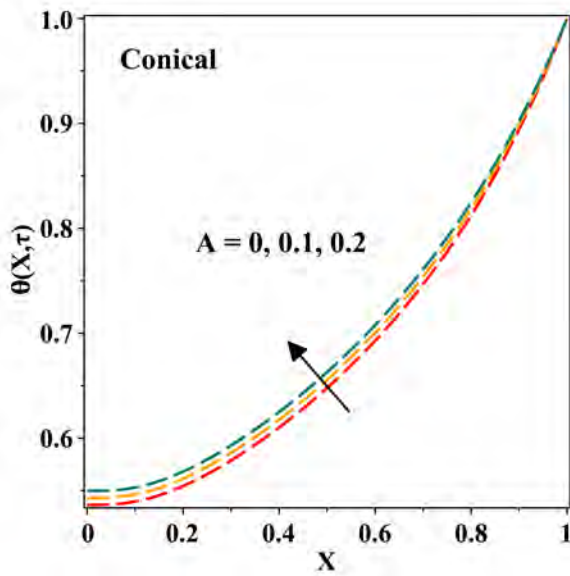

(a)
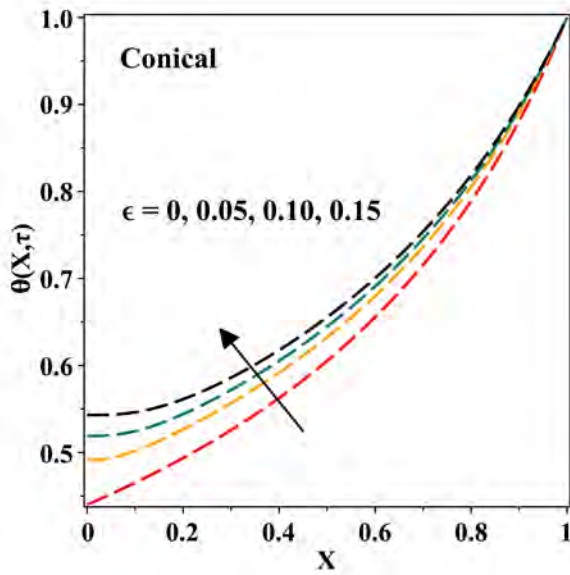
(b)   (c)
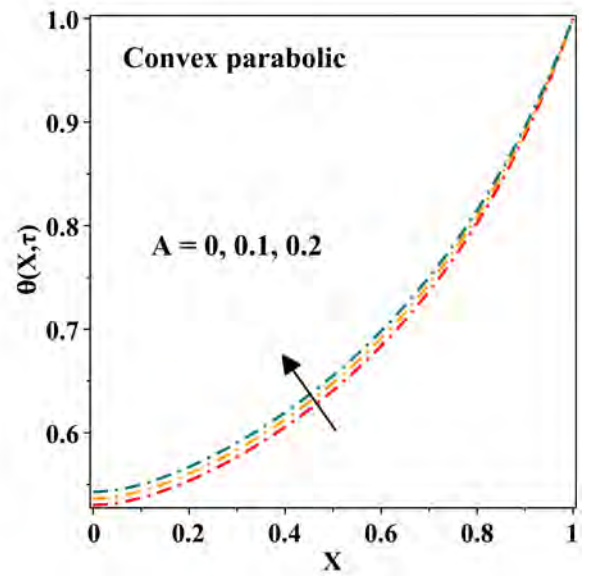
Figure 6.2: Plot of fin temperature values for distinct values of roughness parameter ϵ.

.

(a)

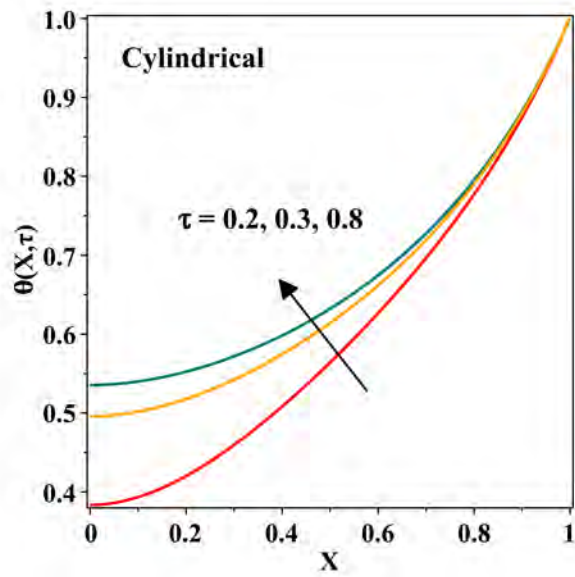(b)   (c)

Figure 6.3: Plot of fin temperature values for distinct values of thermal conductivity parameter A.

.

Figure 6.4: Plot of fin temperature values for distinct values of dimensionless time τ.

.

(a)

(b)   **(c)**

Figure 6.5: Plot of fin temperature values for distinct values of wet porous parameter m_2.

.

116
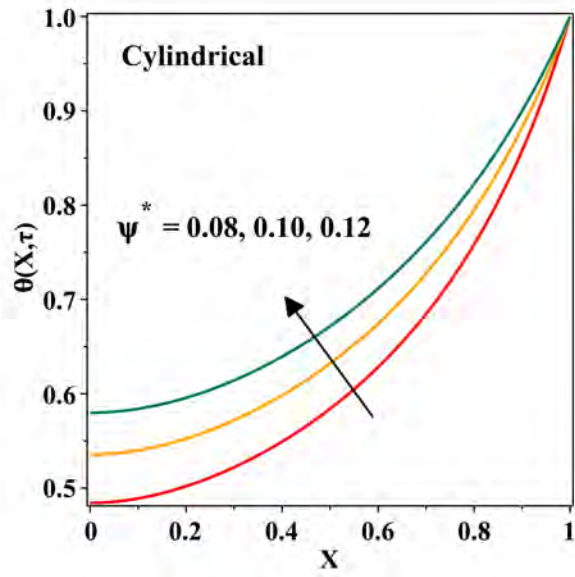
(a)
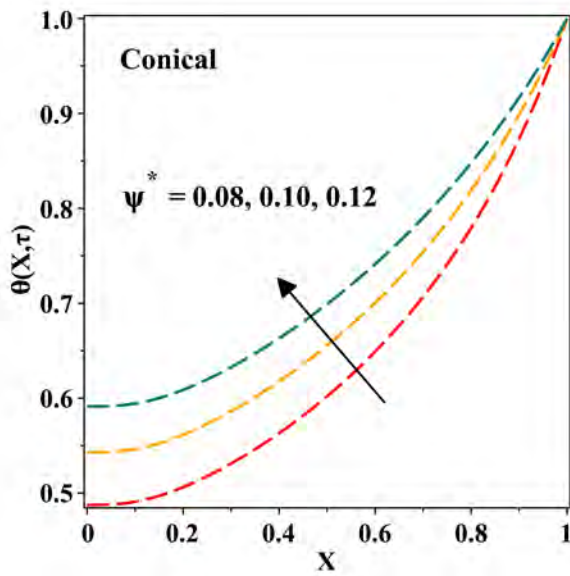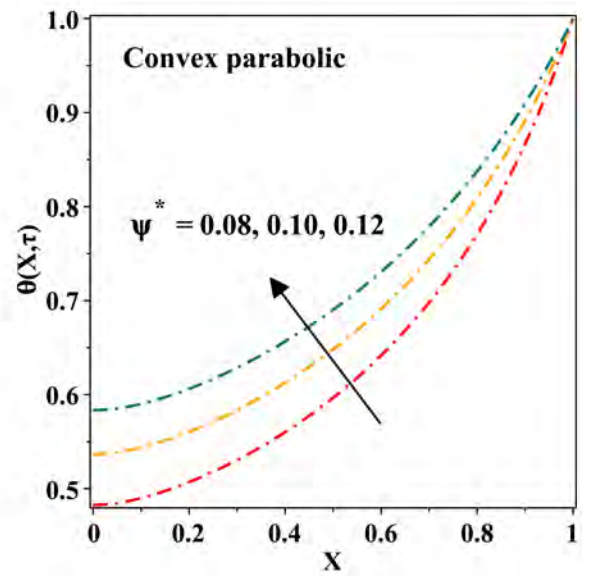
(b)   (c)

Figure 6.6: Plot of fin temperature values for distinct values of base radius to length ratio ψ^*.

.
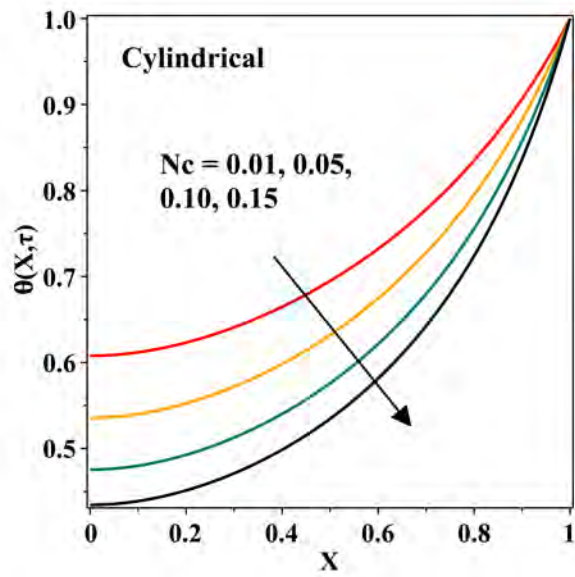
(a)
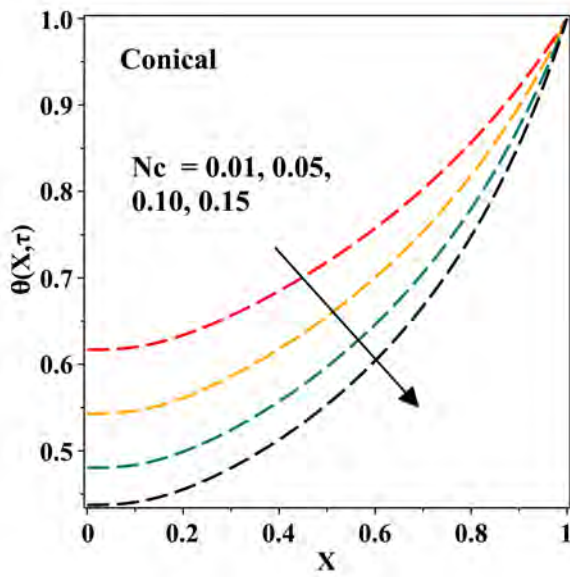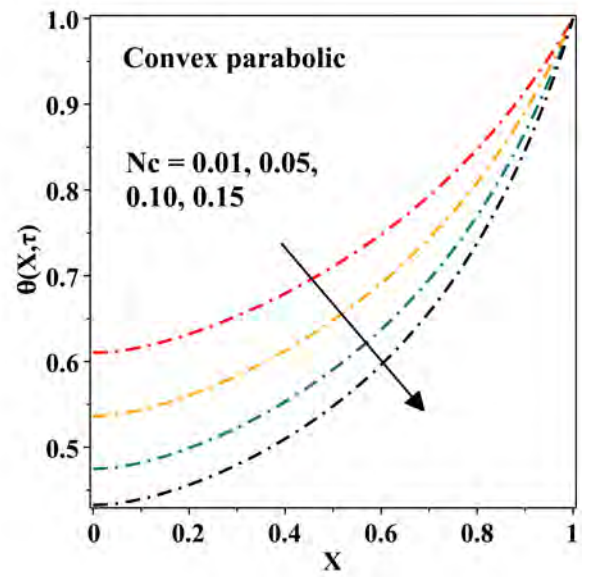
(b)   **(c)**

Figure 6.7: Plot of fin temperature values for distinct values of convective parameter Nc.

.
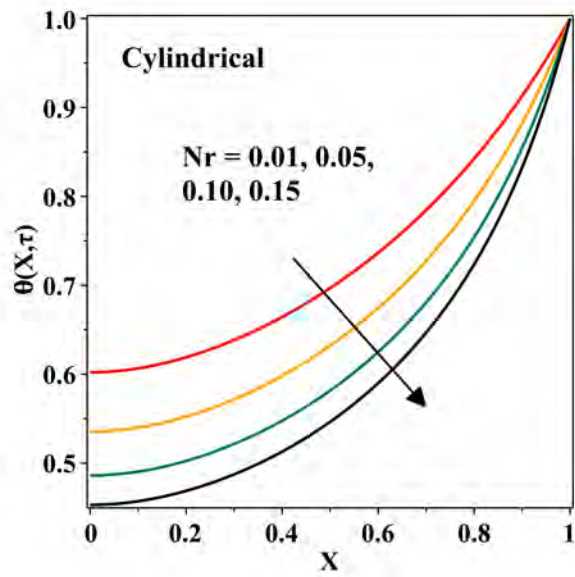
(a)
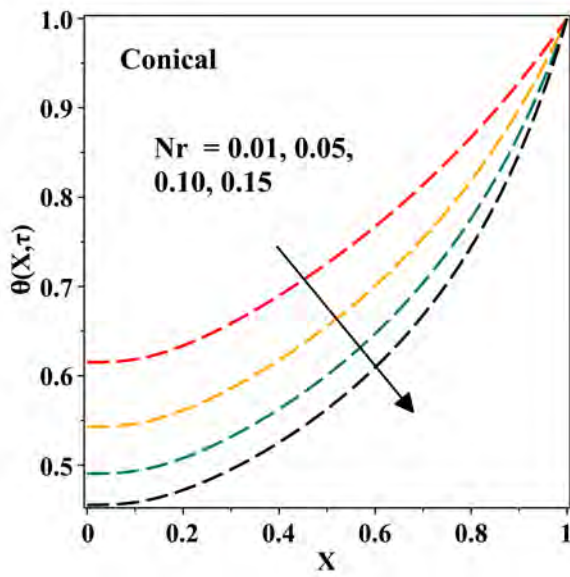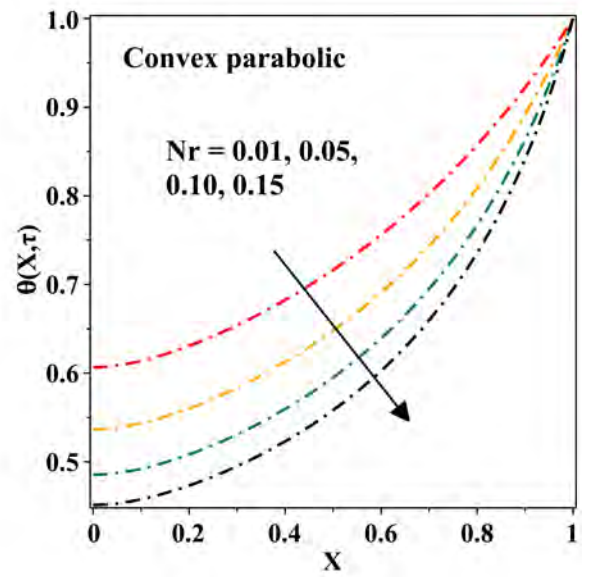
(b)   **(c)**
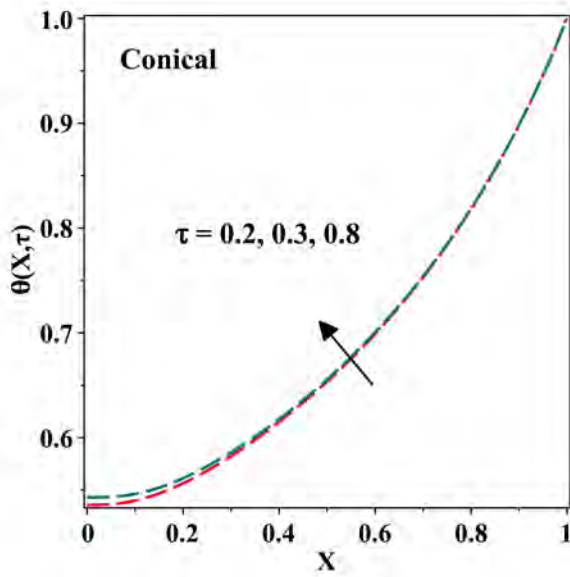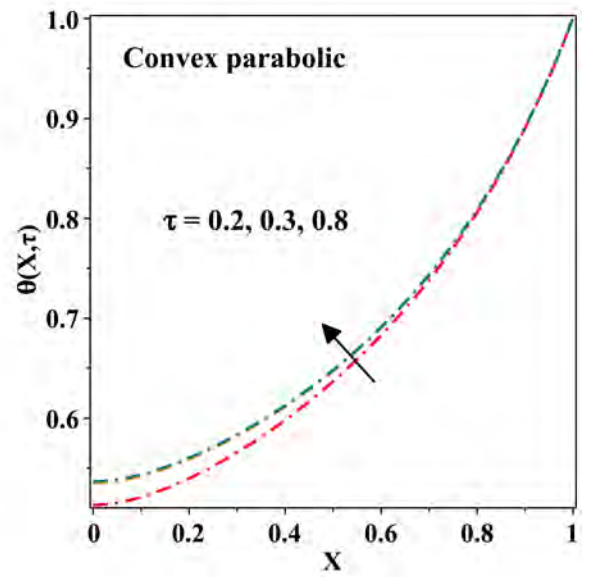
Figure 6.8: Plot of fin temperature values for distinct values of radiative parameter Nr.

.
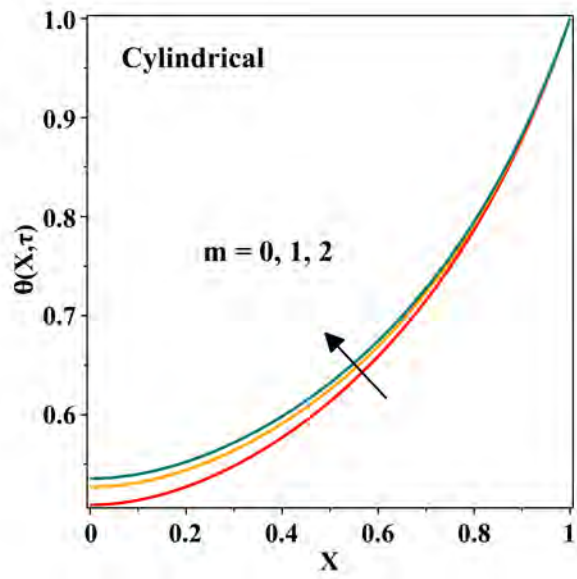
(a)
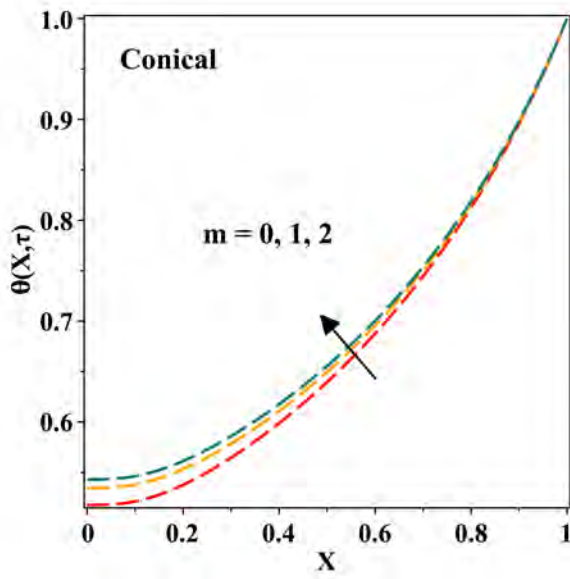
(b)
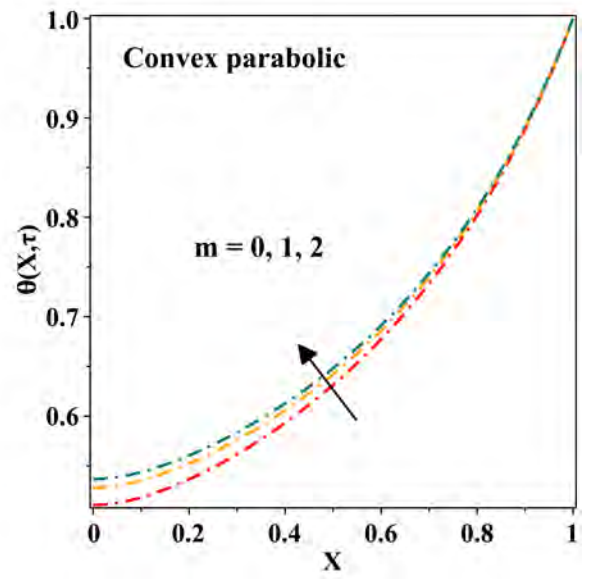
(c)

Figure 6.9: Plot of fin temperature values for distinct values of exponential index m.
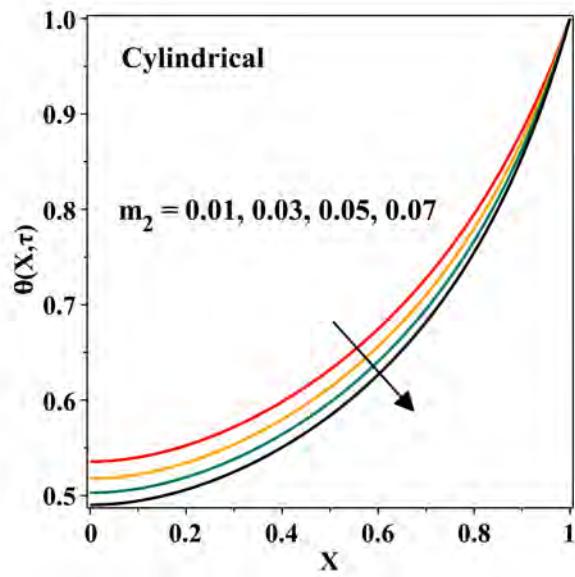
.
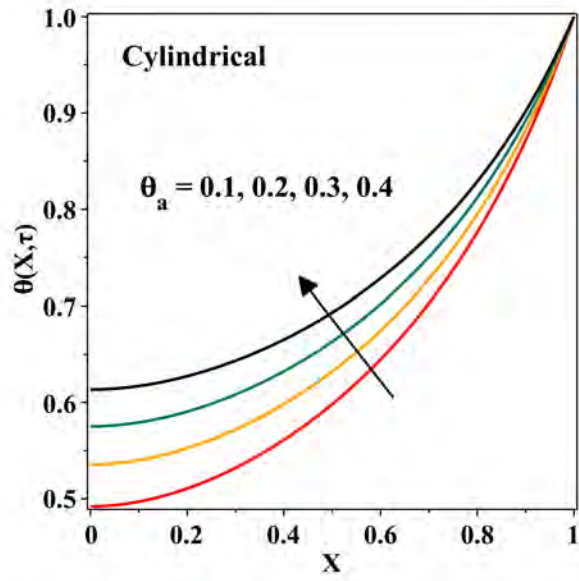
(a)

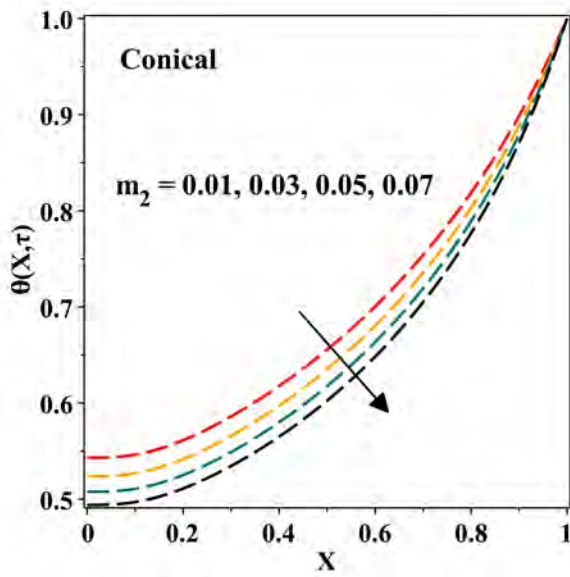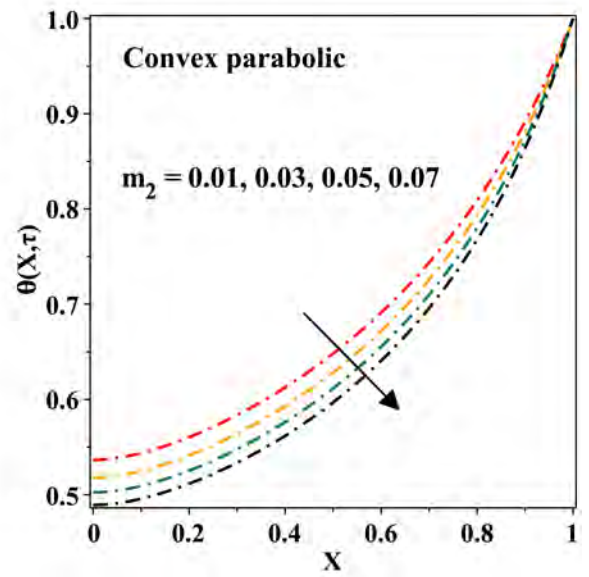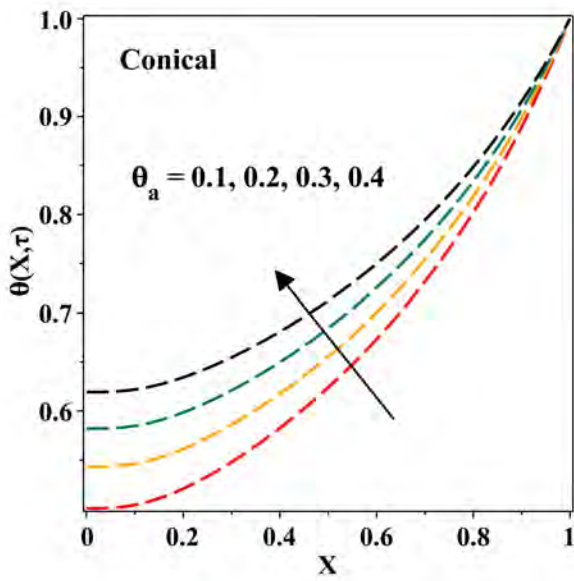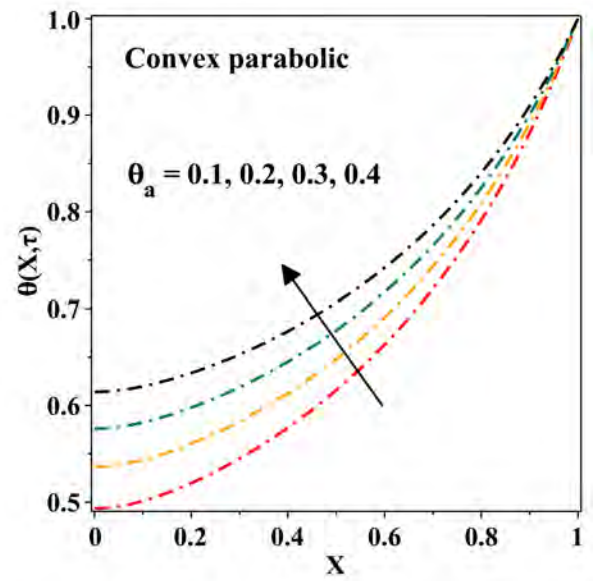(b)   (c)

Figure 6.10: Plot of fin temperature values for distinct values of dimensionless ambient temperature θ_a.

.
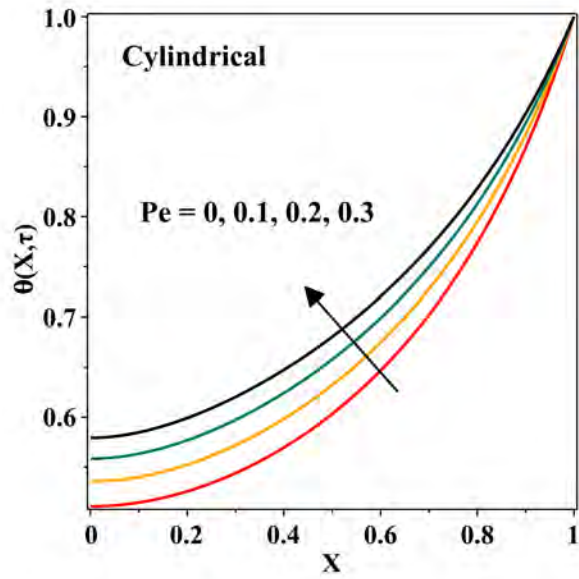
(a)
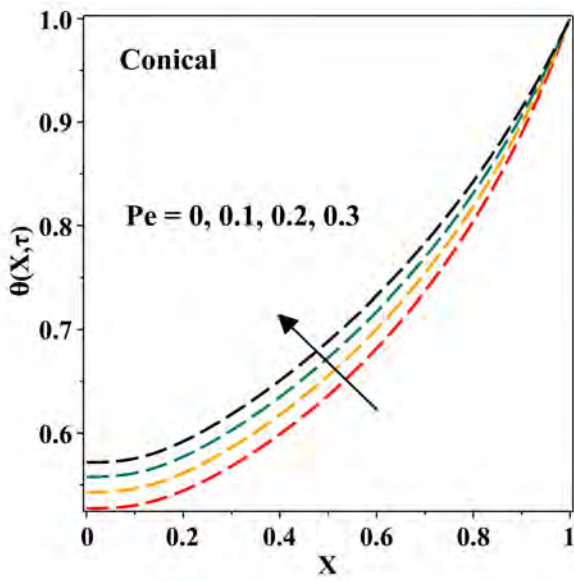
(b)
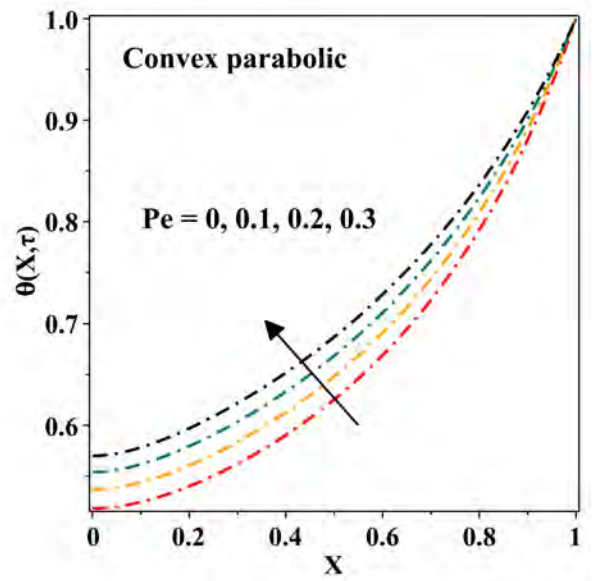
(c)

Figure 6.11: Plot of fin temperature values for distinct values of Peclet number Pe.

.
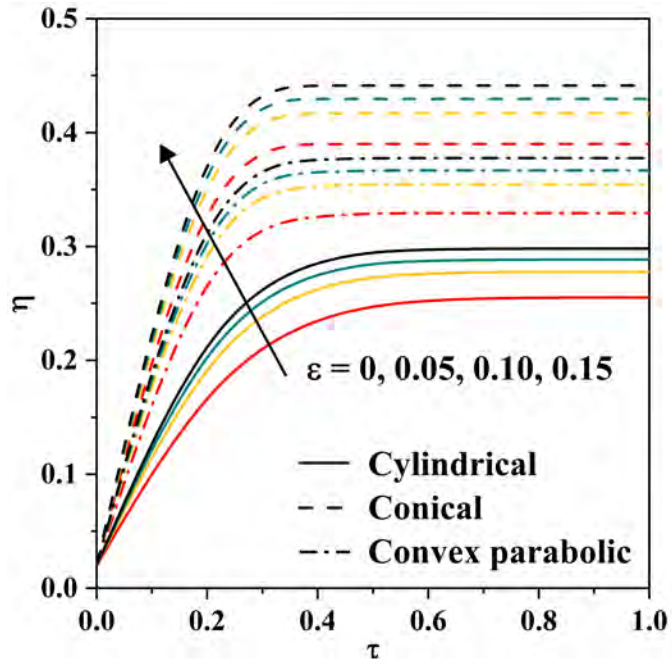
Figure 6.12: Fin efficiency as a function of roughness parameter ϵ and dimensionless time τ.
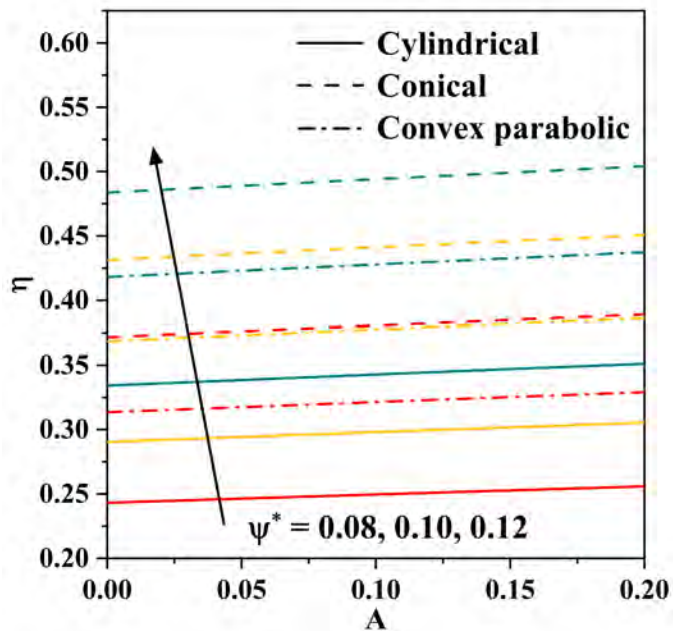
Figure 6.13: Fin efficiency as a function of thermal conductivity parameter A and base radius to length ratio ψ^*.
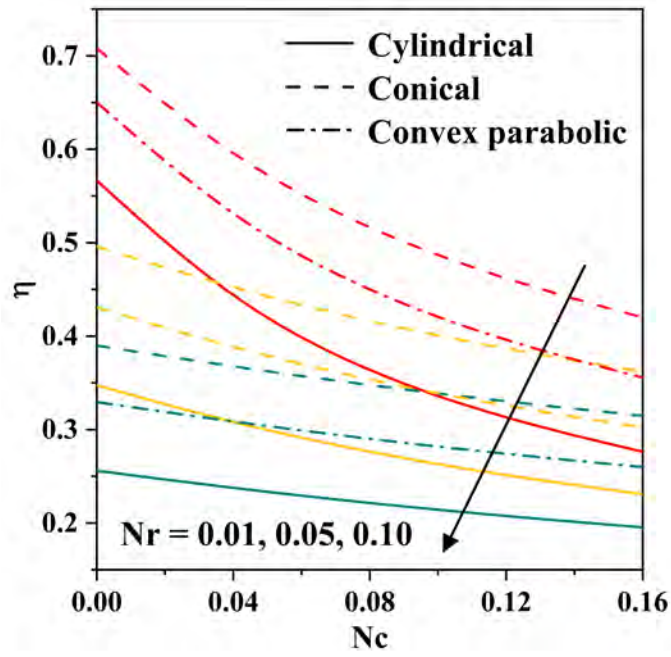
Figure 6.14: Fin efficiency as a function of convective parameter Nc and radiative parameter Nr.
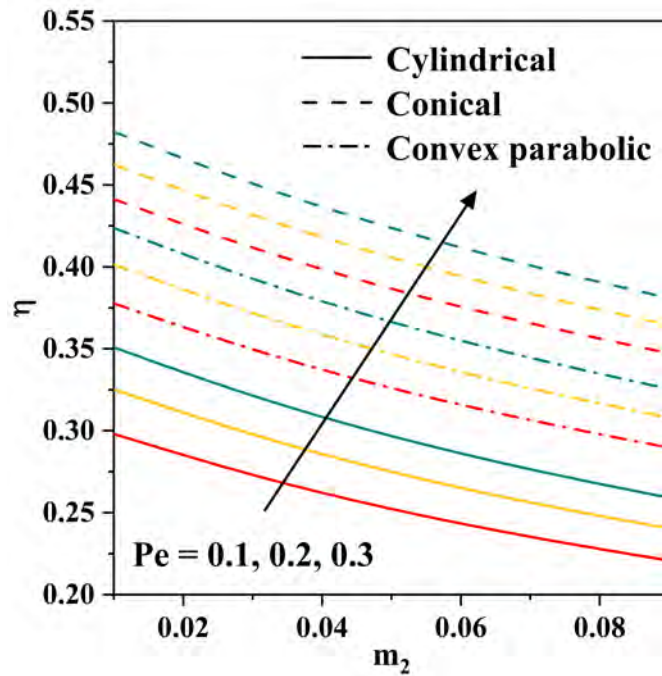
Figure 6.15: Fin efficiency as a function of Peclet number Pe and wet porous parameter m_2.

Chapter 7

Numerical Investigation of Transient Thermal Behaviour of Moving Semi-Spherical Fin of Functionally Graded Material

7.1 Prelims

A variety of engineering applications demand efficient and adaptable fin structures for the intensification of heat exchange. The semi-spherical fin structures are useful in the field of refrigeration, chemical processing systems, aerospace etc. In this regard, the present chapter numerically investigates the transient thermal behaviour of a fully wet semi-spherical fin composed of functionally graded material (FGM). The study incorporates the Darcy model as the fin is made up of porous material. Further, the fin is exposed to convective-radiative heat exchange and is subject to uniform motion. The heat balance equation has been reduced to get a nonlinear PDE which is computed by employing the FDM. The dimensionless terms are grouped together and their influence on the temperature distribution in a semi-spherical fin is studied. The transient fin efficiency has been modelled and its variation with relevant parameters has been graphically depicted. And these are found to be greatly affected by Peclet number, wet porous nature and dimensionless time.

As a main outcome the semi-spherical fin efficiency is positively influenced by the Peclet number.

7.2 Modeling and Interpretation

7.2.1 Heat Transfer
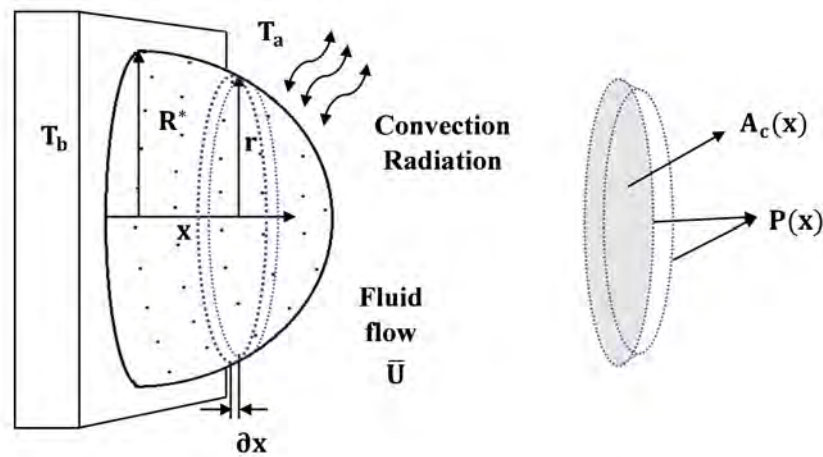
Figure 7.1: Geometrical representation of a functionally graded semi-spherical fin.

Consider a semi-spherical fin of radius R^* mounted on a prime surface of temperature T_b whose physical layout is as pictured in figure 7.1. The fin is fully wetted in a single-phase fluid which also acts as a heat sink with temperature T_a for convective-radiative heat exchanges. The fluid's movement through the pores of the fin and its interaction with the solid surface is governed by the Darcy's law. Further, the fin is subject to motion in the horizontal direction with uniform velocity $\bar{U}$ which can also be interpreted as the flow of a fluid across the stationary fin with a uniform velocity $\bar{U}$. The fin material is an FGM with thermal conductivity as a function of spatial coordinate x. The variation in thermal conductivity can be controlled by the grading parameter a. Initially fin is in thermal equilibrium with the ambient fluid and at time $t \geq 0$, there is a step change in

the temperature and the fin base attains the temperature T_b from T_a. Further the fin tip is considered to be of adiabatic type.

It can be observed from figure 7.1 that the moving fluid's interaction with the fin surface is relative to the shape of the fin. Hence, the heat transfer equation for a moving semi-spherical fin under unsteady conditions is given by,

$$\rho C_p A_c \frac{\partial T}{\partial t} = \frac{d}{dx}\left(k(x)A_c \frac{dT}{dx}\right) - 2\pi r h (1-\hat{\phi})(T-T_a) - 2\pi r h_D(1-\hat{\phi})(\bar{\omega}-\bar{\omega}_s)$$

$$- 2\pi r \rho \bar{v}(x) C_p (T-T_a) - 2\sigma\varepsilon\pi r(T^4 - T_a^4) - \rho C_p \bar{U} A_c \frac{dT}{dx}. \tag{7.2.1}$$

The cross-sectional area of a semi-spherical fin is given by,

$$A_c = \pi(R^{*2} - x^2). \tag{7.2.2}$$

Depending on the variation of thermal conductivity along the $x-$axis i.e., $k(x)$, three types of FGMs can be defined namely:

Case 1: Linear FGM

$$k(x) = k_0(1+ax). \tag{7.2.3}$$

Case 2: Quadratic FGM

$$k(x) = k_0(1+ax^2). \tag{7.2.4}$$

Case 3: Exponential FGM

$$k(x) = k_0 e^{ax}, \tag{7.2.5}$$

where, a is the grading parameter of thermal conductivity.

For three different FGMs the energy equation for a moving semi-spherical fin in equation (7.2.1) by utilizing equations (1.2.6) and (1.2.9) along with the equations (7.2.2) to (7.2.5)

127

reduces to,

Case 1: Linear FGM

$$\frac{\rho C_p R^{*2}}{k_0}\frac{\partial T}{\partial t} = (1+ax)(R^{*2}-x^2)\frac{d^2 T}{dx^2} + \left[a(R^{*2}-x^2)-2x(1+ax)\right]\frac{dT}{dx}$$

$$- \frac{\rho C_p \bar{U}(R^{*2}-x^2)}{k_0}\frac{dT}{dx} - \frac{2h_a(1-\hat{\phi})\sqrt{R^{*2}-x^2}}{k_0}\frac{(T-T_a)^{m+1}}{(T_b-T_a)^m}$$

$$- \frac{2\rho g K\beta_f C_p \sqrt{R^{*2}-x^2}(T-T_a)^2}{\nu_f k_0} - \frac{2\sigma\varepsilon\sqrt{R^{*2}-x^2}(T^4-T_a^4)}{k_0}$$

$$- \frac{2h_a(1-\hat{\phi})l_{fg}\sqrt{R^{*2}-x^2}(\bar{\omega}-\bar{\omega}_s)}{k_0 C_p Le^{\frac{2}{3}}}\frac{(T-T_a)^m}{(T_b-T_a)^m}. \tag{7.2.6}$$

Case 2: Quadratic FGM

$$\frac{\rho C_p R^{*2}}{k_0}\frac{\partial T}{\partial t} = (1+ax^2)(R^{*2}-x^2)\frac{d^2 T}{dx^2} + \left[2ax(R^{*2}-x^2)-2x(1+ax^2)\right]\frac{dT}{dx}$$

$$- \frac{\rho C_p \bar{U}(R^{*2}-x^2)}{k_0}\frac{dT}{dx} - \frac{2h_a(1-\hat{\phi})\sqrt{R^{*2}-x^2}}{k_0}\frac{(T-T_a)^{m+1}}{(T_b-T_a)^m}$$

$$- \frac{2\rho g K\beta_f C_p \sqrt{R^{*2}-x^2}(T-T_a)^2}{\nu_f k_0} - \frac{2\sigma\varepsilon\sqrt{R^{*2}-x^2}(T^4-T_a^4)}{k_0}$$

$$- \frac{2h_a(1-\hat{\phi})l_{fg}\sqrt{R^{*2}-x^2}(\bar{\omega}-\bar{\omega}_s)}{k_0 C_p Le^{\frac{2}{3}}}\frac{(T-T_a)^m}{(T_b-T_a)^m}. \tag{7.2.7}$$

Case 3: Exponential FGM

$$\frac{\rho C_p R^{*2}}{k_0}\frac{\partial T}{\partial t} = e^{ax}(R^{*2}-x^2)\frac{d^2 T}{dx^2} + \left[ae^{ax}(R^{*2}-x^2)-2xe^{ax}\right]\frac{dT}{dx}$$

$$- \frac{\rho C_p \bar{U}(R^{*2}-x^2)}{k_0}\frac{dT}{dx} - \frac{2h_a(1-\hat{\phi})\sqrt{R^{*2}-x^2}}{k_0}\frac{(T-T_a)^{m+1}}{(T_b-T_a)^m}$$

$$- \frac{2\rho g K\beta_f C_p \sqrt{R^{*2}-x^2}(T-T_a)^2}{\nu_f k_0} - \frac{2\sigma\varepsilon\sqrt{R^{*2}-x^2}(T^4-T_a^4)}{k_0}$$

$$- \frac{2h_a(1-\hat{\phi})l_{fg}\sqrt{R^{*2}-x^2}(\bar{\omega}-\bar{\omega}_s)}{k_0 C_p Le^{\frac{2}{3}}}\frac{(T-T_a)^m}{(T_b-T_a)^m}. \tag{7.2.8}$$

The following are the corresponding initial and boundary conditions,

$$T(x,0) = 0, \quad T(0,t) = T_b, \quad \frac{\partial}{\partial x} T(R^*, t) = 0. \tag{7.2.9}$$

The following are dimensionless quantities utilized for non-dimensionalising the energy equation.

$$X = \frac{x}{R^*}, \theta = \frac{T}{T_b}, \theta_a = \frac{T_a}{T_b}, \tau = \frac{k_0}{\rho C_p R^{*2}} t, Nc = \frac{2\rho g K \beta_f C_p T_b R^*}{\nu_f k_0}, Nr = \frac{2\sigma \varepsilon R^* T_b^3}{k_0},$$

$$\bar{\omega} - \bar{\omega}_s = b_2(T - T_a), m_0 = \frac{2h_a R^*(1-\hat{\phi})}{k_0}, m_1 = \frac{2h_a l_f g(1-\hat{\phi}) b_2 R^*}{k_0 C_p Le^{\frac{2}{3}}}, m_2 = m_0 + m_1,$$

$$\beta = aR^*, \alpha = aR^{*2}, Pe = \frac{\rho C_p \bar{U} R^*}{k_0}. \tag{7.2.10}$$

Here, Nr is the radiative term related to radiative heat transfer, Nc is the convective term related to buoyancy effect, m_2 is the wet porous term related to wet and porous nature of fin, β and α are in-homogeneity indices related to grading parameter of thermal conductivity and Pe is the Peclet number related to speed of fin movement.

Substituting the above equation (7.2.10) in equations (7.2.6)-(7.2.8) one respectively gets,

Case 1: Linear FGM

$$\frac{\partial \theta}{\partial \tau} = (1 + \beta X)(1 - X^2) \frac{\partial^2 \theta}{\partial X^2} + (\beta - 2X - 3\beta X^2) \frac{\partial \theta}{\partial X} - Nr\sqrt{(1 - X^2)}(\theta^4 - \theta_a^4)$$

$$- Nc\sqrt{(1 - X^2)}(\theta - \theta_a)^2 - m_2\sqrt{(1 - X^2)}\frac{(\theta - \theta_a)^{m+1}}{(1 - \theta_a)^m} - Pe(1 - X^2)\frac{\partial \theta}{\partial X}. \tag{7.2.11}$$

Case 2: Quadratic FGM

$$\frac{\partial \theta}{\partial \tau} = (1 + \alpha X^2)(1 - X^2) \frac{d^2 \theta}{dX^2} + (2\alpha X - 2X - 4\alpha X^3) \frac{d\theta}{dX} - Nr\sqrt{(1 - X^2)}(\theta^4 - \theta_a^4)$$

$$- Nc\sqrt{(1 - X^2)}(\theta - \theta_a)^2 - m_2\sqrt{(1 - X^2)}\frac{(\theta - \theta_a)^{m+1}}{(1 - \theta_a)^m} - Pe(1 - X^2)\frac{\partial \theta}{\partial X}. \tag{7.2.12}$$

Case 3: Exponential FGM

$$\frac{\partial \theta}{\partial \tau} = e^{\beta X}(1 - X^2)\frac{d^2\theta}{dX^2} + (\beta - 2X - \beta X^2)e^{\beta X}\frac{d\theta}{dX} - Nr\sqrt{(1 - X^2)}(\theta^4 - \theta_a^4)$$

$$- Nc\sqrt{(1 - X^2)}(\theta - \theta_a)^2 - m_2\sqrt{(1 - X^2)}\frac{(\theta - \theta_a)^{m+1}}{(1 - \theta_a)^m} - Pe(1 - X^2)\frac{\partial \theta}{\partial X}.$$

$$(7.2.13)$$

The reduced initial and boundary conditions are given by,

$$\theta(X, 0) = 0, \quad \theta(0, \tau) = 1, \quad \frac{\partial}{\partial X}\theta(1, \tau) = 0.$$

$$(7.2.14)$$

7.2.2   Thermal Efficiency Analysis

The thermal efficiency is heat flux through the fin versus ideal heat flux rate. It is calculated as,

$$\eta = \frac{Q_f}{Q_{ideal}}.$$

$$(7.2.15)$$

The heat flux rate through the fin is given by,

$$Q_f = \int_0^{R^*} \left[\begin{array}{l} \frac{2\pi \rho g K \beta_f C_p \sqrt{R^{*2} - x^2}}{\nu_f}(T - T_a)^2 + 2\sigma\varepsilon\pi\sqrt{R^{*2} - x^2}(T^4 - T_a^4) \\ \\ +h_a2\pi(1 - \hat{\phi})\sqrt{R^{*2} - x^2}\frac{(T - T_a)^{m+1}}{(T_b - T_a)^m} + \frac{h_a2\pi b_2 l_{fg}(1 - \hat{\phi})\sqrt{R^{*2} - x^2}}{C_p Le^{\frac{2}{3}}}\frac{(T - T_a)^{m+1}}{(T_b - T_a)^m} \end{array} \right] dx.$$

$$(7.2.16)$$

The heat flux rate through an ideal fin is given by,

$$Q_{ideal} = \left[\begin{array}{l} \frac{2\pi \rho g K \beta_f C_p}{\nu_f}(T_b - T_a)^2 + 2\sigma\varepsilon\pi(T_b^4 - T_a^4) \\ \\ +h_a2\pi(1 - \hat{\phi})(T_b - T_a) + \frac{h_a2\pi b_2 l_{fg}(1 - \hat{\phi})}{C_p Le^{\frac{2}{3}}}(T_b - T_a) \end{array} \right] \int_0^R \sqrt{R^2 - x^2}dx.$$

$$(7.2.17)$$

In dimensionless form the thermal fin efficiency is given by,

$$\eta = \frac{\int_0^1 \left[Nc(\theta - \theta_a)^2\sqrt{1 - X^2} + m_2\sqrt{1 - X^2}\frac{(\theta - \theta_a)^{m+1}}{(1 - \theta_a)^m} + Nr\sqrt{1 - X^2}(\theta^4 - \theta_a^4) \right] dX}{[Nc(1 - \theta_a)^2 + m_2(1 - \theta_a) + Nr(1 - \theta_a^4)]\int_0^1 \sqrt{1 - X^2}dX}.$$

$$(7.2.18)$$

130

7.3   Numerical Elucidation

The second order nonlinear parabolic PDEs (7.2.11), (7.2.12) and (7.2.13) along with their corresponding initial and boundary conditions as in equation (7.2.14) are the concerned equations. Using the FDM with centered-implicit scheme the solution of the PDEs has been found via the Maple software. The detailed procedure is explained in section (2.3). The results of the present investigation have been extracted by setting $\Delta X = 0.008$ and $\Delta \tau = 0.001$.

7.4   Deliberation of Results

The response of linear, quadratic, and exponential semi-spherical FGM fin structures for variation in significant parameters has been represented via graphs by numerically analysing the equations (7.2.11)-(7.2.13). The contant values presumed throughout the study are: $Nc = 1, Nr = 1, m_2 = 1, m = 2, \theta_a = 0.2, Pe = 1, \alpha = 0.2, \tau = 1$ and $\beta = 0.2$.

Figure 7.2 (a-c) depicts the thermal field of linear, quadratic, and exponential FGM fin structures for a range of power index m related to the heat flow coefficient of convection h. Considering the linear FGM case, it can be clearly noted that the thermal curves are flatter with rise in m values. Here, $m = 0$ and $m \neq 0$ correspond to linear and non-linear variation of heat flow coefficient with fin temperature. As the nonlinearity in the relationship increases the value of h decreases from its value at ambient temperature i.e, h_a leading to decreased heat loss through convection. Thus, a linear relationship between m and h results in lower tip temperatures. Further, the quadratic and exponential FGM cases can be similarly explained.

The thermal attribute of three FGM fin structures for distinct values of radiation

parameter Nr has been represented in figure 7.3 (a-c). The figure dictates that there is a decrease in fin temperature with rise in Nr values. This can be explained as follows. The ratio of heat flow through radiation to that through conduction is taken as the radiative parameter Nr. Hence, as Nr value rises the heat flow through radiation is more than that through conduction resulting in a decrease in fin temperature. Further, the variation in all three cases has a similar explanation.

Figure 7.4 (a-c) reveals the variation in the temperature profile of three considered semi-spherical FGM fin structures for a range of the convective parameter Nc. It can be observed that the temperature curve rises with a downfall in Nc values. This is because the parameter Nc reflects the strength of convection heat flow against conduction heat flow and as Nc values move from 1 to 3 convection mode of heat flow becomes stronger resulting in a reduction in fin temperature. Thus, the hike in the convective parameter results in a decrease in fin tip temperature. Further, in all three cases of FGM fin similar trend is followed.

As pictured in figure 7.5 (a-c), the dimensionless ambient temperature θ_a has a significant impact on the temperature curves of the three distinct FGM fin structures. Here, θ_a is the ratio of surrounding temperature to temperature at the fin base and it has a positive impact on the fin temperature. This is because convective heat flow is governed by Newton's law of cooling which says heat flow rate is directly dependent on the temperature difference. Thus, a rise in θ_a values imply a rise in ambient temperature as compared to base temperature resulting in a decrease in temperature difference. This leads to decrease in convective heat loss and rise in fin temperature. Thus, minimum θ_a helps in the cooling process of the fin. Besides, the discussion holds true for all three kinds of FGM fin structures.

The temperature distribution in three distinct semi-spherical FGM fin structures for various values of Peclet number Pe has been captured in figure 7.6 (a-c). The Peclet number is associated with the fin motion and the sketch in linear case deciphers that the temperature distribution in the fin is positively influenced by the Peclet number. This phenomenon can be justified as follows. The ascending values of the Peclet number represent a jump in the speed of fin. As fin movement gains velocity, the interaction between the ambient fluid and the solid fin surface is given less time for convective heat flow leading to higher values of fin temperature. Thus, for a higher heat flow rate, the Peclet number should be minimized. For the other two cases of semi-spherical FGM fin, a similar explanation holds good.

Figure 7.7 (a-c) reveals the influence of the in-homogeneity index α, β on the temperature distribution of semi-spherical fin structures of linear, quadratic, and exponential FGM. It can be noted that steeper curves have appeared for lower values of the index. The reasoning for the linear case is as follows. The in-homogeneity index is associated with the grading parameter of thermal conductivity. Hence ascending value of the index implies elevation in the grading parameter which results in a hike in thermal conductivity of the fin. Thus, on an average the thermal conductivity will be more in the case of high in-homogeneity index which causes increased conduction leading to high fin temperature. The other two cases can be satisfactorily explained using a similar explanation.

The temperature distribution in a semi-spherical fin with time (dimensionless) τ has been captured in figure 7.8 (a-c). The fin surface temperature rises with time, but the variances are only noticeable at first. This is due to the fact that initially there is no difference in temperature between the fin base and the surrounding. But, as time passes, the heat enters the fin structure via the base causing the local fin temperature to rise.

Gradually with rise in base temperature the heat conduction through the fin picks up resulting in a rise in the fin temperature, but after a certain point, the temperature curve becomes parallel to the x-axis, indicating that the steady-state has been reached.

The wet porous parameter (m_2)'s impact on the temperature curve of a semi-spherical fin has been revealed in figure 7.9 (a-c). The wet porous characteristic, as can be observed, has a favourable influence on the fin heat flow rate. The m_2 takes into consideration the porosity of the fin material along with the humidity near the fin surface. Furthermore, an increase in porosity increases the fin's surface area, and the wet condition of the fin promotes greater heat absorption from the surface, resulting in higher heat loss via convective-radiative ejections. As a result, greater m_2 values improve the fin cooling process. Besides, with time the temperature curves are flatter indicating better temperature distribution.

The function $\eta(Nc, Nr)$ for three types of semi-spherical FGM fin structures has been plotted in figure 7.10. The graph confers that the convective term Nc and the radiative term Nr adversely affect the thermal efficiency. The highest efficiency is achievable only if the entire fin surface temperature equals that at the base. That is only when the temperature distribution is maximal. But as discussed earlier the Nc and Nr negatively influence the temperature distribution resulting in lower fin temperatures. Further, in all three cases, the curves behave similarly and hence a similar explanation holds good. On the other hand, the exponential FGM fin has the highest efficiency and the quadratic FGM fin has the least efficiency with the linear one in between the two. This is because in exponential FGM fin the thermal conductivity varies exponentially with fin length leading to better conduction of heat. Thus temperature distribution is enhanced and hence higher efficiency is achieved. For a similar reason, linear FGM fin performs better than quadratic

FGM fin.

The thermal efficiency η for the three considered semi-spherical FGM fin structures with a simultaneous variation of Peclet number Pe and in-homogeneity index α, β has been illustrated in figure 7.11. As indicated in the plot both Peclet number and in-homogeneity index enhance the thermal efficiency. This is due to better temperature distribution with hike in the values of Pe, α and β. Besides, all three FGM fin structures behave similarly. Further, the exponential FGM fin performs better than the linear FGM fin at lower values of Peclet number and they exchange their positions at higher values of Peclet number. On the other hand, the quadratic FGM fin has the least efficiency compared to the other two.

Figure 7.12 represents the efficiency of semi-spherical FGM fin for simultaneous variation of wet porous parameter m_2 and dimensionless time τ. As pictured the characteristics m_2 degrades the fin efficiency. This is because, in order to achieve high efficiency the temperature distribution in the fin must be equivalent to an ideal fin with $T = T_b$ throughout the fin structure. But the considered parameter reduces the local fin temperature leading to improper distribution of temperature and this causes lower efficiency of the fin structure. On the other hand efficiency increases with time (dimensionless) τ in the beginning and gradually become constant. This is because, at time τ equal to zero there is no heat flow through fin due to zero thermal gradient and as time passes the base temperature rises and heat enters the fin structure. Thus there is an increase in temperature distribution leading to elevation in efficiency and gradually with time the efficiency values become constant indicating the achievement of steady state.

7.5 Denouement

A moving semi-spherical fin made of FGM is the focus of the study. The fin structures made of linear, exponential, and quadratic FGM have been comparatively analysed for temperature distribution and thermal efficiency. The FDM has been employed, and the computations have been graphically depicted and discussed. Listed below are the key outcomes of the study:

- The lower tip temperatures were attained for ascending values of convective, radiative and wet porous characteristics. The exponent m and the surrounding temperature θ_a decelerate the fin cooling process.

- The increase in fin motion and thermal grading enhances the temperature distribution. Further, faster the fin movement and higher the thermal grading, higher is the thermal efficiency.

- The exponential FGM fin is more efficient than the linear and quadratic FGM fin structures except at higher values of Peclet number in which case the linear FGM outperforms the other two.

- The temperature distribution and the thermal efficiency increase with time to a certain extent and gradually attain the steady values.
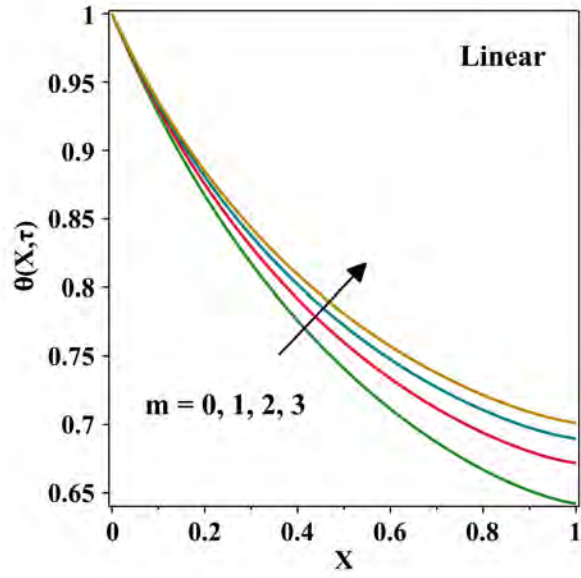
(a)
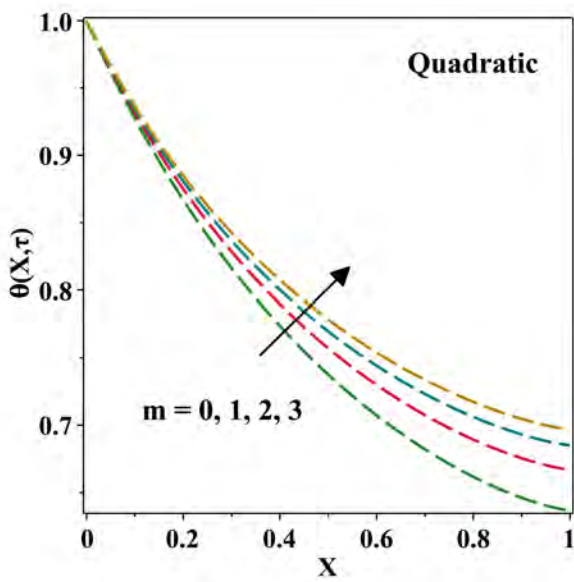
(b)
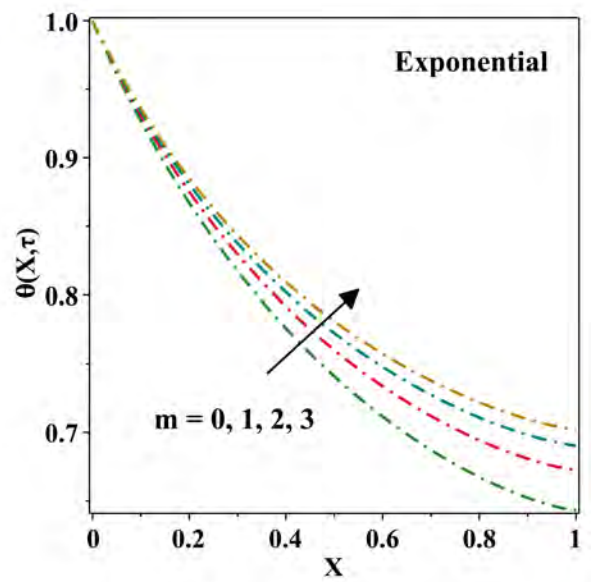
(c)

Figure 7.2: Plot of fin temperature values for distinct values of exponential index m.

.
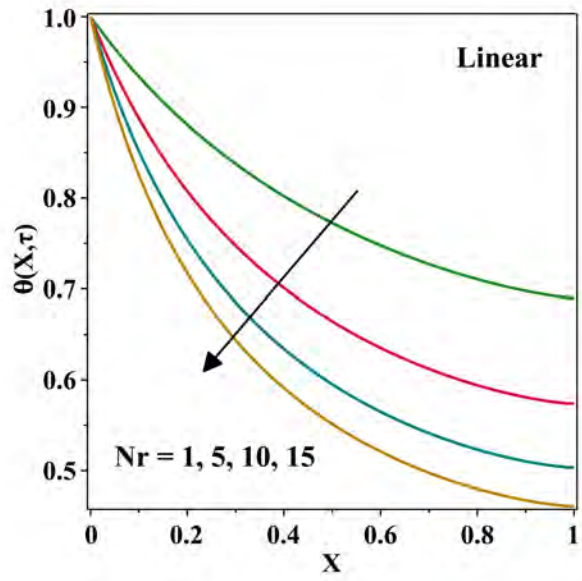
(a)
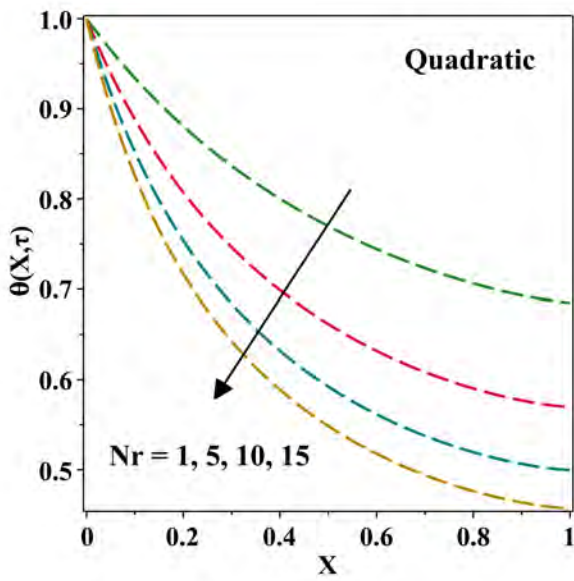
(b)
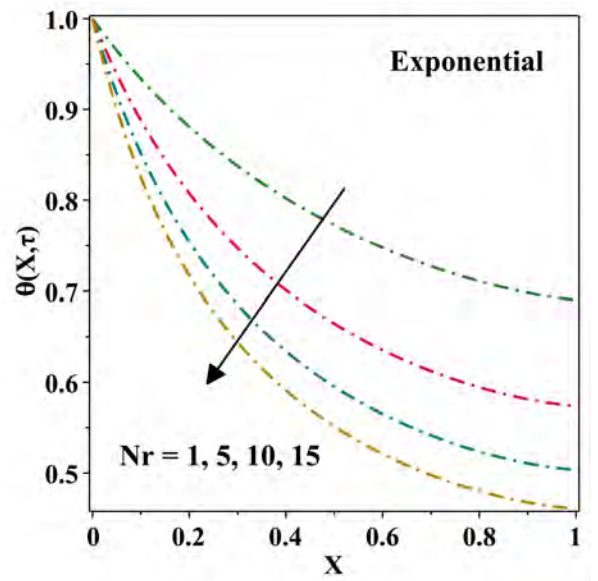
(c)

Figure 7.3: Plot of fin temperature values for distinct values of radiative parameter Nr.

.
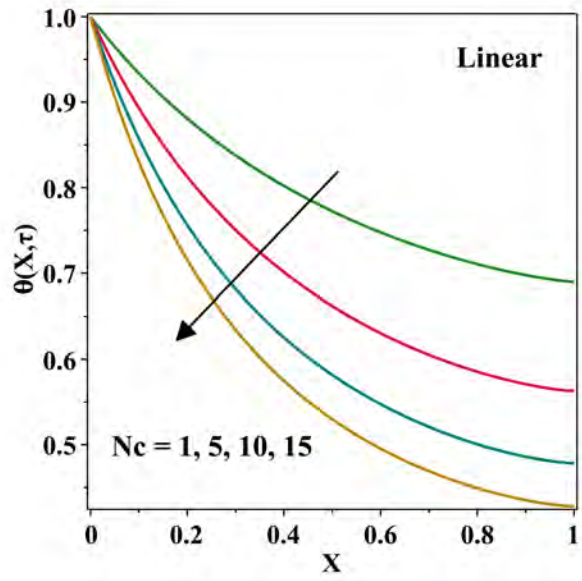
(a)
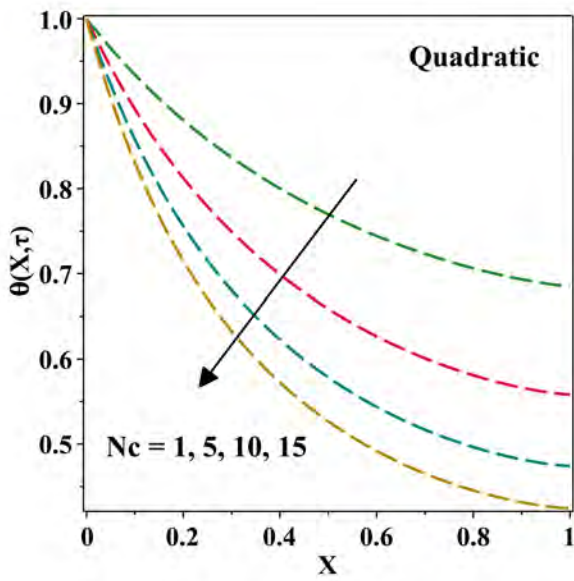
(b)
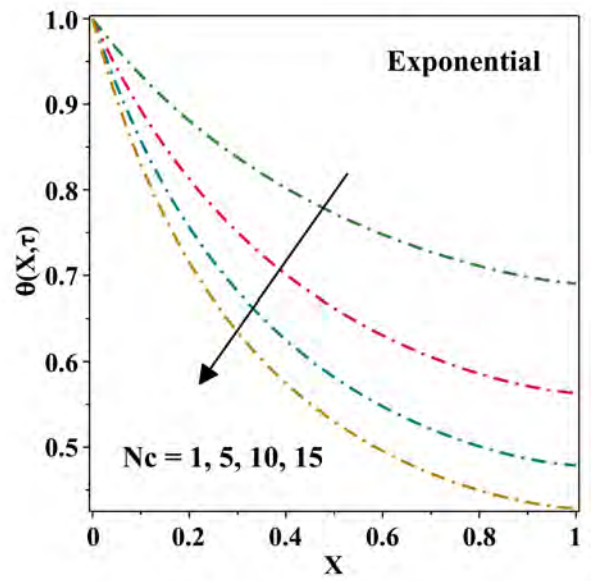
(c)

Figure 7.4: Plot of fin temperature values for distinct values of convective parameter Nc.

.
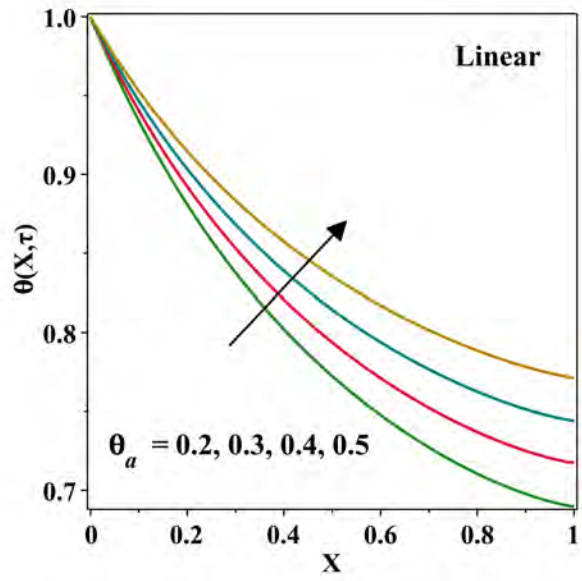
(a)
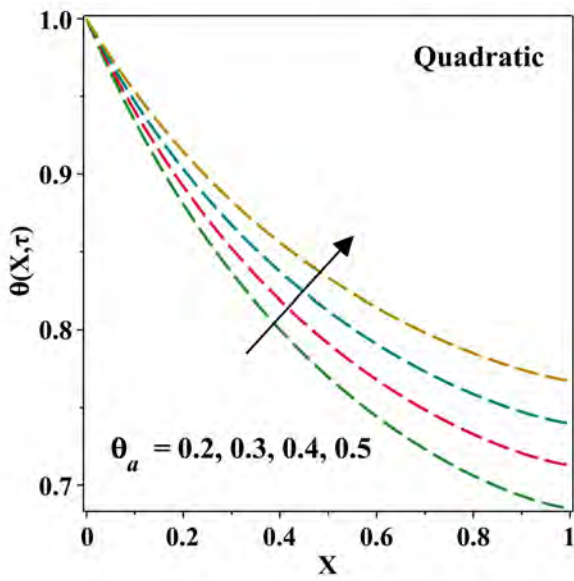
(b)
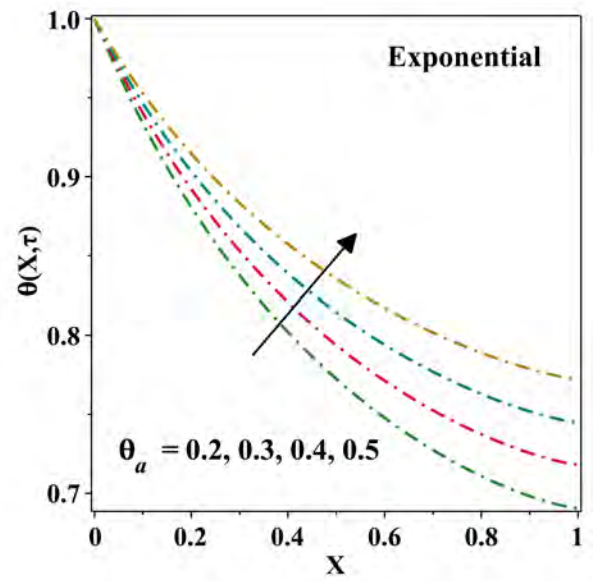
(c)

Figure 7.5: Plot of fin temperature values for distinct values of ambient temperature θ_a.

.
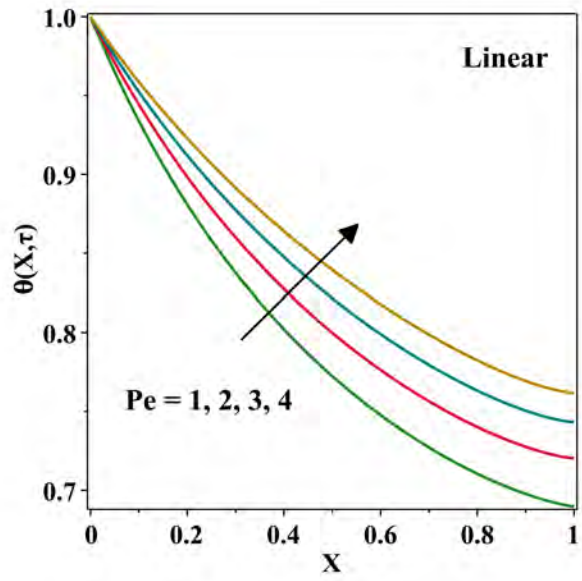
(a)
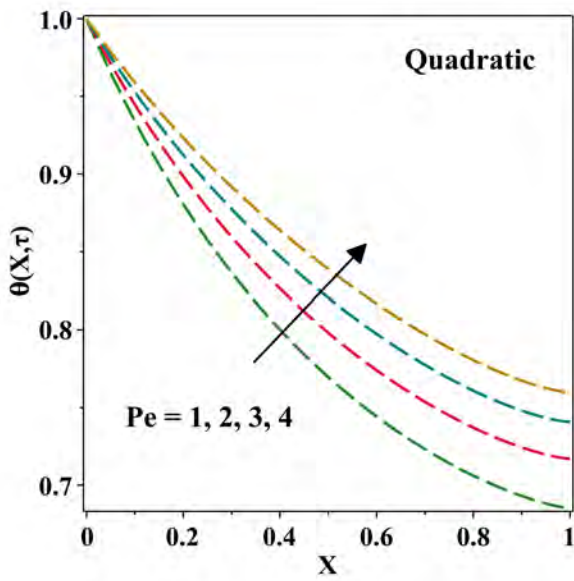
(b)
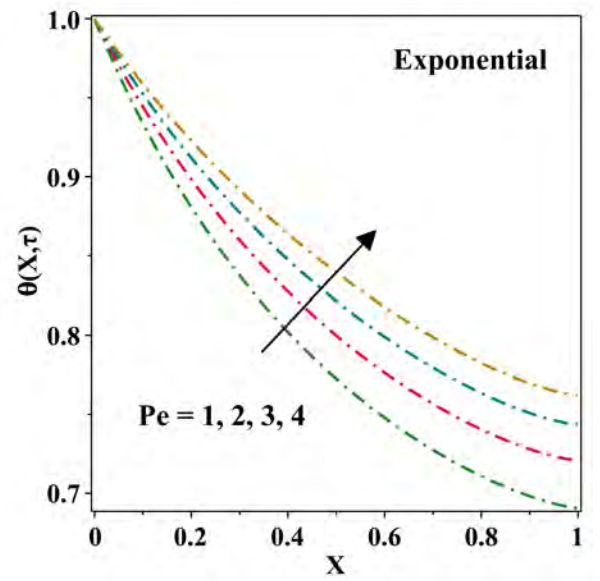
(c)

Figure 7.6: Plot of fin temperature values for distinct values of Peclet number Pe.

.
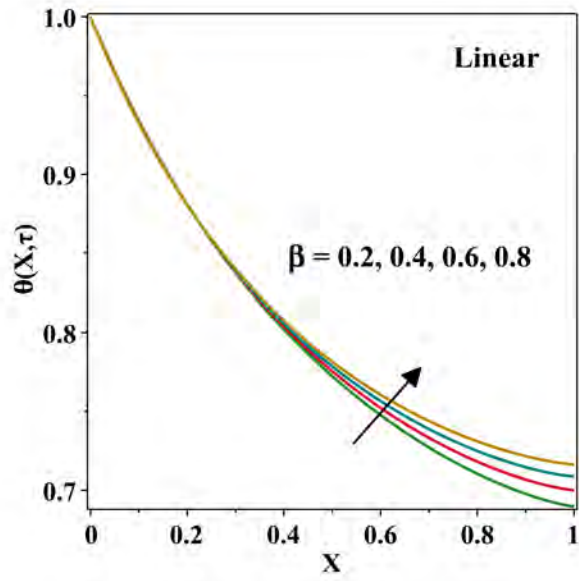
(a)
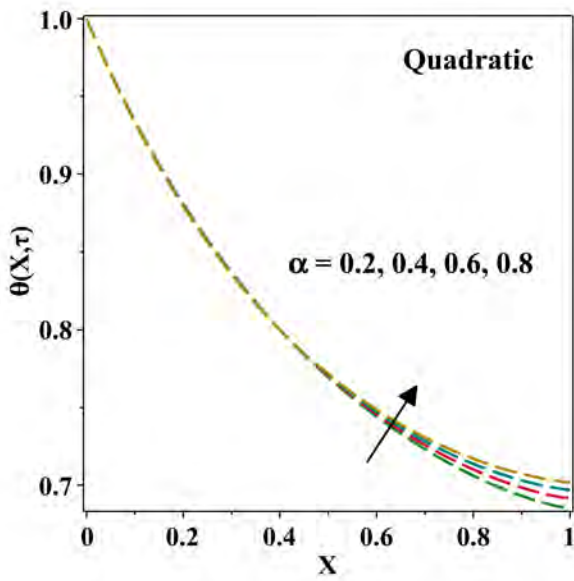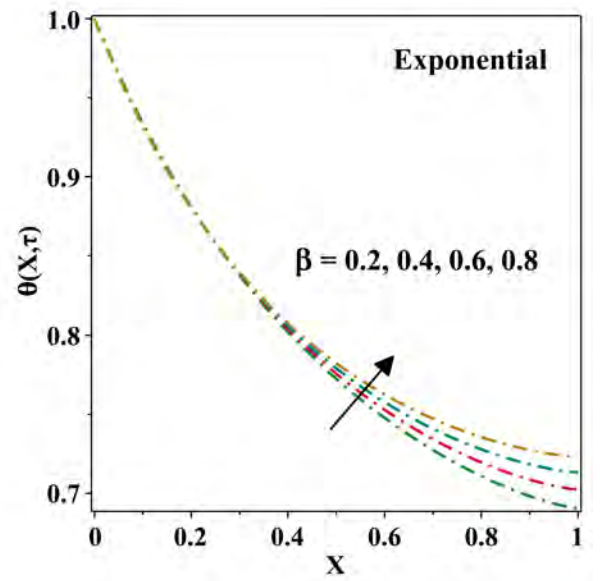
(b)   (c)

Figure 7.7: Plot of fin temperature values for distinct values of in-homogeneity index α, β.
.
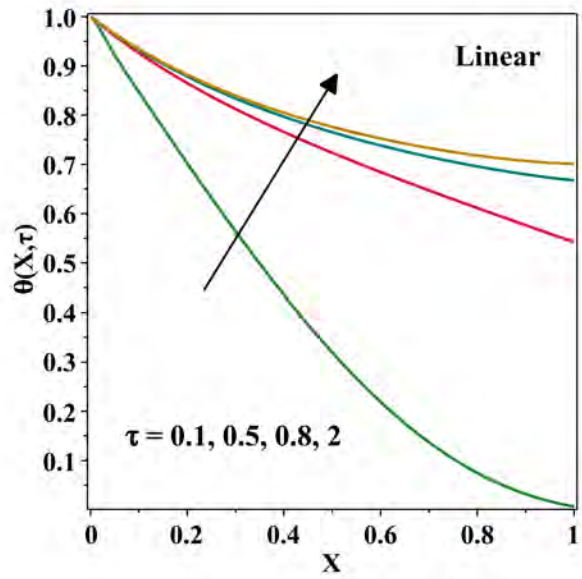
(a)
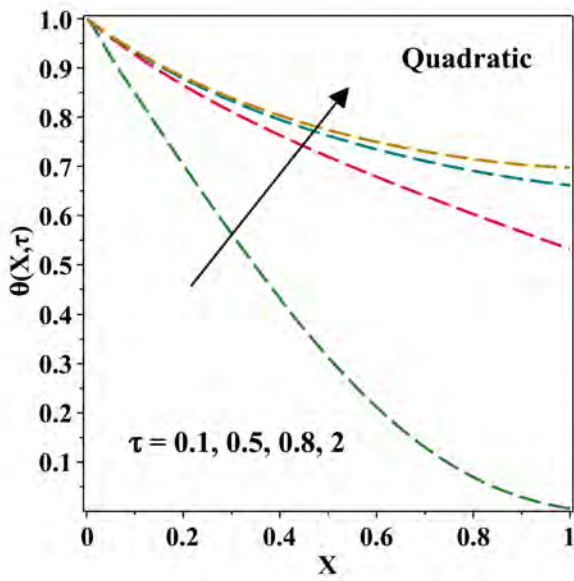
(b)
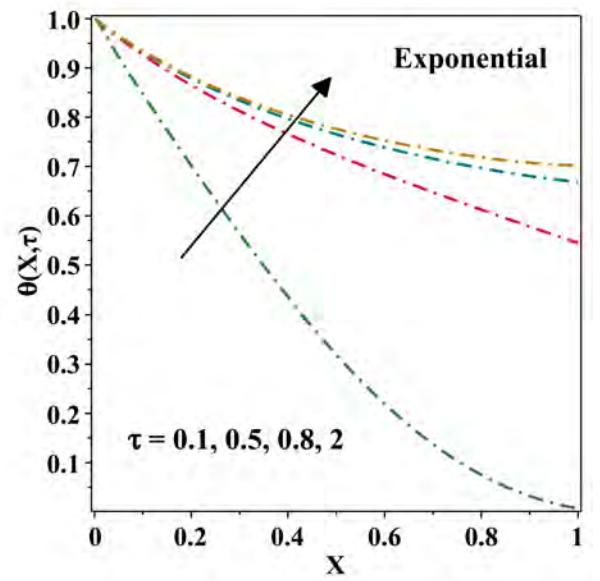
(c)

Figure 7.8: Plot of fin temperature values for distinct values of dimensionless time τ.

.
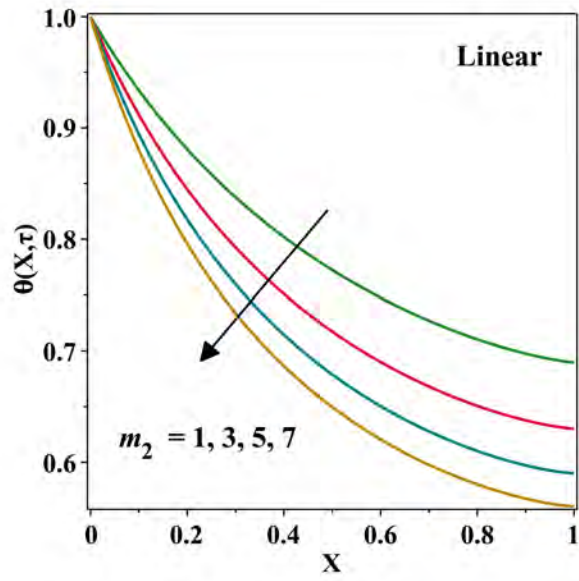
(a)
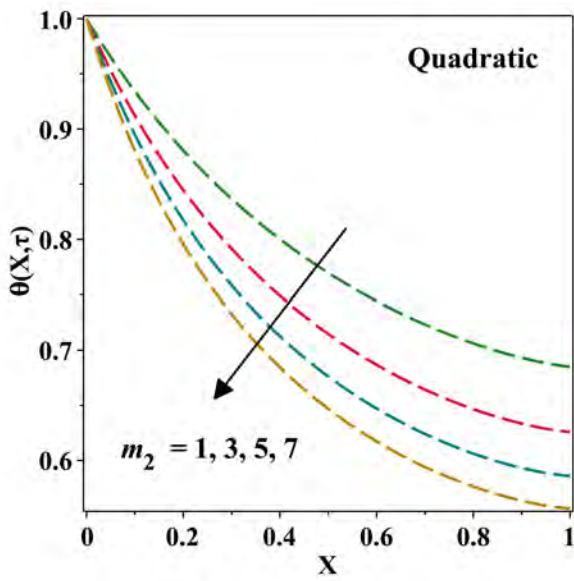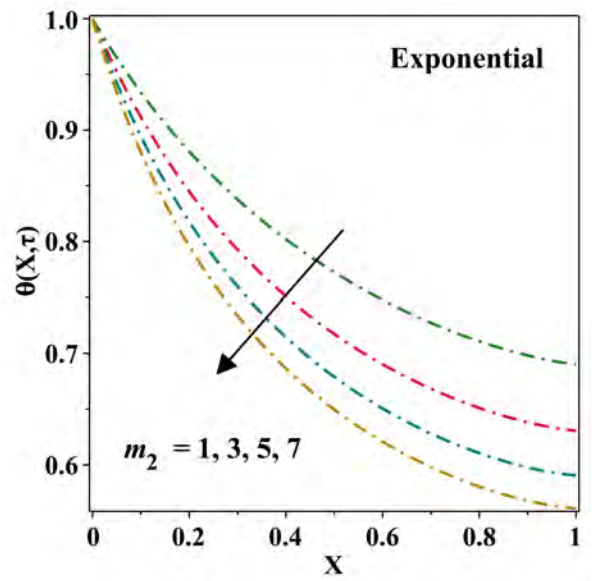
(b)　　　　　　　　　　　　　　　　　(c)

Figure 7.9: Plot of fin temperature values for distinct values of wet porous parameter m_2.

.
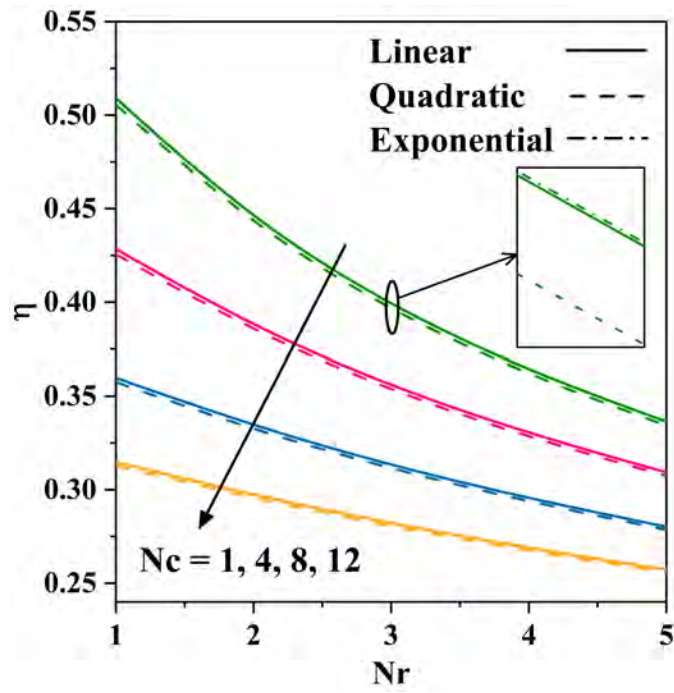
Figure 7.10: Fin efficiency as a function of Nc and Nr.
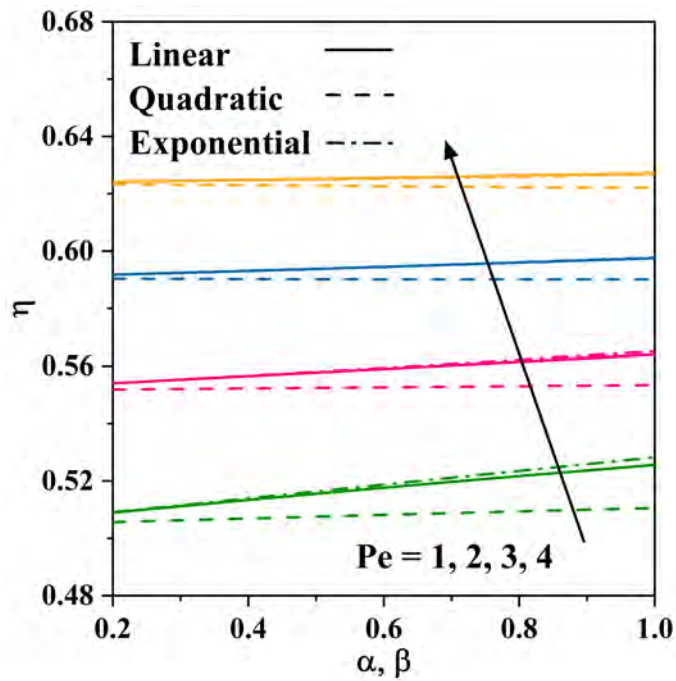
Figure 7.11: Fin efficiency as a function of Pe and α, β.
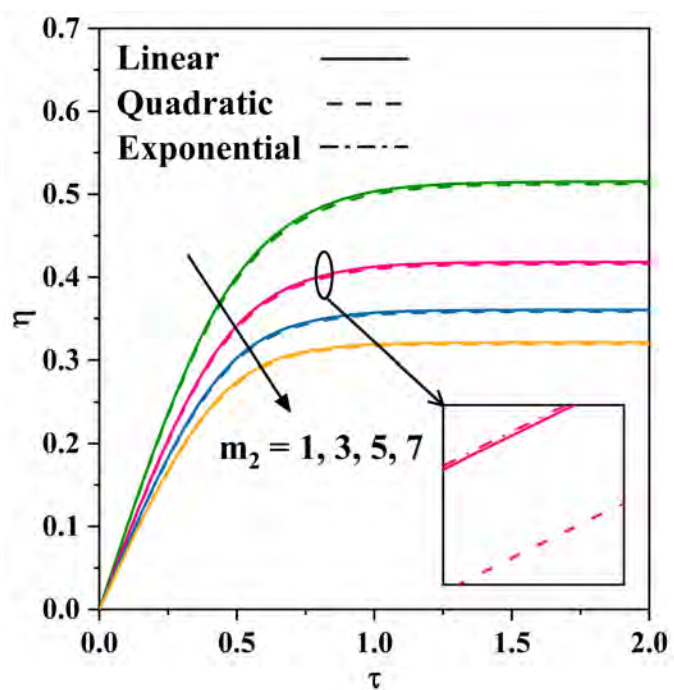
Figure 7.12: Fin efficiency as a function of m_2 and τ.

Chapter 8

Analysis of Entropy Generation in a Longitudinal Fin Exposed to Convection and Radiation

8.1 Prelims

A wet porous moving longitudinal fin composed of linear FGM has been chosen for the analysis. The fin is allowed to stretch/shrink by mounting a mechanism similar to a conveyer belt. The thermal behaviour of the fin and its entropy generation in the presence of convective-radiative heat transmission are the focus of the study. Further, three distinct cases of FGM namely homogeneous, type I (higher thermal grading towards the fin base) and type II (higher thermal grading towards the fin tip) have been comparatively investigated. The derived energy equation is a 2nd order nonlinear ODE and is solved with the aid of the RKF45 method. The fin thermal profile, entropy generation profile, and average entropy generation have been graphically analysed for the thermal conductivity grading parameter, Peclet number, stretching/shrinking parameter, wet porous parameter and other relevant parameters. The entropy generation along fin length as well as the average entropy generated in a fin are discovered to be lowest in the case of homogeneous fin structures followed by type I and type II FGM fin structures. The present investigation

benefits the manufacture and design of FGM fin structures.

8.2   Modeling and Interpretation

A rectangular profiled longitudinal fin structure with dimensions as depicted in figure 8.1 has been considered for the current study. The fin is composed of functionally graded porous material and is exposed to fully wet conditions. Thus, the fluid is allowed to penetrate through the porous fin matrix and its interaction with the solid surface is modelled by employing the Darcy's law. Further, the fin is in contact with and receives heat from a prime surface with temperature T_b and undergoes convective-radiative heat transmission with the ambient fluid at temperature T_a. The fin is subject to motion with a uniform velocity $\bar{U}$ and is allowed to stretch or shrink at a rate $\bar{U}(1 + s^*x)$ by mounting a stretching/shrinking mechanism on its surface. The tip of the fin is assumed adiabatic as there is negligible heat exchange through it when compared to the fin's lateral surfaces. Further, the temperature is assumed to vary only along the $x-$ direction as pictured in the figure 8.1 and hence the study is one-dimensional.
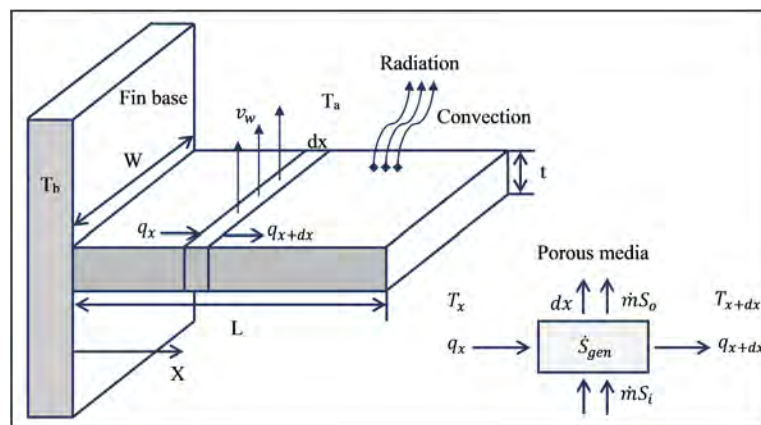
Figure 8.1: Schematic representation of rectangular profiled longitudinal fin.

Considering a small element dx in the fin the energy equation of the fin under steady

conditions can be modelled as,

$$q_x - q_{x+dx} - \rho \bar{v}_w(x) W C_p dx (T - T_a) - \sigma \varepsilon W dx (T^4 - T_a^4) - \rho C_p \bar{U}(1 + s^* x) W t_b \frac{dT}{dx}$$

$$- h(T) W dx (1 - \hat{\phi})(T - T_a) - h_D W dx l_{fg}(1 - \hat{\phi})(\bar{\omega} - \bar{\omega}_s) = 0. \tag{8.2.1}$$

According to Fourier's conduction law, the transfer of heat at distance x from the base is given by,

$$q = -k(x) W t_b \frac{dT}{dx}. \tag{8.2.2}$$

Utilizing equations (1.2.6), (1.2.9) and (8.2.2), the equation (8.2.1) resolves into,

$$t_b \frac{d}{dx}\left[k(x)\frac{dT}{dx}\right] - \frac{\rho g K \beta_f C_p}{\nu_f}(T - T_a)^2 - \sigma \epsilon (T^4 - T_a^4) - \frac{(1 - \hat{\phi})h_a(T - T_a)^{m+1}}{(T_b - T_a)^m}$$

$$- \frac{(1 - \hat{\phi})h_a l_{fg}(\bar{\omega} - \bar{\omega}_s)(T - T_a)^m}{C_p Le^{\frac{2}{3}}(T_b - T_a)^m} - \rho C_p \bar{U}(1 + s^* x) t_b \frac{dT}{dx} = 0. \tag{8.2.3}$$

In equation (8.2.3), $k(x)$ is the thermal conductivity of the material dependent on the axial coordinate x. With k_0 being the thermal conductivity of the homogeneous material, three different variations of k with x are considered namely:

Case 1: Homogeneous with $k(x) = k_0$.

In this case, the fin material is homogeneous and the substitution of the above condition in equation (8.2.3) results into,

$$\frac{d^2T}{dx^2} - \frac{\rho \beta_f g K C_p}{k_0 t_b \nu_f}(T - T_a)^2 - \frac{(1 - \hat{\phi})h_a(T - T_a)^{m+1}}{k_0 t_b (T_b - T_a)^m} - \frac{\sigma \varepsilon}{k_0 t_b}(T^4 - T_a^4)$$

$$- \frac{(1 - \hat{\phi})l_{fg}(\bar{\omega} - \bar{\omega}_s)h_a(T - T_a)^m}{C_p Le^{\frac{2}{3}}k_0 t_b (T_b - T_a)^m} - \frac{\rho C_p \bar{U}(1 + s^* x)}{k_0}\frac{dT}{dx} = 0. \tag{8.2.4}$$

Case 2: Type I FGM with $k(x) = k_0(1 + ax)$.

In this case, the thermal conductivity is k_0 at the base of the fin structure and it increases

149

towards the fin tip. The above condition resolves equation (8.2.3) into,

$$\frac{d^2T}{dx^2} + ax\frac{d^2T}{dx^2} + a\frac{dT}{dx} - \frac{\rho\beta_f gKC_p}{k_0 t_b \nu_f}(T - T_a)^2 - \frac{(1 - \hat{\phi})h_a(T - T_a)^{m+1}}{k_0 t_b(T_b - T_a)^m}$$

$$- \frac{(1 - \hat{\phi})l_{fg}(\bar{\omega} - \bar{\omega}_s)h_a(T - T_a)^m}{C_p Le^{\frac{2}{3}}k_0 t_b(T_b - T_a)^m} - \frac{\rho C_p \bar{U}(1 + s^*x)}{k_0}\frac{dT}{dx}$$

$$- \frac{\sigma\varepsilon}{k_0 t_b}(T^4 - T_a^4) = 0. \tag{8.2.5}$$

Case 3: Type II FGM with $k(x) = k_0(1 + a(L - x))$.

In this case, the thermal conductivity is k_0 at the fin tip and it increases towards the base of the fin. The above condition resolves equation (8.2.3) into,

$$\frac{d^2T}{dx^2} + a(L - x)\frac{d^2T}{dx^2} - a\frac{dT}{dx} - \frac{\rho\beta_f gKC_p}{k_0 t_b \nu_f}(T - T_a)^2 - \frac{(1 - \hat{\phi})h_a(T - T_a)^{m+1}}{k_0 t_b(T_b - T_a)^m}$$

$$- \frac{(1 - \hat{\phi})l_{fg}(\bar{\omega} - \bar{\omega}_s)h_a(T - T_a)^m}{C_p Le^{\frac{2}{3}}k_0 t_b(T_b - T_a)^m} - \frac{\rho C_p \bar{U}(1 + s^*x)}{k_0}\frac{dT}{dx}$$

$$- \frac{\sigma\varepsilon}{k_0 t_b}(T^4 - T_a^4) = 0. \tag{8.2.6}$$

The respective boundary conditions are given below,

$$T = T_b \ at \ x = 0,$$

$$\frac{dT}{dx} = 0 \ at \ x = L. \tag{8.2.7}$$

The following are the dimensionless parameters,

$$\theta = \frac{T}{T_b}, \theta_a = \frac{T_a}{T_b}, X = \frac{x}{L}, \alpha = aL, m_0 = \frac{h_a L^2(1 - \hat{\phi})}{k_0 t_b}, Nc = \frac{\rho g\beta_f KC_p T_b L^2}{\nu_f k_0 t_b},$$

$$m_1 = \frac{h_a l_{fg}(1 - \hat{\phi})b_2 L^2}{k_0 t_b C_p Le^{\frac{2}{3}}}, Nr = \frac{\sigma\varepsilon L^2 T_b^3}{k_0 t_b}, m_2 = m_0 + m_1, Pe = \frac{\rho C_p \bar{U} L}{k_0},$$

$$S = s^* L, \bar{\omega} - \bar{\omega}_s = b_2(T - T_a). \tag{8.2.8}$$

Equations (8.2.4) to (8.2.6) upon non-dimensionalizing resolve into the following non-linear ODEs,

Case 1: Homogeneous

$$\frac{d^2\theta}{dX^2} - Nr(\theta^4 - \theta_a^4) - m_2\frac{(\theta - \theta_a)^{m+1}}{(1 - \theta_a)^m} - Nc(\theta - \theta_a)^2 - Pe(1 + SX)\frac{d\theta}{dX} = 0.$$

(8.2.9)

Case 2: Type I FGM

$$\frac{d^2\theta}{dX^2} + \alpha X\frac{d^2\theta}{dX^2} + \alpha\frac{d\theta}{dX} - Nr(\theta^4 - \theta_a^4) - m_2\frac{(\theta - \theta_a)^{m+1}}{(1 - \theta_a)^m} - Nc(\theta - \theta_a)^2$$

$$- Pe(1 + SX)\frac{d\theta}{dX} = 0.$$

(8.2.10)

Case 3: Type II FGM

$$\frac{d^2\theta}{dX^2} + \alpha(1 - X)\frac{d^2\theta}{dX^2} - \alpha\frac{d\theta}{dX} - Nr(\theta^4 - \theta_a^4) - m_2\frac{(\theta - \theta_a)^{m+1}}{(1 - \theta_a)^m} - Nc(\theta - \theta_a)^2$$

$$- Pe(1 + SX)\frac{d\theta}{dX} = 0.$$

(8.2.11)

The respective dimensionless boundary conditions are,

$$\theta(0) = 1,$$

$$\frac{d\theta(1)}{dX} = 0.$$

(8.2.12)

8.3 Entropy Generation

Estimating the entropy generation in different fin structures exposed to various circumstances is one of the methods of assessing a fin's performance. The entropy generation equilibrium as per second law of thermodynamics can be written as,

$$\sum_{i=1}^{n}\frac{\dot{Q}}{T} + \sum_{i=1}^{n}(\bar{m}_i\dot{S}_i - \bar{m}_0\dot{S}_0) + \dot{S}_{gen} = \frac{d\dot{S}}{dt}.$$

(8.3.1)

Since the study is conducted under steady conditions, $\frac{d\dot{S}}{dt} = 0$. The above equation can be further simplified by noting the input and output in control volume to get,

$$\bar{m}_i(\dot{S}_i - \dot{S}_0) + \dot{S}_{gen} + \frac{q_x}{T_x} - \frac{q_{x+dx}}{T_{x+dx}} = 0. \tag{8.3.2}$$

Considering pressure to be constant both in and out of the porous medium and assuming air to be an ideal gas, the following expression can be extracted for $\dot{S}_i - \dot{S}_0$,

$$\dot{S}_i - \dot{S}_0 = -C_p ln \frac{T(x)}{T_a}. \tag{8.3.3}$$

Further it is known that,

$$q_{x+dx} = q_x - \frac{\partial q_x}{\partial x} dx. \tag{8.3.4}$$

Assuming $T(x + dx) - T(x) \approx 0$ and substituting the above two equations in equation (8.3.2) it results in,

$$-\bar{m}C_p ln \frac{T(x)}{T_a} + \dot{S}_{gen} + \frac{q_x}{T_x} - \frac{q_x - \frac{\partial q_x}{\partial x} dx}{T_{x+dx}} = 0. \tag{8.3.5}$$

The above equation upon simplifying gives,

$$\dot{S}_{gen} = \bar{m}C_p ln \frac{T(x)}{T_a} - \frac{1}{T(x)} \frac{\partial q_x}{\partial x} dx. \tag{8.3.6}$$

After substituting for q_x and simplifying the above equation reduces to,

$$S_{gen}''' = \frac{\dot{S}_{gen}}{W t_b dx} = \frac{\rho g \beta_f K C_p (T - T_a)}{\nu_f t_b} ln\left(\frac{T}{T_a}\right) + \frac{1}{T(x)} \frac{d}{dx}\left(k(x) \frac{dT}{dx}\right). \tag{8.3.7}$$

Further,

$$\frac{S_{gen}''' L^2}{k_0} = \frac{\rho g \beta_f K C_p (T - T_a) L^2}{k_0 \nu_f t_b} ln\left(\frac{T}{T_a}\right) + \frac{L^2}{k_0 T(x)} \frac{d}{dx}\left(k(x) \frac{dT}{dx}\right). \tag{8.3.8}$$

On substituting for $k(x)$ and non-dimensionalizing we get,

Case 1: Homogeneous

$$Ns = Nc(\theta - \theta_a) ln\left(\frac{\theta}{\theta_a}\right) + \frac{1}{\theta} \frac{d^2\theta}{dX^2}. \tag{8.3.9}$$

Case 2: Type I FGM

$$Ns = Nc(\theta - \theta_a)ln\left(\frac{\theta}{\theta_a}\right) + \frac{1}{\theta}\left[(1 + \alpha X)\frac{d^2\theta}{dX^2} + \alpha\frac{d\theta}{dX}\right].$$

(8.3.10)

Case 3: Type II FGM

$$Ns = Nc(\theta - \theta_a)ln\left(\frac{\theta}{\theta_a}\right) + \frac{1}{\theta}\left[(1 + \alpha(1 - X))\frac{d^2\theta}{dX^2} - \alpha\frac{d\theta}{dX}\right].$$

(8.3.11)

On substituting equations (8.2.4) to (8.2.6) respectively in equations (8.3.9) to (8.3.11) all three equations get reduced to equation (8.3.12) given below.

$$Ns = Nc(\theta - \theta_a)\left[ln\left(\frac{\theta}{\theta_a}\right) + 1 - \frac{\theta_a}{\theta}\right] + \frac{Nr}{\theta}(\theta^4 - \theta_a^4) + m_2\frac{(\theta - \theta_a)^{m+1}}{\theta(1 - \theta_a)^m}$$

$$+ \frac{Pe(1 + SX)}{\theta}\frac{d\theta}{dX}.$$

(8.3.12)

Average entropy production in the whole fin can be estimated as,

$$Ns_{avg} = \int_0^1 Ns(X)dX.$$

(8.3.13)

8.4 Numerical Elucidation

The nonlinear second order ODEs namely (8.2.9) to (8.2.11) with insulated boundary condition in equation (8.2.12) have been solved by applying the RKF45 method. In the present analysis, solutions are obtained for the step size 0.001 with the convergence criteria set to 10^{-6}.

8.5 Deliberation of Results

The numerical solutions for the ODEs in equations (8.2.9) to (8.2.11) were derived by utilizing the RKF45 technique. Further these solutions were employed to estimate the entropy generation in a fin given by equations (8.3.9) to (8.3.11) and average entropy

generation in a fin given by equation (8.3.13). This section has been embedded with the suitable discussions for the results derived by the graphical analysis of the obtained solutions.

Figure 8.2 comparatively depicts the thermal conductivity variation in the fin material composed of different types of FGMs for distinct values of grading parameter α. It can be observed that there is no variation in thermal conductivity for homogeneous material, the thermal conductivity increases with grading towards fin base for type I FGM and the thermal conductivity increases with grading towards fin tip for type II FGM. But the average thermal conductivity for both types of FGMs is found to be equal except that the increase in thermal conductivity with grading differs by direction.

Figures 8.3 and 8.4 are of significance as they respectively picturize the comparison of the thermal distribution and entropy generation in a fin composed of homogeneous material against those made from type I and type II FGMs. It can be derived that both the temperature distribution and the entropy generation along the fin length are highest in the case of type II FGM fin and lowest in the case of homogeneous fin. Even though the average thermal conductivity is same in both the cases of FGMs, the increased thermal conductivity towards the fin tip encourages better distribution of temperature towards the tip of the fin. Further the higher production of entropy in type II FGM can be justified by the increased heat transmission within the fin. On the other hand, entropy production rises with a rise in the thermal gradient of the fin structure and hence justifies the increased entropy towards the fin base.

The impact of convective parameter Nc on the thermal profile and entropy generation profile of fin structure made up of type I and type II FGMs has been comparatively represented in figures 8.5 and 8.6 respectively. It can be noted that the fin temperature

decreases, and entropy generation increases with an increase in the parameter Nc. This is because, the parameter Nc accounts for convective heat transfer due to buoyancy effect. Thus, as permeability of the fin structure increases, the penetrability of the ambient fluid through the fin pores increases leading to increased convective heat transmission. Further, the increased movement of heat and an increase in the temperature gradient towards the fin base is the reason for higher entropy production towards the base of the fin structure with the rise in the values of parameter Nc.

Figures 8.7 and 8.8 respectively illustrate the importance of radiative parameter Nr in the thermal and entropy generation analysis of two distinct FGM fin structures. It can be interpreted that fin temperature steeps down towards the fin tip and entropy production elevates towards the fin base with an increase in the parameter Nr. Here, the parameter Nr corresponds to ratio of radiative to conductive heat transfer. Thus, enhancing values of Nr result in increased heat transmission via radiative heat transfer as compared to conductive heat transfer. Thus, it results in lower thermal profiles of fin structures. Further, the hike in the temperature difference towards the fin base with escalating values of Nr result in increased entropy production at that area.

The prominence of wet porous parameter m_2 in the variation of thermal field and entropy production of two distinct types of FGM fin structures has been correspondingly represented in figures 8.9 and 8.10. It can be deciphered that the parameter m_2 has a negative influence on temperature distribution towards the fin tip and positive influence on generation of entropy. This can be interpreted as follows. The parameter m_2 accounts for the porosity and wet nature around the fin structure and hence as it elevates there is increase in the convective heat transmission process resulting in decrease in local fin temperature. Further, this also causes elevation in the temperature gradient towards fin

base leading to increased production of entropy.

Figures 8.11 and 8.12 correspondingly capture the effect of Peclet number Pe on the thermal and entropy fields of type I and type II FGM fin structures. The figures depict the increase in local fin temperature and decrease in generation of entropy for both the kinds of fin structures. Here, Peclet number relates to fin movement and elevation in its values result in faster movement of fin resulting in decrease in time for interaction between ambient fluid and solid fin surface for the process of convective heat transmission. Thus, it results in decreased heat transmission via convection leading to increased local fin temperature. Further, as rise in the values of the Peclet number Pe decreases the thermal gradient values, there is a decrease in the production of entropy.

Figures 8.13 and 8.14 respectively picturize the variations in the thermal and entropy generation profiles of distinct FGM longitudinal fin structures for different values of the thermal conductivity grading parameter α. In general, as α value increases, there is elevation in the local temperature and entropy production in both type I and type II FGM fin structures. This is because the accelerating α values enhance the fin materials' average thermal conductivity resulting in better temperature distribution towards the tip of the fin and lead to enhanced values of temperature. Further, the increase in α values enhance the movement of heat throughout the fin structure leading to increased entropy production.

The energy field and entropy generation profile of type I and type II FGM fin structures for distinct values of ambient temperature θ_a has been illustrated in figure 8.15 and figure 8.16 respectively. Here, it can be noted that accelerating values of θ_a increase the fin temperature throughout its length and also decrease the production of entropy. This can be explained as follows. The dimensionless ambient temperature θ_a has a significant

impact on the convective and radiative heat transmissions as their governing laws depend majorly on the difference in the temperature between the two considered bodies. Thus as θ value rises, the temperature difference between the fin structure and the ambient fluid decreases resulting in lesser heat transmission and leads to higher fin temperature. The higher θ_a values also decrease the local thermal gradient resulting in lesser production of entropy.

Figures 8.17 and 8.18 correspondingly capture the effect of stretching/shrinking parameter S on the thermal and entropy fields of type I and type II FGM fin structures. The figures depict an increase in local fin temperature as well as in generation of entropy for both the kinds of fin structures. Here, $S = 1$ represents stretching and $S = -1$ represents shrinking. The stretching mechanism adds to fin motion and increases the local fin temperature whereas the shrinking mechanism negates the fin motion resulting in a decrease in the local fin temperature. Further, a stretching fin structure is found to generate more entropy as compared to the shrinking one.

The average entropy generation Ns_{avg} in type I FGM, type II FGM and homogeneous material fin structures upon variation in radiative parameter Nr and convective parameter Nc has been pictured in figure 8.19. It can be seen that Ns_{avg} values increase with elevation in the values of Nc and Nr. The observed behaviour is due to the same reasons as discussed before. The variation in Ns_{avg} values for distinct values of stretching/shrinking parameter S and wet porous parameter m_2 has been pictured in figure 8.20. There is an elevation in average entropy values with hike in parameters m_2 and S. The observed behaviour is similar to the case of entropy production and hence can be explained as before. Additionally, the impact of thermal conductivity grading parameter α and the Peclet number Pe on the average entropy generation Ns_{avg} in the distinct fin structures

has been considered in figure 8.21. There is hike in the Ns_{avg} values with parameter α and a dip in Ns_{avg} values with rise in parameter Pe. The behaviour is similar to that observed for the case of entropy generation and follows similar reasons as explained earlier.

8.6   Denouement

The thermal behaviour and entropy generation of a wet porous longitudinal fin made of linear FGM that is subject to convective-radiative heat transmission have been studied. When a fin is subject to continuous motion with constant velocity, three different cases of FGM—homogeneous, type I, and type II—have been comparatively explored. The numerically derived solutions are graphically analysed to derive the following key results.

- Type I FGM fin structures result in lower fin temperatures as compared to type II ones. But fin temperature is lowest in the case of homogeneous ones.

- The entropy generation along fin length as well as the average entropy generated in a fin are lowest in the case of homogeneous fin structures followed by type I and type II FGM fin structures.

- The convective, radiative and wet porous nature of the fin structures result in a decrease in fin temperature along the fin length. But the entropy generation is elevated towards the fin base with a rise in these parameters. Also, average entropy generation is greatly influenced as it increases with these parameters.

- The Peclet number and the ambient temperature result in rise in fin tip temperature whereas decrease the entropy generation towards the fin base. Also, average entropy generation faces a decrease with the acceleration in these parameters.

- A stretching fin structure is found to generate more entropy as compared to the shrinking one.

- The fin temperature, entropy generation and average entropy generation all three are prominently affected by the grading parameter as they elevate with its rise.
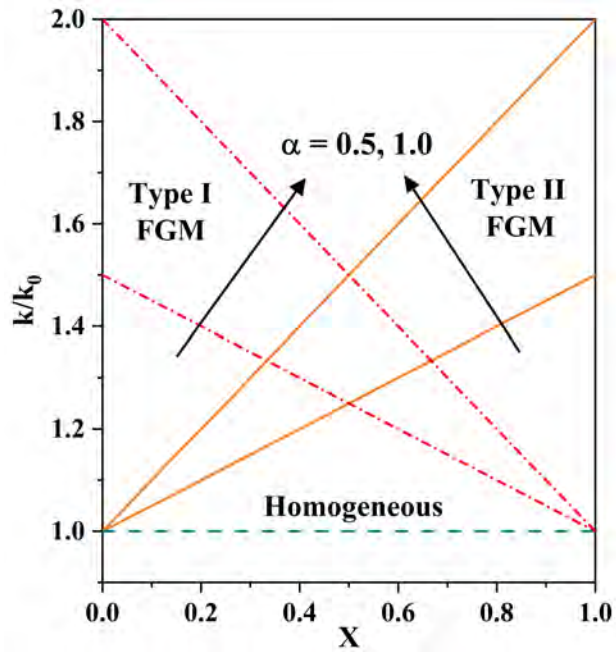
Figure 8.2: Variation in thermal conductivity ratio for distinct values of grading parameter α in different fin structures.
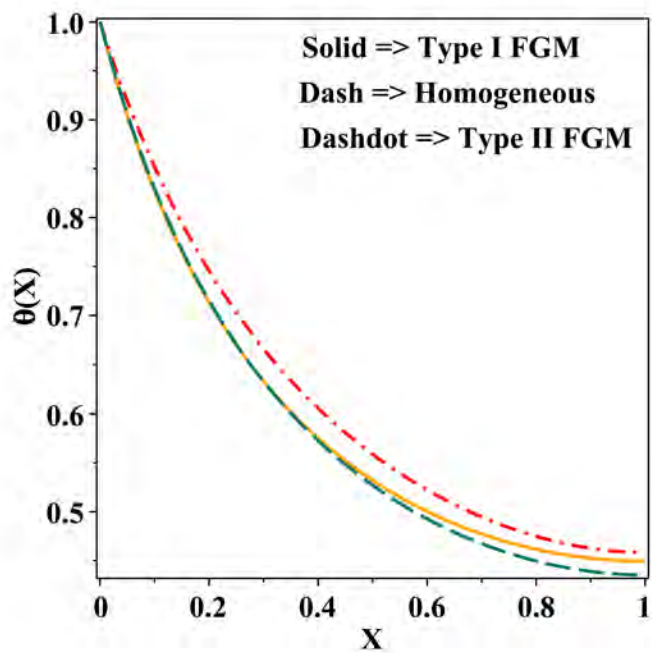
Figure 8.3: Thermal profiles of type I FGM, type II FGM and homogeneous material fin structures.
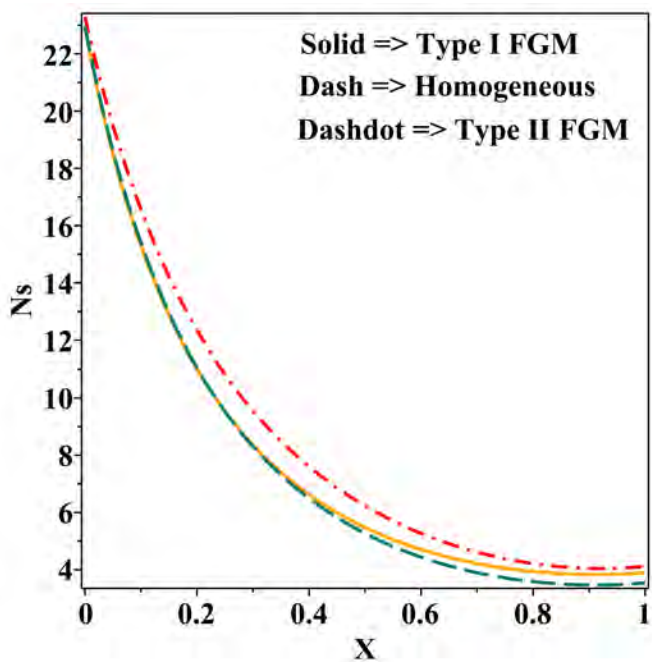
Figure 8.4: Entropy generation in type I FGM, type II FGM and homogeneous material fin structures.
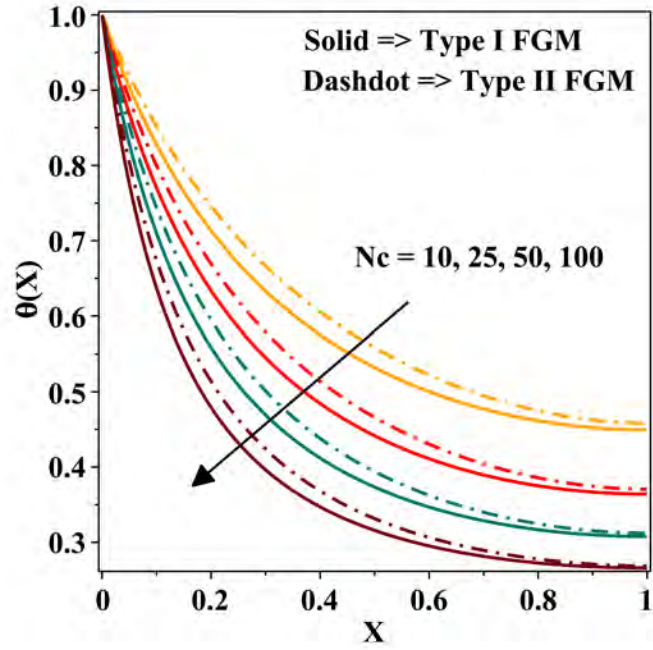
Figure 8.5: Thermal profiles of type I and type II FGM fin structures for distinct values of convective parameter Nc.
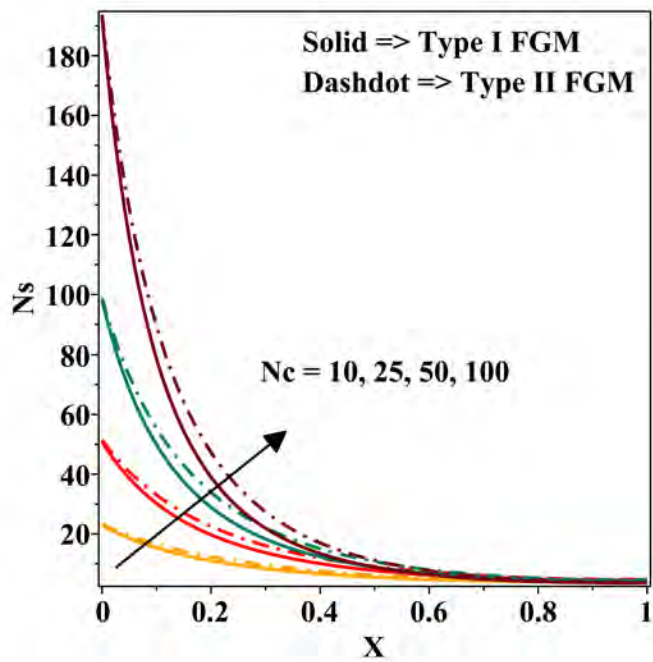
Figure 8.6: Entropy generation in type I and type II FGM fin structures for distinct values of convective parameter Nc.
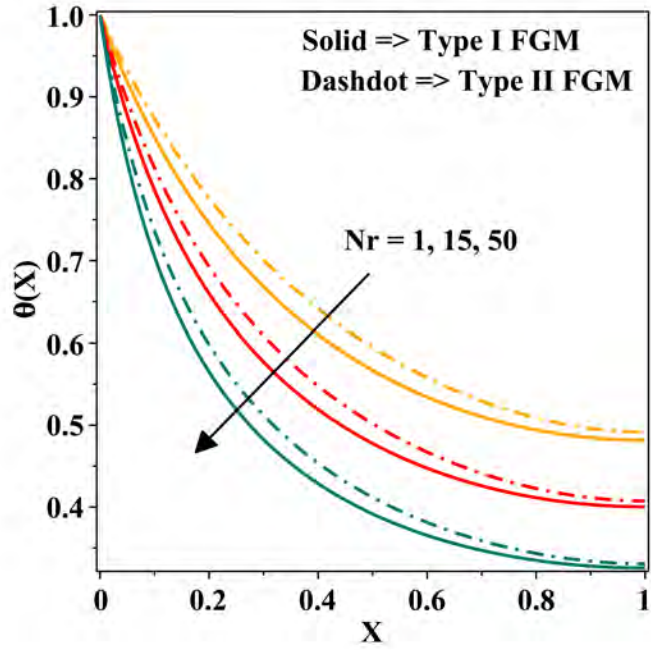
Figure 8.7: Thermal profiles of type I and type II FGM fin structures for distinct values of radiative parameter Nr.
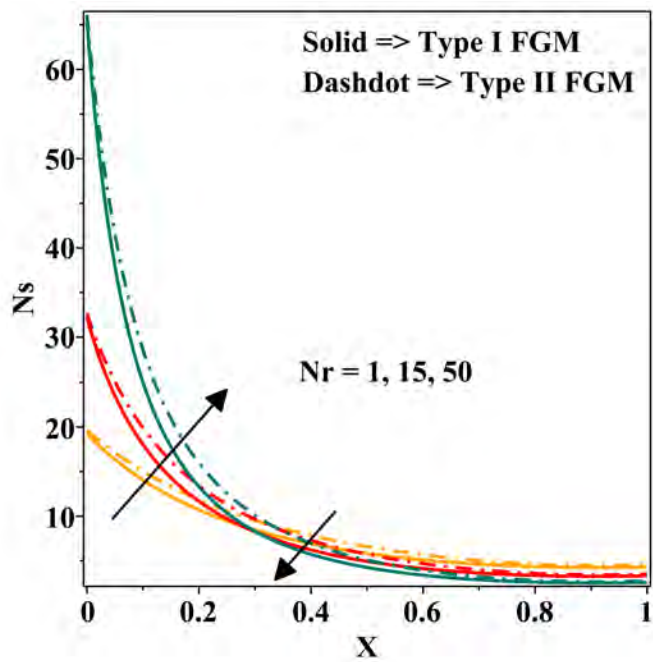
Figure 8.8: Entropy generation in type I and type II FGM fin structures for distinct values of radiative parameter Nr.
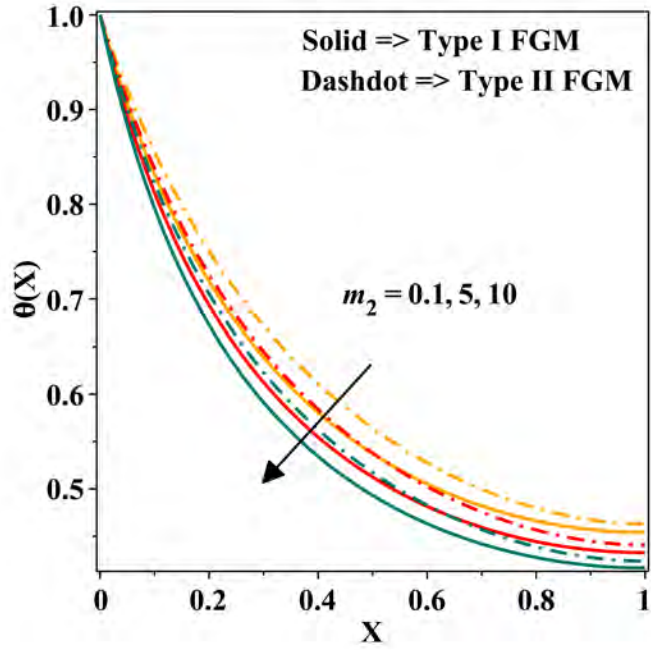
Figure 8.9: Thermal profiles of type I and type II FGM fin structures for distinct values of wet porous parameter m_2.
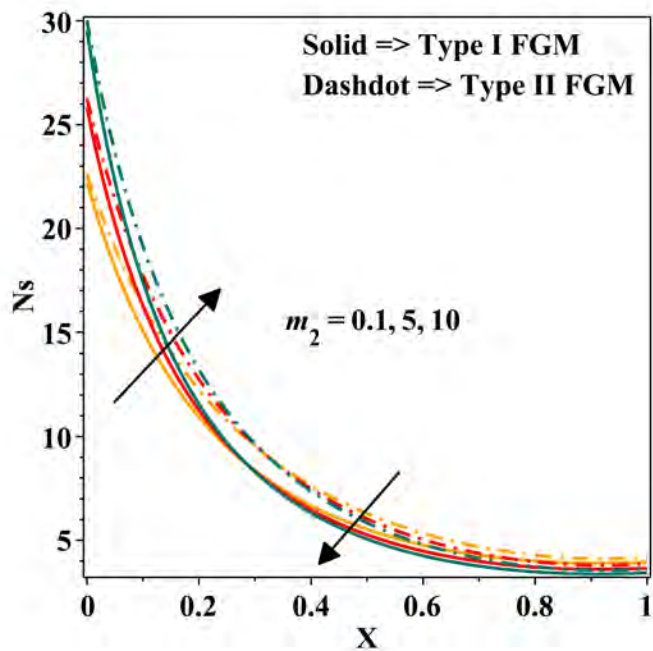
Figure 8.10: Entropy generation in type I and type II FGM fin structures for distinct values of wet porous parameter m_2.
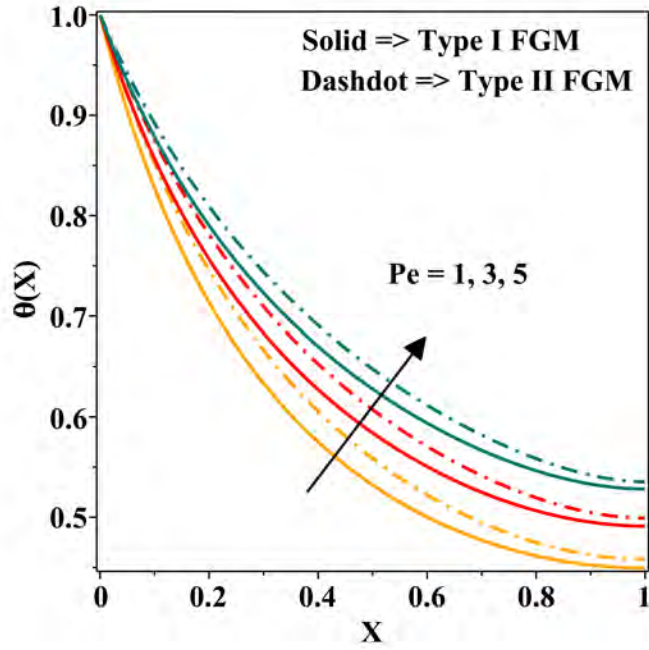
Figure 8.11: Thermal profiles of type I and type II FGM fin structures for distinct values of Peclet number Pe.
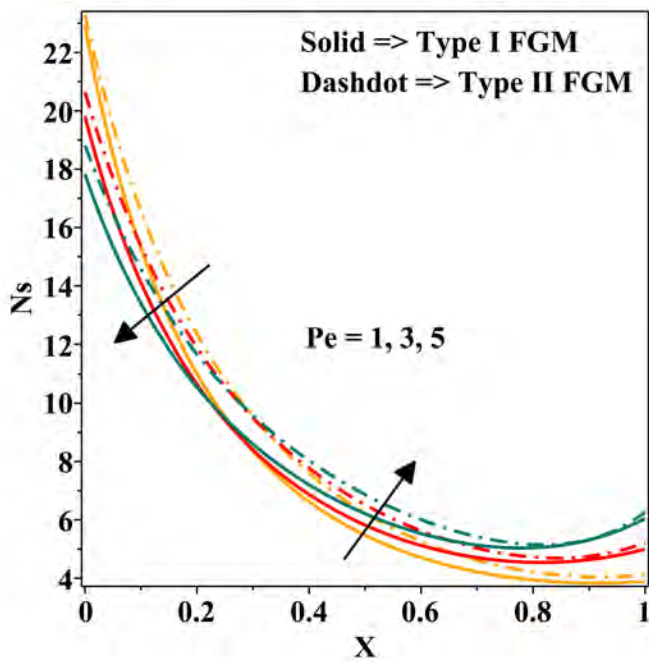
Figure 8.12: Entropy generation in type I and type II FGM fin structures for distinct values of Peclet number Pe.
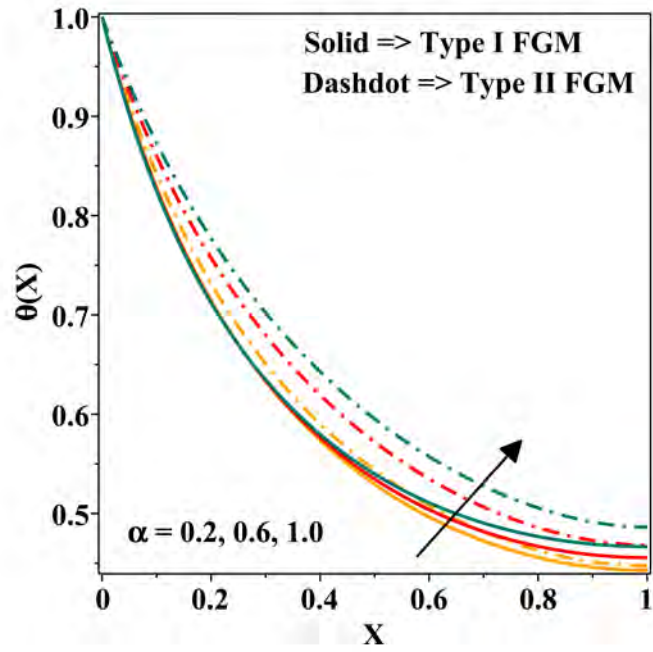
Figure 8.13: Thermal profiles of type I and type II FGM fin structures for distinct values of thermal conductivity grading parameter α.
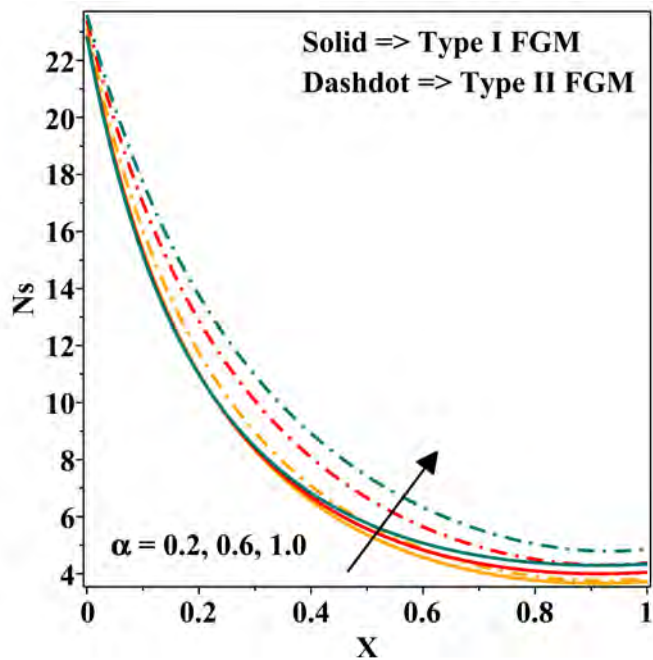
Figure 8.14: Entropy generation in type I and type II FGM fin structures for distinct values of thermal conductivity grading parameter α.
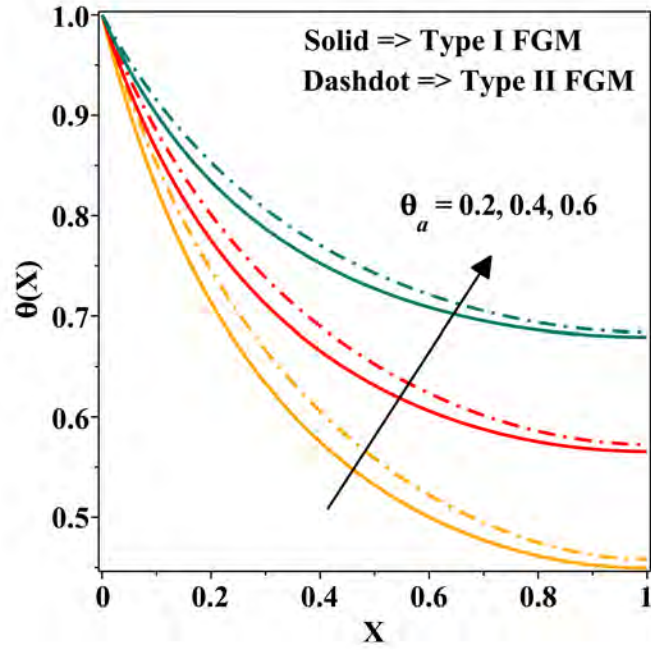
Figure 8.15: Thermal profiles of type I and type II FGM fin structures for distinct values of ambient temperature θ_a.
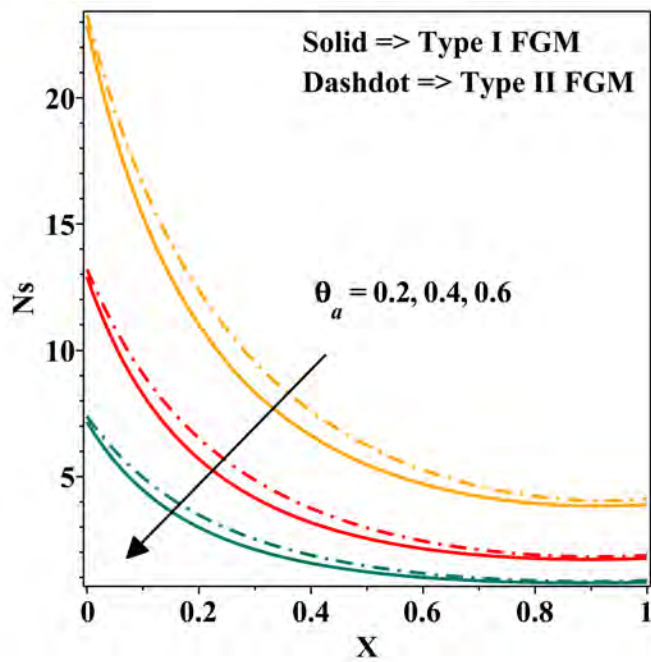
Figure 8.16: Entropy generation in type I and type II FGM fin structures for distinct values of ambient temperature θ_a.
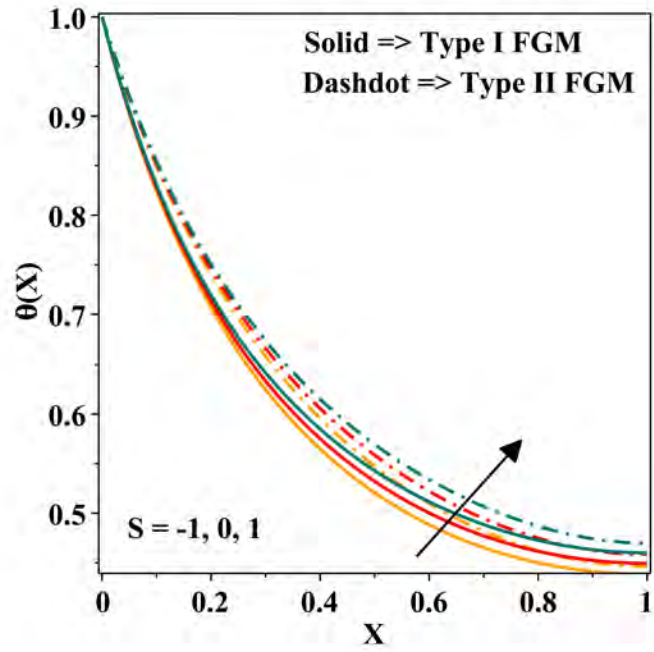
Figure 8.17: Thermal profiles of type I and type II FGM fin structures for distinct values of stretching/shrinking parameter S.
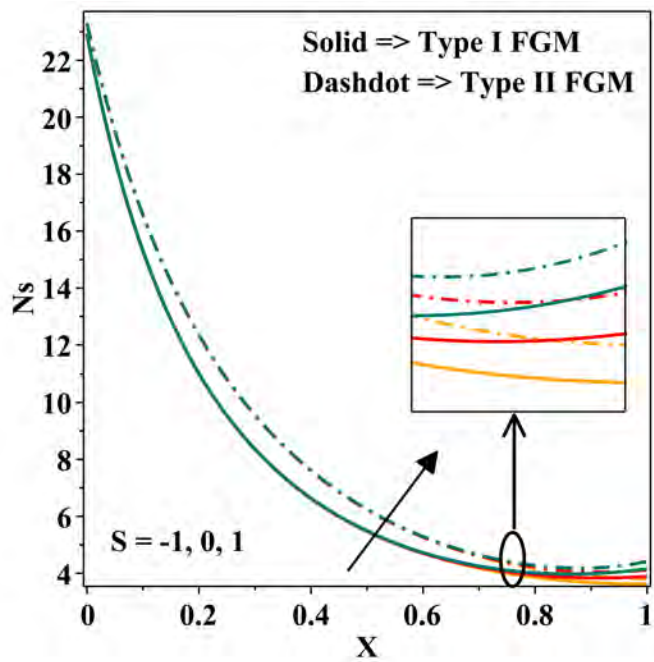
Figure 8.18: Entropy generation in type I and type II FGM fin structures for distinct values of stretching/shrinking parameter S.

167
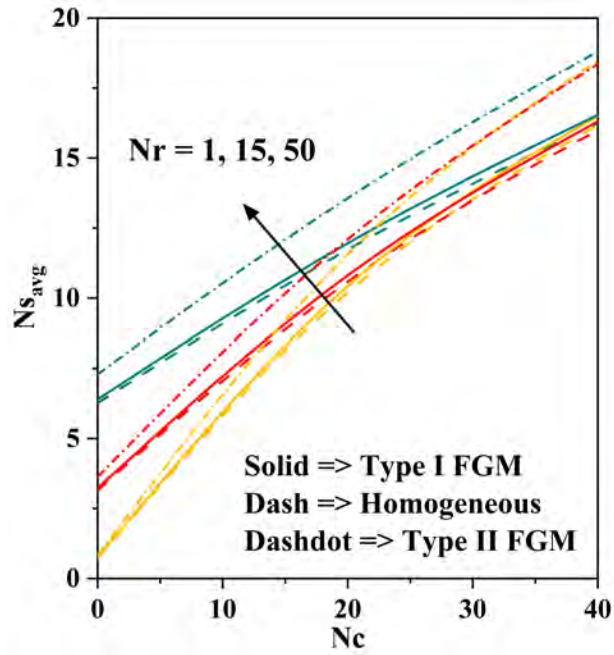
Figure 8.19: Average entropy generation in type I and type II FGM fin structures for distinct values of convective parameter Nc and radiative parameter Nr.
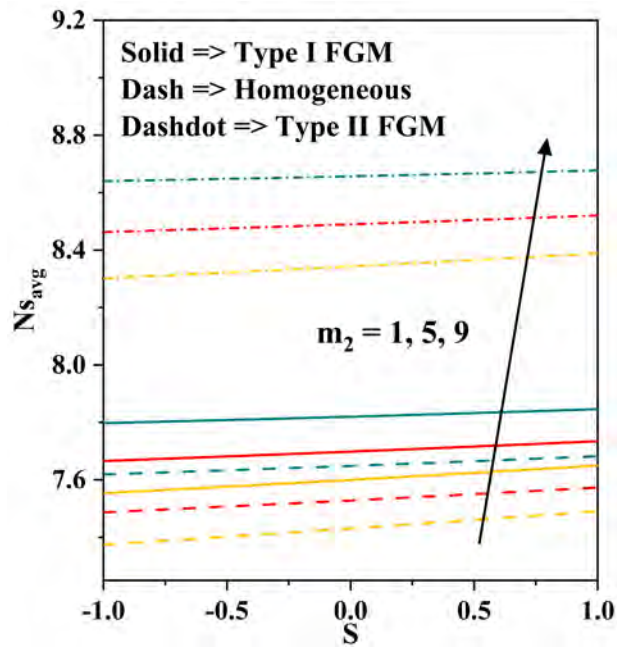
Figure 8.20: Average entropy generation in type I and type II FGM fin structures for distinct values of wet porous parameter m_2 and stretching/shrinking parameter S.
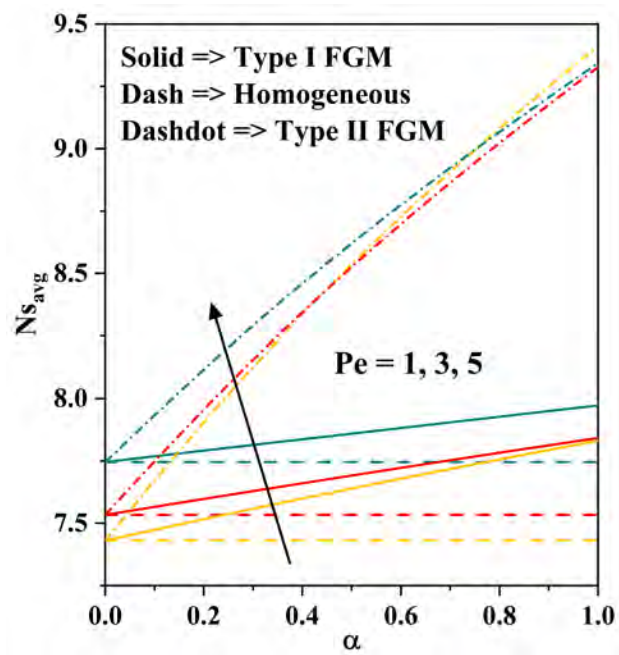
Figure 8.21: Average entropy generation in type I and type II FGM fin structures for distinct values of Peclet number Pe and grading parameter α.

Bibliography

[1] Arslanturk C. *Correlation equations for optimum design of annular fins with temperature dependent thermal conductivity*, Heat and Mass Transfer, 45(4) (2009): 519-525.

[2] Atouei S.A., Hosseinzadeh K., Hatami M., Ghasemi S.E., Sahebi S.A.R. and Ganji D.D. *Heat transfer study on convective–radiative semi-spherical fins with temperature-dependent properties and heat generation using efficient computational methods*, Applied Thermal Engineering, 89 (2015) 299-305.

[3] Ayoobi A, Ramezanizadeh M and Alhuyi-Nazari M. *Optimization of temperature distribution and heat flux functions for cylindrical and conical micro-fins by applying genetic algorithm*, Journal of Thermal Analysis and Calorimetry, 143(6) (2021) 4119-30.

[4] Aziz A. and Bouaziz M.N. *A least squares method for a longitudinal fin with temperature dependent internal heat generation and thermal conductivity*, Energy Conversion and Management, 52(8-9) (2011) 2876-2882.

[5] Aziz A. and Khani F. *Convection–radiation from a continuously moving fin of variable thermal conductivity*, Journal of the Franklin Institute, 348(4) (2011) 640-651.

[6] Aziz A. and Luardini V.J. *Analytical and numerical modeling of steady periodic heat transfer in extended surfaces*, Computational mechanics, 14(5) (1994) 387-410.

[7] Aziz A. and Makinde O.D. *Heat transfer and entropy generation in a two-dimensional orthotropic convection pin fin*, International Journal of Exergy, 7(5) (2010) 579-592.

[8] Aziz A. and Na T.Y. *Periodic heat transfer in fins with variable thermal parameters*, International Journal of Heat and Mass Transfer, 24(8) (1981) 1397-1404.

[9] Aziz A. and Torabi M. *Convective-radiative fins with simultaneous variation of thermal conductivity, heat transfer coefficient, and surface emissivity with temperature*, Heat Transfer-Asian Research, 41(2) (2012) 99-113.

[10] Aziz A., Torabi M. and Zhang K. *Convective–radiative radial fins with convective base heating and convective–radiative tip cooling: homogeneous and functionally graded materials*, Energy Conversion and Management, 74 (2013) 366-376.

[11] Bahrami M., Yovanovich M.M. and Culham J.R. *Role of random roughness on thermal performance of microfins*, Journal of Thermophysics and Heat Transfer, 21(1) (2007) 153-7.

[12] Baslem A., Sowmya G., Gireesha B.J., Prasannakumara B.C., Rahimi-Gorji M. and Hoang N.M., *Analysis of thermal behavior of a porous fin fully wetted with nanofluids: convection and radiation*, Journal of Molecular Liquids, 307 (2020) 112920.

[13] Berrehal H., Dinarvand S. and Khan I. *Mass-based hybrid nanofluid model for entropy generation analysis of flow upon a convectively-warmed moving wedge*, Chinese Journal of Physics, 77 (2022) 2603-2616.

[14] Bhanja D., Kundu B. and Aziz A. *Enhancement of heat transfer from a continuously moving porous fin exposed in convective–radiative environment*, Energy Conversion and Management, 88 (2014) 842-853.

[15] Bhanja D., Kundu B. and Mandal P.K. *Thermal analysis of porous pin fin used for electronic cooling*, Procedia Engineering, 64 (2013) 956-65.

[16] Bhowmik A., Singla R.K., Das R., Mallick A. and Repaka R. *Inverse modeling of a solar collector involving Fourier and non-Fourier heat conduction*, Applied Mathematical Modelling, 38(21-22) (2014) 5126-5148.

[17] Choi S.U. and Eastman J.A. *Enhancing thermal conductivity of fluids with nanoparticles*, (No. ANL/MSD/CP-84938; CONF-951135-29). Argonne National Lab., IL (United States) (1995).

[18] Darvishi M.T., Gorla R.S.R., Khani F. and Gireesha B.J. *Thermal analysis of natural convection and radiation in a fully wet porous fin*, International Journal of Numerical Methods for Heat and Fluid Flow, 26(8) (2016) 2419-2431.

[19] Das R. *Estimation of feasible materials and thermal conditions in a trapezoidal fin using genetic algorithm*, Proceedings of the Institution of Mechanical Engineers, Part G: Journal of Aerospace Engineering, 230(13) (2016) 2356-2368.

[20] Das R. and Kundu B. *Forward and inverse nonlinear heat transfer analysis for optimization of a constructal T-shape fin under dry and wet conditions*, International Journal of Heat and Mass Transfer, 137 (2019) 461-475.

[21] Das R. and Kundu B. *New forward and inverse solutions for wet fins generalized profiles with all nonlinear phenomena*, Journal of Heat Transfer, 143(2) (2021).

[22] Díez L.I., Espatolero S., Cortés C. and Campo A. *Thermal analysis of rough microfins of variable cross-section by the power series method*, International Journal of Thermal Sciences, 49(1) (2010) 23-35.

[23] Din Z.U., Ali A., De la Sen M. and Zaman G. *Entropy generation from convective–radiative moving exponential porous fins with variable thermal conductivity and internal heat generations*, Scientific Reports, 12(1) (2022) 1-11.

[24] Din Z.U., Ali A. and Zaman G. *Entropy generation in moving exponential porous fins with natural convection, radiation and internal heat generation*, Archive of Applied Mechanics, 92(3) (2022) 933-44.

[25] Fallo N., Moitsheki R.J. and Makinde O.D. *Analysis of heat transfer in a cylindrical spine fin with variable thermal properties*, Defect and Diffusion Forum, 387 (2018) 10-22.

[26] Ganji D.D., Rahimi M., Rahgoshay M. and Jafari M. *Analytical and numerical investigation of fin efficiency and temperature distribution of conductive, convective, and radiative straight fins*, Heat Transfer—Asian Research, 40(3) (2011) 233-45.

[27] Gardner K.A. *Efficiency of extended surface*, Journal of Heat Transfer, 67 (1945) 621-631.

[28] Ghadikolaei S.S., Gholinia M., Hoseini M.E. and Ganji D.D. *Natural convection MHD flow due to MoS2–Ag nanoparticles suspended in C2H6O2H2O hybrid base fluid with thermal radiation*, Journal of the Taiwan Institute of Chemical Engineers, 97 (2019) 12-23.

[29] Ghasemi S.E., Valipour P., Hatami M. and Ganji D.D. *Heat transfer study on solid and porous convective fins with temperature-dependent heat generation using efficient analytical method*, Journal of Central South University, 21(12) (2014) 4592-4598.

[30] Gireesha B.J. and Sowmya G. *Heat transfer analysis of an inclined porous fin using Differential Transform Method*, International Journal of Ambient Energy, 43(1) (2020) 3189-3195.

[31] Gireesha B.J., Sowmya G., Khan M.I. and Öztop H.F. *Flow of hybrid nanofluid across a permeable longitudinal moving fin along with thermal radiation and natural convection*, Computer methods and programs in biomedicine, 185 (2020) 105166.

[32] Gireesha B.J., Sowmya G. and Macha M. *Temperature distribution analysis in a fully wet moving radial porous fin by finite element method*, International Journal of Numerical Methods for Heat & Fluid Flow, 32(2) (2019) 453-468.

[33] Gireesha B.J., Sowmya G. and Gorla R.S.R. *Nanoparticle shape effect on the thermal behaviour of moving longitudinal porous fin*, Part N: Journal of Nanomaterials, Nanoengineering and Nanosystems, Proceedings of the Institution of Mechanical Engineers, 234(3-4) (2020) 115-121.

[34] Gorla R.S.R. and Bakier A.Y. *Thermal analysis of natural convection and radiation in porous fins*, International Communications in Heat and Mass Transfer, 38(5) (2011) 638-45.

[35] Hajabdollahi F., Rafsanjani H.H., Hajabdollahi Z. and Hamidi Y. *Multi-objective optimization of pin fin to determine the optimal fin geometry using genetic algorithm*, Applied Mathematical Modelling, 36(1) (2012) 244-54.

[36] Harper D.R. and Brown W.B. *Mathematical equations for heat conduction in the fins of air cooled engines*, NACA Rep. 158, National Advisory Committee on Aeronautics, Washington, DC (1922).

[37] Hassanzadeh R. and Pekel H. *Heat transfer enhancement in annular fins using functionally graded material*, Heat Transfer—Asian Research 42(7) (2013) 603-617.

[38] Hatami M., Ahangar G.R.M., Ganji D.D. and Boubaker K. *Refrigeration efficiency analysis for fully wet semi-spherical porous fins*, Energy Conversion and Management, 84 (2014) 533-540.

[39] Hatami, M. and Ganji, D.D. *Thermal performance of circular convective–radiative porous fins with different section shapes and materials*, Energy Conversion and Management, 76 (2013) 185-193.

[40] Hatami M. and Ganji D.D. *Thermal behavior of longitudinal convective–radiative porous fins with different section shapes and ceramic materials (SiC and Si3N4)*, Ceramics International, 40(5) (2014) 6765-6775.

[41] Hatami M. and Ganji D.D. *Investigation of refrigeration efficiency for fully wet circular porous fins with variable sections by combined heat and mass transfer analysis*, International Journal of Refrigeration, 40 (2014) 140–151.

[42] Hatami M., Hasanpour A. and Ganji D.D. *Heat transfer study through porous fins (Si3N4 and AL) with temperature-dependent heat generation*, Energy Conversion and Management, 74 (2013) 9-16.

[43] Hoshyar H.A., Rahimipetroudi I., Ganji D.D. and Majidian A.R. *Thermal performance of porous fins with temperature-dependent heat generation via the homotopy perturbation method and collocation method*, Journal of Applied Mathematics and Computational Mechanics, 14 (2015) 53–65.

[44] Hosseinzadeh S., Hosseinzadeh K., Hasibi A. and Ganji D.D. *Thermal analysis of moving porous fin wetted by hybrid nanofluid with trapezoidal, concave parabolic and convex cross sections*, Case Studies in Thermal Engineering, 30 (2022) 101757.

[45] Joneidi A.A., Ganji D.D. and Babaelahi M. *Differential transformation method to determine fin efficiency of convective straight fins with temperature dependent thermal conductivity*, International Communications in Heat and Mass Transfer, 36(7) (2009) 757-762.

[46] Khan W.A. and Aziz A. *Transient heat transfer in a functionally graded convecting longitudinal fin*, Heat and Mass Transfer, 48(10) (2012) 1745-1753.

[47] Khani F. and Aziz A. *Thermal analysis of a longitudinal trapezoidal fin with temperature-dependent thermal conductivity and heat transfer coefficient*, Communications in Nonlinear Science and Numerical Simulation, 15(3) (2010) 590–601.

[48] Khani F., Darvishi M.T., Gorla R.S.R. and Gireesha B.J. *Thermal analysis of a fully wet porous radial fin with natural convection and radiation using the spectral collocation method*, International Journal of Applied Mechanics and Engineering, 21(2) (2016) 377-392.

[49] Khatami S. and Rahbar N. *An analytical study of entropy generation in rectangular natural convective porous fins*, Thermal Science and Engineering Progress, 11 (2019) 142-149.

[50] Kiwan S. and Al-Nimr M.A. *Using porous fins for heat transfer enhancement*, Journal of Heat Transfer, 123(4) (2001) 790-795.

[51] Kiwan S. *Thermal analysis of natural convection porous fins*, Transport in Porous Media, 67(1) (2007) 17-29.

[52] Kiwan S. *Effect of radiative losses on the heat transfer from porous fins*, International Journal of Thermal Sciences, 46(10) (2007) 1046-1055.

[53] Kiwan S. *On the natural convection heat transfer from an inclined surface with porous fins*, Transport in Porous Media, 127(2) (2019) 295-307.

[54] Kraus A.D., Aziz A. and Welty J.R. *Extended surface heat transfer*, New York: John Wiley, 2002.

[55] Kundu B., Das R. and Lee K.S. *Differential transform method for thermal analysis of exponential fins under sensible and latent heat transfer*, Procedia Engineering, 127 (2015) 287-294.

[56] Kundu B., Das R., Wankhade P.A. and Lee K.S. *Heat transfer improvement of a wet fin under transient response with a unique design arrangement aspect*, International Journal of Heat and Mass Transfer, 127 (2018) 1239-1251.

[57] Kundu B. and Lee K.S. *Fourier and non-Fourier heat conduction analysis in the absorber plates of a flat-plate solar collector*, Solar Energy, 86(10) (2012) 3030-3039.

[58] Kundu B. and Lee K.S. *A non-Fourier analysis for transmitting heat in fins with internal heat generation*, International Journal of Heat and Mass Transfer, 64 (2013) 1153-1162.

[59] Kundu B. and Lee K.S. *Exact analysis for minimum shape of porous fins under convection and radiation heat exchange with surrounding*, International Journal of Heat and Mass Transfer, 81 (2015) 439-448.

[60] Kundu B. and Yook S.J. *An accurate approach for thermal analysis of porous longitudinal, spine and radial fins with all nonlinearity effects–analytical and unified assessment*, Applied Mathematics and Computation, 402 (2021) 126124.

[61] Lambert M.A. and Fletcher L.S. *Thermal contact conductance of spherical rough metals*, Journal of Heat Transfer, 119(4) (1997) 684-90.

[62] Lane H.J. and Heggs P.J. *Extended surface heat transfer—the dovetail fin*, Applied Thermal Engineering, 25(16) (2005) 2555-2565.

[63] Ma J., Sun Y. and Li B. *Simulation of combined conductive, convective and radiative heat transfer in moving irregular porous fins by spectral element method*, International Journal of Thermal Sciences, 118 (2017) 475-487.

[64] Manohar G.R., Venkatesh P., Gireesha B.J., Madhukesh J.K. and Ramesh G.K. *Dynamics of hybrid nanofluid through a semi spherical porous fin with internal heat generation*, Partial Differential Equations in Applied Mathematics, 4 (2021) 100150.

[65] Moitsheki R.J. and Harley C. *Transient heat transfer in longitudinal fins of various profiles with temperature-dependent thermal conductivity and heat transfer coefficient*, Pramana, 77(3) (2011) 519-532.

5

[66] Moradi A., Hayat T. and Alsaedi A. *Convection-radiation thermal analysis of triangular porous fins with temperature-dependent thermal conductivity by DTM*, Energy Conversion and Management, 77 (2014) 70-77.

[67] Mosavat M., Moradi R., Takami M.R., Gerdroodbary M.B. and Ganji D.D. *Heat transfer study of mechanical face seal and fin by analytical method*, Engineering Science and Technology, an International Journal, 21(3) (2018) 380-388.

[68] Mosayebidorcheh S., Farzinpoor M. and Ganji D.D. *Transient thermal analysis of longitudinal fins with internal heat generation considering temperature-dependent properties and different fin profiles*, Energy Conversion and Management, 86 (2014) 365-370.

[69] Murray W.M. *Heat transfer through an annular disk or fin of uniform thickness*, Trans. ASME, J. Appl. Mech., 60 (1938) A78.

[70] Nabati M., Jalalvand M. and Taherifar S. *Sinc collocation approach through thermal analysis of porous fin with magnetic field*, Journal of Thermal Analysis and Calorimetry, 144(6) (2021) 2145-2158.

[71] Najafabadi M.F., Rostami H.T., Hosseinzadeh K. and Ganji D.D. *Thermal analysis of a moving fin using the radial basis function approximation*, Heat Transfer, 50(8) (2021) 7553-7567.

[72] Ndlovu P.L. *Numerical analysis of transient heat transfer in radial porous moving fin with temperature dependent thermal properties*, Journal of Applied and Computational Mechanics, 6(1) (2020) 137-144.

[73] Oguntala G., Abd-Alhameed R., Sobamowo G. and Abdullahi H.S. *Improved thermal management of computer microprocessors using cylindrical-coordinate micro-fin heat sink with artificial surface roughness*, Engineering Science and Technology, an International Journal, 21(4) (2018) 736-44.

[74] Oguntala G.A., Sobamowo G.M., Abd-Alhameed R.A. and Noras J.M. *Numerical study of performance of porous fin heat sink of functionally graded material for improved thermal management of consumer electronics*, IEEE Transactions on Components, Packaging and Manufacturing Technology, 9(7) (2019) 1271-1283.

[75] Oguntala G.A., Sobamowo G.M., Eya N.N. and Abd-Alhameed R.A. *Investigation of simultaneous effects of surface roughness, porosity, and magnetic field of rough porous microfin under a convective–radiative heat transfer for improved microprocessor cooling of consumer electronics*, IEEE Transactions on Components, Packaging and Manufacturing Technology, 9(2) (2018) 235-246.

[76] Poulikakos D. and Bejan A. *Fin geometry for minimum entropy generation in forced convection*, Journal of Heat Transfer, 104(4) (1982) 616-623.

[77] Ramzan M., Dawar A., Saeed A., Kumam P., Watthayu W. and Kumam W. *Heat transfer analysis of the mixed convective flow of magnetohydrodynamic hybrid nanofluid past a stretching sheet with velocity and thermal slip conditions*, Plos one, 16(12) (2021) e0260854.

[78] Roy P.K., Mallick A., Mondal H. and Sibanda P. *A modified decomposition solution of triangular moving fin with multiple variable thermal properties*, Arabian Journal for Science and Engineering, 43 (2018) 1485–1497.

[79] Sahoo R.R. *Thermo-hydraulic characteristics of radiator with various shape nanoparticle-based ternary hybrid nanofluid*, Powder Technology, 370 (2020) 19-28.

[80] Sabbaghi S., Rezaii A., Shahri G.R. and Baktash M.S. *Mathematical analysis for the efficiency of a semi-spherical fin with simultaneous heat and mass transfer*, International Journal of Refrigeration, 34(8) (2011) 1877-1882.

[81] Sahu M. and Sarkar J. *Steady-state energetic and exergetic performances of single-phase natural circulation loop with hybrid nanofluids*, Journal of Heat Transfer, 141(8) (2019) 082401

[82] Sharqawy M.H. and Zubair S.M. *Efficiency and optimization of straight fins with combined heat and mass transfer- An analytical solution*, Applied Thermal Engineering, 28 (2008) 2279-2288.

[83] Singla R.K. and Das R. *Application of decomposition method and inverse prediction of parameters in a moving fin*, Energy Conversion and Management, 84 (2014) 268-281.

[84] Singh S., Kumar D. and Rai K.N. *Analytical solution of Fourier and non-Fourier heat transfer in longitudinal fin with internal heat generation and periodic boundary condition*, International Journal of Thermal Sciences, 125 (2018) 166-175.

[85] Sowmya G. and Gireesha B.J. *Analysis of heat transfer through different profiled longitudinal porous fin by differential transformation method*, Heat Transfer, 51(2) (2022) 2165-2180.

[86] Sowmya G., Gireesha B.J. and Berrehal H. *An unsteady thermal investigation of a wetted longitudinal porous fin of different profiles*, Journal of Thermal Analysis and Calorimetry, 143(3) (2021) 2463-2474.

[87] Sowmya G., Gireesha B.J. and Makinde O.D. *Thermal performance of fully wet longitudinal porous fin with temperature-dependent thermal conductivity, surface emissivity and heat transfer coefficient*, Multidiscipline Modeling in Materials and Structures, 16(4) (2019) 749-764.

[88] Sowmya G., Gireesha B.J., Khan M.I., Momani S. and Hayat T. *Thermal investigation of fully wet longitudinal porous fin of functionally graded material*, International Journal of Numerical Methods for Heat & Fluid Flow, 30(12) (2020) 5087-5101.

[89] Sowmya G., Gireesha B.J. and Madhu M. *Analysis of a fully wetted moving fin with temperature-dependent internal heat generation using the finite element method*, Heat Transfer, 49(4) (2020) 1939–1954.

[90] Sowmya G., Gireesha B.J. and Prasannakumara B.C. *Scrutinization of different shaped nanoparticle of molybdenum disulfide suspended nanofluid flow over a radial porous fin*, International Journal of Numerical Methods for Heat & Fluid Flow, 30(7) (2019) 3685-3699.

[91] Sun Y.S. and Xu J.L. *Thermal performance of continuously moving radiative–convective fin of complex cross-section with multiple nonlinearities*, International Communications in Heat and Mass Transfer, 63 (2015) 23-34.

[92] Sundar L.S., Sharma K.V., Singh M.K., Sousa A.C. *Hybrid Nanofluids Preparation, Thermal Properties, Heat Transfer and Friction Factor—A Review*, Renew Sustain Energy Rev, 68 (2017) 185–198.

[93] Talbi N., Kezzar M., Malaver M., Tabet I., Sari M.R., Metatla A. and Eid M.R. *Increment of heat transfer by graphene-oxide and molybdenum-disulfide nanoparticles in ethylene glycol solution as working nanofluid in penetrable moveable longitudinal fin*, Waves in Random and Complex Media, (2022) 1-23 https://doi.org/10.1080/17455030.2022.2026527.

[94] Torabi M. and Aziz A. *Thermal performance and efficiency of convective–radiative T-shaped fins with temperature dependent thermal conductivity, heat transfer coefficient and surface emissivity*, International Communications in Heat and Mass Transfer, 39(8) (2012) 1018-1029.

[95] Torabi M., Aziz A. and Zhang K. *A comparative study of longitudinal fins of rectangular, trapezoidal and concave parabolic profiles with multiple nonlinearities*, Energy, 51 (2013) 243-256.

[96] Turkyilmazoglu M. *Efficiency of heat and mass transfer in fully wet porous fins: exponential fins versus straight fins*, International Journal of Refrigeration, 46 (2014) 158-164.

[97] Turkyilmazoglu M. *Stretching/shrinking longitudinal fins of rectangular profile and heat transfer*, Energy Conversion and Management, 91 (2015) 199-203.

[98] Turkyilmazoglu M. *Efficiency of the longitudinal fins of trapezoidal profile in motion*, Journal of Heat Transfer, 139(9) (2017) 094501.

[99] Turkyilmazoglu M. *Heat transfer from moving exponential fins exposed to heat generation*, International Journal of Heat and Mass Transfer, 116 (2018) 346-351.

[100] Turkyilmazoglu M. *An optimum profile of a special pin fin: full solutions*, International Journal of Numerical Methods for Heat and Fluid Flow, 30(11) (2020) 4945-4954.

[101] Turkyilmazoglu M. *Thermal management of parabolic pin fin subjected to a uniform oncoming airflow: Optimum fin dimensions*, Journal of Thermal Analysis and Calorimetry, 143 (2021) 3731-373.

[102] Vahabzadeh A., Ganji D.D. and Abbasi M. *Analytical investigation of porous pin fins with variable section in fully-wet conditions*, Case Studies in Thermal Engineering, 5 (2015) 1-12.

[103] Varun Kumar R.S., Sowmya G. and Prasannakumara B.C. *Significance of non-Fourier heat conduction in the thermal analysis of a wet semi-spherical fin with internal heat generation*, Waves in Random and Complex Media, 18 (2022) 1-7.

[104] Yang Y.T. and Chien S.K. *A double decomposition method for solving the periodic base temperature in convective longitudinal fins*, Energy Conversion and Management, 49(10) (2008) 2910-2916.

[105] Yildirim A., Yarimpabuç D. and Celebi K. *Transient thermal stress analysis of functionally graded annular fin with free base*, Journal of Thermal Stresses, 43(9) (2020) 1138-1149.

Nomenclature

A	thermal conductivity parameter
A_b	area of the fin base (m^2)
A_c	cross-sectional area of the fin (m^2)
$\bar{A}_c$	rough pin fin cross-sectional area (m^2)
B	amplitude of input temperature
B^*	emissivity parameter
C	fin taper ratio
C_p	specific heat at constant pressure (J/kgK)
$(C_p)_1$	specific heat at constant pressure of first nanoparticle (J/kgK)
$(C_p)_2$	specific heat at constant pressure of second nanoparticle (J/kgK)
$(C_p)_f$	specific heat at constant pressure of base fluid (J/kgK)
$(C_p)_{nf}$	specific heat at constant pressure of nanofluid (J/kgK)
$(C_p)_{hnf}$	specific heat at constant pressure of hybrid nanofluid (J/kgK)
C_T	temperature ratio
F_{f-a}	shape factor for radiation heat transfer
G	generation parameter
K	permeability (m^2)
L	length of the fin (m)
Le	Lewis number
M	thermogeometric parameter
Nc	convection parameter
Nr	radiative parameter
Ns	entropy generation number
Ns_{avg}	average entropy production

P	fin perimeter (m)
$\bar{P}$	rough pin fin perimeter (m)
Pe	Peclet number
Q	dimensionless heat transfer rate
$\dot{Q}$	heat transfer rate (W)
R	radius (dimensionless)
R^*	radius of fin (m)
$\bar{R}$	tip to base radius ratio
S	stretching/shrinking parameter of the fin
$\dot{S}$	entropy $(Jkg^{-1}K^{-1})$
S'''_{gen}	entropy generation $(Jm^{-3}K^{-1})$
T	local fin temperature (K)
T_a	ambient temperature (K)
T_b	base temperature (K)
T_{bm}	average base temperature (K)
T_s	sink temperature (K)
$\bar{U}$	constant velocity of the fin (ms^{-1})
Ve	Vernotte number
W	width (m)
X	dimensionless length
a	grading parameter of thermal conductivity
b_2	variable parameter $(1/K)$
g	acceleration due to gravity (ms^{-2})
h	heat transfer coefficient (W/m^2K)
h_a	heat transfer coefficient at temperature T_a (W/m^2K)
h_D	uniform mass transfer coefficient kg/m^2s
l_{fg}	latent heat of water evaporation (J/kg)
k	thermal conductivity (J/kg)
k_0	thermal conductivity of the homogeneous material (W/mK)
k_a	thermal conductivity at temperature T_a (W/mK)
k_{eff}	effective thermal conductivity of the material (W/mK)

k_f thermal conductivity of the base fluid (W/mK)

k_{nf} thermal conductivity of the nanofluid (W/mK)

k_{hnf} thermal conductivity of the hybrid nanofluid (W/mK)

m power index of heat transfer coefficient

$\bar{m}$ mass flow rate (kg/s)

$m_{\bar{\sigma}}$ mean absolute surface slope

m_0, m_1 constants

m_2 wet porous parameter

n pin fin shape factor

n_1 wet fin parameter

q base heat transfer rate (W)

q^* internal rate of heat generation (W/m^3)

q_a^* internal rate of heat generation at temperature T_a (W/m^3)

r fin radius or radial direction (m)

r_t tip radius (m)

r_b base radius of the pin fin (m)

s shape factor

s^* rate of stretching/shrinking of the fin $(1/m)$

t time (s)

$t^*(x)$ fin thickness at distance x (m)

t_b fin base thickness (m)

$\bar{v}_w,$ velocity of the fluid passing through the fin (m/s)

w_1 mass of first nanoparticle (g)

w_2 mass of second nanoparticle (g)

w_f mass of base fluid (g)

x axial coordinate of the fin (m)

Greek symbols

ρ density (kg/m^3)

ρ_1 density of the first nanoparticle (kg/m^3)

ρ_2 density of the second nanoparticle (kg/m^3)

ρ_f density of the ambient fluid (kg/m^3)

ρ_{nf} density of the nanofluid (kg/m^3)

ρ_{hnf} density of the hybrid nanofluid (kg/m^3)

α, β in-homogeneity index

α^* measure of thermal conductivity variation with temperature $(1/K)$

β^* measure of surface emissivity variation with temperature $(1/K)$

β_f volumetric thermal expansion coefficient of the ambient fluid $(1/K)$

β_{nf} volumetric thermal expansion coefficient of the nanofluid $(1/K)$

β_{hnf} volumetric thermal expansion coefficient of the hybrid nanofluid $(1/K)$

Ω angle of inclination

ψ dimensionless frequency of oscillation

ψ^* base radius to length ratio

$\bar{\psi}$ frequency of oscillation (s^{-1})

ν fin shape parameter

ν_f kinematic viscosity of the ambient fluid (m^2/s)

ϵ relative roughness

ϵ_g internal heat generation parameter $(1/K)$

ϵ_G non-dimensional internal heat generation parameter

ε surface emissivity of fin

ε_s surface emissivity of fin at temperature T_s

η fin efficiency

$\hat{\phi}$ porosity

φ solid volume fraction of nanoparticles

φ_1 solid volume fraction of first nanoparticle

φ_2 solid volume fraction of second nanoparticle

μ_f dynamic viscosity of the base fluid (kg/ms)

μ_{nf} dynamic viscosity of the nanofluid (kg/ms)

μ_{hnf} dynamic viscosity of the hybrid nanofluid (kg/ms)

χ sphericity

θ non-dimensional temperature

θ_a dimensionless ambient temperature

θ_s dimensionless sink temperature

τ	dimensionless time
τ_0	thermal relaxation time (s)
σ	Stefan-Boltzmann constant $(W/m^2 K^4)$
$\bar{\sigma}$	roughness standard deviation (m)
$\bar{\omega}$	humidity ratio of the saturated air
$\bar{\omega}_s$	humidity ratio of the surrounding air
δ	a geometrical quantity that defines the tip semi-fin thickness (m)

Subscripts

gen	generation
i	inlet
o	outlet
p	particle
S	solid

Publications

1. "Heat transfer analysis of longitudinal fins of trapezoidal and dovetail profile on an inclined surface", Physica Scripta (IOP Publishing) (Scopus) (SCI) (IF-3.081), 96 125209 (2021).

2. "Effects of stretching/shrinking on the thermal performance of a fully wetted convective-radiative longitudinal fin of exponential profile", Applied Mathematics and Mechanics (Springer) (Scopus) (SCI) (IF-3.918), 43(3) 389-402 (2022).

3. "Numerical investigation of efficiency of fully wet porous convective-radiative moving radial fin in the presence of shape-dependent hybrid nanofluid", International Communications in Heat and Mass Transfer (Elsevier) (Scopus) (SCI) (IF-6.782), 138 106341 (2022).

4. "Numerical investigation of transient thermal behaviour of fully wet and porous moving semi-spherical fin", Physica Scripta (IOP Publishing) (Scopus) (SCI) (IF-3.081), 97(8) 085220 (2022).

5. "Transient thermal investigation of a fully wet porous convective-radiative rough cylindrical pin fin", Heat Transfer (Wiley Online Library) (Scopus), (2023) https://doi.org/10.1002/htj.22809.

6. "Study on efficiency of fully wet porous trapezoidal fin structures in the presence of

convection and radiation", JNNCE Journal of Engineering & Management (JJEM), 5(2) 66-72 (2022).

7. "Effect of periodic heat transfer on the transient thermal behaviour of a convective-radiative fully wet porous moving trapezoidal fin", Applied Mathematics and Mechanics (Springer) (Scopus) (SCI) (IF-3.918), (2023) (Accepted).

8. "Thermal performance of stretching/shrinking fully wet porous cylindrical and conical pin fin structures by differential transformation approach", International Journal of Modern Physics B (World Scientific) (Scopus) (SCI) (IF-1.404), (Revised manuscript submitted).

9. "Analysis of entropy generation in a fully wet moving porous longitudinal fin exposed to convection and radiation: Homogeneous and functionally graded materials", Journal of Thermal Analysis and Calorimetry (Springer) (Scopus) (SCI) (IF-4.755), (Revised manuscript submitted).

10. "Impact of shape-dependent hybrid nanofluid on transient heat transfer and efficiency of a fully wet porous longitudinal fin", has been submitted for possible publication in Arabian Journal for Science and Engineering (Springer).

11. "Study on efficiency of convective-radiative moving semi-spherical fin of functionally graded material", has been submitted for possible publication in ZAMM - Journal of Applied Mathematics and Mechanics (Wiley Online Library).

12. "An unsteady thermal investigation of a convective-radiative porous exponential fin subject to heat generation and periodic boundary condition", has been submitted for possible publication in Physica Scripta (IOP Publishing).

13. "Transient thermal analysis of a convective-radiative fully wet porous inclined exponential fin with internal heat generation: non-Fourier approach", has been submitted for possible publication in Communications in Theoretical Physics (IOP Publishing).

14. "Impact of non-Fourier heat conduction on transient thermal behaviour of fully wet convective-radiative moving trapezoidal fin", has been submitted for possible publication in International Journal of Modelling and Simulation (Taylor and Francis).

15. "Mass-based hybrid nanofluid flow over an unsteady exponential moving porous fin under fully wetted condition", has been submitted for possible publication in Heat and Mass Transfer (Springer).

16. "Role of surface roughness on the transient thermal behaviour of distinct profiled convective-radiative wet porous moving pin fin structures", has been submitted for possible publication in Waves in Random and Complex Media (Taylor and Francis).

17. "An unsteady thermal analysis of a convective-radiative moving porous inclined semi-spherical fin subject to heat generation", has been submitted for possible publication in Brazilian Journal of Physics (Springer).

18. "Impact of stretching/shrinking on entropy generation of a fully wet moving convective-radiative longitudinal fin by Optimal Homotopy Analysis Method (OHAM)", has been submitted for possible publication in International Communications in Heat and Mass Transfer (Elsevier).

Physica Scripta

PAPER

Heat transfer analysis of longitudinal fins of trapezoidal and dovetail profile on an inclined surface

B J Gireesha[1,*], M L Keerthi[1] and K M Eshwarappa[2]

[1] Department of PG Studies and Research in Mathematics, Kuvempu University, Shankaraghatta-577451, Shivamogga, Karnataka, India
[2] Department Studies in Physics, Davangere University, Shivagangotri, Davangere, Karnataka, India
[*] Author to whom any correspondence should be addressed.

E-mail: bjgireesu@gmail.com, keerthiholalur@gmail.com and eshwarappa–km@yahoo.com

Abstract

The trapezoidal and dovetail profiled longitudinal fin structures exposed to a convective-radiative environment and mounted on an inclined surface have been considered for the analysis. The fin structures have been assumed to be porous and fully wet in nature. The Darcy model has been implemented to simulate the fluid-solid interactions. Further, the convective and radiative heat transfer coefficients have been taken to be temperature-dependent. The resulting equation has been reduced by introducing the non-dimensional quantities and then solved by employing the Runge-Kutta Fehlberg 4th–5th order method along with the shooting technique. The effect of tip tapering, angle of inclination, fully wet nature, porosity, internal heat generation, and other pertinent parameters on the fin thermal profile and fin heat transfer rate has been presented graphically and discussed. It has been inferred that the dovetail fin profile achieves the highest heat transfer rate followed by rectangular and trapezoidal fin profiles provided the internal heat generation is minimal. The present work is significant for fin design purposes and also acts as a verification tool for future research.

Nomenclature

$A(x)$	cross-sectional area of the fin at distance x (m²)
A_b	area of the fin base (m²)
B	emissivity parameter
C	fin taper ratio
C_p	specific heat at constant pressure (J KgK⁻¹)
G	generation parameter
K	permeability (m²)
L	length of the fin (m)
Le	Lewis number
Nr	radiative parameter
Nc	natural convection parameter
Q	dimensionless heat transfer rate
T	local fin temperature (K)
T_a	ambient temperature (K)
T_s	sink temperature (K)
T_b	base temperature (K)

Study on Efficiency of Fully Wet Porous Trapezoidal Fin Structures in the Presence of Convection and Radiation

B.J. Gireesha[1]*, M.L. Keerthi[1], D.O. Soumya[1]

[1]*Department of PG Studies and Research in Mathematics, Kuvempu University, Shankaraghatta-577451, Shivamogga, Karnataka, India.

bjgireesu@gmail.com, keerthiholalur@gmail.com, soumyado510@gmail.com

Abstract

The thermal behaviour of fully wet porous trapezoidal profiled longitudinal fin structures in the presence of natural convection and radiation has been scrutinized in the present analysis. The rectangular and trapezoidal profiles have been comparatively analysed. The Darcy's law has been incorporated to study the solid-fluid interactions. Further, the internal heat generation has been assumed to be a linear function of temperature. The obtained non-linear second order ordinary differential equation has been reduced and evaluated numerically. The impact of fully wet condition, porous nature, internal heat generation and other relevant parameters on the thermal profile and efficiency of trapezoidal and rectangular fin profiles has been interpreted graphically and discussed. It has been derived that the rectangular fin profile is more efficient than the trapezoidal profile.

Keywords: Natural convection, porous, trapezoidal profile, fully wet longitudinal fin, fin efficiency, internal heat generation.

1. Introduction

The fin, which is an extra surface attached to the primary surface, is significant in amplifying the cooling process. Fin structures are generally applied in the engineering field to improve heat transfer rates by expanding surface area and adding material attachment. In their work, Kraus et al [11] have comprehensively covered the basic concepts regarding the extended surface heat transfer.
Porous fin is implemented to extend the surfaces of a system, resulting in effective heat transfer amplification. Hence Kiwan and Al Nimr [9] provided a unique technique that uses porous fins to improve heat transmission from a given surface. Kiwan [10] explored the role of radiation heat transfer on a convective porous extended surface with respect to a vertical isothermal surface. The Darcy model was used by Gorla and Bakier [4] to examine the thermal performance of extended porous

surface of rectangular profile. To solve a model representing heat transport in a radial porous fin, Jooma and Harley [6] used the Crank-Nicolson technique. Sobamowo et al [18] used the developed exact results to examine the impact of thermal-model factors on the permeable fin's energy performance. Martins-Costa et al [13] used the Oberbeck–Boussinesq approximation with Darcy's law to scrutinize the thermal profile of a porous rectangular fin.

The wetted fin, as opposed to a dry one, allows for greater heat circulation. As a result, the totally wet situation has piqued people's attention, and numerous works have been conducted as a result. Hatami and Ganji [5] investigated the mass and heat transfer in a porous radial wet fin by 4th order Runge Kutta and Least Square method and the impact of Darcy number on the energy field has also been investigated. The radiation heat transfer in the permeable fully wet fin has been studied by Darvishi et al [2]. The Darcy model was

APPLIED MATHEMATICS AND MECHANICS (ENGLISH EDITION)

Effects of stretching/shrinking on the thermal performance of a fully wetted convective-radiative longitudinal fin of exponential profile[*]

B. J. GIREESHA[1,†],   M. L. KEERTHI[1],   G. SOWMYA[2]

1. Department of PG Studies and Research in Mathematics, Kuvempu University, Shankaraghatta 577451, India;

2. Department of PG Mathematics, The National College (Auto), Bangalore 560070, India

Abstract   The present investigation focuses on the thermal performance of a fully wet stretching/shrinking longitudinal fin of exponential profile coated with a mechanism like a conveyer belt. The modeled equation is non-dimensionalized and solved by applying the Runge-Kutta-Fehlberg (RKF) method. The effects of parameters such as the wet parameter, the fin shape parameter, and the stretching/shrinking parameter on the heat transfer and thermal characteristics of the fin are graphically analyzed and discussed. It is inferred that the negative effects of motion and internal heat generation on the fin heat transfer rate can be lessened by setting a shrinking mechanism on the fin surface. The current examination is inclined towards practical applications and is beneficial to the design of fins.

Key words   fully wet longitudinal fin, convection, exponential profile, internal heat generation, moving fin

Chinese Library Classification   O361
2010 Mathematics Subject Classification   34B27, 74A15, 74S05

Nomenclature

A,	thermal conductivity parameter;	h_{D},	uniform mass transfer coefficient;
$A(x)$,	cross-sectional area of the fin, m^2;	h_{a},	coefficient of convective heat transfer at
A_{b},	area of the fin base, m^2;		T_{a}, W/(m^2·K);
T_{a},	ambient temperature, K;	h,	coefficient of convective heat transfer,
b_2,	variable parameter, K^{-1};		W/(m^2·K);
c_p,	specific heat at constant pressure,	G,	generation number;
	J/(kg·K);	k_{a},	thermal conductivity at T_{a}, W/(m·K);

Numerical investigation of efficiency of fully wet porous convective-radiative moving radial fin in the presence of shape-dependent hybrid nanofluid

M.L. Keerthi [a], B.J. Gireesha [a,*], G. Sowmya [b]

[a] Department of PG Studies and Research in Mathematics, Kuvempu University, Shankaraghatta, 577451 Shivamogga, Karnataka, India
[b] Department of Mathematics, MS Ramaiah Institute of Technology, Banglore 54, India.

ARTICLE INFO

ABSTRACT

The main focus of the study is a fully wet porous fin of radial profile exposed to convective-radiative heat exchange with the hybrid nanofluid flowing past it with a constant velocity of U. In the analysis, spherical-spherical, spherical-cylindrical, and spherical-platelet shape combinations of two nanoparticles are considered. The mixture model is employed to assess all the thermophysical attributes of the hybrid nanofluid except thermal conductivity and dynamic viscosity, which are estimated by applying the nanoparticle volume fraction-based interpolation method. The fin model with the applied conditions results in an ordinary differential equation which is made dimensionless and then numerically resolved by applying the Runge Kutta Fehlberg (RKF) 4-5th ordered technique. The effect of Peclet number, wet fin parameter, thermogeometric parameter, nanoparticle volume fraction, convective parameter, radiative parameter, exponential index, empirical shape factor and ambient temperature (dimensionless) on the energy field and thermal gradient profiles of the radial fin subjected to shape-dependent hybrid nanofluid flow has been graphically analysed. Furthermore, the thermal fin efficiency has been modelled and its variation with the significant parameters has been examined. One of the major outcomes was that efficiency increases with nanoparticle volume fraction. Further, it is significantly affected by the shape factor of the nanoparticles and achieves the highest value for spherical-platelet combination. The results obtained motivate further study of nanotechnology assisted extended surface technology.

1. Introduction

Excess heat generation in thermal components is unavoidable in a wide range of engineering applications. This excessive heat might have a negative impact on the operation and functionality of such components. As a result, the reliable operation of such components necessitates the use of appropriate cooling technology. Although different cooling processes have long been used to remove heat, fins or extended surfaces play a vital role in increasing the heat transfer rate. Kraus et al. [1] have put in an encyclopaedic effort in compiling the advancements in the field of extended surface technology. Because of their widespread use in industry, researchers have always sought new techniques to improve their performance and make them more flexible to the needs of the field.

Gorla and Bakier [2] investigated the simultaneous effect of convective and radiative heat losses on the porous fin's purpose and found that the radiative environment enhances the fin heat transfer rate.

In the heat exchange process, the fin material is crucial and, in this regard, Khan and Aziz [3] examined three distinct sorts of functionally graded materials and found that they improved the rate of heat transmission through the fin. Further, they employed the finite difference approach (FDM) to investigate the transient thermal behaviour of the fin. Practically, the thermophysical attributes of the fin material fluctuate with temperature and in this direction, Darvishi et al. [4] explored the thermal nature of a radial fin, assuming that thermal conductivity is a function of local fin temperature. They conferred that variable thermal conductivity has a significant impact on the distribution of temperature in the fin structure. Additionally, Atouei et al. [5] have investigated the semi-spherical fin structures by considering temperature-sensitive physical features as well as heat absorption criteria and have developed the solutions using least squares and collocation approaches. Studies were also conducted by considering alternative geometries to the basic fin structure since varied application areas necessitate flexible

---

* Corresponding author.
  E-mail address: bjgireesu@gmail.com (B.J. Gireesha).

ORIGINAL ARTICLE

HEAT TRANSFER WILEY

Transient thermal investigation of a fully wet porous convective–radiative rough cylindrical pin fin

B. J. Gireesha[1] ⬤ │ **M. L. Keerthi[1]** │ **K. M. Eshwarappa[2]**

[1]Department of PG Studies and Research in Mathematics, Kuvempu University, Shankaraghatta, Shivamogga, Karnataka, India

[2]Department Studies in Physics, Davangere University, Shivagangotri, Davangere, Karnataka, India

Correspondence
B. J. Gireesha, Department of PG Studies and Research in Mathematics, Kuvempu University, Shankaraghatta-577451, Shivamogga, Karnataka, India.
Email: bjgireesu@kuvempu.ac.in

Abstract

The microelectromechanical systems technologies frequently produce rough surfaces, and the repercussion of roughness on the thermal performance is more prominent in structures of smaller dimensions. In this regard, the present article intends to examine the unsteady thermal behavior of a fully wet, porous, and rough micropin-fin structure under convective–radiative conditions. Here, a pin fin of a cylindrical profile has been chosen. The problem is modeled by incorporating the roughness parameters in the perimeter and cross-sectional area of the pin fin. Further, the study of the porous structure has been carried out by implementing the Darcy model. The resulting partial differential equation is nonlinear and of the second order which has been solved by employing the finite difference method. The impact of the roughness parameter, wet porous parameter, dimensionless time, convective parameter, base radius-to-length ratio, radiative parameter, thermal conductivity parameter, power index, and ambient temperature on the thermal performance and efficiency of rough micropin-fin structures has been established graphically. According to the findings, for 0.15% rise in roughness, the rough micropin fin has 12% more thermal drop rate and 13% less efficiency than the smooth one. Further, the work

Physica Scripta

PAPER

Numerical investigation of transient thermal behaviour of fully wet and porous moving semi-spherical fin

M L Keerthi[1], **B J Gireesha**[1,*] and **G Sowmya**[2]

[1] Department of PG Studies and Research in Mathematics, Kuvempu University, Shankaraghatta-577451, Shivamogga, Karnataka, India
[2] Department of Mathematics, MS Ramaiah Institute of Technology, Banglore-54, India
[*] Author to whom any correspondence should be addressed.

E-mail: keerthiholalur@gmail.com, bjgireesu@gmail.com and g.sowmya34@gmail.com

Abstract

A variety of engineering applications demand efficient and adaptable fin structures for the intensification of heat exchange. The semi-spherical fin structures are useful in the field of refrigeration, chemical processing systems, aerospace etc. In this regard, the present article numerically investigates the transient thermal behaviour of a fully wet semi-spherical fin. The study incorporates the Darcy model as the fin is made up of porous material. Further, the fin is exposed to convective-radiative heat exchange and is subject to uniform motion. The heat balance equation has been reduced to get a nonlinear partial differential equation (PDE) which is computed by employing the finite difference method (FDM). The dimensionless terms are grouped together and their influence on the temperature distribution in a semi-spherical fin is studied. Also, the instantaneous heat transfer rate and the transient fin efficiency have been modelled and their variations with relevant parameters have been graphically depicted. And these are found be strong functions of Peclet number, wet porous nature and dimensionless time. As a main outcome the semi-spherical fin efficiency is positively influenced by the Peclet number. Along with the fundamental point of interest the results presented benefit the fin designing purposes.

Nomenclature

$A_c(x)$	=	fin cross-sectional area as a function of $x (m^2)$;
A_b	=	area of the fin base (m^2);
b_2	=	variable parameter $(1/K)$;
C_p	=	specific heat at constant pressure (J/kgK);
g	=	acceleration due to gravity (m/s^2);
h_D	=	uniform mass transfer coefficient (kg/m^2s);
h_a	=	coefficient of convective heat transfer at temperature $T_a(W/m^2K)$;
h	=	coefficient of convective heat transfer (W/m^2K);
K	=	permeability (m^2);
k_{eff}	=	effective thermal conductivity of the material (W/mK);
k	=	thermal conductivity (W/mK);
Le	=	Lewis number;
m_0, m_1	=	constants;
m_2	=	wet parameter;
Nc	=	convective parameter;
Nr	=	radiative parameter;
P	=	fin perimeter (m);
Pe	=	Peclet number;
p	=	exponential index of coefficient of convective heat transfer;
Q	=	non-dimensional heat flow rate;
q	=	heat flow rate (W);
R	=	radius of semi-spherical fin (m);